Sterols and oxysterols in brain and the immune system.

Meljon, Anna

Sterols and oxysterols in brain and the immune system

Anna Meljon

A thesis submitted to Swansea University in fulfilment of the requirements for the degree of Doctor of Philosophy

Swansea University

2014

ProQuest LLC.
789 East Eisenhower Parkway
P.O. Box 1346
Ann Arbor, MI 48106 – 1346

Summary

This project investigates sterol and oxysterol content of murine brain and macrophages. Oxysterols are oxidised forms of cholesterol implicated in a wide array of biological functions.

The compounds were analysed with LC-MS LTQ-Orbitrap high resolution system, which provides a highly sensitive and accurate tool for analysis of metabolites.

We profiled a sterol content of newborn murine brain and identified a broad spectrum of oxysterols. Some of these compounds are implicated in neurogenesis, a number of other oxysterols derived from desmosterol were identified in brain tissue for the first time.

We analysed murine model of human disease arising from reduced ability to produce cholesterol (SLOS). The sterol profile showed an altered level of cholesterol precursors and generally lowered concentration of oxysterols.

Next, we moved to analysis of brain lipidome from animals with disrupted mechanisms of cholesterol metabolism. Cholesterol hydroxylase Cyp46a1 provides the mechanism of cholesterol removal from the brain. The study of the knock out mice did not reveal the existence of any compensatory mechanisms. The results showed mainly the reduction in cholesterol synthesis.

We profiled a sterol content of Cyp27a1-/- mouse brain. Cyp27a1 participates in bile acid synthesis. The steroid profile revealed changed pattern of mono- and polihydroxylated sterols suggesting an upregulation of an alternative pathway of bile acid synthesis. We also analysed the consequence of deficiency of another enzyme involved in bile acids synthesis Cyp7b1. In brain of Cyp7b1-/- mouse we found elevated levels of known Cyp7b1 substrates, and increased concentration of other, putative substrates for this enzyme.

The last experimental chapter concentrates on analysis of murine macrophages treated with interferon β and γ. The treatment induced an increased production of 25-hydroxycholesterol. This links sterol metabolism with mechanisms of immune defence.

Declarations and Statements

This work has not previously been accepted in substance for any degree and is not being concurrently submitted in candidature for any degree.

Signed

Date 12/11/2014

This thesis is the result of my own investigations, except where otherwise stated. Where correction services have been used, the extent and nature of the correction is clearly marked in a footnote(s).

Other sources are acknowledged by footnotes giving explicit references. A bibliography is appended.

Signed

Date 12/11/2014

I hereby give consent for my thesis, if accepted, to be available for photocopying and for inter-library loan, and for the title and summary to be made available to outside organisations.

Signed

Date 12/11/2014

Acknowledgements

I would like to thank my family, supervisors, colleagues and friends for their support and encouragement during the course of this research and while writing this document. I would like to express my gratitude to my supervisor Professor William Griffiths for his support and guidance over the years. Thank you for patience and kindness while sharing your knowledge in mass spectrometry. Your hard work can be a true inspiration! I am grateful to Dr. Yuqin Wang for sharing her experience and practical skills in mass spectrometry, LC and molecular biology.

I would like to thank to Professor Gareth Brenton and Dr. Ruth Godfrey for letting me use their laboratory and instruments. I would like to express my sincere gratitude to all the members of the EPSRC centre for giving me their time and passing knowledge in mass spectrometry. Special thanks to Mr. John Tregembo for his help with technical issues in the lab.

I am indebted to Professor David Russell from University of Texas Southwest Medical Centre Dallas and Professor Cedric Shackleton from Children's Hospital Oakland Research Institute for providing me with the brain samples and to Dr. Mathieu Blanc from Edinburgh University for sending me the macrophage samples. I would also like to thank to Professor Norman Javitt from New York University School of Medicine and Professor Hans-Joachim Knölker from Technical University of Dresden for synthesising the analytical standards.

My thanks also go to my friends and colleagues for nice and supportive atmosphere in the lab. Special thanks go to Dr. Alwena Morgan, Dr. Peter Crick for their help and input while writhing this thesis.

Table of contents

List of figures

List of tables

ACAT	acetyl:CoA:cholesterol acyltransferase
BBB	blood brain barrier
C_{18}	octadecyl carbon chain
CH25H	cholesterol 25-hydroxylase
CID	collision induced dissociacion
CNS	central nervous system
CYP	cytochrome P450
CYP11A1	cytochrome P450 11A1
CYP27A1	cytochrome P450 27A1
CYP3A4	cytochrome P450 3A4
CYP39A1	cytochrome P450 39A1
CYP46A1	cytochrome P450 46A1
CYP7A1	cytochrome P450 7A1
CYP7B1	cytochrome P450 7B1
CYP8B1	cytochrome P450 8B1
CTX	cerebrotendinous xanthomatosis
Da	Dalton
DHCR7	3β-hydroxysterol-D7-reductase, 7-dehydrocholesterol reductase
ESI	electrospray ionisation
FT	Fourier transformation
g	gram
GC	gas chromatography
GC-MS	gas chromatography mass spectrometry
GP	Girard P
HDL	high density lipoproteins
HMG-CoA	3-hydroxy-3-methylo-glutarylo-Coenzyme A
HPLC	high pressure liquid chromatography
HSD3B7	hydroxysteroid dehydrogenase
INSIG	insulin-induced gene protein
INF	interferon

INFα	Interferon alpha
INFβ	Interferon beta
INFγ	Interferon gamma
INFAR1	Interferon alpha/beta receptor alpha chain
L	liter
LC-MS	liquid chromatography mass spectrometry
LDL	low density lipoproteins
LIPID MAPS	lipid metabolites and pathways strategy
LXR	liver X receptor
m	milli (10^{-3})
μ	micro (10^{-6})
m/z	mass to charge ratio
MALDI	matrix assisted ionisation
mCMV	murine cytomegalovirus
MS^n	tandem mass spectrometry
n	nano (10^{-9})
p	pico (10^{-12})
ppm	parts per million
RA	relative abundance
RF	radio frequency
RIC	reconstructed ion chromatogram
RP	reverse phase
RRT	relative retention time
SCAP	SREBP-escort protein
SIM	selected ion monitoring
SLOS	Smith-Lemli-Opitz Syndrome
SPE	solid phase extraction
SREBP	sterol response element binding protein
SRM	selected reaction monitoring
STAT	Signal Transducer and Activator of
TIC	total ion chromatogram

Gene and protein nomenclature

Human protein abbreviations are written with al the letters in uppercase, mice protein abbreviations are written with only the first letter in uppercase and the remaining letters in lower case.

Gene abbreviations are italicised, with uppercase and lowercase letters following the pattern for proteins.

1 Introduction

1.1 Origins of oxysterols

Cholesterol is present at various degrees in all animal cells where it plays vital physiological functions. As a constituent of cell membranes cholesterol modulates fluidity of the lipid bilayer [1] [2] [3] [4] while its metabolically active pool serves as precursors of oxysterols, bile acids and steroid hormones.

The cholesterol molecule is based on a cyclopentanoperhydrophentanthrene core with a hydroxyl group attached to one side and a isooctyl chain bound to the other end (Figure 1.1). Such a "design" of cholesterol provides a unique feature: the cyclic frame with the hydroxyl group is more polar than the non-polar hydrocarbon tail. However, this property can by altered by addition of hydrophilic groups either to the ring structures or to the chain. The gradation of polarity within steroid molecules as well as the possibility of alteration their hydrophilic properties have profound physiological consequences, such as translocation through biological membranes or interactions with regulatory proteins, just to name a few.

Cholesterol derivatives which share its tetracyclic nucleus, are known as steroids; to this group belong oxysterols, bile acids and steroid hormones. On the contrary, opening of any of the ring structures gives an origin to compounds known as *seco*-sterols, exemplified by vitamin D_3.

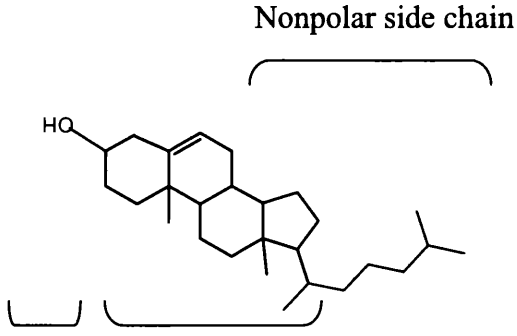

Figure 1.1 Structure of cholesterol

In the animal body cholesterol originates either from the diet or can be biosynthesised. Dietary cholesterol is absorbed from the intestine, and then is distributed to tissues via the circulation. Steroids have a very low solubility in aqueous solutions, so in order to be transported in the blood they need to be coupled to proteins, forming complexes known as lipoproteins. The transport of cholesterol and its derivatives from the intestine is carried out in Low Density Lipoproteins (LDL), while an excess of sterols is removed from the tissues in High Density Lipoproteins (HDL) which transfer the sterols to the liver. These two classes of lipoproteins are different in steroid composition and the proteins involved in their transport.

Although cholesterol can be obtained from a diet, all cells can biosynthesise sterols *de novo*. High intake of cholesterol from the diet suppresses the rate of its *de novo* synthesis by the body, hence the homeostasis relays on both dietary and indigenous pools of cholesterol. For humans the level of dietary cholesterol absorbed per day ranges between 300-700 mg compared to approximately 800 mg synthesised in the liver [5].

In humans the liver is responsible for biosynthesis of the majority of body cholesterol, which is later distributed across tissues, with the exception of the brain. Brain is separated from the peripheral circulation by blood brain barrier which is formed by tight connections of endothelial cells. BBB prevents the entry of microorganisms and compounds such as endotoxins from entering the CNS. This structure is selectively permeable allowing the passage of small molecules such as water by means of passive diffusion, while active transport is needed for compounds such as glucose and amino acids. The blood brain barrier prevents larger lipophilic molecules such as cholesterol from entering the nervous tissue, therefore all cholesterol in the brain must be produced *in situ*.

Cholesterol is *de novo* biosynthesised in the mevalonate pathway. In general, the pathway can by divided into four main blocks. In the first one acetyl-CoA is transformed into 3-hydroxy-3-methylglutarl-CoA (HMG-CoA). In the next stage HMG-CoA is reduced to form mevalonic acid. This is a rate-limiting step in the mevalonate pathway and is catalysed by the enzyme HMG-CoA reductase. HMG-CoA reductase is controlled by a negative feedback mechanism with the final product of the pathway, cholesterol. Mevalonate is then transformed into isopentenyl

pyrophosphate. The condensation of six molecules of isopentenyl pyrophosphate leads to the formation of squalene. In the final part of the pathway linear squalene is transformed into a tetracyclic structure, lanosterol, which is later modified to form cholesterol. The transition from lanosterol to cholesterol can by achieved in two separate pathways utilising either 7-dehydrocholesterol or desmosterol (24-dehydrocholesterol) as the intermediates. 7-Dehydrocholesterol and desmosterol are reduced by actions of specific reductases to form cholesterol. Oxysterols, for example 25-hydroxycholesterol, can be produced from hydroxylation of cholesterol and also have a regulatory role on the mevalonate pathway. The scheme of mevalonate pathway is presented in Figure 1.2 [6]. The control loop of HMG-CoA reductase is disturbed in cells of patients suffering from defects of cholesterol synthesis such as Smith-Lemli-Opitz Syndrome (SLOS). SLOS arises from the malfunction of 7-dehydrocholesterol reductase, which leads to accumulation of 7- and its isomer, 8-dehydrocholesterol, accompanied by reduced levels of cholesterol.

The general pathway of cholesterol removal from the body proceeds via the formation of bile acids. Bile acids are polar derivatives of cholesterol, the transformation of cholesterol into bile is carried out via oxysterols as intermediate metabolites. The main role of bile is to serve as detergents aiding the emulsification, digestion and adsorption of lipids and fat soluble vitamins from food. Recently a new function of bile acids emerged when these compounds were found to be ligands to nuclear receptors.

In humans the main pool of bile acids is generated in the liver, where they are conjugated with either taurine or glycine. Then bile acids are transported to and enriched in the gall bladder, from where they are excreted into the duodenal part of the intestine. In the intestine bile can be either re-absorbed via the enterohepatic circulation or removed from the body with the faeces.

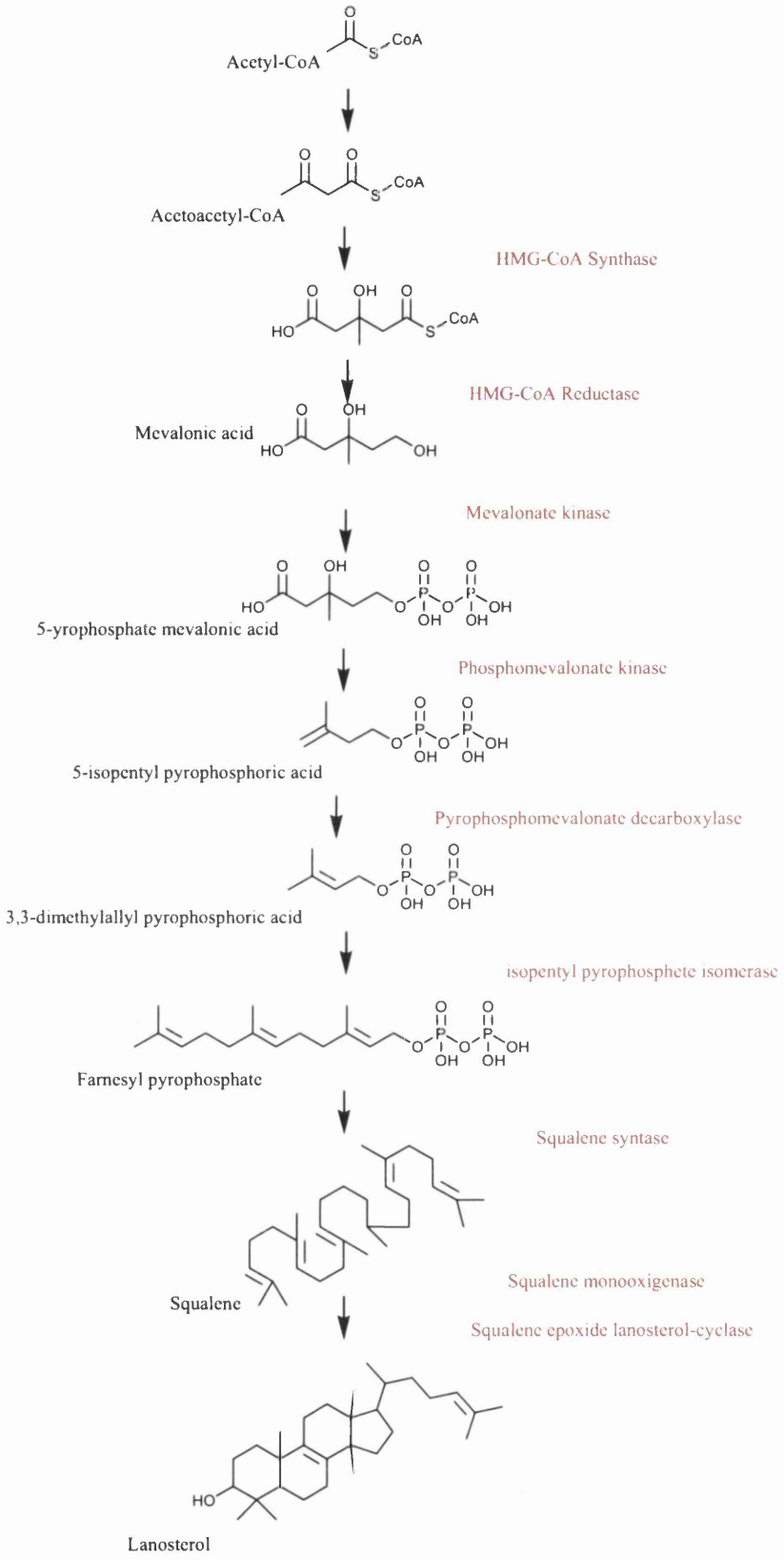

Figure 1.2 Simplified overview of cholesterol synthesis pathways under the feed-back control of cholesterol and oxysterols exemplified by 25-hydroxycholesterol. (Modified from ref. [6])

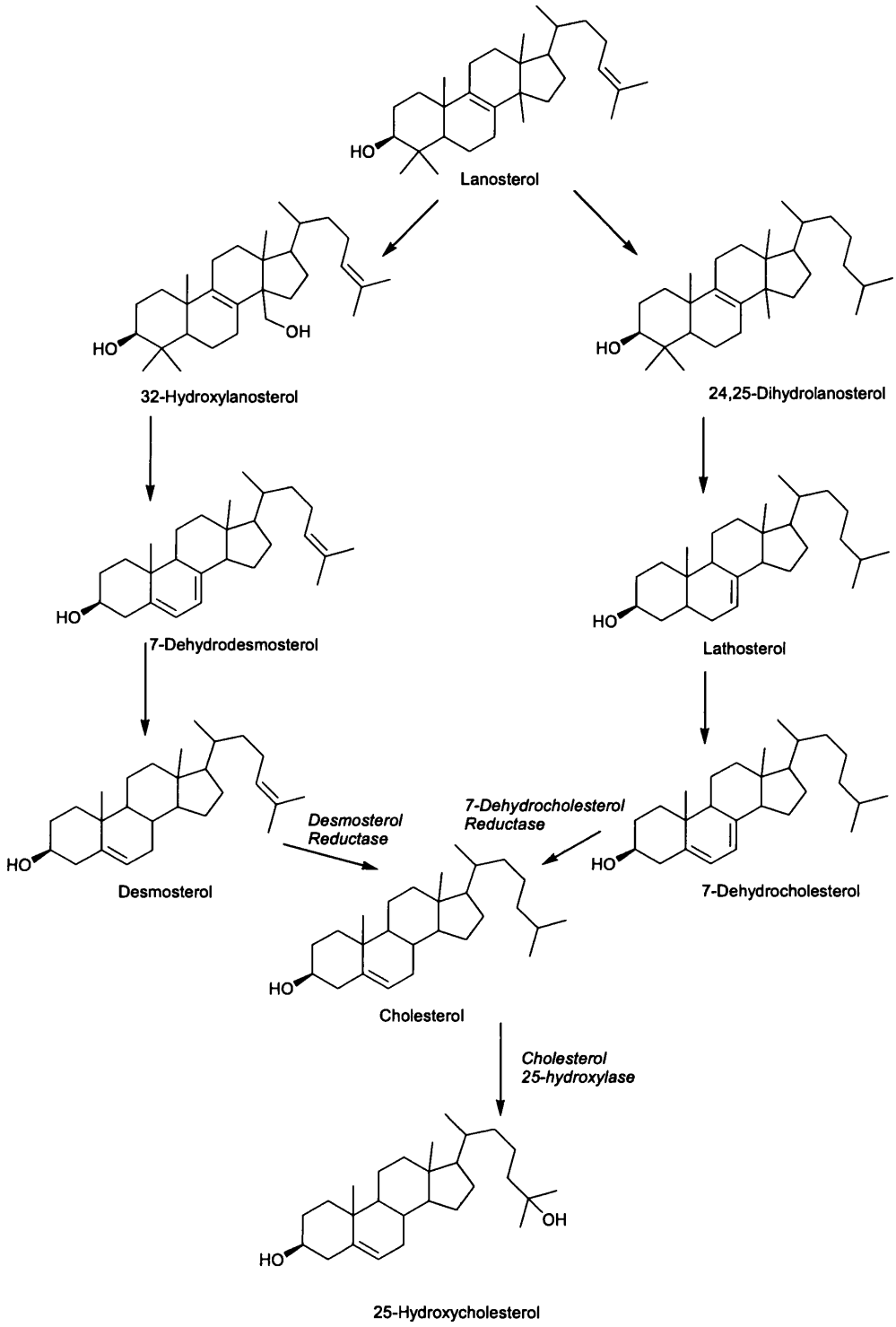

Figure 1.3 - continued

1.2 Characteristics of oxysterols

Oxysterols are mono- or polyoxygenated derivatives of cholesterol or its precursors. These compounds are precursors to bile acids, steroid hormones and vitamin D_3, they serve as transport routes for cholesterol and have also biological activity as ligands to receptors. The oxygen-containing group can be attached to the sterol molecule in form of a hydroxyl (hydroxycholesterol), a ketone (keto- o oxocholesterol) or carboxylate group (acid derivatives of cholesterol). Hydroxylation or generation of a ketone group is possible on either the steroid core or on the alkyl chain, while the carboxylate function applies only to the side-chain.

Cholesterol derivatives possessing an additional oxygen-containing group are less hydrophobic, which has multiple consequences for their physical and physiological properties. Oxygenated forms of cholesterol can pass more readily through biological membranes, therefore increasing the rate of transportation in cells.

Oxysterols can be generated by either enzymatic or non-enzymatic mechanisms. An overview of oxysterols found in human and rodent brain is presented in Figure 1.4 and Figure 1.5.

Non-enzymatic reactions include autoxidation or reaction with ozone. Autoxidation preferably occurs at the allylic C7 carbon and tertiary C25 carbon. This generates 7α-hydroxy-, 7β-hydroxy-, 7-keto- and 25-hydroxycholesterol, respectively. Generation of ozone by antibody-catalysed reactions was reported by Wentworth et al [7]. This reaction is likely to occur in sites affected by inflammation. Exposure to ozone causes opening of oxysterol ring structures leading to formation of *seco*-sterols.

Enzymes involved in the metabolism of cholesterol predominantly belong to the family of cytochrome P450 (Cyp monoxygenases, with the exception to cholesterol 25-hydroxylase [8]. The Cyp enzymes are an ancient family of proteins involved in sterol metabolism in animals, plants, yeast and some classes of bacteria. Most of bacteria do not have Cyp proteins, however the strains that express these enzymes includes bacteria employed in synthesis of therapeutical agents such as streptomycin (Streptomce)s and anti-cancer drugs (Myxobacteria) [9, 10]. On the contrary, Cyp can be targeted in patogens such as Mycobacteria [11] and fungi [12]. Azoles-based fungicides inhibit Cyp51, preventing from conversion of lanosterol to

fungal sterol – ergosterol. This class of anti-fungal drugs is used to treat a wide range of pathogent in medical in agricultural use [13-15]. Many Cyp enzymes are responsible for metabolism of xenobiotics. Cholesterol 25-hydroxylase, which is not a Cyp enzyme, is expressed in various tissues including heart, lung and kidney and its activity can be upregulated during the immune response. Its cellular localisation is limited to endoplasmatic reticulum and Golgi apparatus.

Cyp7a1 and Cyp27a1 initiate the two main metabolic pathways of bile acid biosynthesis: the "classical" also known as the "neutral" and the "alternative", which can be also referred to as "acetic" pathways. The main, "classical", route is initiated by hydroxylation of cholesterol at the 7α position catalysed by the endoplasmatic reticulum enzyme Cyp7a1. This reaction is a major regulator and rate limiting step in the bile acid biosynthesis. Cyp7a1 is a hepatic enzyme, hence this reaction is limited to the liver.

In the "alternative" pathway the formation of bile acids starts from hydroxylation the alkyl chain at the 27 position. It worth noting that this nomenclature is not equivocal due to 25R stereochemistry introduced by hydroxylation of the terminal C-26 carbon. Hence a molecule previously named 27-hydroxycholesterol possessing (25R)26-hydroxyl group is re-named into 26-hydroxycholesterol [16], however many authors still use the name 27-hydroxycholesterol. This reaction of 26-hydroxylation is performed by the mitochondrial enzyme Cyp27a1, ubiquitously expressed by various cells [17]. including neurons and glia [18-20].

Cyp7a1 is a cytochrome P450 microsomal hepatic enzyme that converts cholesterol to 7α-hydroxycholesterol. Cyp27a1 is a ubiquitously expressed enzyme confined to mitochondria. It not only metabolizes cholesterol to 27-hydroxycholesterol, but also transforms resulting oxysterol into 27-carboxylic acid. Deficiency of CYP27A1 in humans is linked to metabolic disorder Cerebrotendinous Xantomatosis [21].

7α- and 27-hydroxylation are initial steps of bile acid formation. 27-hydroxylated cholesterol and 27-carboxlic acid can be further hydroxylated by CYP7B1, an enzyme specifically catalysing 7α-hydroxylation of oxysterols. Two human disorders are associated with malfunction of CYP7B1: liver failure in children

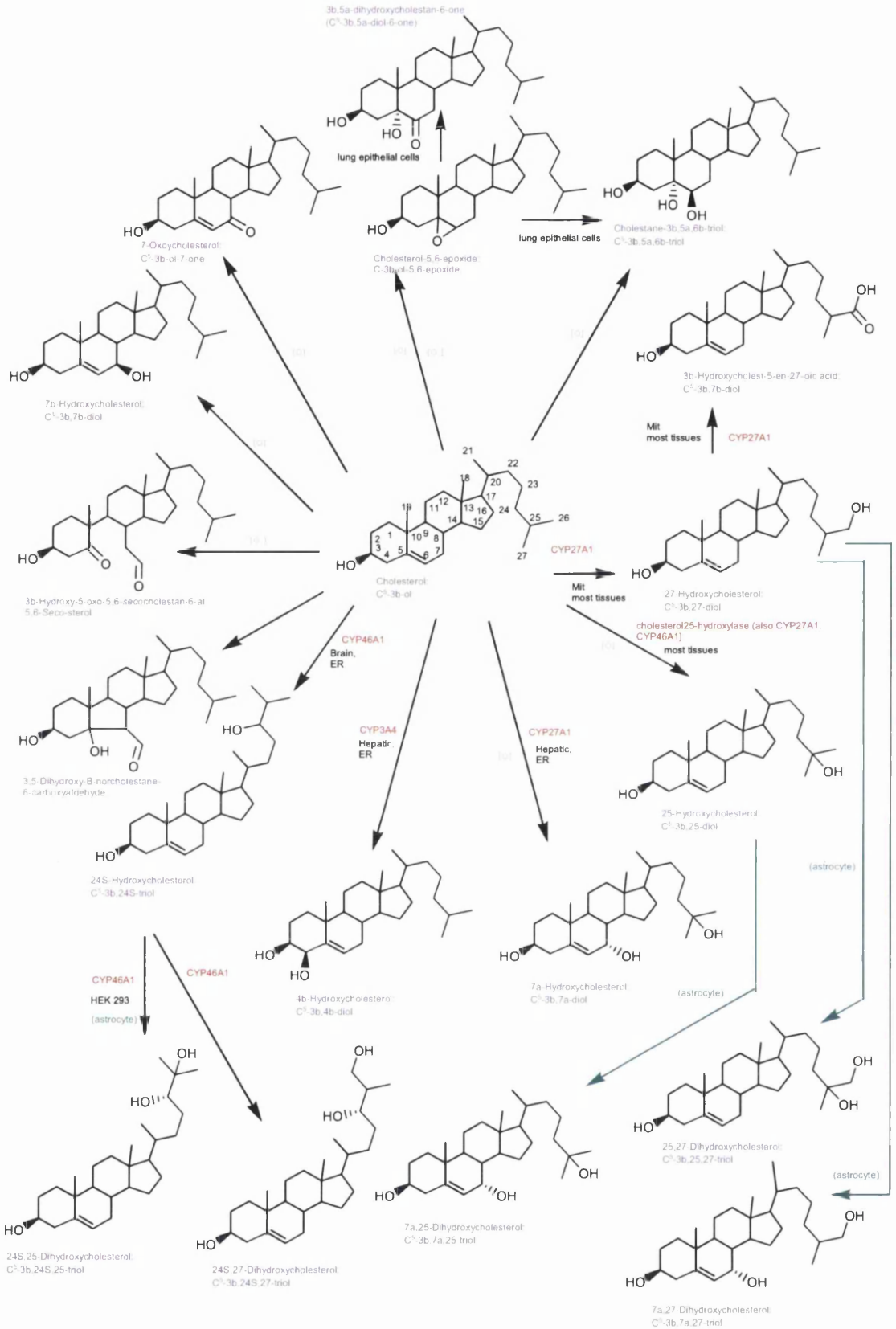

Figure 1.4 Oxysterols identified in human and rat brain. Enzymes indicated in red, subcellular locations abbreviated as follows: Endoplasmatic reticulum (ER), Mitochondria (Mit), Peroxisome (Pos), Cytosol (Cyt). Reproduced from ref. [22].

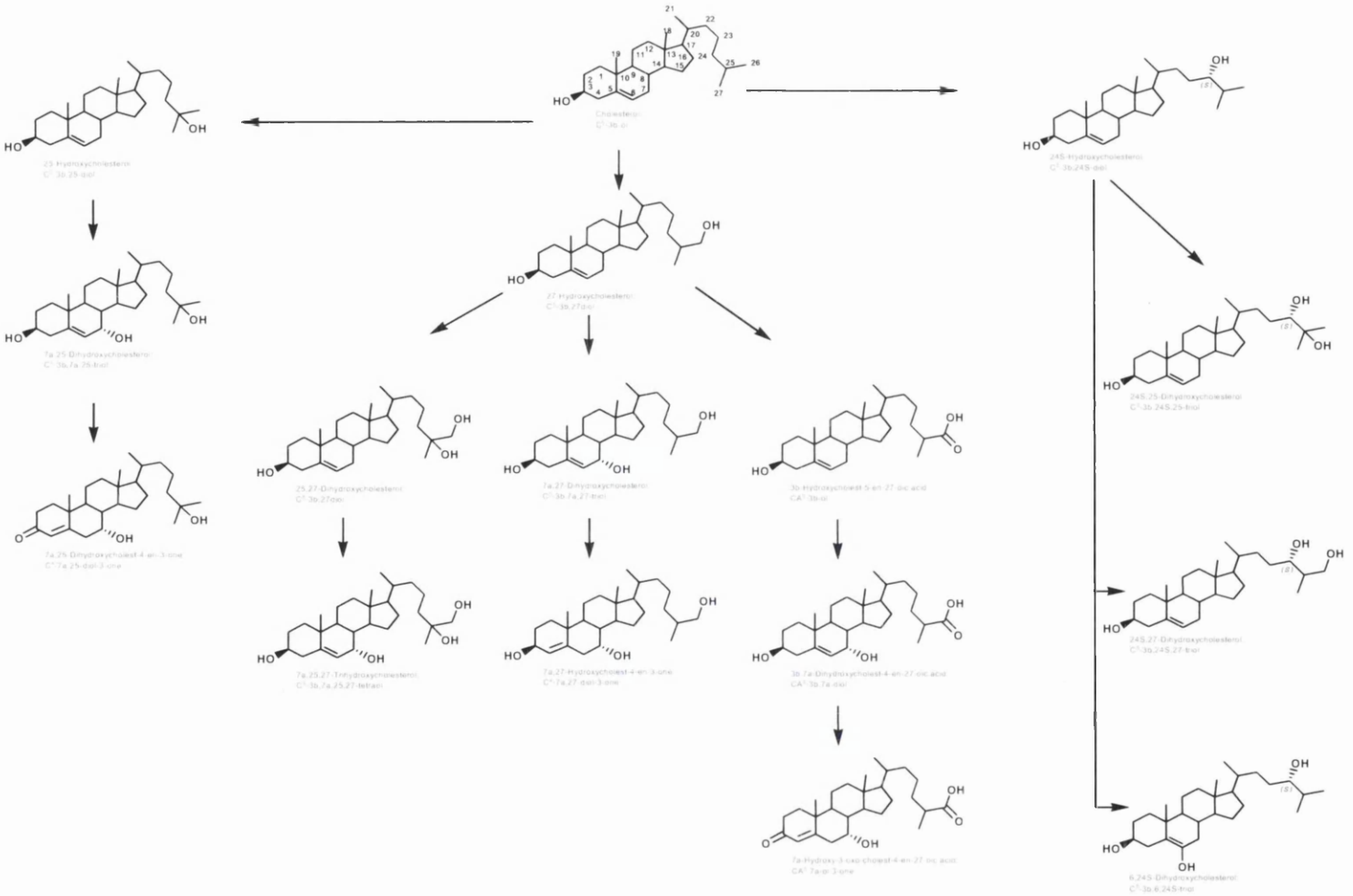

Figure 1.5 Oxysterols identified in human and rat brain – continued.

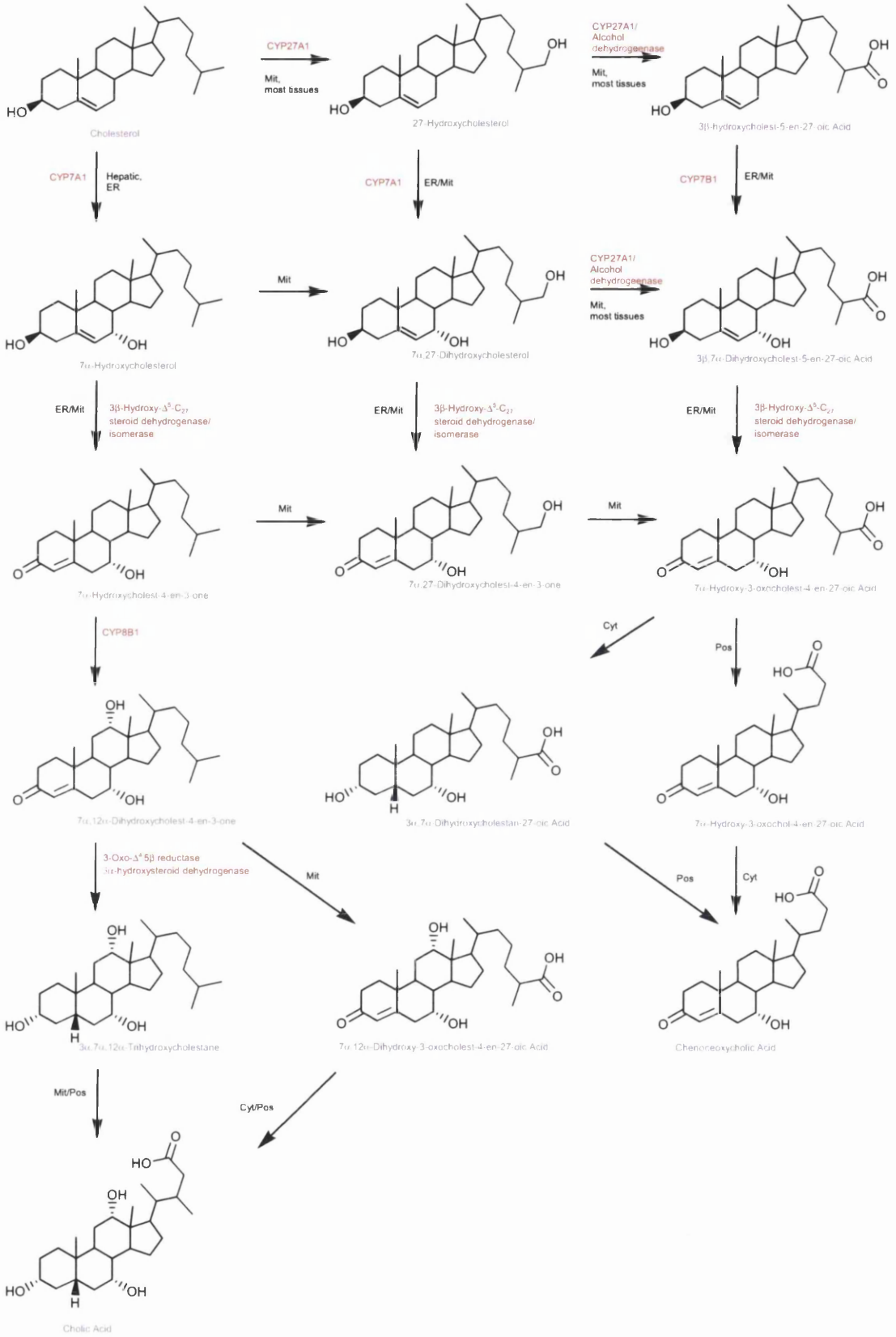

Figure 1.6 Simplified bile acid biosynthesis pathways in man. Endoplasmatic reticuclum (ER),Mitochondria (Mit), Peroxisome (Pos), Cytosol (Cyt). Reproduced from ref. [22].

and spastic paraplegia [23-25]. The schematic view presenting bile acid biosynthesis pathways is shown in Figure 1.6.

CYP11A1 resides in mitochondria and is expressed mainly in steroidogenic tissues, where it catalyzes the conversion of cholesterol to pregnenolone. This is obtained by double hydroxylation at positions C20 and C22, followed by a cleavage of the side chain.

CYP46A1 is detected specifically in nervous tissue where is found in microsomes. This monoxygenase converts cholesterol to 24*S*-hydroxycholesterol, and to much lesser degree 27- and 25-hydroxycholesterol. Cyp3a4, similarly to CYP7A1, is expressed in hepatic microsomes, and converts cholesterol to 4β-hydroxylation and, to in minor degree, 25-hydroxycholesterol.

Some cytochrome CYP450 based cholesterol/oxysterol hydroxylases can target other compounds apart from cholesterol, CYP3A provides 4β- and 25-hydroxylation of cholesterol [26] and 6β-hydroxylation of testosterone [27]. On the contrary, the catalytic activity of other enzymes such as CYP11A1 is limited to cholesterol as the substrate [28]. Moreover, the products generated by these enzymes, are rarely limited to one oxysterol, as an example is a CYP46A1 hydroxylating 27-, 25- and 24S-positions of cholesterol [29, 30].

1.3 Oxysterols as pleiotropic modulators of cell physiology

Initially oxysterols were recognised for their role in cholesterol homeostasis [31], however more recent studies show that their control reaches far beyond sterol synthesis [32]. Oxygenated derivatives of cholesterol exert a wide range of functions affecting cell survival and apoptosis [33-37] viability of cancer cells [38, 39] embryogenesis [40] and immune response [41] (more details in chapter 1.5 Roles of oxysterols in immunity).

The hypothesis of oxysterols acting as suppressors of cholesterol biosynthesis was proposed by Kandutch [42] in the 1970's. According to this, oxysterols, rather than abundant cholesterol, modulate the mevalonate pathway via negative feed back loop. Later findings confirmed that oxysterols are acute governors of cholesterol production and furthermore, disposal. This control is executed either on the enzymatic level by accelerating the degradation of a mevalonate pathway enzyme

HMG-CoA reductase or on a transcriptional level by altering the expression of genes involved in catabolism and anabolism of cholesterol.

Oxysterols were proven to accelerate an ubiquitin-dependant degradation of HMG-CoA reductase, which is the rate-limiting enzyme required for synthesis of cholesterol. A number of oxysterols can increase the rate of ubiquitination of the reductase, which leads to quicker proteolysis of the protein [43].

In addition to removal of the biosynthetic enzyme, oxysterols alter the level of cholesterol by controlling the expression of genes involved in sterol biosynthesis/metabolism. In the mevalonate pathway the expression of a number of enzymes is suppressed by increased concentration of oxysterols, the down regulated enzymes include squalene synthase, HMG-CoA synthase, and as mentioned before HMG-CoA reductase [44].

The control over expression of genes can be mediated by transcription factors that respond to changing levels of sterols in the environment such as Liver X Receptors (LXRs) and Sterol Regulatory Element Binding Protein (SREBP).

While SREBP induces cholesterol production and uptake, LXR is responsible for its increased disposal from the cell. Further studies on these two transcription factors proved that cross talk between SREBP and LXR affects a wide range of cell functions not only directly related to lipid homeostasis [45].

LXRα and β belong to the class of nuclear receptors, which after heterodimerisation with the Retinoid X Receptor (RXR) act as transcription factors regulating expression of genes. LXRα is mainly expressed in adipose tissue, the liver and the intestine and controls cholesterol homeostasis. LXRβ is ubiquitously expressed across the body and is important in functioning of brain [46] and the immune system [47]. Natural ligands for LXR are oxysterols such as 22R-, 25-, 27-, 24S-hydroxycholesterol, 24S,25-epoxycholesterol and the cholesterol precursor - desmosterol. Recent study also showed that LXR can be induced by 25- and 26-hydroxy-7-dehydrocholesterol, which are metabolites of 7-dehydrocholesterol generated by CYP27A1 [48].

Upon activation, LXR-RXR heterodimers binds to the LXR-response element of the regulated genes, which can result in either stimulation and inhibition of transcription. Non-active dimers binds to complexes containing corepressors and in this form LXR can suppress the expression of genes.

LXRs up-regulates genes involved in cholesterol homeostasis such as Cyp7a1 (in mouse) catalyse hydroxylation of cholesterol [49], ABCA1 and ABCD1 responsible for removal of cholesterol from the cells [50, 51] and Apolipoprotein E which mediates cholesterol transport [52]. LXR is also a main governor of expression of Niemann-Pick type C1 protein, which is involved in intracellular cholesterol trafficking [53].

In brain LXR ligands stimulate neurogenesis of murine midbrain as well as development of dopaminergic neurons [46]. This finding is of special importance as loss of dopaminergic neurons is the characteristic feature of Parkinson's disease [54]. LXR is involved in alleviation of inflammatory response by promoting expression of genes expressing anti-inflammatory proteins TYRO-3, AXL and MER [36, 55] or polyunsaturated fatty acids [56, 57]. In macrophages LXR activated by desmosterol suppresses the inflammatory response provoked by Toll Like Receptors (TLR) activation [35, 58]. LXR ligands are also reported to alleviate symptoms of neurodegenerative diseases such as Alzheimer's disease and Parkinson's disease in murine models. Inflammatory processes are believed to contribute to the etiology of these disorders [59, 60].

As opposed to LXRs, low concentration of cholesterol "activate" SREBP. The inactive form of SREBP is coupled to the escort protein SCAP which interacts with an ER protein anchored to membrane – Insig [61].

SREBPs are present in three main isoforms *SREBP1a, SREBP1c and SREBP2*. SREBP1s primarily control lipogenesis with SREBP1a highly expressed in immune cells and SREBP1c is abundant in various organs, especially liver and adipose [61, 62]. SREBP2 is responsible for biosynthesis and uptake of cholesterol [35, 56, 63].

SREBP binds to SCAP which responds to the changes in cholesterol concentration. SCAP contains a sterol-sensing domain, which is activated by cholesterol, but not by side-chain hydroxylated oxysterols such as 25-hydroxycholesterol [64]. Interestingly, similar domains were also identified in HMG-CoA reductase, Patched and Nieman-Pick C1 protein which are believed to interact with sterols [65]. At high concentration of cellular cholesterol, cholesterol binds to SCAP which, in turn, changes its conformation in order to bind to the ER resident protein Insig [66]. When cholesterol is scarce SCAP can detach from Insig and the

SCAP-SREBP complex can be transported to Golgi where SREBP is transformed to its active form.

Insig is expressed in two isoforms INSIG1 and INSIG2, which directly retain the complex with SREBP and SCAP by the ER membrane [35, 67]. INSIG, unlike SCAP, can bind oxysterols possessing a hydroxyl group in the side-chain, such as 24S-, 25- or 27-hydroxycholesterol. Binding of oxysterols by Insig augments binding with SCAP, as well as decreases the rate of Insig degradation [68].

The HMG-CoA reductase gene is a target for SREBP regulation, as the key enzyme in the mevalonate pathway and is subjected to control from both cholesterol and oxysterol levels. SREBP also stimulates expression of the LDL receptor, which uptakes cholesterol-lipoprotein complexes leading its to decreased concentration in the circulation[69].

As mentioned before SREBP is not the only protein which respond to cellular cholesterol. NPC1 protein contains a sterol-sensing domain highly homologous to SREBP. Mutations in NPC1 gene are found in patient suffering from Niemann-Pick type C1 disease. This is a neurovisceral disorder characterised by an accumulation of lipids, which in brain leads to neurodegeneration. NPC1 protein binds cholesterol by binding its 3β-hydroxyl group together with the cyclic core inside a structural pocket [70]. NCP1 participates in transport of cholesterol from late endosome/lyzosomes to the endoplasmatic reticulum, where it can be estrified, or transferred across the membrane to the extracellular matrix [71]. Defect in NPC1 causes malfunction of SREBP and LXR action, what leads to an accumulation of intracellular cholesterol. In macrophages these disturbance of the sterol homeostasis contributes to development of atherosclerosis [72].

Patch (PTCH1), protein implicated in embryonic morphogenesis and suppression of carcinogenesis, also capable to bind cholesterol, however the binding domain differs from that of SREBP and NPC1. PTCH1 belongs to Hedgehog signalling pathway. Disruptions in this pathway during embryogenesis result in teratogenic malformation of the foetus, such as holoprosencephaly [73], while malfunction in an adulthood leads to development of cancer [74]. PTCH1 is a membrane receptor which upon binding cholesterol activates next protein - Smoothened (Smo) [75]. Activated Smo triggers a cascade of reactions which alter expression of transcription factors, such as glioma-related oncogenes. This leads to

activation or suppression of the target genes including the ones belonging to Hedgehog pathway, thus creating negative and positive feedback control [76, 77]. What is interesting, not only cholesterol affects Hedgehog pathway, oxysterols were also characterised as potent ligands for Smo protein [74, 78, 79].

As exemplified by Niemann-Pick type C1 protein and Sonic Hedgehog pathway, sterols can exert function of secondary messengers in signal transduction cascades, finely tuning wide range of processes. However, this dependencies are still not fully understood and require further study to in order to evaluate their possible therapeutic importance.

1.4 Cholesterol and oxysterols in the brain

Brain is the most cholesterol-rich organ, and contains 2-3% of the total body weight. In an adult, healthy animal blood brain barrier (BBB) is impermeable for cholesterol therefore its entire pool is synthesised *in situ*. Peripherally generated cholesterol can be used by central nervous system during embryogenesis and in newly born animals before the full formation of BBB. In adult mammals BBB can be compromised in a pathological states such as multiple sclerosis [80], epilepsy [81], Alzheimer Disease [82], meningitis [83] or infection with parasite Trypanosoma [84].

In a normal physiological state of an adult mammalian brain entire cholesterol is created in an autonomic mevalonate. BBB is formed by tight junctions of endothelial cells of the capillary vessels surrounding the CNS which impede diffusion of cholesterol [85]. As opposed to that, more hydrophilic forms of cholesterol - oxysterols can freely migrate through the barrier, therefore hydroxylation of cholesterol can be used as an exit route for brain-generated sterols. In addition to that, it was showed that some steroids of plant origin such as sitosterol and campesterol can be accumulated in the brain, which suggests some sort of flux mechanism of these sterols [86, 87].

Cholesterol is present predominantly in unesterified form in CNS; only in young animals small quantities of cholesteryl and desmosterol esters were detected [88]. The increased amount of esterified cholesterol is associated with neurodegenerative disorders such as multiple sclerosis [89].

Cholesterol in the brain tissue is generally divided into two polls: metabolically inactive which is "locked" inside myelin sheets and metabolically

accessible cholesterol present in cellular membranes of neurons and astrocytes. Myelination of neuronal axons by oligodendrocytes is carried out from later stages of embryonic development, accelerates in postnatal period and lasts until adolescence [90-95]. In adult rodent brain cholesterol confined to myelin sheets accounts for 70% of the total pool. The highest rate of cholesterol synthesis occurs during intense myelination, which in mice occurs at the 3 weeks age [94], and decreases in elder animals. Cholesterol in human brain is characterised by an unusually long half-life time, [88, 96-99], which reflect its relatively inert position within myelin envelope.

The remaining 30% of cholesterol is metabolically active and present in various aspects of brain development. It appears that formations of synapses depends on the supply of cholesterol not only provided by neurons but also additionally biosynthesised by glia [100-102].

Cholesterol can not leave the brain through BBB *per se*, however its 24S-hydroxylated analogue can freely cross the barrier and by peripheral circulation be transported to the liver. Further metabolism is initiated by hydroxylation at 7α position catalysed by microsomal, hepatical enzyme Cyp39A1 [103], in subsequent steps 7α,24S-dihydroxycholesterol is transformed into bile acids.

24S-Hydroxylation is the main exit route for cholesterol, however hydroxylations at C25 and C27 are also present in brain but to much lesser degree [104]. It is estimated that around 60% of cholesterol efflux from CNS is performed via 24S-hydroxylation [105]. This transformation is provided by brain-specific, ER enzyme Cyp46a1, which is expressed in neurones, however its expression in the whole brain vary between anatomical regions [47, 49]. The deletion of this gene surprisingly does not cause the increase in the level of cholesterol, but instead it reduces the rate of its synthesis [106].

Although the majority of 24S-hydroxycholesterol is metabolised exogenously, 25-hydroxylation of this oxysterol was reported in cultured astrocytes yielding 24S,25-dihydroxycholesterol. Also 27-hydroxycholesterol was metabolised in the same manner by astrocytes [56]. For some of these transformation can be responsible Cyp46a1 which was reported to have 25- or 27-hydroxylase activity towards 24S-hydroxycholesterol. The generation of 24S,25-dihydroxycholesterol and 24S,27-dihydroxycholesterol by CYP46A1 was shown in *CYP46A1* transfected HEK cells and in vitro by an isolated enzyme [107].

Furthermore, 7α-hydroxylation activity was detected in brain derived microsomes for 25- and 27-hydroxycholesterol, but not 24S-hydroxycholesterol. The 7α-hydroxylation was followed by conversion of 3β-hydroxo-5-ene group into 3-oxo-4-ene conformation [108].

27-hydroxycholesterol is produced by ubiquitously expressed enzyme Cyp27a1, which was found also in neurons and glia [19]. The defection of CYP27A1 is associated with a metabolic disorder with neurological impairment Cerebrotendinous Xanthomatosis [21]. 27-Hydroxycholesterol is also LXR ligand, although less potent than 24S-hydroxycholesterol [109].

Recently, also another side chain-oxidised sterol: 25-hydroxycholesterol has been demonstrated to be produced by brain cells astrocytes [110]. This oxysterol is produced as a part of humoral response to pathogens, its role in the brain remains unknown.

Brain is an endocrine organ involved in production of steroid hormones such as pregnenolone. The biosynthesis of this involves 20S- and 22R-hydroxylation of cholesterol followed by a cleavage of the side chain. 20S-hydroxycholesterol was detected in rat brain [111] while 22R-hydroxycholesterol was found in human CNS. Pregnenolone is synthesised from cholesterol by mitochondrial enzyme CYP11A1, also known as P450scc (Cytochrome P450 side chain cleavage) which is expressed in rodent brain [112-114].

24S,25-Epoxycholesterol, as opposed to other oxysterols, does not originate from the modification of cholesterol, but is produced in a shunt of a mevalonate pathway leading to synthesis of cholesterol. Synthesis of 24,25EC is from the activity of the 2,3-oxidosqualene cyclase (OSC) [115-117]. OSC catalysis the transformation of 2,3(*S*)-monooxidosqualene (MOS) to lanosterol or the 24,25EC precursor 2,3(*S*):22(*S*),23-dioxidosqualene (DOS) to 24(*S*),25-epoxylanosterol. This is followed by conversion of lanosterol and 24(*S*),25-epoxylanosterol into cholesterol and 24,25EC, respectively.

Under physiological conditions the synthesis of cholesterol dominates [118]. The presence of 24S,25-Epoxycholesterol was shown in developing and new born brain, which is not surprising, considering high rate of cholesterol synthesis in this organ [119, 120]. Recently, this oxysterol was shown to promote neurogenesis via LXR in foetal murine brain [121]. 24S,25-Epoxycholesterol is synthesised by various

cells in vitro including, neuronal cell line SN4741 (AM unpublished observations), ovarian cells [68] and fibroblasts (AM unpublished observations). 24S,25-Epoxycholesterol is a potent ligand of LXR [109] and SREBP inhibitor, which enables this oxysterol to participate in the control of cholesterol biosynthesis. As this oxysterol is synthesised in parallel to cholesterol it can serve as an early warning signal against its over-production [122].

In work of Mcdonald and colleagues [123] were also identified ring-hydroxylated derivatives such as 4β-hydroxycholesterol and 5,6-epoxycholesterol. In humans 4β-hydroxycholesterol is biosynthesised by 4β-hydroxylation of cholesterol catalysed by ER enzyme CYP3A4 [124], predominantly expressed in the liver and, to much lesser degree, in the brain [125]. 5β,6β-Epoxycholesterol is considered as a product of cholesterol autooxidation and lipid peroxidation [126] showing cytotoxic properties in *in vitro* systems [127, 128].

1.5 Roles of oxysterols in immunity

The first evidences that alteration of lipid metabolism can be a part of the immune system emerged relatively recently when in 2009 Diczfalusky and colleagues reported upregulated production of 25-hydroxycholesterol by macrophages treated with LPS and type I and II interferons *in vitro*. Moreover, increased levels of 25-hydroxycholesterol were also detected in blood of mice and volunteers who were administered LPS intravenously [129]. Since then the cross talk between immune response and sterol metabolism has been a subject of intense research. Sterols and cholesterol intermediates play a role in both innate [130, 131] and adaptive immunity [130, 132], they are involved in the antiviral response [133], differentiation of lymphocytes [134] and immunoglobulin production [130].

Treatment of macrophages with interferon γ or murine cytomegalovirus (MCMV) activates cholesterol 25-hydroxylase, the activation is mediated by signalling the protein Stat1 [135]. Interferon γ, by binding to IFN γ receptor activates Stat1 protein, which binds to the promoter of cholesterol 25-hydroxylase, enhancing its expression. Also incubation of macrophages with virus increased expression of cholesterol 25-hydroxylase. Macrophages infected with virus alter their lipid metabolism by suppression of the mevalonate pathway [133], therefore it is feasible,

that increased concentration of 25-hydroxycholesterol can inhibit cholesterol synthesis via SREBP.

Moreover, 25-hydroxycholesterol produced as a part of the antiviral response has antiviral properties. In vitro it inhibits the internalisation of a broad number of coated viral species into the host cell [136], by altering the cellular membrane. Increased concentration of 25-hydroxycholesterol prevents viral-cellular membrane fusion which is required for virus entry. The antiviral properties were shown for pathogens responsible for chronic infections such as human immunodeficiency virus, vesicular stomatitis virus, herpes simplex virus 1 and murine gammaherpex virus [136], as well as for acutely infectious species such as Ebola virus, Nipah virus, Russian Spring-Summer Encephalitis and Rift Valley fever virus.

The antiviral activity of 25-hydroxycholesterol was also assessed in vivo. Humanised mice which received injection with 25-hydroxycholesterol prior to HIV infection had 80% less HIV mRNA than controls. Furthermore, mice with a knockout of cholesterol 25-hydroxylase were more susceptible for murine gammaherpex virus infection.

The mechanisms of antiviral properties may involve alteration of membrane properties as well as the inhibition of geranylgeranylation of protein, however they were not fully elucidated [133].

25-Hydroxycholesterol can be further hydroxylated by the action of CYP7B1 yielding 7α,25-dihydroxycholesterol, which was found to be a chemotropic agent recognised by the receptor EBI2 in B cells [132, 137]. B cells belong to lymphocytes and are involved in humoral adaptive immunity. The pivotal function of B cells is production of antibodies in response to pathogenic antigens. B cells also present antigens to other cells involved in humoral response, furthermore they can become memory B cells important in response to repeated exposure to the antigen. In mammals B cells are produced in bone marrow but maturation and differentiation is performed in secondary lymphoid tissues such as spleen.

Differentiating B cells migrate within this tissue directed by the gradient of 7α,25-dihydroxycholesterol sensed by the G-protein coupled receptor EBI2. Migration of B cells from and to follicular areas of the spleen is essential for specialisation of these cells into the one recognising antibodies presented by T-cells [138].

7α,25-Dihydroxycholesterol is further metabolised by 3β-HSD into 7α,25-dihydroxycholest-4-ene-3-one, which is lacking the biological activity of its hydrogenated analogue.

CH25H and CYP7B1 are expressed in lymphoid stromal cells, while in dendritic cells the expression of CH25H is inhibited [139].

The second main class of lymphocytes are T cells which, as opposed to B-cells, are involved in the cellular part of the immune response. Liver X Receptor activation inhibits differentiation of T cells into Th17 subpopulations, this suppression of T cell transition is linked to mitigation of inflammatory symptoms of encephalomyelitis [140].

1.6 Metabolomics of sterols

Metabolomics is an emerging branch of "omic" studies concentrating on the analysis of small molecule metabolites present in biological matrices. Unlike genomics, transcriptomics or proteomics, metabolomics focuses on final products of cellular biochemistry. Genomics analyses structure and function of the genome of an organism (genomics), however, genes are transcribed under tight control and the entire genome is not actively transcribed. Transcriptomics concentrates on mRNA transcripts, though under posttranscriptional control these may not be translated into active proteins. Proteomics measures the levels of proteins expressed by the organism [141] including the proteins that are in a metabolically inert form. As the activity of proteins can be inhibited by the environment, their presence may not translate into production of a final metabolite. Hence metabolomics is an ultimate tool in assessing a current biological condition of the organism.

Metabolomics is the analyses of small molecules (molecular weight <1,000 Da) which can be either products of cellular anabolism or catabolism. Molecules that are generated in non-enzymatic processes such as autoxidation can also contribute to the metabolome. This generates a great number of structurally and functionally diverse compounds. Such a quantity of potential analytes can be embraced with two approaches, i.e. global or targeted metabolomics [142].

The global methodology applies when the analytes of interest are not well characterised, and the aim is to qualify and quantify the highest possible number of compounds. This methodology can be used for an analysis of sample derived from a

patient suffering from unknown disease when the obtained data is compared to data from healthy individual in order to characterise metabolites unique for the disorder.

The targeted approach (metabolite profiling) is used when analysed molecules are defined to some extent prior to experiment, thus enabling optimisation of the analytical methodology for the detection of compounds of interest. This methodology was adopted by research bodies such as Lipid Metabolites and Pathways Strategies (LIPID MAPS) in USA, and The European Lipidomics Initiative and European Network for Oxysterol Research.

Although the class of analytes is defined, the actual analysis provides two main challenges. Firstly, the compounds can be present at very different levels making the detection of low-abundance molecules difficult, and secondly, structural similarity of compounds may make them difficult to separate.

These challenges can be addressed by using multiple separation methods during sample preparation/analysis and employing a detector capable of identifying closely related molecules. This can be achieved by using a solid phase extraction (SPE) technique followed by liquid chromatography (LC) coupled to a mass spectrometry (MS) detector. While SPE and LC will provide the separation based on polarity of analytes, MS will separate them further according to their mass to charge ratio (m/z).

Mass spectrometry provides a sensitive and specific analysis of molecules, hence its popularity in metabolite profiling studies. The principle of mass spectrometry is separation of ionised molecules in electric or magnetic field according to their mass to charge ratio. Furthermore, ions can be fragmented which provides additional information regarding structure. These features allow measurement of known analytes as well as putatively identify the structures of novel compounds. A schematic diagram of the methodology used in the analysis of oxysterols is presented in Figure 1.7.

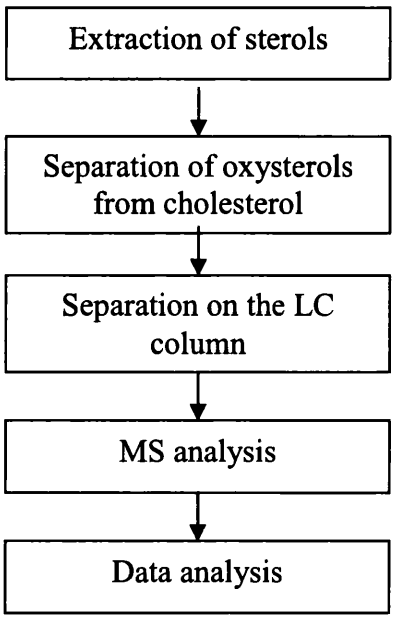

Figure 1.7 Schematic sequence of events for the analysis of oxysterols extracted from biological material

1.7 Extraction of sterols from biological matrices

The biochemical composition of cells, tissues and other biological matrices is extremely complex. This means that the compounds of interest are surrounded by a high number of other compounds, which may interfere with analysis. To reduce the impact of the matrix, the chosen technique should favour the predetermined analytes such as sterols. The ultimate extraction method provides a high yield of analyte while simultaneously reducing the amount of other, unwanted substances.

The performance of the extraction can be assessed by the addition of an internal standard. This should be done at the start of the extraction protocol, so the potential loss of standard during the procedure mirrors the loss of the target lipids.

The most common extraction method for lipids is a liquid extraction with organic solvents. During the extraction only the analytes which are soluble can be transferred to the solvent; non soluble substances, such as proteins, carbohydrates will precipitate. The efficiency of extraction depends on polarity of solvents compared against the polarity of analytes, therefore the selection of solvents affects the type of

isolated lipids, for example cholesteryl esters will be extracted with high efficiency by hexane, while non esterified cholesterol can be isolated by ethanol.

Two most traditionally used methods for lipid extraction are Folch [143] and Bligh-Dyer [144] methods. Folch protocol was originally developed for the isolation of brain lipids. According to this procedure tissue is homogenised with mixture of chloroform and methanol (2:1;v/v), then water or saline is added. The final volumetric ratio of chloroform, methanol and water (saline) is 8:4:3. The solvents then separate into two layers: lower, containing mainly chloroform and methanol and upper – predominantly aqueous. Lipids are present in chloroform rich-phase while water-soluble contaminants are transferred into water-rich solution. Bligh and Dyer modified the previous method to accommodate for an extraction of tissues containing higher proportion of water. McDonald has optimised the method for an extraction of oxysterols, by replacing methanol with ethanol [123]. In this method tissue is initially homogenised in ethanol, with subsequent addition of chloroform and saline solution. Also pure ethanol was used as solvent for extraction of hepatic lipids with satisfactory results [145]. An ultimate method for lipid extraction has not been developed, the efficiency of each method depends on the nature of lipids as well as the nature of used tissues accounting for varied results produced by different laboratories.

1.8 SPE for fractionation and enrichment of lipids

Solid phase extraction (SPE) is a technique used for the separation, purification and enrichment of compounds present in analysed material. In regards to oxysterols, there is a requirement to separate these from much more abundant lipids. Lipid extract contains mainly phospholipids, triacylglycerols, esters of cholesterol and cholesterol. Presence of these molecules in the solution would have detrimental effect on further analytical processing, for instance lipids present at high concentrations are prone to precipitation in more aqueous solutions.

In the SPE technique the mixture of analytes is passed through solid, porous material (stationary phase), aided by the flow of a solvent (mobile phase). Depending on the affinity of the analyte to the mobile and solid phases the analyte can be either flushed out by the mobile phase or retained by the solid phase. In general, classification of SPE is based on the type of affinity used; it can be polarity of

molecules (reverse and normal phase SPE) or ionic interactions (cation and anion exchange SPE).

Ion exchange SPE is rarely used in lipidomics as many lipids are electrically neutral. The most commonly used SPE is a reversed phase. In this type of SPE, the stationary phase is made of non-polar material which interacts with lipids while the mobile phase consists of polar solvents. For this type of SPE van der Waals forces provide weak, reversible binding of analyte to stationary phase. The stationary phase material is usually silica with attached hydrophobic hydrocarbon chains (ODS or 18) with a high affinity to hydrophobic analytes, the stationary phase is packed inside a cartridge. The retention of the compound is determined by its polarity, the non-polar stationary phase will interact stronger with non-polar analytes, while more polar molecules will be eluted. A gradient of mobile phases of decreasing polarity will gradually elute less polar compounds. This allows for subsequent isolation of separate classes of lipids [146].

The flow of the mobile phase can be aided either by applying a positive pressure to the top of the cartridge or by applying the negative pressure at the bottom. To improve efficiency of the work flow, SPE cartridges can be mounted on a manifold providing a negative pressure to the cartridges via vacuum manifold.

Reversed phase SPE is widely used for isolation of oxysterols. Oxysterols are present at levels three orders of magnitude lower than cholesterol, therefore simultaneous detection of these compounds is difficult due to the limited dynamic range of instruments. Cholesterol is also susceptible to autoxidation and oxysterols generated in this process would interfere with endogenous compounds. Oxysterols are more polar than cholesterol therefore are easier to elute with polar solvent than cholesterol which requires a more non-polar mobile phase.

In our methodology sterols in solid tissues are extracted by ethanol, which is subsequently diluted to 70% ethanol with water. Media retained after cell culture is added to ethanol to form a 70% solution. This is applied onto a reversed phase SPE cartridge. More polar oxysterols are eluted from the column while cholesterol and more hydrophobic compounds such as cholesteryl esters and triacylglicerydes are bound to the stationery phase. Cholesterol can be eluted from the column by ethanol. This method was used for extraction of oxysterols from plasma [147] and brain [148].

For the separation of mixtures containing high concentration of compounds of varied polarity "recycling" SPE can be used. In this method the mixture of analytes is

initially dissolved in high organic content solvent. This is passed through the SPE column, allowing non-polar compounds to be retained by the column. The resulting effluent is diluted with polar solvent, such as water and re-applied onto the SPE column, in this cycle more polar compounds will be bound by the solid phase. In following cycles the polarity of the eluent is increased, allowing more polar compounds to be captured by the solid phase. The step-wise increase in the polarity of solution is required for retaining molecules of diverse polarity, as the dilution of the solvent at the initial stage with water would cause non-polar analytes to precipitate. The original method was described by Liere and colleagues [149] for the separation of brain steroids. Griffiths has adapted this system for the analysis of oxysterols.

1.9 Mass spectrometry

The analysis of the lipidome presents distinct challenges; the analytes are often present at a trace-level, furthermore the compounds may be structurally closely related which complicates identification. For these reasons, mass spectrometry, with high sensitivity and specificity, is a commonly chosen tool in the study of lipids.

In general, the mass spectrometer can be divided into following parts: (1) an inlet, releasing the sample, (2) a source, where the analyte is ionised, (3) a mass analyser, that provides the means to discriminate the molecules according to their m/z ratio, (4) a detector that detects separated ions and (5) a data collection and analysis systems which facilitates further processing of obtained information. A diagram of the mass spectrometer used in this work is presented in Figure 1.10.

1.9.1 Inlet

The sample is injected into an ion source from an inlet. This device can be as simple as a syringe containing a mixture of analytes, when all compounds are introduced to the ion source simultaneously; this approach is commonly used in shot-gun metabolomics. Alternatively the syringe may contain material separated prior to injection, for example with SPE techniques.

More commonly analytes are separated before applying them into the source either by High Pressure Liquid Chromatography (HPLC) or Gas Chromatography (GC) systems, which provide separation of compounds in a real time, just before entering the mass spectrometer.

1.9.2 Ion sources

Ionisation of the sample can be achieved in a number of ways, where charge is transferred onto electrically neutral molecules. Most ionisation techniques for GC-MS are based on the formation of a molecular cation caused the loss of an electron from an exited molecule, however charge can be also acquired by a chemical reaction with an ion that is already electrically charged.

The choice of ionisation technique must consider the physical state of the analysed material and its chemical stability. With liquid samples, the fluid is electrically charged and ions sprayed into the source. This mechanism is exploited in electrospray ionisation. Solid samples can be ionised by matrix-assisted laser desorption/ionisation where the matrix provides a support for the sample, and is bombarded with a light beam able to ionised molecules. Some ionisation techniques are gently producing only a molecular or pseudomolecular ions, others, cause generation of fragment ions. The profile of these fragments can provide additional information regarding the structure of the original molecule [146].

The electrospray ionisation (ESI) technique is commonly used in metabolomics studies and was also used in our work. The electrospray is generated when the liquid is passed through a metal capillary in a strong electric field. The ESI source contains the spray capillary, which serves as one electrode. A counter electrode (sample orifice) is separated from the capillary by 0.3-1 cm. The liquid containing the analyte is passed through the metal capillary and sprayed into the space between the capillary and the orifice. Charged droplets are generated and as they travel in the electric field they loose solvent resulting in a spray of ions of analytes (

Figure 1.8 and Figure 1.9).

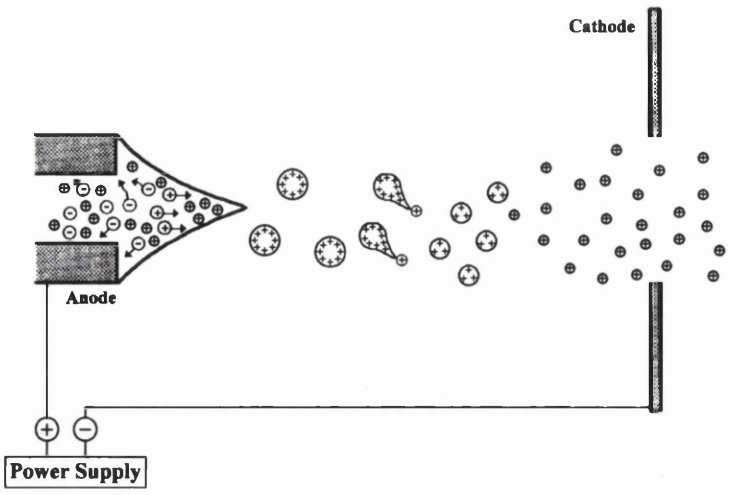

Figure 1.8 Schematic figure of ESI process. A positive potential is applied to the capillary, which becomes an anode. An electric potential of the anode forces positively charged ions to the surface of the meniscus. Upon the destabilisation of the meniscus are released positively charged droplets which are transformed into ions. Reproduced from ref. [22].

The liquid used for delivery of the sample to the electrospray capillary is usually an aqueous mixture of volatile solvents. To increase conductivity of an otherwise electrically neutral mixture, formic acid is often added. The presence of organic solvents aids evaporation, which may be assisted by a nebulising gas, often applied to the electrospray capillary. A stream of gas can be also used to direct the spray into the orifice. The nebulising gases is usually an inert gas, for example nitrogen.

Electrospray is generated when a potential difference is applied between the two electrodes. The optimum voltage is determined by the geometry of the source, dimensions and position of the sprayer, sample flow rate and composition of the solvent. Positive potential on the capillary will force anions to deposit on the walls of the tube, while cations are ejected with the solvents. When the repulsion forces between ions on the liquid surface are stronger than the surface tension, the surface of the liquid changes its properties allowing for formation of the Taylor cone. With sufficiently high electric field the Taylor cone forms a jet which is later dispersed into the spray. Rayleigh limit defines the amount of charge that liquid can accumulate before forming the Taylor cone. Ejected droplets travel in the direction of the counter electrode gradually loosing the solvents. The charge density on the surface of the droplets increases and, upon reaching the Rayleigh limit, the droplet decomposes generating a jet of small droplets.

A

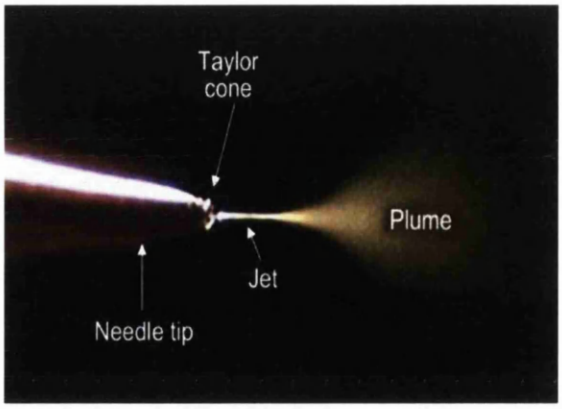

B

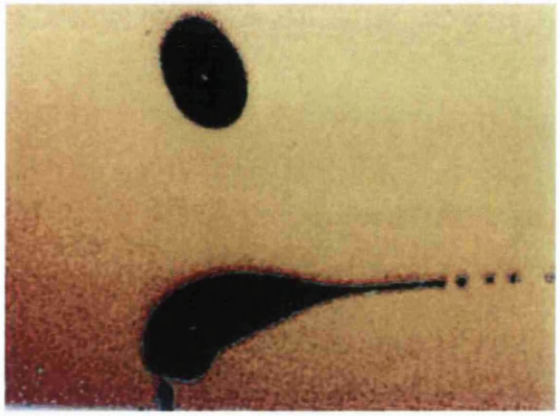

Figure 1.9 The image of ESI process acquired by a high-powered microscope. In panel A is shown the spray generated from a needle tip. Electric potential applied to the needle forces the liquid to become charged and to form a structure known as a Taylor cone. Panel B presents a droplet released form the capillary. Upon loosing the solvent the density of the charge contained by the droplet increases, this leads to the formation of smaller droplets and gas-phase ions. Reproduced from ref. [22].

The "daughter" droplets continue to travel, and to facilitate the loss of the solvent at this stage the spray can be passed through heated capillary e.g. on instruments manufactured by Thermo Scientific, or through a number of skimmers e.g. on instruments from Waters. As the droplets further shrink, ionised molecules are desorbed form the surface and continue to travel to the mass analyser.

1.9.3 Mass analysers

Ionised molecules are transferred into the mass analyzer, where they are separated according to their mass to charge ratio. This can be achieved either in a magnetic or in electric field, or in a combination of both. Mass analysers can be also characterised by the duration of segregation, where either a continuous stream of ions

is analysed (scanning analysers) or, alternatively, a portion of ions is released and the analysis is performed in pulsed-like mechanism (trap analysers).

In magnetic analysers ions travelling from the source are subjected to magnetic field, which alters the trajectory of ions accordingly to their momentum, which in turn is a consequence of their m/z ratios. Only ions of predefined m/z values will be passed through an exit slit and reach the detector. The magnetic field is scanned to generate a mass spectrum.

Quadrupole analyzers consists of four parallel rods. The rods generate an oscillating electric field by altering their Radio Frequency (RF) and Direct Current (DC) voltages. These voltages are arranged so that only selected ions can pass through this system, while other particles will collide on the quadrupole. The voltages are scanned to generate a mass spectrum.

Time of Flight (TOF) analysers measure the time required for ions to pass through a drift tube. In order to precisely measure the time ions spend flying in the tube, they need to be released simultaneously at a precise time point. This require either the source to produce the ions in a pulsating manner or ions generated continuously are gated and released in intervals.

The last group of instruments is based on the ion trap principles: ions are confined in the trap where the manipulation of RF and DC potentials allows for a precise separation of particles. Commonly used traps include: quadrupole ion trap, ion cyclotron resonance and, the most recently developed, Orbitrap.

The above mentioned analysers can be used either as a stand-alone instruments or can be interfaced to form hybrid machines. One of the coupled analyzers is Linear ion Trap-Orbitrap (LTQ-Orbitrap) which was used in this work.

LTQ-Orbitrap

The general principles of LTQ-Orbitrap operations are as follow: (1) ions from the source are loaded into the linear ion trap, (2) the linear ion trap axially injects the ions into the C-trap, (3) the C-trap focuses the ions, and a smaller cloud, of ions are (4) injected into the Orbitrap, where (5) axial oscillations of ions in an electric field allows for separation. Schematic representation is shown in Figure 1.9.

The ions from the source are focused into a precise stream which flows into the ion trap. In an older model, the LTQ-Orbitrap XL, ions are directed by a tube lens/skimmer. In a newer version, LTQ-Orbitrap Velos, this was substituted with S-lenses. The S-Lens consists of a stack of metal ring plates (apertures) under RF

frequency. Changing electric field applied to the apertures controls the movement of ions so the molecules are focused into a precise stream [150].

The first analyser, the Linear ion Trap, provides for ion storage, isolation and fragmentation. Ions from the S-lens are loaded into the trap and upon reaching a predefined number, the trap can start further processing of the ions. This sequence of loading the trap followed by the analysis is referred to as a scan. Alternatively the linear ion trap can only serve as storage device for ions that are transferred into the Orbitrap for analysis.

The linear ion trap in the LTQ-Orbitrap Velos is a dual cell analyser, which means that it contains two consecutive linear traps, each enclosed in a separate cell. In the first, high pressure, cell ions are trapped, isolated and can be subjected to fragmentation. The second cell, low pressure, provides efficient ejection of separated ions.

Ions in the linear trap can be analysed intact, in this mode the analyser gives the mass of intact ions. The second mode involves fragmentation of ions. In this mode precursor (parent) ions are subjected to collision with inert gas eg. helium, which produces fragment (daughter) ions that are subjected to analysis. This fragmentation method is called Collision Induced Dissociation (CID). Obtained fragment ions can be isolated and subjected to another cycle of fragmentation, this process is named a multi-stage fragmentation. In the nomenclature the number of fragmentations is characterised by the power of MS. One cycle of mass selection and fragmentation would be annotated by MS^2, while MS^n stands for a general multi-stage fragmentation. A disadvantage of CID fragmentation is a poor trapping capacity of the trap for lower mass ions. This results in detection only of ions with masses higher than 1/3 mass of its precursor. This limitation does not apply to Pulsed Q Dissociation (PQD) method which allows for the detection of low mass fragment ions (ref).

Alternative to CID and PQD methods, ions from the source can be simply stored in the LTQ from where they are passed into the C-Trap which focuses the cloud of ions and injects them into Higher Energy Collisional Dissociation (HCD) collision cell. In the HCD cell ions are fragmented and product ions are transported back via the C-Tap to the Orbitrap analyser. HCD method allows for detection of low mass fragment ions, unlike CID where only fragment ions with mass larger that 30% of parent ion are detected. Moreover, detection in the Orbitrap provides a benefit of

high mass accuracy. The HCD method, however, provides lower chromatographic resolution, as the scanning rate is lower due to the Orbitrap's longer duty cycle.

Scans performed by the LTQ-Orbitrap can be also subdivided accordingly to scan method: (1) full scan, (2) selected ion monitoring (SIM), (3) selected reaction monitoring (SRM) and (4) consecutive reaction monitoring (CRM). Full scan produces a plain spectrum of a sample, within a defined m/z range. Although it gives general information regarding the analyte, it may be not very discriminative, as ions present at low level would be dominated by other components such as impurities at higher levels. SIM, however, is a tailored method when only a defined mass will be scanned. SRM is similar, where only fragment ions generated in a unique reaction are monitored, such as for a characteristic neutral loss. In the CRM method two or more consecutive collision cycles occur and in each cycle only a selected ion is subjected to further fragmentation. The following cycle only occurs if the predefined ions are detected. (5) The final scan is the product ion scan where all the fragment ions (above the 1/3 cut off) are detected after fragmentation of a parent ion.

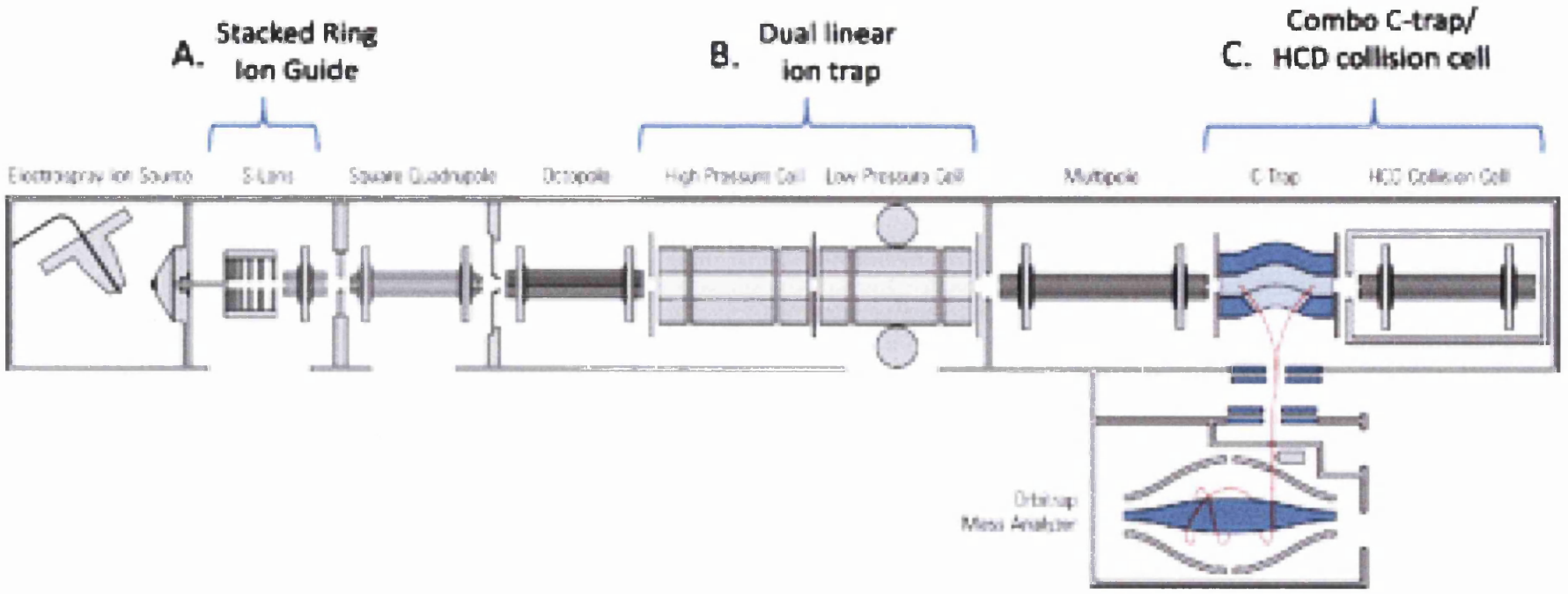

Figure 1.9 Schematic overview of LTQ-Orbitrap Velos. (reproduced from Orbitrap Velos Hardware manual)

1.9.4 Detectors

Ions released by the analyser are passed into the detector. In general, ions hitting the walls of the detector produce a stream of secondary particles such as electrons or photons which can be quantified. Ions are released from the analyser accordingly to their *m/z* ratio, which limits the number of particles simultaneously interacting with the detector. Signal generated in this process is low and to allow for a precise measurement needs to be enhanced. For this reason detector are often coupled with amplifiers, which are responsible for signal enhancement.

The main types of detectors used are Faraday cup and secondary electron multipliers (SEM). The Faraday cup ion collector is on older type of instruments and is used for a detection of relatively abundant streams of ions. SEM instruments are more modern and provide a much higher sensitivity of measurement. In SEM detector contains metal surfaces emitting secondary electrons following contact with ions. Positively charged ions hit the metal surface of the first dynode which releases electrons (for negatively charged ions there is a conversion dynode), the electrons are directed into a system of multiplying dynodes. Multiplication (gain) of the electron beam can be obtained either in a discrete (step-wise) or continuous method. In a discrete multiplier electrons hit a sequence of metal plates, on each stage emitting an increased number of particles. In a continuous multiplier, the electrons are interacting with a continuous surface capable of emitting an amplified number of electrons. The latter type of detector was used in the linear ion trap detection system of the LTQ-Orbitrap Velos system [151, 152]. The in the Orbitrap detection is through an image current generated by ions oscillating around a central spindle.

1.10 High Pressure Liquid Chromatography

The separation of compound with High Pressure/Performance Liquid Chromatography (HPLC) utilises the difference in the affinity of analytes to the stationary phase and the mobile phase of the system. The mobile phase consists of a mixture of organic solvents and buffer, which under high pressure flows through the stationery phase, which is a porous material tightly packed in a supporting tube (column). The time of the travel of analytes through the stationary phase is called the retention time. Different compounds have different retention times, which allows for the separation of analytes. In general, HPLC types can be distinguished depending on the mechanism of interaction that determines the separation of compounds by the chromatographic system. HPLC can be divided into: partition, adsorption, ion and exchange.

Partition chromatography is the most popular method of separation. In this method the analytes are partitioned as the sample moves across the stationary phase propelled by the movement of the mobile phase. The polarity of the analyte versus polarity of the phases controls the velocity of separated molecules. This chromatography can be divided into normal and reversed phase chromatography. Normal phase chromatography utilises a polar stationary phase which can be made of bare silica. Separation is achieved by the movement of non-polar solvent such as chloroform as the mobile phase. Separated analytes must be readily soluble in non-polar solutions.

In reversed phase chromatography the stationary phase is nonpolar. The most popular material is silica with bond tetra (C4), octa (C8) or octadecyl (C18) carbon chains. Shorter chains are more efficient in separation of large molecules possessing many hydrophobic groups such as proteins, longer alkyl chains are used in analysis of small molecules, for example lipids. The mobile phase used is a combination of polar organic and inorganic solvents. HPLC is the commonly coupled to the MS detector as mobile phase can easily form electrospray. To increase ionisation efficiency the solvents can be enriched with components such as formic acid or ammonia.

Components of the HPLC system

A high and stable pressure of flowing mobile phase is needed for efficient separation and this is provided by a specialised instrument – HPLC system. It consists of a number of modules controlling sample delivery as well as the flow and temperature of the mobile phase during the separation. The Dionex Ultimate 3000 HPLC system, used in the present work, is divided into an autosampler, pump module with reservoir of the mobile phase and temperature control compartment where the column (stationary phase) is housed. A schematic representation of the HPLC system is presented in Figure 1.10.

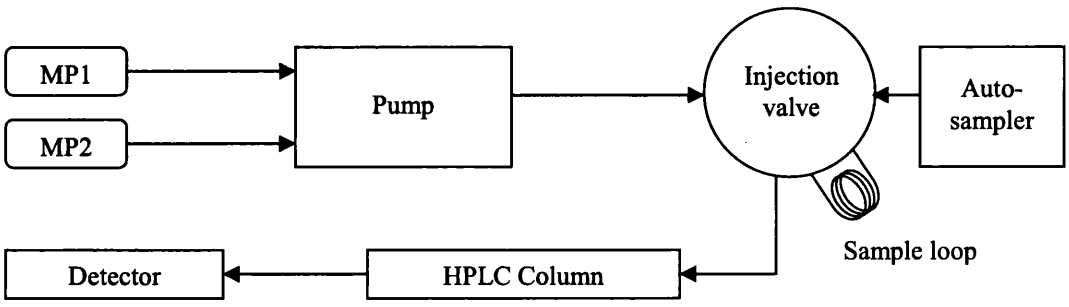

Figure 1.10 Schematic representation of HPLC instrument (MP – mobile phase).

The flow of mobile phases is propelled by a system of pumps and pump valves. This maintains a steady flow of defined composition of mobile phases. The Ultimate 3000 system can combine solvents from up to four different reservoirs, however, the most common is a composition of two mobile phases. The alteration of the ratios of different solutions enables a change in the polarity of a final mobile phase, which accelerates and improves separation of analytes.

The autosampler (injector) injects the sample into a continuously flowing stream of the mobile phase. Sample is withdrawn from a cooled vial by a needle and fills the sample loop. The flow of the solvent through the sample loop is controlled by a six-port injection valve. The stator switches the ports allowing for removal of the sample from the loop and injecting it to the mobile phase system with a minimum in disruption of the flow.

Depending on the use of multiple mobile phases the elution can be divided into isocratic or gradient. In an isocratic flow the composition of mobile phases remains constant throughout the entire analysis. This method is commonly used for analysis of well-defined compounds, such as quantification of an active ingredient during the pharmaceutical quality control. Gradient elution is obtained when the proportion of solvents in the mobile phase is changed in a programmed manner. This can be either continuous or step-wise, while the speed of transition between the solvents and can be proportional to time (linear gradient) or can be increased/decreased with time of the analysis (curved gradient). In this way it is possible to slow down the elution of the least retained compounds and accelerate migration of the analytes with the highest column affinity. Gradient flow is therefore used for separation of a complex compositions of analytes, such as in metabolomics studies.

The mobile phase is pumped through the column where the sample is fractionated into the different analytes. The column is kept in a temperature-controlled chamber, as the fluctuations of temperature affect the viscosity and pressure of solvents. Variations of these affect the retention time of eluted compounds as well as the resolution of peaks. Higher temperature decreases the viscosity of mobile phase allowing faster analysis, however, this solution is not appropriate for thermally labile compounds. These can be separated at an ambient temperature equal to the temperature of the room where the instrument is housed, usually maintained constant by an air-condition system.

1.11 Analysis of sterols with LC-MS

The analysis of steroid compounds can be challenging due to their chemical and physical properties. Sterols are lacking a strong chromophore which makes them unsuitable for high sensitivity UV-based analysis, mass spectral detection can be difficult due low volatility (important in GC-MS) and low ionisation efficiency (in LC-MS). Low solubility in aqueous solutions affects the selection of solvents used in LC-MS. Moreover, oxysterols are present at very low levels compared to a high excess of cholesterol. Cholesterol is also susceptible for autoxidation, producing non-endogenous oxysterols.

These issues can be mitigated by separating oxysterols from cholesterol at an early stage of sample preparation and by providing a chemical derivatisation of sterols. For LC-MS derivatisation can improve ionisation of compounds as well as increase their solubility. Ionisation efficiency is particularly important as it increases the sensitivity of mass spectroscopic detection for compounds present at trace level in biological material [88, 153, 154]. During chemical derivatisation for LC-MS a molecule of interest is coupled to a readily ionisable compound.

Derivatisation of oxysterols followed by LC-MS analysis was used in the work of Honda and colleagues[155]. In their study sterols present in human plasma were derivatised with picolinic acid; the resulting material was purified with a C_{18} SPE cartridge. The material was further fractionated with HPLC using a Hypersil GOLD column with a gradient mobile phase. The composition of mobile phase at the beginning of the separation was more polar (acetonitrile:methanol:water, 40:40:20, v/v), reducing the water content with the duration of the run (acetonitrile:methanol:water, 45:45:10, v/v), to the solvents was added 0.1% formic acid. The detection limit of derivatised sterols were established at the picogram level on the column. Piconyl ester of cholesterol were detected on the level of 0.1pg, which was almost 4000 times higher than in the analysis of cholesterol in its native state.

Other derivatisation method used in the studies of sterol by LC-MS employs a precharged quaternary nitrogen moiety present in reagents: Girard T ((Hydrazinocarbonylmethyl)trimethylammonium chloride) and Girard P reagent (1-(Carboxymethyl)pyridinium chloride hydrazide). The ability of Girard T reagent to form hydrazones with steroids possessing an oxo group was described in work of Wheeler and Rosado-Lojo [156]. Girard reagents are hydrophilic and increase solubility of derivatised sterols in water-based solutions, this feature was utilised for the separation of ketosteroids from other sterols [157]. With the development of LC-MS technology Girard reagents were recognised as a steroid derivatisation agent, providing an easily ionisable moiety [158-160].

As Girard reagents form hydrazones only with sterols possessing an oxo function, Griffiths' group developed a methodology allowing the use of this application for a wider group of steroids [148]. Sterols possessing 3β-hydoxy-5-ene or 3β-hydoxy-5α-hydrogen functions can be transformed into 3-oxo-4-ene or 3-oxo groups by action of a bacterial enzyme cholesterol oxidase as described by Brooks et al. [161]. The resulting compounds can be subjected to derivatisation with Girard P reagent and analysed on MS instrument. Obtained analytes can be separated prior to MS detection with capillary [162] or reverse phase HPLC [148]. This approach was also evaluated for MALDI-MS [158, 163, 164]. The MS signal intensity was improved by Girard P derivatisation by a factor of 1000 [162]. This methodology was used in LC-MS analysis of brain [120, 148, 165, 166], cerebrospinal fluid [167] and plasma [168].

1.12 Aims of the project

LC-MS methodology has been employed for the analysis of sterols present in various biological matrices including nervous tissue. This work was focused on detailed profiling of a sterol content of murine brain. The study included a number of brain samples derived from animals at various stages of development as well as nervous tissue from animal models of human metabolic disorders. The second part of the project concentrated on the alteration of the lipidome as part of the immune response to pathogens.

The main objectives of this work:

1. Modification of an existing LC method for detailed analysis of murine brain tissue.
2. Analysis of new born mouse brain with regard to neurosterols promoting neurogenesis.
3. Investigation of oxysterol biomarkers present in brain of murine model of human disease Smith-Lemli-Opitz.
4. Study of nervous tissue derived from Cyp46a1 deficient mice in order to establish a possible alternative metabolic pathways of cholesterol removal from the brain.
5. Analysis of lipid profile of brain from mice with disrupted synthesis of bile acids, representing models of human disorders Spastic Paraplegia type 5 and Cerebrotendinous Xanthomathosis.
6. Investigation of sterol content of murine macrophages as apart of the immune response.

Chapter 2

2 Materials and methods

2.1 Materials

2.1.1 Reagents and solvents

Solvents were from Fisher-Scientific (Loughborough, Leicestershire, UK). Water, acetonitrile, methanol and propan-2-ol were HPLC grade while ethanol was analytical grade. Acetic acid 100% was from VWR International Ltd (Poole, Dorset, UK) and formic acid 98/100% from VWR International S.A.S. (Briare, France). Potassium phosphate buffer made from potassium dihydrogen phosphate (KH2PO4) was from Sigma-Aldrich (Japan). Sterol/oxysterol standards were purchased from Avanti Polar Lipids (Alabaster, AL, USA). Cholesterol oxidase from Streptomyces sp. was obtained from Sigma-Aldrich (Saint Louis, MO, USA) and GP reagent [1-(carboxymethyl)pyridinium chloride hydrazide] from TCI Europe (Zwijndrecht, Belgium). SPE cartridges, Certified Sep-Pak C18, 3cm3, 200 mg, were from Waters Inc (Elstree, UK).

2.1.2 Reference standards

The list of reference standards is presented in Table 2.1.

2.1.3 Preparation of standard solutions

Stock solutions of standard compounds were prepared by dissolving 1 mg of 24(R/S)-[26,26,26,27,27,27-$^{2}H_{6}$]hydroxycholesterol, 1 mg of 7-[25,26,26,26,27,27,27-$^{2}H_{7}$]oxocholesterol and 10 mg of [25,26,26,26,27,27,27-$^{2}H_{7}$]cholesterol in 10 mL of propan-2-ol. Working solutions were made by diluting of 10 µL of the 1 ng/µL oxysterol stock solutions with 990 µL of 99.9% ethanol.

Table 2.1 Reference standards used for the work.

No	Steroid/Sterol/Oxysterol *Common* and	Steroid/Sterol/Oxysterol Systematic name	Supplier
1.	22(R)-hydroxycholesterol	cholest-5-en-3β,22(R)-diol	Avanti Polar Lipids (Alabaster, AL, USA)
2.	24(R)-hydroxycholesterol	cholest-5-en-3β,24(R)-diol	
3.	24(S)-hydroxycholesterol	cholest-5-en-3β,24(S)-diol	
4.	25-hydroxycholesterol	cholest-5-en-3β,25-diol	
5.	7α,26-dihydroxycholesterol	cholest-(25R)-5-en-3β,7α,26-triol	
6.	7β,26-dihydroxycholesterol	cholest-(25R)-5-en-3β,7β,26-triol	
7.	7α,25-dihydroxycholesterol	cholest-5-en-3β,7α,25-triol	
8.	7β,25-dihydroxycholesterol	cholest-5-en-3β,7β,25-triol	
9.	24(R),25-epoxycholesterol	cholest-5-en-24(R),25-epoxy-3β-ol	
10.	desmosterol	cholest-5,24-dien-3β-ol	
11.	6-dehydrocholesterol	cholest-5,6-dien-3β-ol	
12.	7-dehydrocholesterol	cholest-5,7-dien-3β-ol	
13.	8(9)-dehydrocholesterol	cholest-5,8(9)-dien-3β-ol	
14.	8(14)-dehydrocholesterol	cholest-5,8(14)-dien-3β-ol	
15.	24(R/S)-[26,26,26,27,27,27-$^{2}H_6$]hydroxycholesterol		
16.	7-[25,26,26,26,27,27,27-$^{2}H_7$]oxocholesterol		
17.	[25,26,26,26,27,27,27-$^{2}H_7$]cholesterol		
18.	19-hydroxycholesterol	cholest-5-en-3β,19-diol	Steroloids
19.	26-hydroxycholesterol	cholest-(25R)-5-en-3β,26-diol	
20.	27-hydroxycholesterol	cholest-(25S)-5-ene-3β,27-diol	Technische Universität Dresden
21.	(24Z)27-hydroxydesmosterol	cholest-(24Z)-5,24-diene-3β,27-diol	
22.	(24E)27-hydroxydesmosterol	cholest-(24E)-5,24-diene-3β,27-diol	
23.	20R,22R-dihydroxycholesterol	cholest-5-en-3β,20R,22R-triol	previous studies in Swansea University
24.	22-oxocholesterol	cholest-5-en-22-oxo-3β-ol	
25.	24-oxocholesterol	cholest-5-en-20-oxo-3β-ol	

2.1.4 Isolation of sterols/oxysterols from mouse brains

Newborn wild type and SLOS

Lipid extracts of neonatal mouse brains were a gift from Dr. C.H. Shackleton, Oakland Children's Hospital, California. Newborn mouse brain was homogenised and initially extracted in methanol:chloroform (1:1, v/v), and re-extracted in methanol. The combined extracts were taken to dryness and shipped to Swansea.

The lipid extracts of newborn mouse brain, equivalent of 100 mg of wet tissue, were solubilised in 1.05 mL of 99.9% ethanol containing 50 ng of 24(R/S)-[$^2H_6$]hydroxycholesterol, 50 μg of [$^2H_7$]cholesterol and ultrasonicated for 15 min at room temperature. Then 0.45 mL of water was added and the mixture was sonicated for another 15 min. The mixture was centrifuged at 14,000 g at 4 °C for 60 min and the supernatant was collected. The extraction procedure was repeated on the lipid residue (with a second 1.05 mL ethanol containing reference standards and addition of 0.45 mL of water) and the supernatants combined (final volume 3 mL).

Adult Cyp46a1 deficient mice

Lipid extracts of brains from Cyp46a1 deficient mice were a gift from Dr. D.W. Russell, University of Texas Southwestern Medical Center at Dallas, Dallas. Lipids were extracted from brains of four 15 week old female mice, two *Cyp46a1-/-* animals and two wild type (wt, *Cyp46a1+/+*) controls. Brain tissue (0.4 – 0.5 g, wet weight) was homogenised in phosphate buffer solution (1.2 mL), then was added 6 mL of chloroform and methanol (1:2, v/v, 6 mL) mixture. After further homogenisation the sample was centrifuged (1,360 g) for 10 min at 4 ^{O}C. Resulting supernatant was transferred to a fresh tube where again chloroform (2 mL) and phosphate buffer (2 mL) were added. Following further centrifugation the organic phase was removed and solvents evaporated. The dried lipid residue was shipped to Swansea.

Lipids extract corresponding to 100 mg of brain wet weight were dissolved in 1.05 mL of ethanol containing 50 ng of 24R/S-[$^2H_6$]hydroxycholesterol and 50 μg of [$^2H_7$]cholesterol and ultrasonicated for 15 min at room temperature. Water (0.45 mL) was added to the mixture and the extract was sonicated for another 15 min. The mixture was centrifuged at 14,000 g at

4 °C for 60 min and the supernatant was retained. The residue was extracted again and the supernatants were combined.

Adult Cyp27a1 and Cyp7b1 deficient mice

Brain samples disinfected from mice carrying mutations in *Cyp7b1* were generated at Edinburgh University. In the experimental procedure were used samples obtained from 13 and 23 month old male mice. Brain samples from mice with disrupted *Cyp27a1* were purchased from Jackson Laboratory (US).

A single chemosphere of the brain (approximately 200 mg) was weighted and the tissue was transferred into a glass/teflon homogeniser. To the tissue was added 2.10 mL of ethanol enriched with 100 ng of 24R/S-[$^2H_6$]hydroxycholesterol and 100 μg of [$^2H_7$]cholesterol. The mixture was homogenised by 30 passes of the pestle followed by sonication for 15 minutes. To the extract was added 0.9 ml of water was and the homogenate was sonicated for another 15 min. The liquid content of the homogeniser was transferred into a separate tube, while the remaining tissue residue in the homogeniser was extracted for the second time. The extract were brought together and centrifuged at 14,000 g at 4 °C for 60 min. The supernatant was collected and divided in two aliquots. One aliquot (corresponding to 100 mg of the biological material) was used in further work.

2.1.5 Isolation of oxysterol/sterols from macrophages

Isolation and treatment of macrophages

Lipid extracts of bone marrow derived macrophages (BMDM) and media were supplied by Dr. M. Blanc from Edinburgh University, UK. Macrophages were extracted form mice and treated in Edinburgh, while lipid extraction and MS analysis was performed in Swansea.

The procedure of isolation of the macrophages and the detail of the treatment are detailed in publication of Blanc et al. [135]. Macrophages were isolated from mice femur and tibia. Extracted cells were flushed with Dulbeco Modified Eagle Medium (DMEM) supplemented with 1% penicillin-streptomycin solution and centrifugated for 5 minutes. The cell pellet was retained and resuspended in DMEM/F12 + GlutaMAX enriched with 10% Fetal Bovine Serum (FCS), 10% L929 conditioned medium (containing Colony-stimulating factor Csf1) and Penicillin/Streptomycin.

For the interferon challenge murine recombinant Interferon gamma (IFNγ) and Interferon Beta 1 (IFNβ) were diluted in complete medium. These were added to cells at a final concentration of 10 U/ml or 25 U/ml respectively.

The construction of the GFP-encoding Murine Cytomegalovirus (MCMV-GFP, originally named: pSM3fr-rev) used in this study was described in the publication of Angulo et al. [169]. The virus was propagated in mouse NIH-3T3 fibrobasts. The amount of infectious MCMV/MHV-68 present in the viral stock was quantified by plaque assay on p53 -/- MEF monolayers in 48-well plates.

Extraction of Oxysterols and Sterols.

Treated cells (10^6) were separated from medium (retained for subsequent extraction) and washed twice with 3mL of ice cold phosphate phosphate buffer. A further 1.6ml of ice cold PBS was added to each plate and cells scraped into a 2mL microcentrifuge tube. The cells were centrifuged at 600g (4° C) for 5 min, the supernatant discarded, and 1ml of 99.9% ethanol added to the cell sediment. To the cell sediment in 1ml of 99.9% ethanol, 1.1ml of 99.9% ethanol containing 20ng of [$^2H_6$]24(R/S)-hydroxycholesterol and 1μg of [$^2H_7$]cholesterol (both Avanti Polar Lipids) was added, with sonication in an ultrasonic bath (5 min). Following centrifugation at 14,000g (4° C) for 60 min, 0.9ml of water was added drop-wise to the supernatant to give a solution of 3ml of 70% ethanol.

To extract secreted oxysterols, incubation medium (2ml) was added drop-wise, with sonication in an ultrasonic bath (5 min), to 4.7ml of 99.9% ethanol containing 20 ng of [$^2H_6$]24(R/S)-hydroxycholesterol and 1μg of [$^2H_7$]cholesterol to give a solution of 6.7ml of 70% ethanol.

2.1.6 Separation of oxysterols from sterols with SPE

During the sample preparation cholesterol can become autooxidised. Oxysterols generated in this process alter an indigenous oxysterol profile of analysed material; therefore it is crucial to separate oxysterols from cholesterol in an initial SPE procedure. A Certified Sep-Pak C18 (200 mg, Waters) cartridge were rinsed with 4 mL of 99.9% ethanol followed by an wash with 6 mL of 70% ethanol to equilibrate the solid phase. The solutions of extracted sterols and the internal standards in 70% ethanol were applied onto the cartridge and allowed to flow at a rate of 0.25 mL/min. The flow of the solvents through the cartridge was enhanced by a

negative pressure applied to the outlet of the cartridge via a vacuum manifold (Vacuum Processing Station, Agilent). Resulting flow-through was collected.. A wash with 4 mL 70% ethanol was similarly collected and combined with the flow-through to give fraction SPE1-FR1 (

Figure 2.2). This fraction is expected to contain oxysterols [167]The column was washed further with 4 mL of 70% ethanol (SPE1-Fr2) and cholesterol eluted from the cartridge with 2 mL of 99.9% ethanol (SPE1-Fr3). A final 2 mL of 99.9% ethanol was applied to the column to elute more hydrophobic sterols from the cartridge (SPE1-Fr4). Each fraction was divided into two equal volumes i.e. (SPE1-FR1A) and (SPE1-FR1B) and all fractions were dried under vacuum with Scanspeed concentrator (Scanvac) and reconstituted in 100 μL of propan-2-ol.

2.1.7 Oxidation of sterols/oxysterols with cholesterol oxidase

Sterols/oxysterols with a 3β-hydroxy-5-ene or 3β-hydroxy-5α-hydrogen functions were transformed to 3-oxo-4-ene and 3-oxo analogues with cholesterol oxidase from *Streptomyces sp.* (Figure 2) [161]. To the fractions "A" from above was added solution of 1 mL 50 mM phosphate buffer (pH7) containing 3.0 μL of cholesterol oxidase (2 mg/mL in H_2O, 44 units/mg of protein). The mixtures were incubated for 1 h at 37 °C, and the reactions were terminated with 2 mL of methanol. The (B) fractions were treated in an identical manner but in the absence of cholesterol oxidase and with the 2 mL of added methanol containing 50 ng of 7-[$^2H_7$]oxocholesterol.

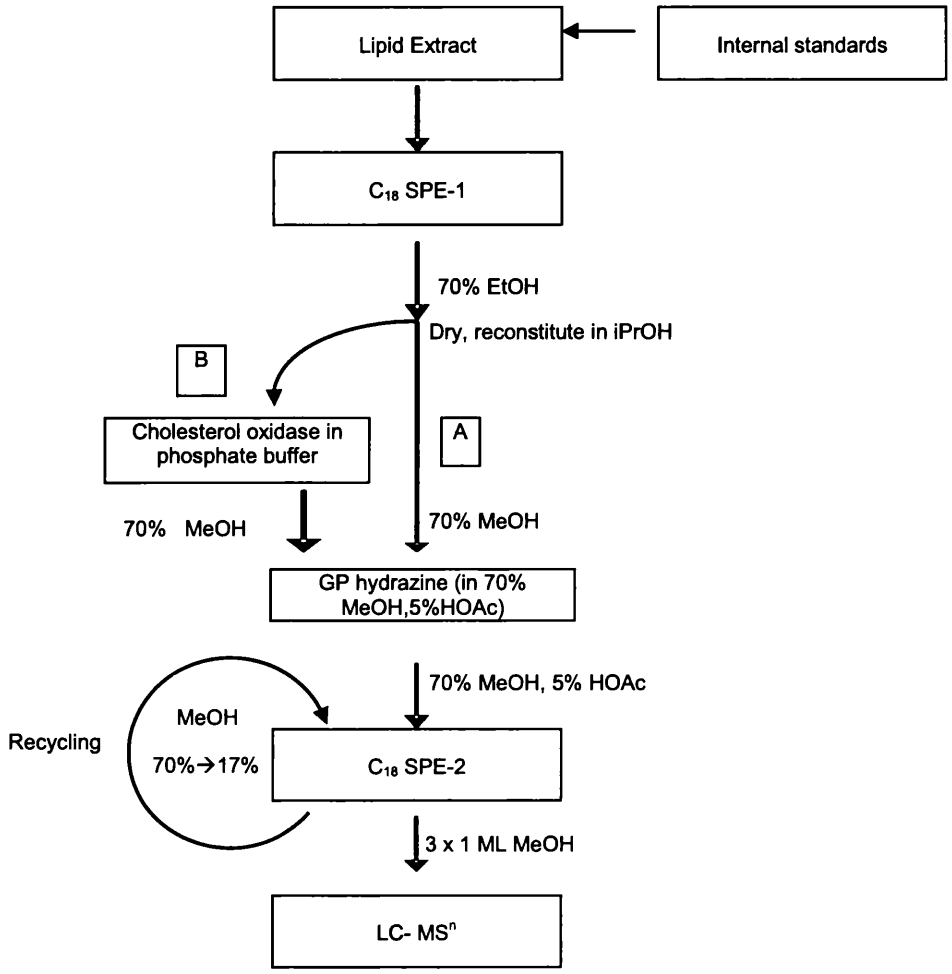

Figure 2.1 Analytical protocol for the analysis of sterols and oxysterols extracted from biological material (brain tissue, cells, media). Extract was split into two portions, one is directly subjected to GP derivatisation (A), while the second one is incubated for 1 h with cholesterol oxidase (B) and then derivatised with GP reagent. In fraction A only sterols naturally possessing 3-oxo moiety are derivatised, in fraction B sterols with 3β-hydroxy-4-ene and 3β-hydroxy-5α-hydrogen will be converted to is 3-oxo analogues, which allows the derivatisation reaction. Recycling procedure for SPE2 was applied in order to separate and remove the excess of GP reagent.

2.1.8 Derivatisation sterols/oxysterols with Girard P reagent

Neutral sterols/oxysterols are electrically inert and, therefore, poorly ionised in the API process. To overcome this issue we applied a derivatisation method to enhance their analysis. Sterols/oxysterols possessing an oxo group (either naturally or via treatment with cholesterol oxidase (Figure 2.1) were derivatised with the GP reagent which contains a pre-ionised quaternary nitrogen (Figure 2.2) [160]. To each of the fractions from above was added 1 mL of phosphate buffer, 150 µL of glacial acetic acid and 150 mg of GP hydrazine (Figure 2.1). Glacial acetic acid added to the mixture increases the rate of hydrazone formation [156]. The mixture was incubated at room temperature overnight in the dark. We call the combined process of oxidation with cholesterol oxidase and derivatisation with GP reagent as a "charge-tagging".

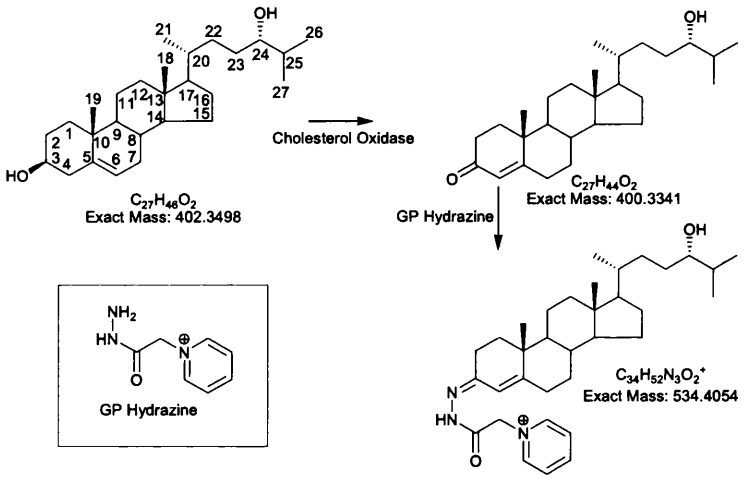

Figure 2.2 The process of charge-tagging by derivatisation with Girard P reagent. Oxysterol possessing 3-oxo group forms positively charged hydrazones with GP hydrazine.

2.1.9 Purification of sterols/oxysterols with SPE

Derivatised sterols/oxysterols were separated from the excess of GP hydrazine by a recycling method [148]. Sterol/oxysterol molecules, even when derivatised to the GP hydrazones, are still prone to precipitation in highly aqueous solutions. To tackle this problem a recycling method was used, where initially analytes were dissolved in 70% methanol, and recycled on a second 200 mg certified Sep-Pak C18 cartridge (SPE2). Prior to application of sample the column was washed with 6 mL of 100% methanol and 6 mL of 10% methanol before conditioning with 4 mL of 70% methanol. The flow of solvent through the column was aided by a negative pressure applied to the column outlet by a vacuum manifold. The derivatisation mixtures from above (~3 mL ~70% methanol) were applied to the column and effluent retained. The sample tube was then washed with 1 mL of 70% methanol and applied to the column followed by a column wash of 1 mL 35% methanol. The effluents were pooled (now ~ 5 mL) and diluted with 4 mL of water to give 9 mL of 35% methanol. This solution was then applied to the column and the flow-through collected, followed by a wash with 1 mL of 17% methanol. The flow-through and wash were diluted with 9 mL of water to give 19 mL of ~ 17% methanol. This solution was again loaded on the column followed by a wash with 6 mL of 10% methanol. At this point all the derivatised sterols/oxysterols are retained on the column while excess derivatisation reagent is in the 10% methanol wash. Derivatised sterols/oxysterols were then eluted in three separate 1 mL portions of 100% methanol (SPE2-FR1, FR2, FR3) followed by 1 mL of 99.9% ethanol (SPE2-FR4). For subsequent analysis of oxysterols the first 2 mL were combined while for sterol analysis 3 mL were combined.

2.1.10 LC–MS and MS^n analysis

The mass spectral work presented in this thesis was done with two instruments. LTQ Orbitrap XL was used for the analysis of neonatal brains and Cyp46a1 deficient brain. The brain tissue from animals with Cyp27a1 and Cyp7b1 deficiencies and were analysed with LTQ Orbitrap Velos. The study of macrophages was performed on both systems: LTQ Orbitrap XL for the first, preliminary part of the study, while LTQ Orbitrap Velos was used for the main body of the macrophage analysis.

LTQ Orbitrap XL or LTQ Orbitrap Velos (Thermo Fisher Scientific, UK) was paired with a Dionex Ultimate 3000 LC HPLC system (Dionex, UK). For the data processing and analyte quantification was used Thermo-Fisher MS software Xcalibur.

Liquid chromatography Dionex Ultimate 3000 LC HPLC system consists of degasser, pump unit, flow control module, column compartment and autosampler (Figure 2.3). Sample is stored until injection in temperature-controlled tray in the autosampler. The sample is withdrawn by the needle and loaded into a sample loop of defined volume. In the next step the analytes are removed from the loop and injected to flowing mobile phase.

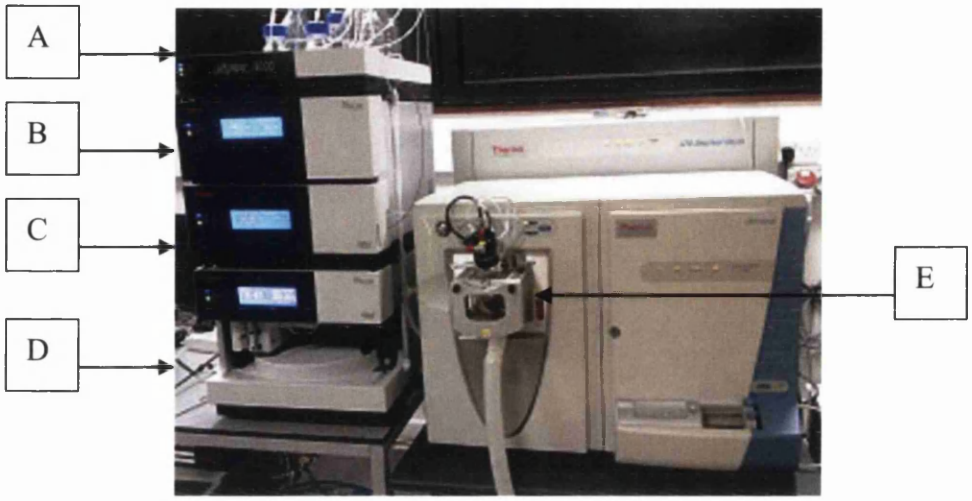

Figure 2.3 Thermo Scientific Dionex Ulitmate 3000 HPLC system. Mobile phases from reservoirs are passed through degassers (A) propelled by the pumps (B). The separation is performed by the HPLC column homed in column compartment (C), the sample is withdrawn from vials kept under stable conditions in the sampler (D). Analytes are transferred to the ESI probe of LTQ Orbitrap Velos (E) from Thermo Scientific.

The separation was performed using a Hypersil GOLD reversed–phase column (50 x 2.1 mm, 1.9 μm, Thermo-Scientific) at ambient temperature at flow rate 200 μL/ min.

For the separation of analytes was used 17 minute long HPLC gradient, however for the separation and quantification of closely eluting compounds was used gradient with altered elution profile lasting for 23 minutes.

Mobile phase A consisted of 0.1% formic acid in 33.3% methanol, 16.7% acetonitrile. Mobile phase B consisted of 0.1% formic acid in 63.3% methanol, 31.7% acetonitrile.

(A)

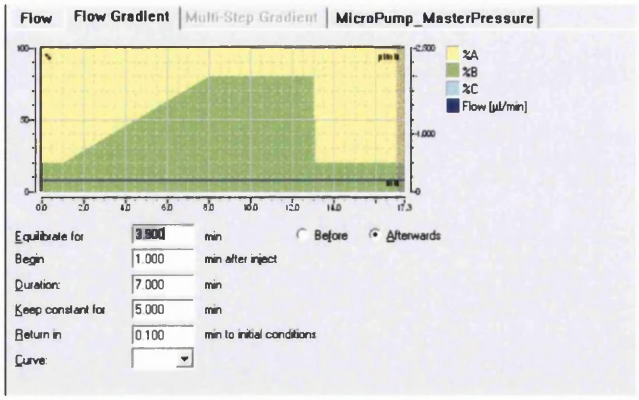

(B)

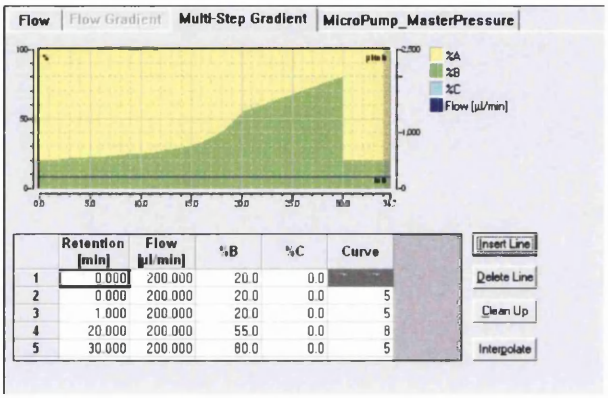

Figure 2.4. Gradient elution programs used for the separation of GP-derivatised oxysterols, programs were controlled with Chromeleon software. Gradient 1 ("short") where the change between the mobile phases is linear (length of the run 17 min) and Gradient 2 where applied curved mobile phases transition (length of the run 32 min). Mobile phase A was 33.3% methanol, 16.7% acetonitrile and 0.1% formic acid, B was 63.3% methanol, 31.7% acetonitrile and 0.1% formic acid. The images were reproduced from the Chromelon instrument control program.

In the "short" gradient the elution started with 20% B lasted for 1 min, then the proportion of B was raised to 80% B over the next 7 min and maintained at this level for further 5 min, before returning to 20% B in 0.1 min. The column was re-equilibrated for a further 3.9 min, giving a total run of 17 min.

The flow through the ESI probe was maintained at 200 µL/ min, The temperature of the capillary was set at 300°C, sheet gas flow was 25 arbitrary units/min, auxiliary gas flow was 5 arbitrary units/min. The voltage applied to the probe was 5 kV.

The LTQ-Orbitrap mass spectrometer was calibrated using Cal Mix (Thermo-Finnigan) and mass-tuned using GP charge-tagged 19-hydroxycholesterol prior to each analytical run. Subsequent tests of LC, MS and MS^n systems were performed by injecting GP charge-tagged 19-hydroxycholesterol (1 pg/μL in 60% methanol, 0.1% formic acid) onto the reversed-phase column and eluting into the ESI source at a flow-rate of 200 μL/min. The analysis of this reference compound was repeated periodically during the analytical batch (every 10 injections) to assure mass accuracy and monitor chromartographic performance. For the analysis of GP charge-tagged sterols/oxysterols, the methanol eluents from the SPE2 fractions was diluted to give solution of 60% methanol. The volume of injected solution ranged between 20μL and 35 μL depending of obtained intensity of analytes.

The LTQ-Orbitap XL or Velos instruments were operated in positive ion mode, using three different scan events. For the plain mass spectrum, we utilised a FTMS scan in the Orbitrap over the *m/z* range 400-605 at 30,000 resolution (full width at half-maximum height, fwhm, definition) was performed followed by data dependent MS^2 ($[M]^+ \rightarrow$) and MS^3 ($[M]^+ \rightarrow [M-79]^+ \rightarrow$) events in the Linear Quadrupole Ion Trap. These MS^n scans in the LTQ were performed in parallel to acquisition of the high-resolution MS scan by the Orbitrap. For the MS^2 and MS^3 scans were performed at the normalised collision energy at 30% and 35% (instrument settings) respectively. In order to select monoisotopic ions the precursor-ion isolation width was set at 2 (LTQ Orbitral XL) or 1 (LTQ Orbitral Velos). A precursor-ion inclusion list was defined according to the *m/z* of the $[M]^+$ ions of expected sterols/oxysterols so that MS^2 was preferentially performed on these ions in the LTQ if their intensity exceeded a preset minimum (500 counts). If a fragment-ion corresponding to a neutral loss of 79 Da from the precursor-ion was observed in the MS^2 event and was above a minimal signal setting (200 counts), MS^3 was performed on this fragment (Figure 2.5).

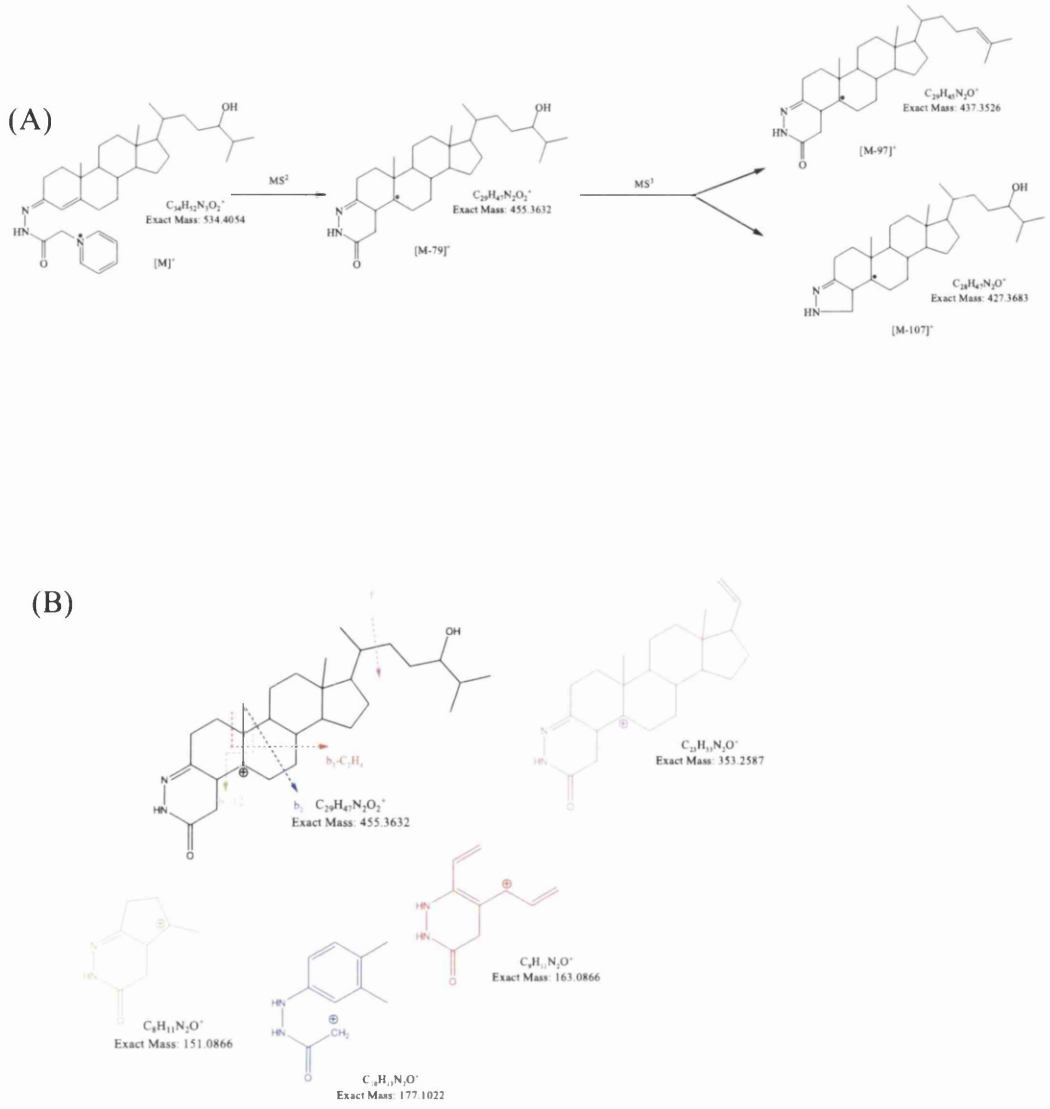

Figure 2.5 Schematic representation of (A) MS^2 and MS^2 performed on ions in inclusion list or most abundant ions and (B) MS^3 fragmentation of sterol/oxysterol GP hydrazones. GP-tagged 24S-hydroxycholesterol is shown as an example.

Quantification of sterols/oxysterols

For the quantification of sterols/oxysterol we exploited stable isotope dilution methodology. Oxysterols were quantified using 24(S/R)-[$^2H_6$]hydroxycholesterol, while sterols were quantified against [$^2H_7$]cholesterol. The quantity of sterols/oxysterols in fractions (A) represent the sum of sterols/oxysterols oxidised by cholesterol oxidase generating a 3-oxo group and those which naturally contain an oxo group. To separate sterols/oxysterols with these structures, quantities in fractions (B) are subtracted from fractions (A). The difference (A-B) represents the quantity of sterols/oxysterols with a 3β-hydroxy group subsequently oxidised to the 3-oxo group, while the quantities in (B) represent sterols/oxysterols with a natural oxo group. 7-[$^2H_7$]Oxocholesterol was use as the to quantify sterols/oxysterols which naturally possess an oxo group and are preserved in fractions (B).

The concentration of analyte of interest was calculated by dividing the analyte peak area divided by the peak area of isotopically labelled internal standard and multiplied by the known concentration of internal standard.

$$\frac{A_a \times M_i}{A_i} = M_a$$

Where:

M_a = concentration of analyte

M_i = concentration of internal standard

A_a = analyte peak area

A_i = internal standard peak area

Karu et al. [148] shown that various GP-derivatised sterols/oxysterols with a 3-oxo-4-ene structure give a similar intensity of response upon analysis by LC-ESI-MS. This allows the use of 24(R/S)-[$^2H_6$]hydroxycholesterol and [$^2H_7$]cholesterol as internal standards for oxysterols and sterols respectively. Once GP tagged 7-oxocholesterol and 24-hydroxycholesterol also give similar response in LC-ESI-MS thereby allowing the use of 7-[25,26,26,26,27,27,27-$^2H_7$]oxocholesterol as the internal standard for (B) fractions.

Chapter 3

3 Analysis of oxysterols in neonatal mouse brain

3.1 Introduction

Unesterified oxysterols in an adult mouse brain are dominated by a large excess of cholesterol (10 - 20 μg/mg wet weight in most species). This causes an analytical difficulty in the study of relatively scarce oxysterols. However, this can be overcome by the analysis of a brain isolated from a new born animal. Mouse belongs to altricial species, which means that a new born mouse is entirely dependant on its mother. Myelination in the neonatal brain has not started and cholesterol levels are similar to most other organs (2 – 4 μg/mg). The level of cholesterol increases rapidly in mouse brain over a three week period during which myelination proceeds [88]. Thus, the newborn mouse offers an opportunity to study the sterol content of brain in the absence of masking levels of myelin-derived cholesterol.

Essentially all cholesterol present in the brain is derived from de novo synthesis, this is also true of newborn mouse, where at least 90% of cholesterol in the brain has been synthesised in the brain [170]. In the developing foetus, after closure of the blood brain barrier (BBB), and in the very young animal, desmosterol levels are elevated indicating a rapid de novo synthesis of sterols [88, 120, 170]. An active mevalonate pathway in the developing foetus is further confirmed by appreciable levels of 24S,25-epoxycholesterol [120].

In adult mammals cholesterol levels in brain are maintained at a constant level by the equilibrium between cholesterol synthesis via mevalonate pathway and cholesterol removal via 24S-hydroxylation reaction. 24S-Hydroxycholesterol is able to cross the BBB and is transported by the circulation to the liver for further metabolism [171]. The foetal mouse brain is characterised by low expression of cholesterol 24-hydroxylase (Cyp46a1), which consequently retains newly synthesised cholesterol within the brain [170]. The increase in the level of cholesterol is accompanied by upregulated expression of *Cyp46a1* and an increase in 24S-hydroxycholesterol levels [29, 172].

24S-Hydroxycholesterol, 24S,25-epoxycholesterol, [109, 173], and 22R-hydroxycholesterol are ligands to the liver X receptors (LXRs) in vitro. Moreover, 22R-hydroxycholesterol participates as an intermediate in the transformation of cholesterol into pregnenolone by the cytochrome P450 (Cyp) side-chain cleavage enzyme (P450SCC, Cyp11a1). This enzyme first hydroxylates cholesterol at 22R position, then at 20R position; resulting 20R,22R-dihydroxycholesterol is cleaved forming pregnenolone. Pregnenolone serves a precursor for

neurosteroid biosynthesis [174]. 22R-Hydroxycholesterol has been reported in human brain as well as to have neuroprotective effects against amyloid beta toxicity in vitro [175, 176].

The aim of this work is to present a comprehensive profile of oxysterols and sterols present in a new born mouse brain. Without the masking effect of cholesterol it would be possible to evaluate the levels of indigenous oxysterols isolated from the brain. Furthermore, this study includes the analysis of oxysterols implicated in neurogenesis found in an embryonic brain [120].

3.2 Results

Oxysterols in newborn mouse brain

Monohydroxycholesterols

Cholesterol molecule possessing one additional hydroxyl subjected to derivatisation with Girard reagent upon ionisation will produce a molecular ion of *m/z* 534.4054. The reconstructive ion chromatogram (RIC) of this *m/z* from newborn mouse brain using chromatographic Gradient 1 and Gradient 2 (gradient elutions showed in Figure 2.4) is shown in Figure 3.1 A and Figure 3.1B, respectively. The analysis of chromatogram for *m/z* 534.4054 showed two dominating peaks eluting at 7.41 min and 7.72 min. Based on comparison with authentic standards these were identified as *syn* and *anti* conformers of GP-tagged 24S-hydroxycholesterol. The MS^3 ($[M]^+ \rightarrow [M-79]^+ \rightarrow$) spectra of both peaks are identical (Figure 3.2B) and show the triad of low mass fragment ions *m/z* 151 (*b1-12), 163 (*b3-C2H4) and 177 (*b2) characteristic of the GP-derivatised 3-oxo-4-ene structure (formed following cholesterol oxidase treatment), and a distinctive ion at 353 ('*f), which is characteristic of the 24-hydroxy group (Figure 2.5) [148]. 24S-Hydroxycholesterol is generated in the Cyp46a1 catalyzed hydroxylation of cholesterol [29].

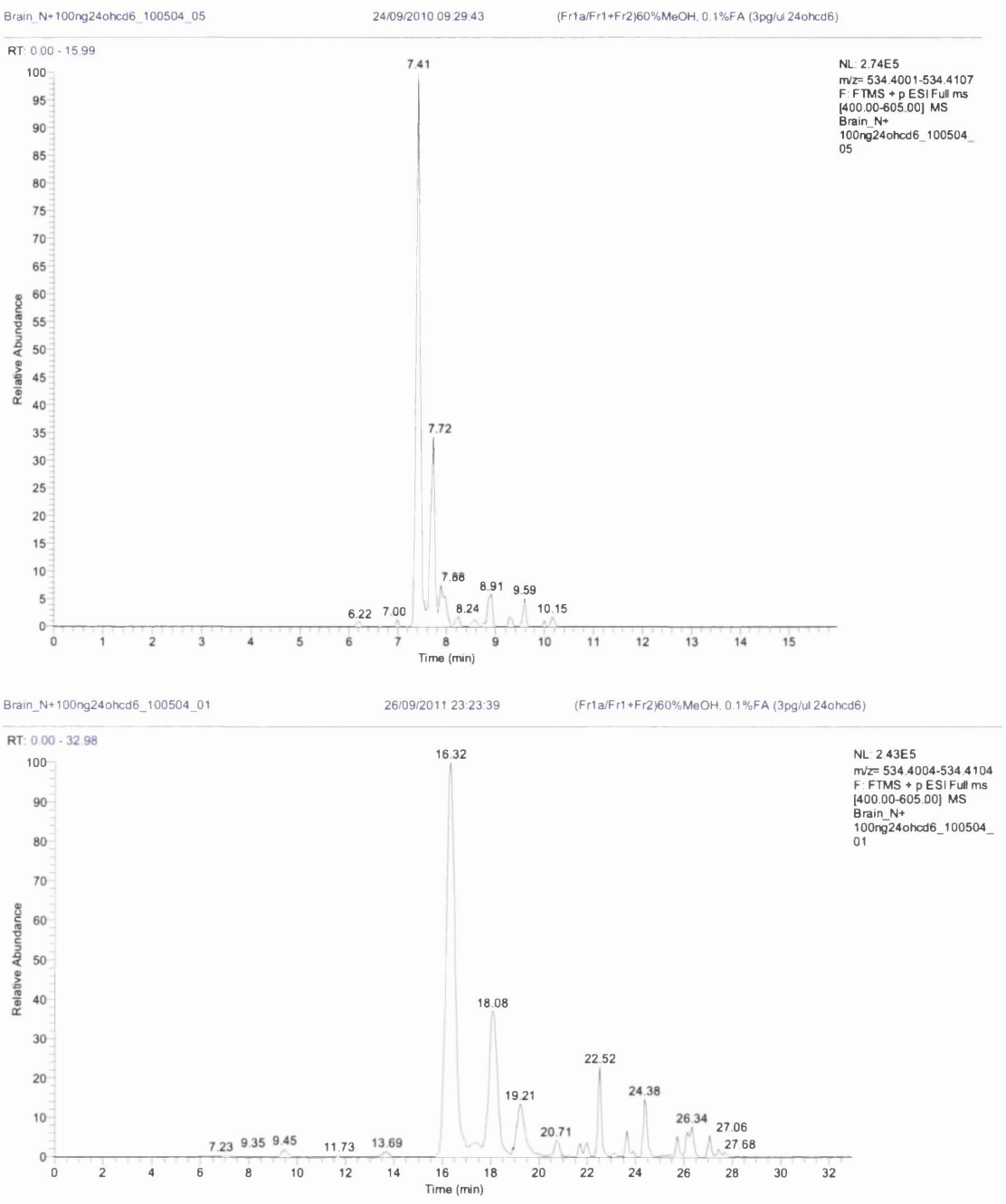

Figure 3.1 Monohydroxycholesterols in newborn mouse brain. (A and B) RIC of *m/z* 534.4054 ± 10 ppm utilising gradients 1 (short) and 2 (long), respectively.

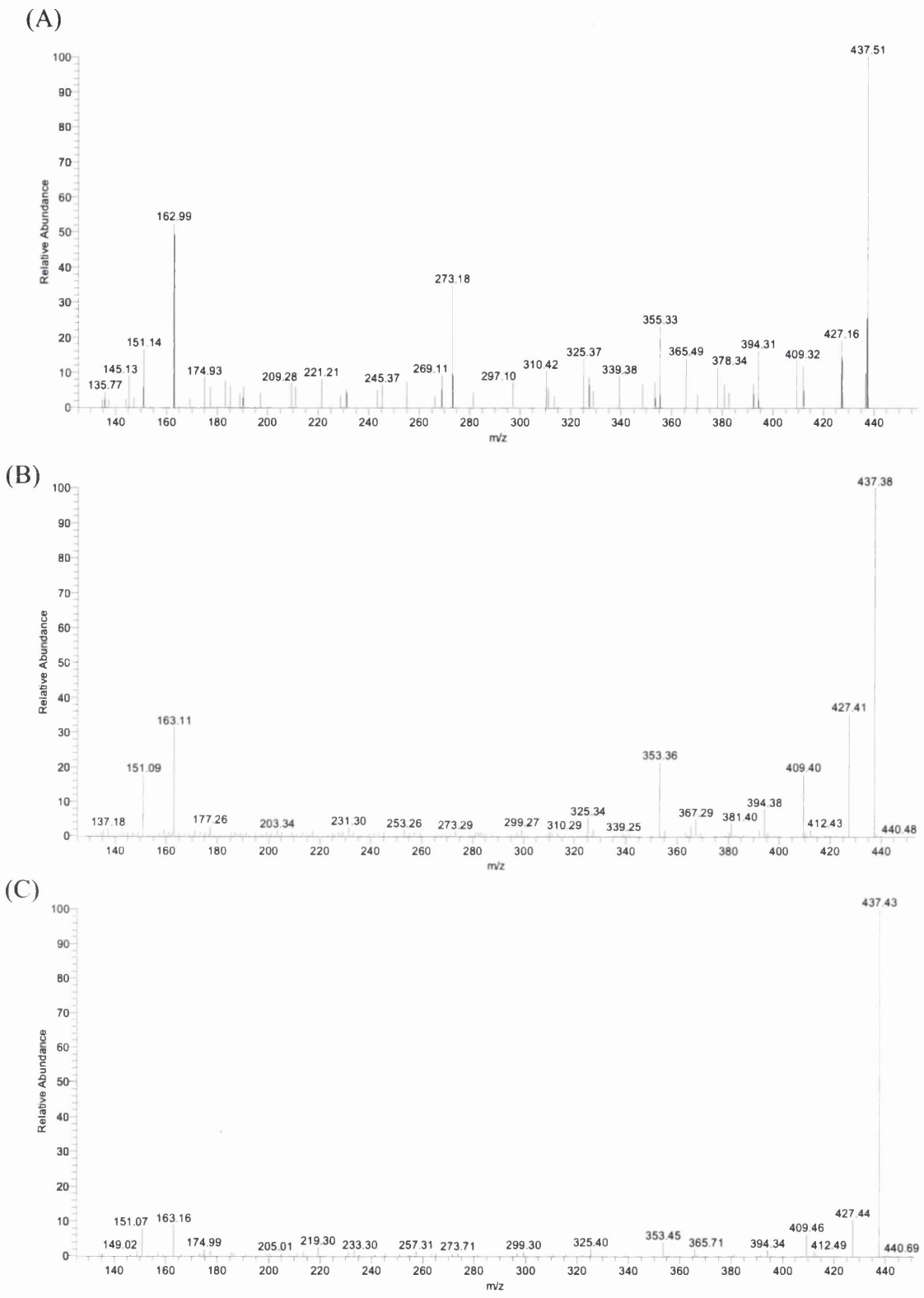

Figure 3.2 Monohydroxycholesterols in newborn mouse brain - cont. (A - C) MS^3 spectra referring to GP-tagged oxysterols. (A) 22R-hydroxycholesterol (22R-HC), (B) 24S-hydroxycholesterol (24S-HC), (C) 25-hydroxycholesterol (25-HC).

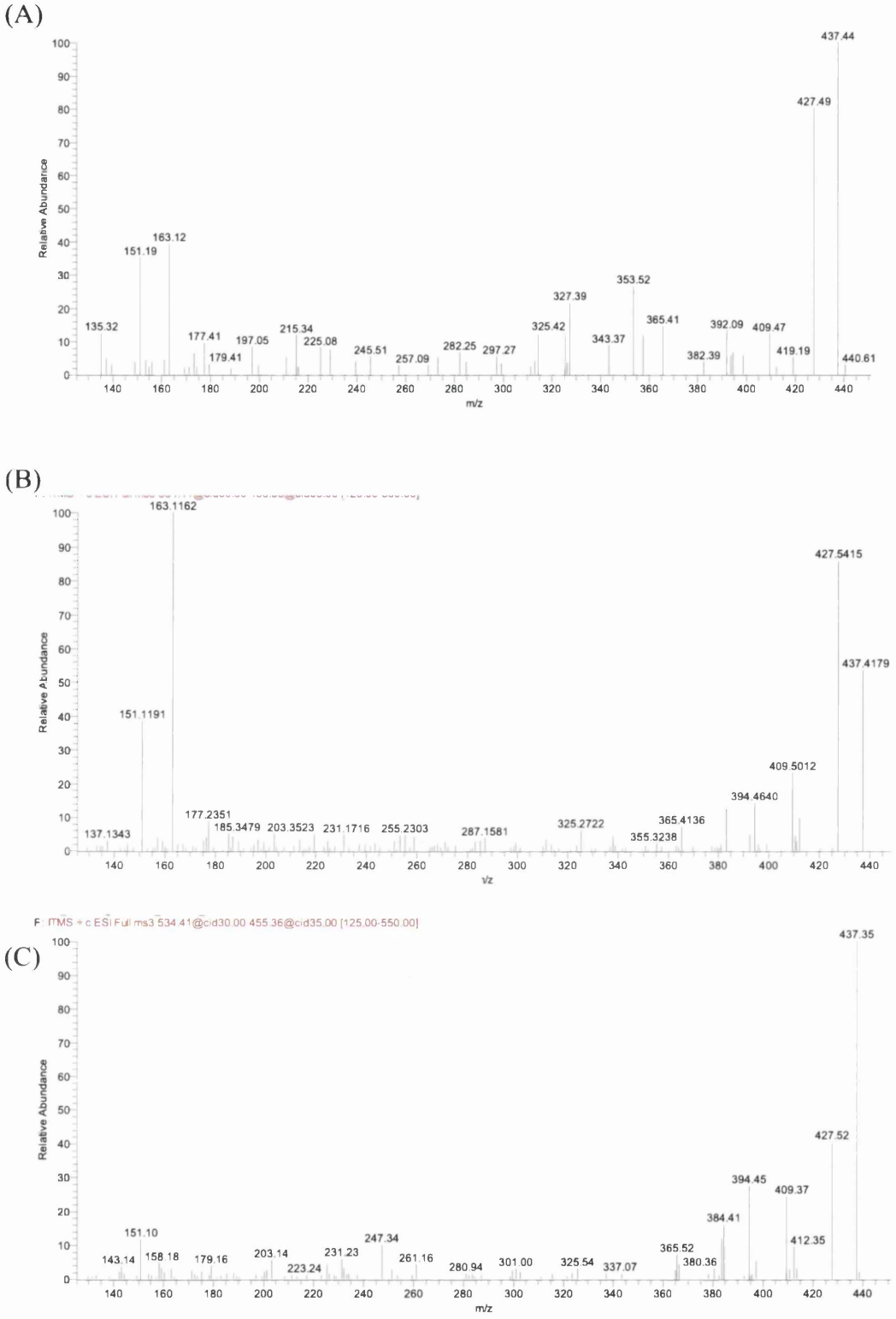

Figure 3.3 Monohydroxycholesterols in newborn mouse brain - cont. MS^3 spectra referring to GP-tagged oxysterols. (A) 26-hydroxycholesterol (cholest-(25R)-5-ene-3β,26-diol, 26-HC), (B) X-hydroxycholesterol (X-HC), and (C) 7α-hydroxycholesterol (7α-HC). Assignment is based on a comparison of retention time, exact mass and MSn spectra with those of authentic standards.

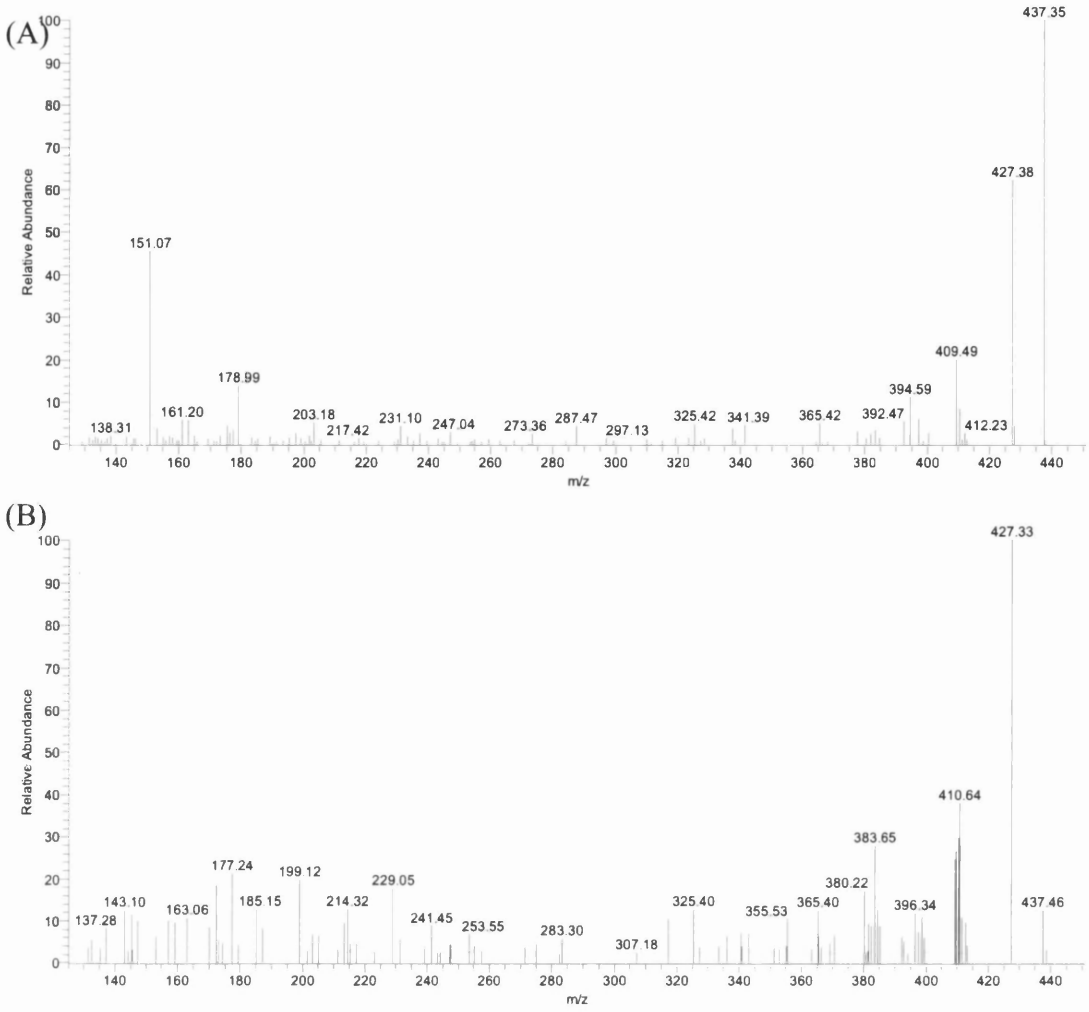

Figure 3.4 Monohydroxycholesterols in newborn mouse brain - cont. MS^3 spectra referring to GP-tagged oxysterols. (A) 7 β-Hydroxycholesterol, (B) 6-hydroxycholesterol.

The Cyp46a1 enzyme is normally expressed in neurons. In newborn mouse brain the level of 24S-hydroxycholesterol was determined to be 0.510 ± 0.082 ng/mg, (mean ± standard deviation, n = 6). This value is considerably lower than that published for the adult mouse (30 – 60 ng/mg) [172, 177-179]. This is not surprising as expression of Cyp46a1 is detected until late embryonic development in mouse [172], and in human Lütjohann et al have shown that CYP46A1 activity is minor in neonates [180]. GP-tagged 24S-, 25- and 26-hydroxycholesterols (cholest-(25R)-5-ene-3β,26-diol) give closely eluting peaks but characteristically different MS^3 spectra (Figure 3.2B-C and Figure 3.3A). This enables the identification of all three oxysterols. However, in this study the comparatively high level of 24S-hydroxycholesterol and low levels of the other two closely eluting oxysterols (<0.010 ng/mg) made accurate quantification of the minor oxysterols difficult. This issue was mitigated by utilising the extended chromatographic gradient (Gradient 2) which improved

the resolution of these isomers and make quantitative estimates of oxysterol concentrations (Figure 3.1). 25-Hydroxycholesterol is formed from cholesterol either by cholesterol 25-hydroxylase (Ch25h) [8] or in Cyp46a1 catalysed reactions [29, 107], while 26-hydroxycholesterol is formed in Cyp27a1 catalysed reactions [181]. Further analysis of the RIC of *m/z* 534.4054 reveals in Figure 3.1A a minor peak at 8.24 min with retention time and MS^3 spectrum 13 identical to charge-tagged 24R-hydroxycholesterol. Reference to the authentic standard indicates that this compound elutes as *syn* and *anti* conformers with the earlier eluting component eluting at 7.88 min. These conformers elute at 19.21 and 20.71 min with the longer gradient (Figure 3.1B). The level of 24R-hydroxycholesterol was determined to be 0.061±0.006 ng/mg. 24R-Hydroxycholesterol has not previously been characterised in brain. In mouse Cyp46a1 accounts for production of 80% of the 24-hydroxycholesterol content of plasma and Lund et al suggested the remainder may be formed in a reaction catalysed by Cyp27a1 as earlier studies in pig revealed that the hepatic mitochondrial sterol 27-hydroxylase has 24-, 25- and (25R),26-hydroxylase activity [182]. It is uncertain whether the 24R-isomer found here in newborn brain is formed as a minor product of Cyp46a1 activity in brain or is an import product hepatically derived from Cyp27a1 oxidation of cholesterol. 24R-Hydroxycholesterol was not detected in young adult female mouse brain. Preceding the major peaks in the RIC of *m/z* 534.4054 is a minor peak eluting at 6.22 min in Figure 3.1A, identified by retention time and its MS^3 spectrum (Figure 3.2A) to correspond to GP-tagged 22R-hydroxycholesterol (0.010 ± 0.002 ng/mg). The presence of a hydroxy group at the C-22 is characterised by an abundant ion at *m/z* 355 (*f') resulting from a cleavage of the C-20 – C-22 bond α to the 22-hydroxy group, and at *m/z* 273 corresponding to the charge-tagged ABC rings. 22R-Hydroxycholesterol is formed from cholesterol by P450SCC (Cyp11a1) as a first step of pregnenolone synthesis via 20R,22R-dihydroxycholesterol. The enzyme is expressed in adult rodent brain and also during embryogenesis [183]. Other monohydroxycholesterols identified in newborn mouse brain were 7α-, 7β- and 6-hydroxycholesterols, at levels of 0.048 ± 0.022, 0.039 ± 0.015 and 0.019 ± 0.014 ng/mg (Figure 3.3C, Figure 3.4A and B). The hydroxylation of the B ring of the tetracyclic nucleus results in an altered pattern of low mass fragment ions in the MS^3 spectra. 7α- or 7β-Hydroxylation causes a shift in the *b3-C2H4 ion from *m/z* 163 to 179. There is an elevated abundance of the ion at *m/z* 151 (*b1-12) in the spectrum of the 7β-isomer compared to the 7α-isomer, while the peaks at *m/z* 231 and 394 are more intense in the spectrum of the 7β isomer. 7β-Hydroxycholesterol can be formed enzymatically in a Cyp7a1 catalyzed reaction, but Cyp7a1 is expressed only in liver [184]. Both 7α- and 7β-hydroxycholesterol can be

produced by autoxidation of cholesterol during sample preparation and storage [185], or they may be formed endogenously by reaction of cholesterol with reactive oxygen species (ROS) [186]. In some, but not all samples, a peak giving MS2 and MS3 spectra identical to those of the authentic standard of 6β-hydroxycholesterol was observed (Table 3.1). 6β-Hydroxycholesterol can be generated from 5,6-epoxycholesterol by hydrolysis and dehydration [126]. The remaining chromatographic peak to be characterised corresponds to a 14 hydroxycholesterol eluting at 8.91 min in Figure 3.1A and at 22.52 min in Figure 3.1B (0.045 ± 0.015 ng/mg). The MS^n spectra suggest hydroxylation at a primary or secondary carbon on the C17 side-chain (Figure 3.3B). One possibility is cholest-(25S)-5-ene-3β,27-diol, however, the retention time does not correspond to that of the authentic standard, which elutes just before the 25R isomer (we use the nomenclature suggested by lipid maps where 26-hydroxycholesterol corresponds to cholest-(25R)-5-ene-3β,26-diol [16]). In summary, the pattern in newborn brain is of one dominating monohydroxycholesterol, i.e. 24S-hydroxycholesterol (Figure 3.1A and B), this is similar to what is observed here in the young female adult and to published data for adult mouse brain [177, 179]. However, it is noteworthy that an array of monohydroxycholesterols isomers are observed in newborn mouse brain, and that a similar situation exists in embryonic brain [120].

Oxo and epoxycholesterols and hydroxydesmosterols

Cholesterol modified with additional epoxy- or oxo- groups or possessing a second insaturated bond and a hydroxyl group, following GP charge-tagging will give an $[M]^+$ ion at *m/z* 532.3898. RICs for this *m/z* are shown in Figure 3.6A and Figure 3.6B separated with the short and long gradient, respectively. The two peaks eluting at RT 6.80 and 7.01 min in Figure 3.6A correspond to the *syn* and *anti* conformers of GP-tagged 24S,25-epoxycholesterol (0.067 ± 0.012 ng/mg). In Figure 3.6B the corresponding peaks are at 12.47 and 13.93 min, respectively. The MS^3 spectra are identical to those of the authentic standard, giving the characteristic low mass ions at *m/z* 151, 163 and 177, and side-chain cleavage fragment ions at 325 ('*e), 353 ('*f) and 367 ('*g) (Figure 3D). The chromatographic peak eluting at 7.79 min in Figure 3.6A was identified as GP-tagged 24-oxocholesterol (0.031 ± 0.008 ng/mg). The presence of a 24-oxo group rather than the 24,25-epoxide is indicated by the elevated abundance of the $[M\text{-}79\text{-}CO]^+$ ion (*m/z* 425) compared to the $[M\text{-}79\text{-}H2O]^+$ ion (*m/z* 435) (Figure 3.8B versus Figure 3.7B). 24-Oxocholesterol is an isomerisation product of 24S,25-epoxycholesterol formed during the derivatisation procedure.

Table 3.1 Steroids, sterols and oxysterols in newborn mouse brain

Steroids, sterols and oxysterols identified by LC-ESI-MSn in brain following SPE and charge-tagging with GP-hydrazine. In the absence of authentic standards presumptive identifications based on exact mass, MSn spectra and retention time are given. Samples from 6 mice were analysed. For comparison values for 15 week female animals are given in parenthesis.

After cholesterol oxidase and GP-tagging		Originating structure				
Mass	Steroid/Sterol/Oxysterol Systematic name	Steroid/Sterol/Oxysterol *Common* and Systematic name	RT G1	RT G2	AS	Mean concentration ng/mg ± SD (n = 6)
448.2959	Pregn-4-ene-3,20-dione 3-GP	*Progesterone* Pregn-4-ene-3,20-dione	2.20	--	Y	(ND) 0.001±0.001a
514.3792	Cholesta-4,7,24-trien-3-one 3-GP	*7-Dehydrodesmosterol* Cholesta-5,7,24-trien-3β-ol	10.85	--	N	(5.65±8.76)b 41.159±2.503b
514.3792	Cholesta-4,6,24-trien-3-one 3-GP	Cholesta-4,6,24-trien-3β-olc	11.59	--	N	(ND) 113.330±7.018b
516.3948	Cholesta-4,24-dien-3-one 3-GP	*Desmosterol* Cholesta-5,24-dien-3β-ol	11.33	--	Y	(104.29±14.84)b 493.986±18.062 b
516.3948	Cholesta-4,7-dien-3-one 3-GP	*7-Dehydrocholesterol* Cholesta-5,7-dien-3β-ol	12.07	--	Y	(ND) 210.484±8.319b
516.3948	Cholesta-4,6-dien-3-one 3-GP	Cholesta-4,6-dien-3β-old	12.28	--	Y	(ND) 46.692±6.736b
518.4105	Cholest-4-en-3-one 3-GP	*Cholesterol* Cholest-5-en-3β-ol	12.83	--	Y	(16025.62±758.1 1) 2221.297±31.67 8
518.4105	Cholest-4-en-3-one 3-GP	Cholest-4-en-3-one	12.83	--	Y	(NA) 2.034±1.271
532.3898	X-Hydroxycholest-4,24-dien-3-one 3-GP	*X-Hydroxydesmosterol* Cholesta-5,24-diene-3β,X-diol	5.97	8.80	N	(ND) 0.002±0.002a
532.3898	24S,25-Epoxycholest-4-en-3-one 3-GP	*24S,25-Epoxycholesterol* 24S,25-Epoxycholest-5-en-3β-ol	6.80 7.01	12.4713 .93	Y	(0.03 ± 0.04)a 0.067±0.012a
532.3898	26-Hydroxycholest-4,24Z-dien-3-one 3-GP	*(24Z),26-Hydroxydesmosterol* Cholesta-5,24Z-diene-3β,26-diol	7.16	14.75	Y	(<0.01)a 0.048±0.009a

532.3898	Y-Hydroxycholest-4,24-dien-3-one 3-GP	*Y-Hydroxydesmosterol* Cholesta-5,24-diene-3β,Y-diol	7.42	16.25	N	(ND) 0.188±0.046a
532.3898	26-Hydroxycholest-4,24E-dien-3-one 3-GP	*(24E),26-Hydroxydesmosterol* Cholesta-5,24E-diene-3β,26-diol	7.94	16.85	Y	(ND) 0.015±0.004a
532.3898	Cholest-4-ene-3,24-dione 3-GP	*24-Oxocholesterol* 3β-Hydroxycholest-5-en-24-one (24S,25-Epoxycholest-5-en-3β-ole)	7.79	18.27	Y	(0.34±0.03)a 0.031±0.008a
532.3898	Cholest-4-ene-3,22-dione 3-GP	*22-Oxocholesterol* 3β-Hydroxycholest-5-en-22-one	8.05	19.77	Y	(ND) 0.060±0.025a
532.3898	7β-Hydroxycholesta-4,24-dien-3-one 3-GP	*7β-Hydroxydesmosterol* Cholesta-5,24-diene-3β,7β-diol	8.67	21.79	N	(ND) 0.020±0.006a
532.3898	7α-Hydroxycholesta-4,24-dien-3-one 3-GP	*7α-Hydroxydesmosterol* Cholesta-5,24-diene-3β,7α-diol	9.29	23.65	N	(ND) 0.024±0.012a
532.3898	6-Hydroxycholesta-4,24-dien-3-one 3-GP	*6-Hydroxydesmosterol* Cholesta-4,24-diene-3β,6-diol (Cholest-24-ene-3β,5α,6β-triol/5,6-Epoxycholest-24-en-3β-olf)	9.66	24.48	N	(ND) 0.023±0.011a
534.4054	22R-Hydroxycholest-4-en-3-one 3-GP	*22R-Hydroxycholesterol* Cholest-5-ene-3β,22R-diol	6.22	9.45	Y	(ND) 0.010±0.002a
534.4054	24S-Hydroxycholest-4-en-3-one 3-GP	*24S-Hydroxycholesterol* Cholest-5-ene-3β,24S-diol	7.41 7.72	16.32 18.08	Y	(27.14±1.71) 0.510±0.082
534.4054	25-Hydroxycholest-4-en-3-one 3-GP	*25-Hydroxycholesterol* Cholest-5-ene-3β,25-diol	7.58	17.42	Y	(0.77±0.26)a 0.004±0.001a
534.4054	24R-Hydroxycholest-4-en-3-one 3-GP	*24R-Hydroxycholesterol* Cholest-5-ene-3β,24R-diol	7.88 8.24	19.21 20.71	Y	(ND) 0.061±0.006
534.4054	26-Hydroxycholest-(25R)-4-en-3-one 3-GP	*(25R),26-Hydroxycholesterol* Cholest-(25R)-5-ene-3β,26-diol	8.04	19.74	Y	(0.33±0.07)a 0.009±0.004a
534.4054	X-Hydroxycholest-4-en-3-one 3-GP	*X-Hydroxycholesterol* Cholest-5-ene-3β,X-diol	8.91	22.52	N	(ND) 0.045±0.015a
534.4054	7β-Hydroxycholest-4-en-3-one 3-GP	*7β-Hydroxycholesterol* Cholest-5-ene-3β,7β-diol	9.59	24.38	Y	(0.04±0.01)a 0.039±0.015a
534.4054	7α-Hydroxycholest-4-en-3-one 3-GP	*7α-Hydroxycholesterol* Cholest-5-ene-3β,7α-diol	10.15	26.14	Y	(<0.01)a 0.048±0.022a
534.4054	6-Hydroxycholest-4-en-3-one 3-GP	*6-Hydroxycholesterol* Cholest-4-ene-3β,6-diol (Cholestane-3β,5α,6β-triol/5,6-Epoxycholestan-3β-olg)	10.51	27.06	Y	(ND) 0.019±0.014a

550.4003	24,25-Dihydroxycholest-4-en-3-one 3-GP	*24,25-Dihydroxycholesterol* Cholest-5-ene-3β,24,25-triol (24S,25-Epoxycholest-5-en-3β-olh)	3.95 4.62	3.88 4.97	Y	(0.16±0.13)a 0.731±0.439a
550.4003	20R,22R-Dihydroxycholest-4-en-3-one 3-GP	*20R,22R-Dihydroxycholesterol* Cholest-5-ene-3β,20R,22R-triol	4.48	4.57	Y	(0.01±0.01)a 0.020±0.007a
564.4160	24(or 25)-Hydroxy-25(or 24) methoxycholest-4-en-3-one 3-GP	*Hydroxymethoxycholesterol* 3β,24(or25)-dihydroxycholest-5-ene-25(or24)-methoxide (24S,25-Epoxycholest-5-en-3β-oli)	6.18 6.68	9.32 11.18	Y	(0.12±0.02) 0.294±0.177a
		Total *24S,25-Epoxycholesterol* **24S,25-Epoxycholest-5-en-3β-ol** (24S,25-Epoxycholest-5-en-3β-ol + 3β-Hydroxycholest-5-en-24-onee + Cholest-5-ene-3β,24,25-triolh + 3β,24(or25)-hydroxycholest-5-ene-25(or24)-methoxide[i]				(0.64±0.02)a 1.123 ± 0.304a

RT G1 = Retention time/min with Gradient 1; RT G2 = Retention time/min with Gradient 2; AS = Authentic standard; Y = Yes, N= No; SD = Standard deviation; ND = Not detected, NA = Not analysed.

a Quantitative estimates based on [2H6]cholest-5-ene-3β,24(R/S)-diol internal standard and GP-tagged 3-oxo-4-ene compounds giving similar ESI-MS response.

b Quantitative estimates based on [2H7]cholest-5-en-3β-ol internal standard and GP-tagged 3-oxo-4-ene compounds giving similar ESI-MS response.

c Possible isomerisation product of cholesta-5,7,24-trien-3β-ol.

d Possible isomerisation product of cholesta-5,7-dien-3β-ol.

e 3β-Hydroxycholest-5-en-24-one is an isomerisation product of 24S,25-epoxycholest-5-en-3β-ol.

f Cholesta-4,24-diene-3β,6-diol is a likely decomposition product of cholest-24-ene-3β,5α,6β-triol and/or 5,6-epoxycholest-24-en-3β-ol.

g Cholest-4-ene-3β,6-diol is a decomposition product cholestane-3β,5α,6β-triol and/or 5,6-epoxycholestan-3β-ol.

h Cholest-5-ene-3β,24,25-triol is a hydrolysis product of 24S,25-epoxycholest-5-en-3β-ol.

i 3β,24(or25)-Dihydroxycholest-5-ene-25(or24)-methoxide is a methanolysis product of 24S,25-epoxycholest-5-en-3β-ol.

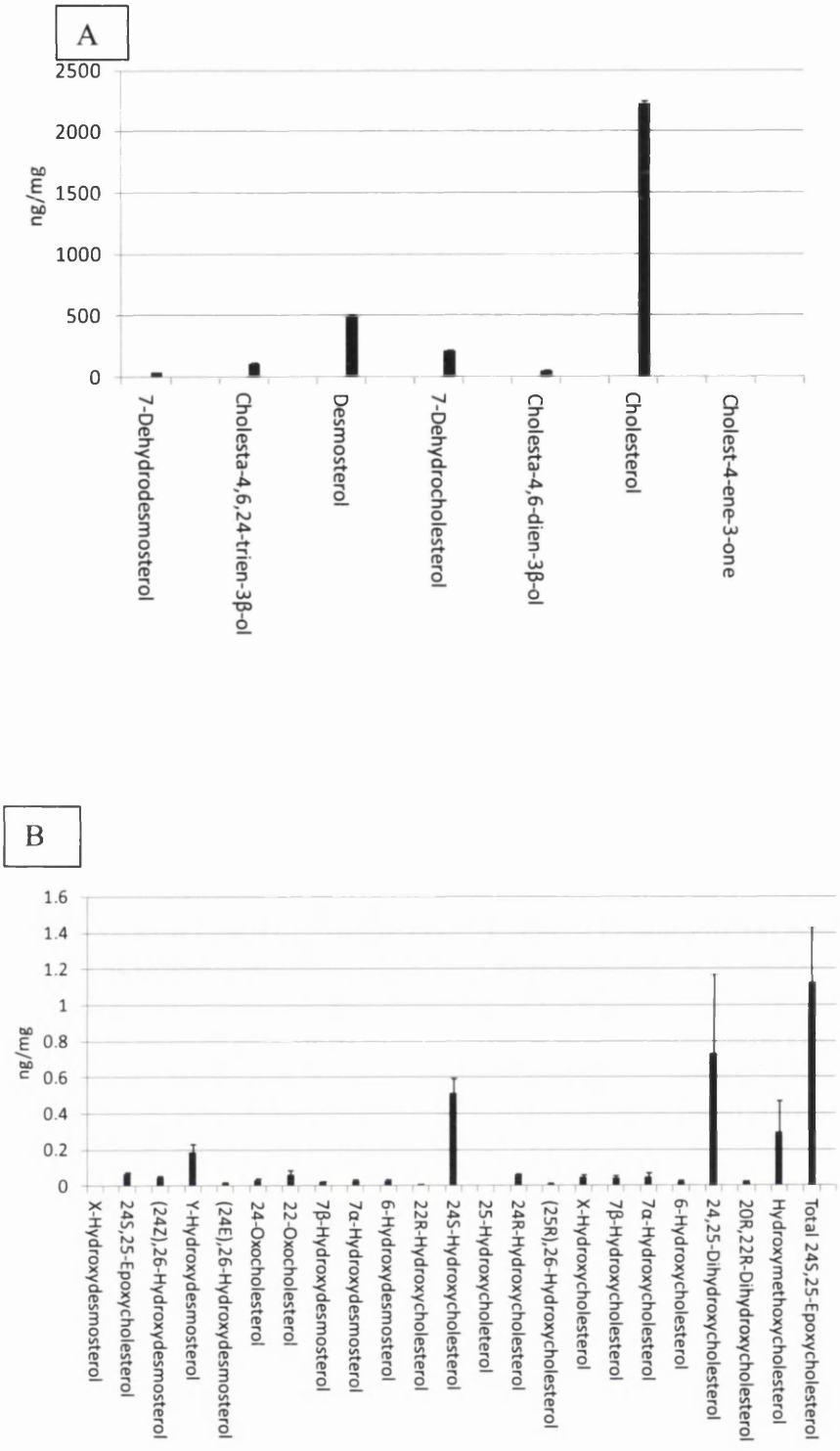

Figure 3.5 Sterols and oxysterols identified in mouse brain. Charge-tagged with GP-hydrazine (A) sterols and (B) oxysterols identified by LC-ESI-MS^n in newborn brain.

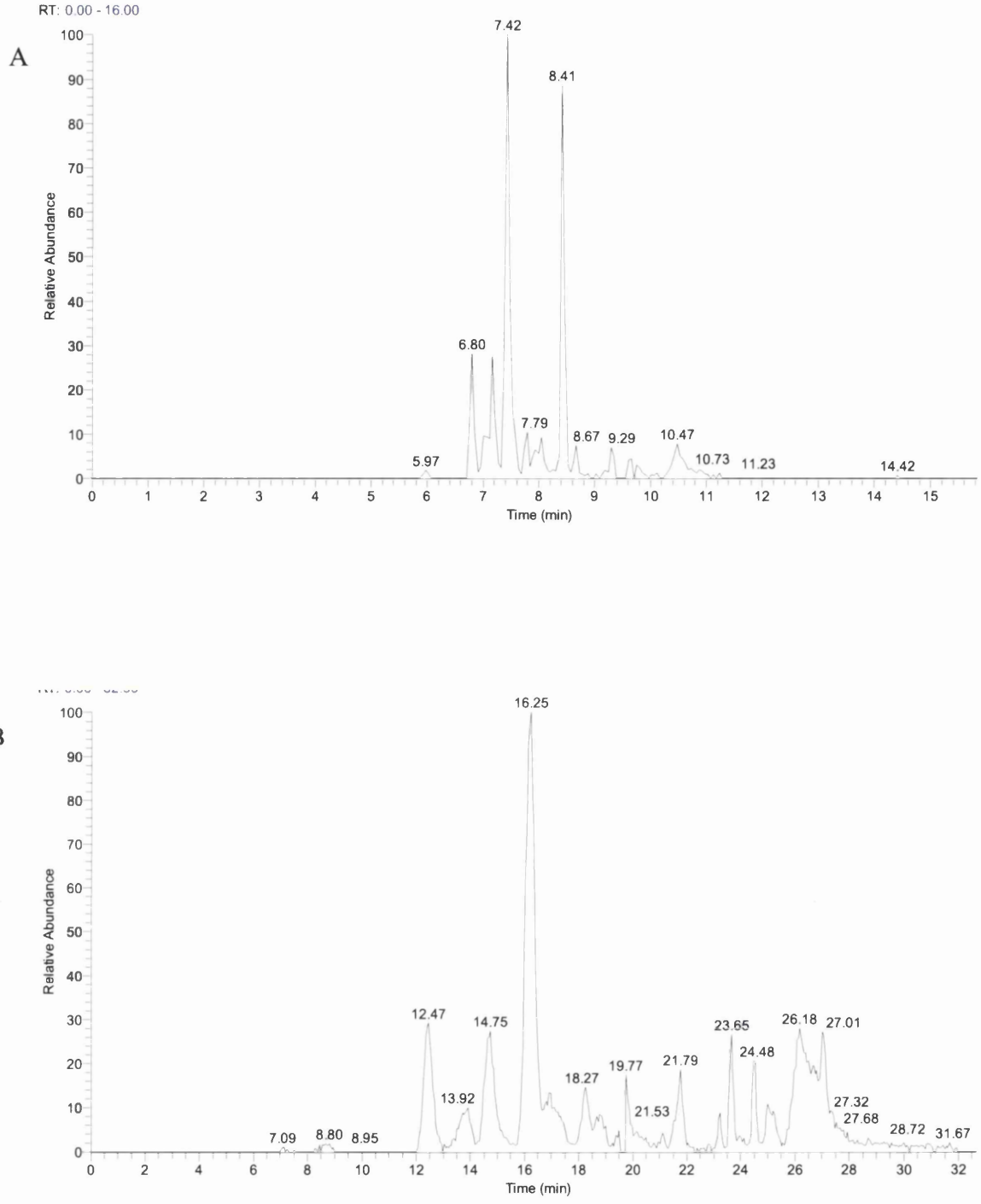

Figure 3.6 Oxo-, epoxycholesterols and hydroxydesmosterols in newborn mouse brain. RIC of *m/z* 532.3898 ± 10 ppm acquired using (A) the short and (B) long gradient.

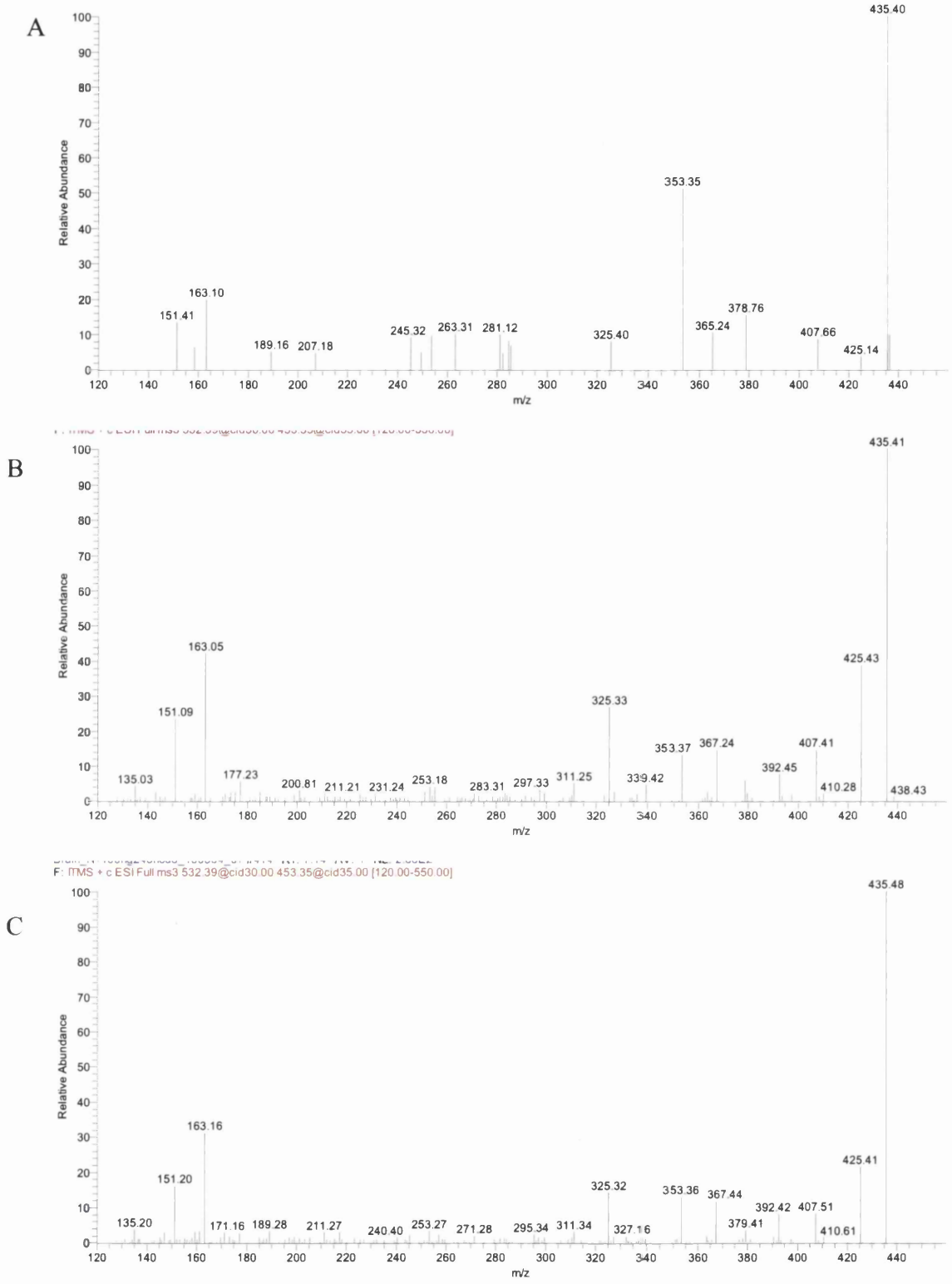

Figure 3.7 MS^3 spectra ($[M]^+ \rightarrow [M-79]^+ \rightarrow$) spectra assigned to GP-tagged oxysterols: (A) X-hydroxydesmosterol (X-HD), (B) 24S,25-epoxycholesterol (24,25-EC), (C) (24Z),26-hydroxydesmosterol (cholesta-5,24Z-diene-3β,26-diol, 26-HD(24Z)).

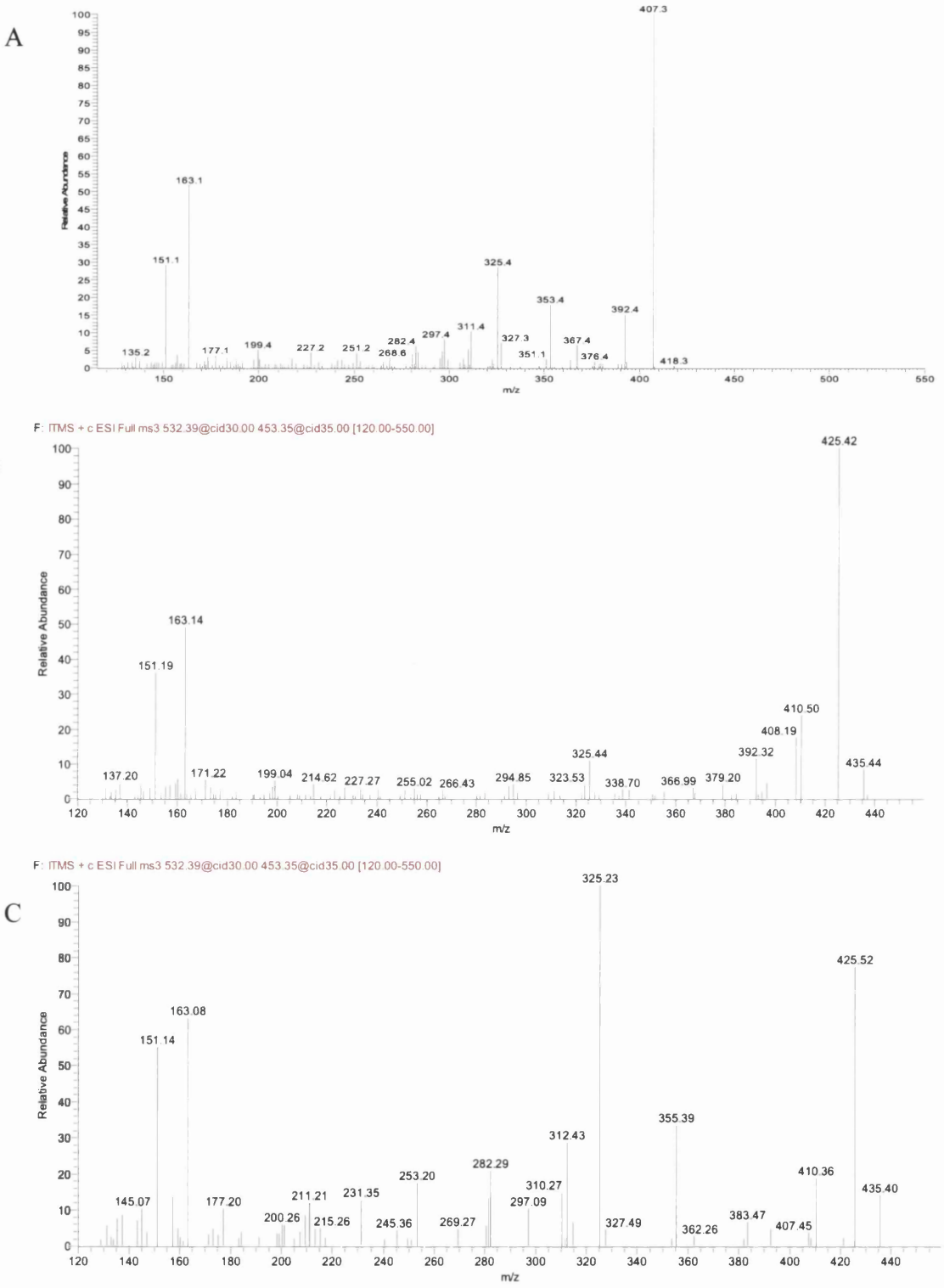

Figure 3.8 MS^3 spectra ($[M]^+ \rightarrow [M-79]^+ \rightarrow$) and (F) $[M]^+ \rightarrow [M-97]^+ \rightarrow$ spectra assigned to GP-tagged oxysterols. (A) Y-hydroxydesmosterol (Y-HD), (B) 24-oxocholesterol (24-OC), (C) 22-oxocholesterol (22-OC).

The peak with retention time 8.05 min in Figure 3.6A subjected to MS^3 fragmentation gave a spectrum characteristic of GP-tagged 22-oxocholesterol (0.060 ± 0.025 ng/mg) (Figure 3.8C). Similar to GP-tagged 24-oxocholesterol, the MS^3 spectrum of 22-oxocholesterol shows a distinctive peak at *m/z* 425 ($[M-79-CO]^+$), however, the base peak is at *m/z* 325 ('*e) with additional peaks at *m/z* 297 ('*e-CO) and *m/z* 282 ('*e-CO-NH) (Figure 3.8). Other intense peaks are at 355 (*f') and 312 (*f'-CO-NH) in addition to the low mass triad 151, 163 and 177. The '*e ion at *m/z* 325 results from cleavage of the C-17 – C-20 bond β to the 22-oxo group, probably via a McLafferty-like rearrangement eliminating the side-chain as an enol [148]. The *f' fragment ion is generated by a cleavage α to the 22-oxo 15 group with elimination of either a ketene or CO and an alkene. Further CO and NH moieties are eliminated from the remnants of the derivatising group to give ions at *m/z* 327 and 312, respectively. 22-Oxocholesterol has not previously been reported in the literature regarding brain tissue, however the role of side-chain has been discussed in older literature [187, 188]. The dominant peak in the RIC of *m/z* 532.3898 is at 7.42 min in Figure 3.6A and 16.25 min in Figure 3.6B (0.188 ± 0.046 ng/mg) and is not easy to assign. The MS3 ($[M]^+ \rightarrow [M-79]^+ \rightarrow$) spectrum is completely dominated by the $[M-79-18]^+$ ion at *m/z* 435. This suggests the analyte readily loses H_2O from the $[M-79]^+$ ion, possibly forming a conjugated diene derived from a sterol with hydroxy and alkene groups α,β to one another. The presence of minor ions at *m/z* 151, 163, 325 ('*e) and 353 ('*f) indicated that the unsaturation and hydroxylation are on the side-chain. As the spectrum showed the dominating loss of water, we applied a different pattern of MS^3 fragmentation. Only one peak is evident appearing at 7.42 min, and the corresponding MS^3 spectrum is shown in Figure 3.8A. The spectrum is compatible with a GP-tagged sterol unsaturated and hydroxylated in the side-chain, possibly 23-hydroxydesmosterol. There is a precedent for C-23 hydroxylation is hypothesised as a part of bile acid synthesis, however 23-hydroxylation of desmosterol has not been reported [189]. Interestingly, cholesterol free mouse has an essentially unaltered pattern of bile acid pattern even though desmosterol is the dominant sterol [190]. It should be noted, however, that C-23 is an allylic site in desmosterol and is thus susceptible to non-enzymatic oxidation. An equivalent peak was not observed in the corresponding chromatogram from young adult female brain. The partial identification of a hydroxylated desmosterol encouraged us to search for further isomers of this molecule. Pikuleva and Javitt demonstrated that desmosterol can be 26-hydroxylated in vitro by human recombinant CYP27A1 [191], while Heverin et al

have identified this oxysterol in the cholesterol free mouse [190]. Brain-specific Cyp46a1 is known to hydroxylate cholesterol at 24- and 27-positions [107], however desmosterol is not recognised by this enzyme as a substrate [172], therefore it is unlikely that Cyp46a1 can contribute to formation of 26-hydroxlated desmosterol. The retention time of authentic charge-tagged (24Z),26-hydroxydesmosterol (cholesta-5,24Z-diene-3β,26-diol) run with the short gradient is 7.16 min and a peak appearing in the RIC of *m/z* 532.3898 at this retention time (0.048 ± 0.009 ng/mg) gives a spectrum essentially identical to that of the authentic standard (Figure 3.7C). By using the longer chromatographic gradient (24Z),26-hydroxydesmosterol was completely separated from the second peak of 24S,25-epoxycholesterol (Figure 3.6A and Figure 3.6B). Hydroxylation of the terminal carbon of desmosterol introduces Z or E stereochemistry about the C-24-25 double bond, and these isomers are readily resolved by utilising the extended gradient allowing the identification also of (24E),26-hydroxydesmosterol (cholesta-5,24E-16 diene-3β,26-diol) eluting at 16.85 min in the chromatogram of newborn brain (0.015 ± 0.004 ng/mg). A minor peak in Figure 3.6A is seen at 5.97 min, the MS^3 spectrum (Figure 3.7A) is again compatible with a GP-tagged hydroxydesmosterol with an added hydroxy group on the side-chain (0.002 ± 0.002 ng/mg). Further scrutinised RIC of *m/z* 532.3898 (Figure 3.6A) revealed peaks at 8.67 and 9.29 min that give MS^3 spectra compatible with GP-tagged 7β- and 7α-hydroxydesmosterols, respectively (0.020 ± 0.006 and 0.024 ± 0.012 ng/mg). The 7α isomer is probably formed, at least in part, endogenously in a Cyp catalysed hydroxylation of desmosterol as Cyp7a1 has activity towards desmosterol. MS^3 spectrum of the peak appearing at 9.66 min corresponds to a GP-tagged 6-hydroxydesmosterol (0.023 ± 0.011 ng/mg), which can be derived from 5,6-epoxydesmosterol [126]. The hydroxydesmosterol molecules described here have not previously been found in brain, and of the isomers characterised only (24Z),26-hydroxydesmosterol is found in the young adult.

Dihydroxycholesterols

Introduction of two hydroxyl groups to a cholesterol molecule and pairing to GP hydrazone will produce an ion of *m/z* 550.4003. Figure 3.9 shows a relevant RIC which reveals two major peaks eluting at 3.95 min and 4.62 min corresponding to the *syn* and *anti* conformers of GP-tagged 24,25-dihydroxycholesterol (0.731 ± 0.439 ng/mg) (Figure 3.11A). The hydroxylation at C-24 and C-25 is indicated by fragment ions *m/z* 325 ('*e), 353 ('*f), 367 ('*g) and 381 ('*h). The presence of hydroxylation at C-25 is further confirmed by the dominating ion *m/z* 453 originating from the loss of water from $[M-79]^+$ ion. 24,25-

Dihydroxycholesterol can he produced by hydrolysis of unstable 24S,25-epoxycholesterol. 24S,25-Epoxycholesterol can be also undergo methanolysis giving hydroxymethoxycholesterol isomers (0.294 ± 0.177 ng/mg) (Figure 3.10). Analysis of the RIC of *m/z* 564.4160 showed a peak doublet with retention times and MS^3 fragmentation profiles identical to those obtained during the analysis of the GP-tagged reference standard (Figure 3.11A). The $[M-79-32]^+$ ion (*m/z* 453) is formed during the elimination of a methoxy group. The combined concentration of 24S,25-epoxycholesterol (0.067 ng/mg), 24-oxocholesterol (0.031 ng/mg), 24,25-dihydroxycholesterol (0.731 ng/mg) and hydroxymethoxycholesterol (0.294 ng/mg) equals 1.123 ± 0.304 ng/mg. 24S,25-Epoxycholesterol is a by-product of the mevalonate pathway, so the comparatively high level of this oxysterol is not unexpected for a developing tissue with high rate of cholesterol synthesis.

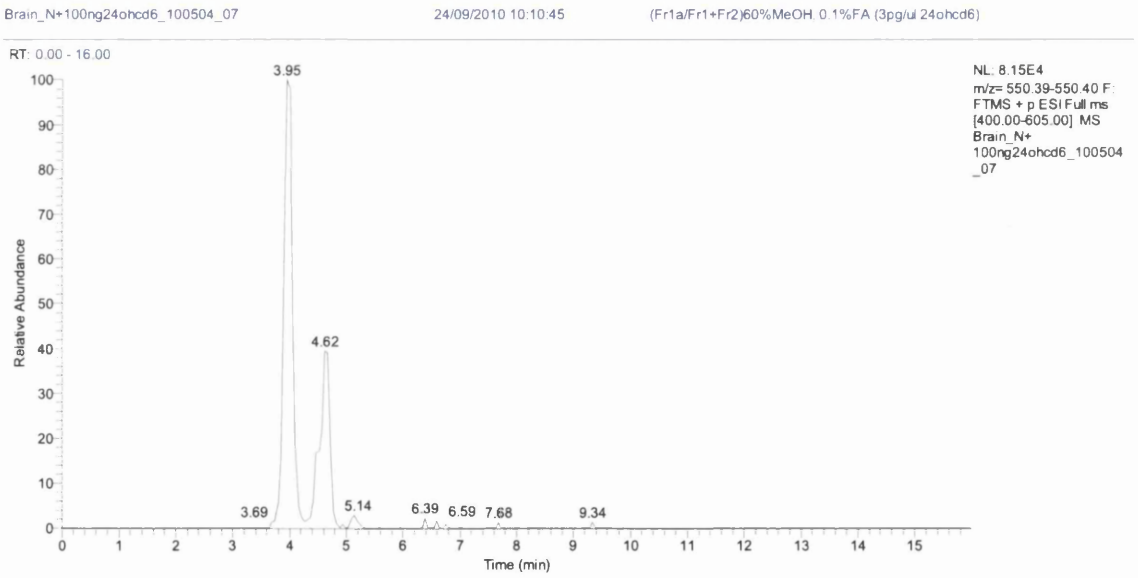

Figure 3.9 Dihydroxycholesterols in brain of newborn mouse. RIC of *m/z* 550.4003 ± 10 ppm recorded using the short gradient.

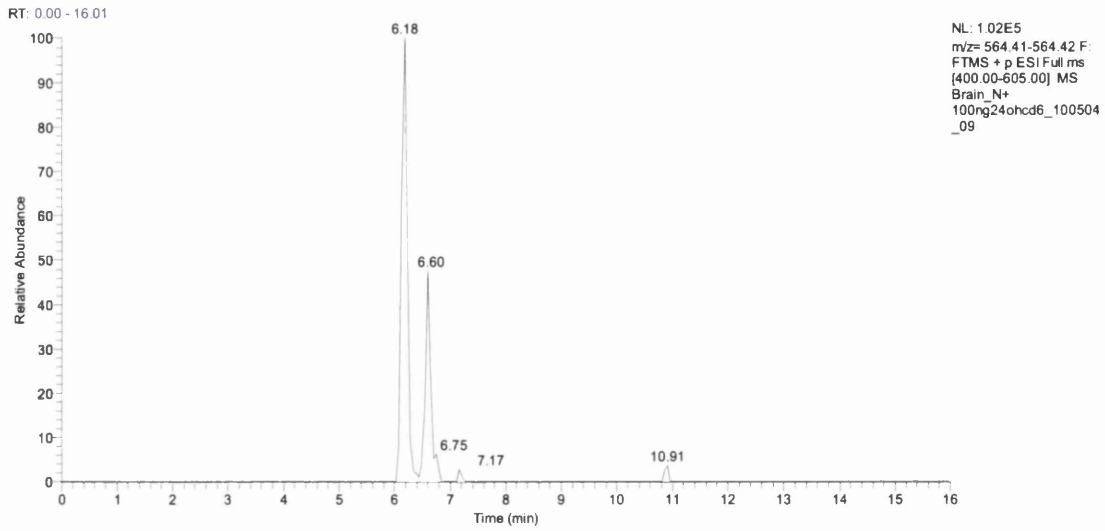

Figure 3.10 RIC of *m/z* 564.4160 ± 10 ppm obtained using the short gradient.

Figure 3.9 reveals a shoulder (4.48 min) on the leading edge of the peak at 4.62 min. This is partially resolved with the longer gradient. Acquired MS^3 spectrum point at the presence of 20R,22R-dihydroxycholesterol (0.020 ± 0.007 ng/mg) (Figure 3.11B) providing the first direct evidence for the presence of this cholesterol metabolite in brain. 20R,22R-Dihydroxycholesterol is an intermediate in the conversion of cholesterol to pregnenolone. Its presence in newborn brain lends weight to the argument that neurosteroids are formed in brain, rather than just passengers from the circulation.

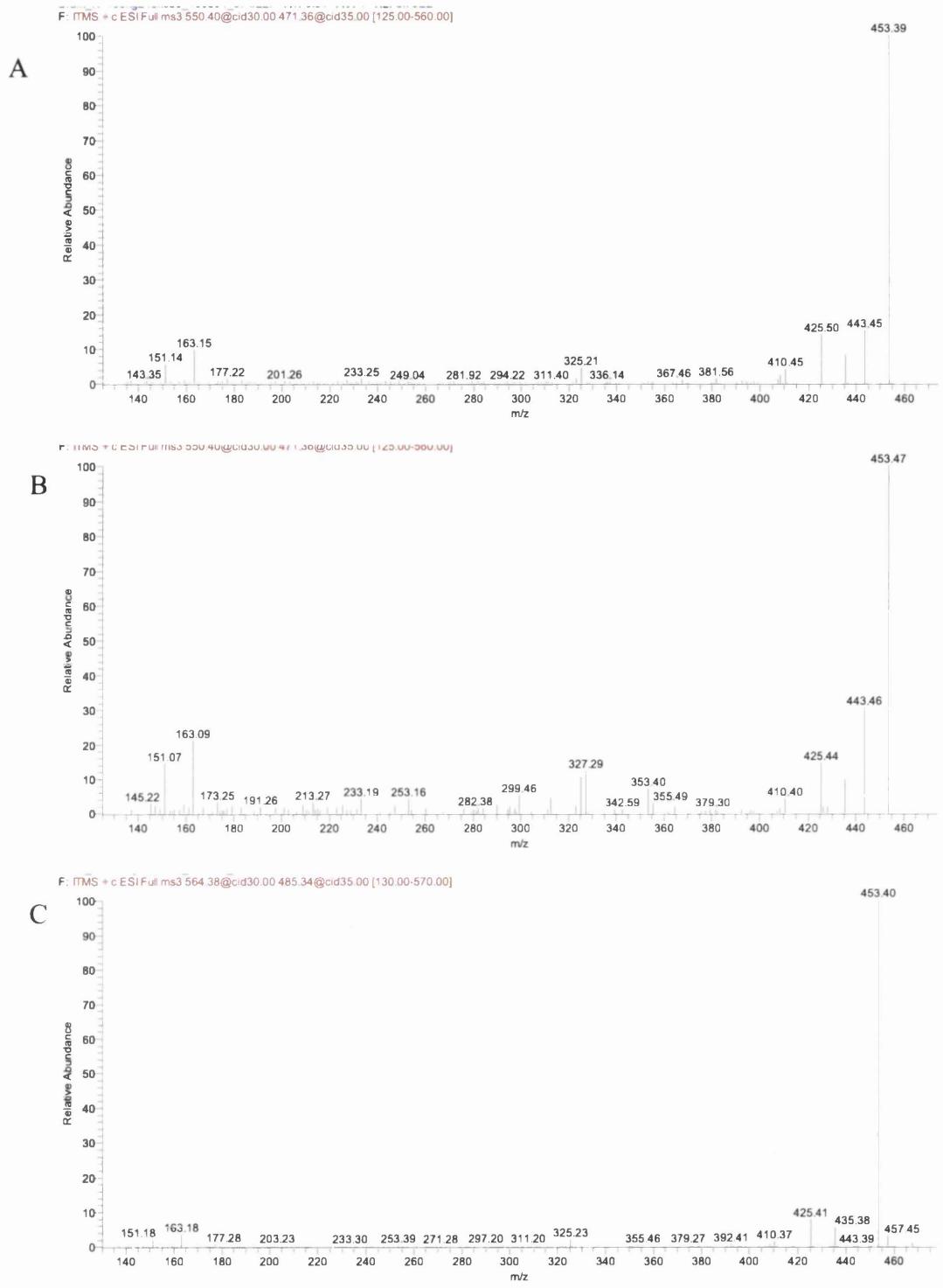

Figure 3.11 MS^3 ($[M]^+ \rightarrow [M-79]^+ \rightarrow$) spectra assigned to GP-tagged (A) 24,25-dihydroxycholesterol (24,25-DiHC) and (B) 20R,22R-dihydroxycholesterol (20,22-DiHC) and 24-hydroxy-25-methoxycholesterol (or the 25-hydroxy-24-methoxy isomer, 24,25-HMC).

Sterols in newborn mouse brain

During the SPE fractionation of the brain extract, cholesterol and its precursor's desmosterol and 7-dehydrocholesterol eluted in fraction 3 (SPE1-FR3). The sterols were derivatised with GP reagent and analysed by LC-MS. Obtained eluent contained a high concentration of cholesterol. To avoid overloading of LC-MS system the solution was diluted by a factor of 10,000 – 20,000 prior to injection. The RIC of *m/z* 518.4105 corresponding to GP charge-tagged cholesterol is shown in Figure 3.12. The major component elutes at 12.83 min and gives an MS3 spectrum identical to that of GP-tagged cholesterol (Figure 3.13).The concentration of cholesterol in newborn brain was calculated to be 2.221 ± 0.032 μg/mg. Similar level was found utilising a GC-MS methodology in work of Marcos et al [192]. These values compare with levels in the young female adult determined here of 16.026 ± 0.758 μg/mg and with literature values for the adult of 10 – 20 μg/mg (9;21;31;35). Cholest-4-en-3-one is also present in newborn brain but at a level of about 0.1% that of cholesterol.

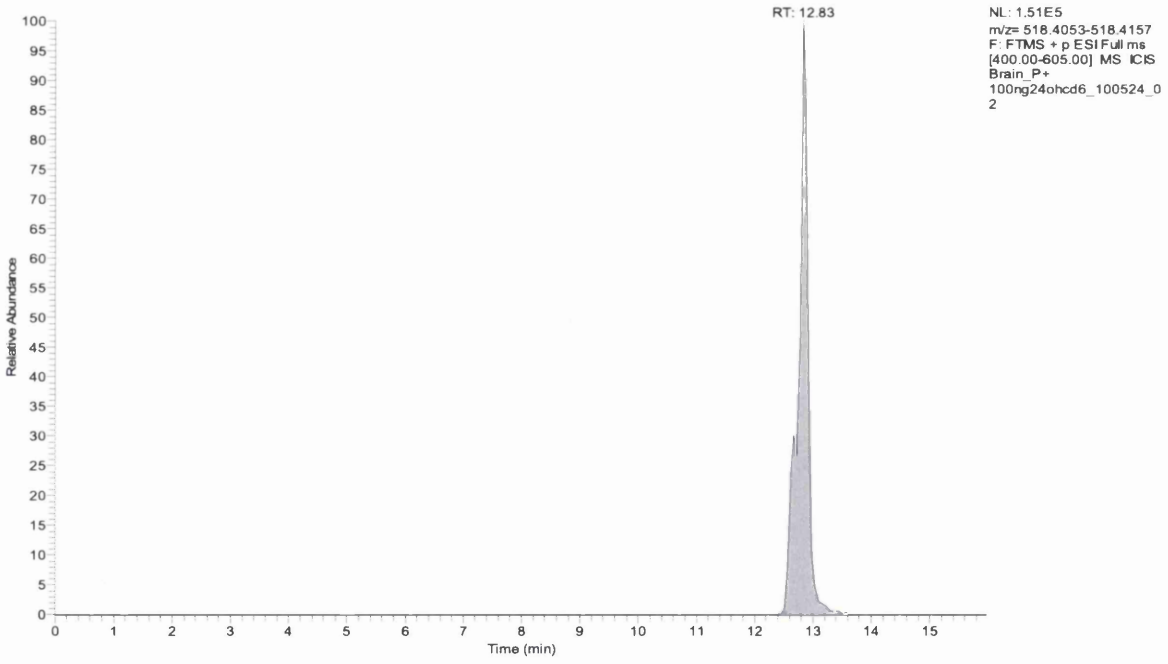

Figure 3.12 Cholesterol in brain of newborn mouse. RIC of *m/z* 518.4105 ± 10 ppm generated with the short gradient.

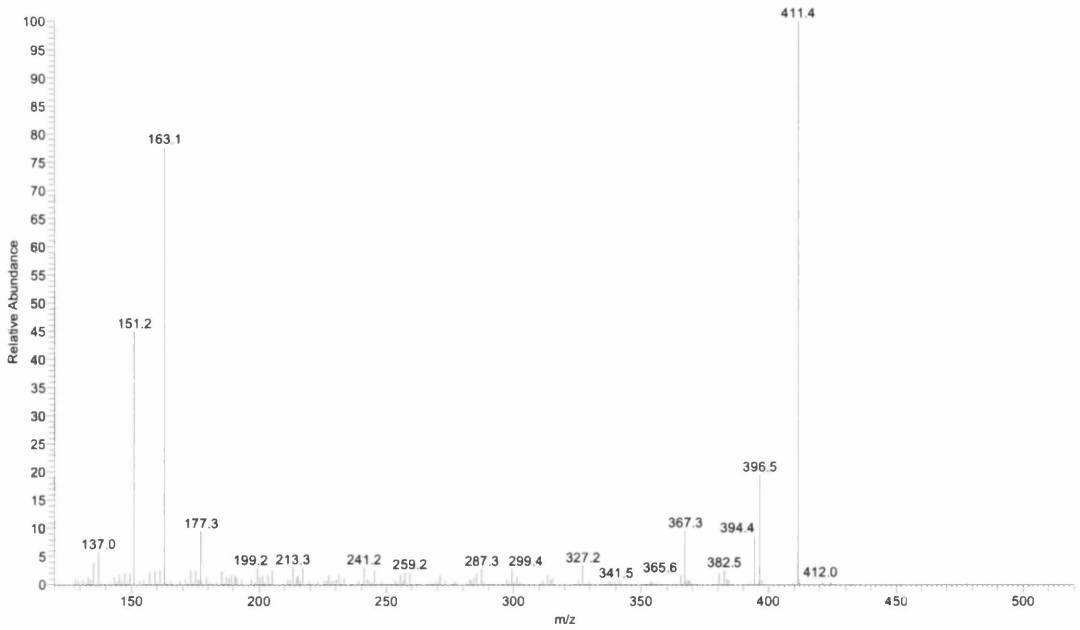

Figure 3.13 MS^3 ($[M]^+ \rightarrow [M-79]^+ \rightarrow$) spectra assigned to GP-tagged cholesterol

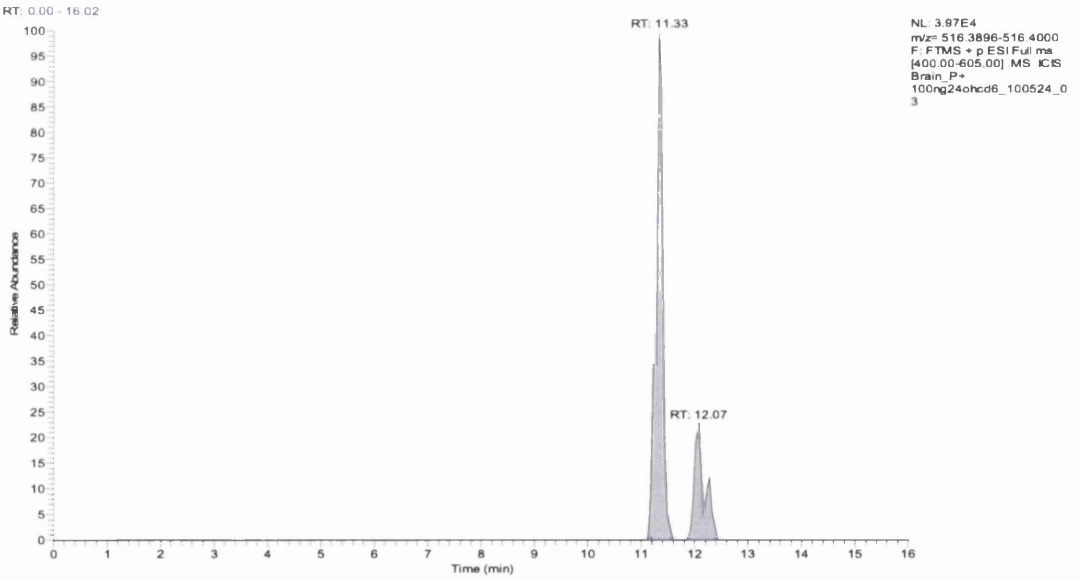

Figure 3.14 Dehydrocholesterols in newborn mouse brain. RIC of *m/z* 516.3948 ± 10 ppm generated with the short gradient.

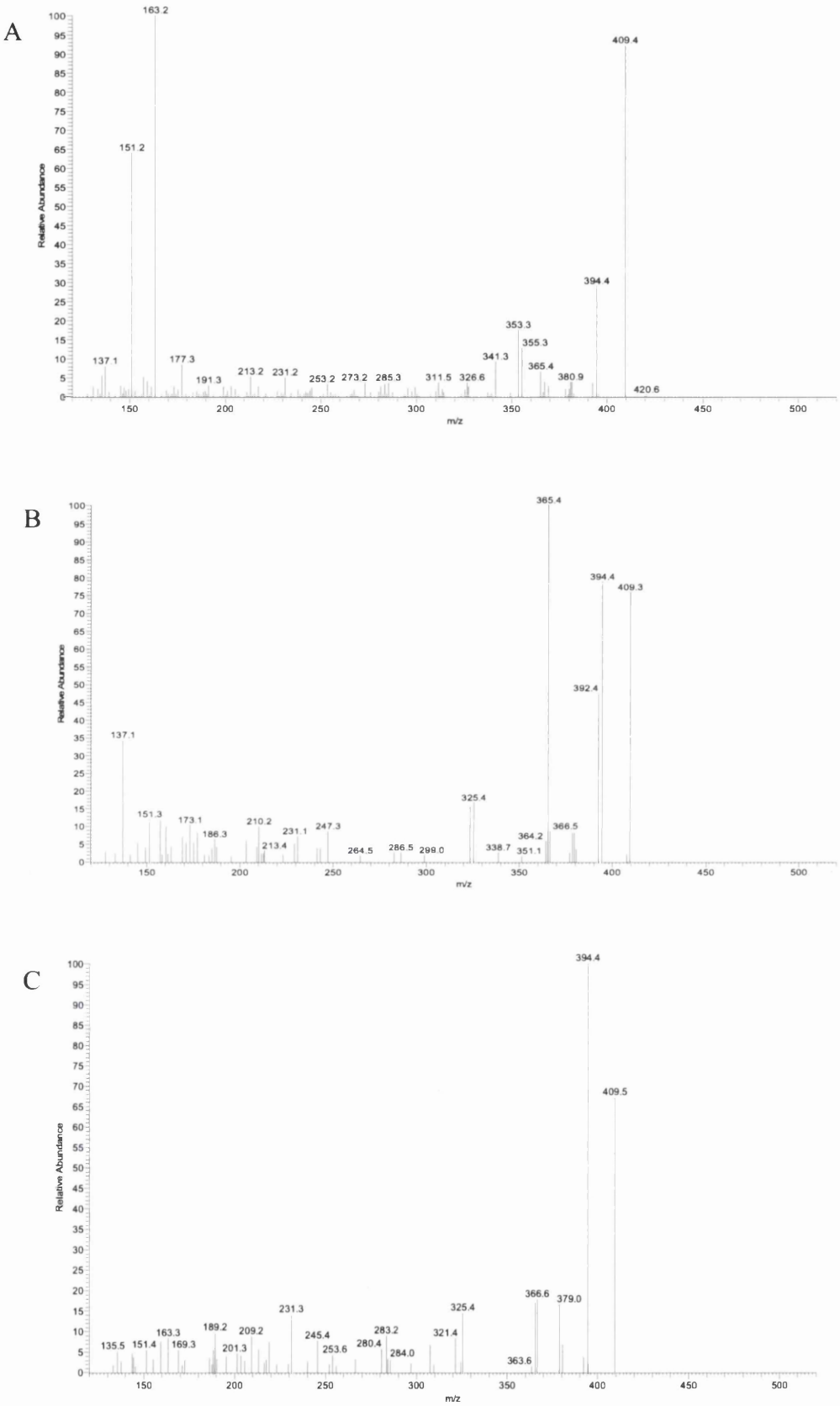

Figure 3.15 MS^3 spectra of peaks eluting at 11.33, 12.07 and 12.28 min and corresponding to GP-tagged desmosterol (A), 7-dehydrocholesterol (B) and cholesta-4,6-dien-3β-ol (C).

The RIC for *m/z* 516.3948 corresponding in *m/z* to GP-tagged desmosterol and 7-dehydrocholesterol revealed one major peak with a second appearing as a doublet (Figure 3.14). The first peak eluting at 11.33 min was identified as GP-tagged desmosterol (493.986 ± 18.062 ng/mg) (Figure 3.15A). This corresponds to about 20% of the total sterol content of newborn brain and agrees well with the value determined by Tint et al for 22 day foetus [170]. Tint et al also showed a reduced expression of neuronal 24-dehydrocholesterol reductase (*Dhcr24*) in the foetus and newborn animal which accounts for the high level of desmosterol. The first component of the second peak eluting at 12.07 min gives an MS^3 spectrum identical to that of GP-tagged 7-dehydrocholesterol (Figure 3.15B). The second component at 12.28 min gives an MS^3 spectrum which we identify as cholesta-4,6-dien-3β-ol (Figure 3.15C). This may be an isomerisation product of 7-dehydrocholesterol. Each analyte is present at high concentration in newborn brain: i.e. 210.484 ± 8.319 ng/mg, and 46.692 ± 6.736 ng/mg, respectively.

High concentration of desmosterol and 7-dehydrocholesterol which are cholesterol precursors shows a high rate of cholesterol synthesis during neonatal development. These also agrees with earlier publications which show that in the developing foetus and suckling newborn the rates of sterol accumulation in brain are greatest [94]. Quan et al measured both desmosterol and cholesterol levels in the CNS of mice and at their earliest time point of 2 days-old, desmosterol made up 30% of total sterols, while at day 15 desmosterol had "essentially disappeared" [94]. The high levels of desmosterol in the newborn animal are particularly interesting in light of recent data indicating that desmosterol can suppress SREBP processing and activate LXR target genes [193, 194]. The precursor of desmosterol is 7-dehydrodesmosterol. A component eluting at 10.85 min in the RIC for *m/z* 514.3792 (Figure 3.16) gives an MS^3 spectrum commensurate with that expected for GP-tagged 7-dehydrodesmosterol (41.159 ± 2.503 ng/mg), Figure 3.17A, and a latter eluting peak at 11.59 min is assigned to cholesta-4,6,24-trien-3β-ol (113.33 ± 7.018) (Figure 3.17B). This may be an isomerisation product of 7-dehydrodesmosterol. Again a high level of cholesterol precursors in newborn brain can be explained by a low expression of *Dhcr24*.

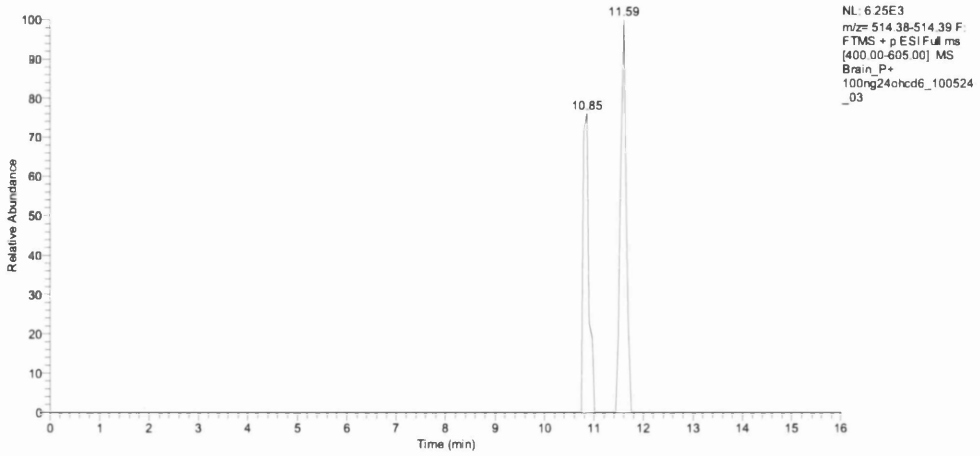

Figure 3.16 RIC of *m/z* 514.3792 ± 10 ppm corresponding to cholesterol precursors in newborn mouse brain.

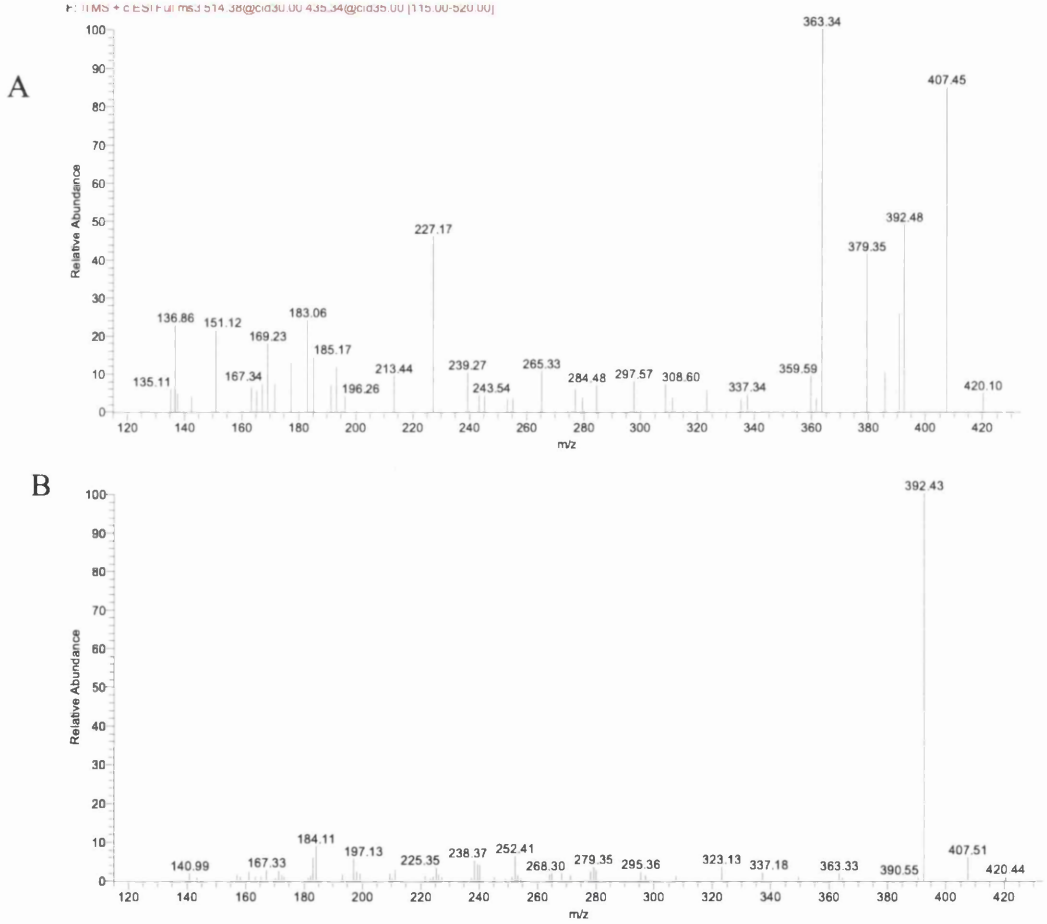

Figure 3.17 MS3 spectra of peaks eluting at 10.85 and 11.59 min in RIC 514.3792 presumptively identified as GP-tagged 7-dehydrodesmosterol (A) and cholesta-4,6,24-trien-3β-ol (B), respectively. The presumptive identifications are made due to the absence of authentic standards.

3.3 Conclusion

In this work was identified and quantified a high number of oxysterols and cholesterol precursors. The most abundant oxysterol found is an "exit" metabolite of cholesterol – 24S-hydroxycholesterol. The other monohydroxysterols found were 25-, 26-, 7α, 7β, 6β - hydroxycholesterol. 25-Hydroxycholesterol is implicated in the immune response [133], however its role in the brain remains unknown. 26- and 7α-hydroxycholesterol are precursors of bile acid biosynthesis, although 7α-hydroxylase is a liver specific enzyme and presence of this oxysterol is probably derived from the circulation. In this work was detected and quantified the C21-neurosteroid progesterone and its biosynthetic precursors 22R-hydroxycholesterol and 20R,22R-dihydroxcholesterol in newborn brain. We confirmed the presence of major amounts of the LXR and Insig ligand 24S,25-epoxycholesterol in developing nervous tissue [120]. Moreover, a number of oxysterols derived from desmosterol were identified. This is the first report of the (24Z),26-hydroxydesmosterol isomer in a biological system.

Chapter 4

4 Analysis of oxysterols in Dhcr7D3-5/T93M mouse brain

4.1 Introduction

Deficiency of 3β-hydroxysterol-D7-reductase (7-dehydrocholesterol reductase, DHCR7) in humans is associated with Smith–Lemli–Opitz syndrome (SLOS). This autosomal recessive disorder is caused by malfunction of enzyme catalysing conversion of 7-dehydrocholesterol into cholesterol in the last step of cholesterol biosynthesis via the Kandustch–Russell pathway (Figure 1.2) [195]. Increased levels of the cholesterol precursor 7-dehydrocholesterol, and of 8-dehydrocholesterol as a consequence of DHCR7 inefficiency accumulate in tissues and in the circulation and serve as a diagnostic marker [196]. The phenotype includes dysmorphia and mental retardation [197, 198]. SLOS occurs at a relatively high incidence rate varying from 1 in 10,000 to 1 in 60,000. For Caucasian populations carrier frequency for mutant alleles may be as high as 1 in 30, but it is probable that the condition often goes undiagnosed as patients with a mild disorder may have little evident phenotype, while early foetal loss may result in the severely affected [197].

In this work were used brain samples derived from heterozygous animals, containing one null allele (deletion of coding exons 3,4,5) and one T93M mutation on Dhcr7, i.e. Dhcr7D3-5/T93M [192, 199]. Homozygous animals die shortly after birth [200, 201], while the animals used in this work carry a hypomorfic mutation and present only a mild phenotype.

The mechanisms responsible for formation of the phenotype are still not elucidated. It is not clear whether the symptoms are developing as a consequence an accumulation of 7-dehydrocholesterol or, perhaps, 7-dehydrocholesterol is subjected to further metabolism generating abnormal, toxic compounds. In this study will be analysed the sterol content of the brain with disrupted mechanism of cholesterol biosynthesis leading to an accumulation of 7-dehydrocholesterol. The compensatory mechanism for reduced synthesis of cholesterol will be investigated as well as possible downstream metabolites of 7-dehydrocholesterol.

4.2 Results

In mammalian brain oxysterols are dominated by the excess of cholesterol. In Autoxidation of cholesterol can lead to production of artificial oxysterols at levels comparable to those found endogenously. 7-Dehydrocholesterol, a hallmark of SLOS, is prone to autoxidation at even higher degree than cholesterol [202]. In order to reduce the risk of formation of autoxidation products of these sterols they were separated from oxysterols at an early stage of sample preparation via SPE methodology.

Cholesterol and dehydrocholesterols

Dehydrocholesterols oxidised with Cholesterol oxidase and GP charge-tagged give an $[M]^+$ ion of *m/z* of 516.3948. The RIC recorded using a short gradient for this *m/z* from newborn SLOS mouse brain is shown in Figure 4.1 A. The MS^3 ($[M]^+ \rightarrow [M-79]^+ \rightarrow$) spectrum of the major peak eluting at 11.07 min (Figure 4.1 C) shows low mass fragment ions at *m/z* 137 ($*b_1$-26) and 151 ($*b_1$-12) characteristic of the GP-derivatised 3-oxo-4,7-diene structure [3]. Other characteristic ions include *m/z* 409 formed by loss of CO group from $[M-79]^+$ ion, *m/z* 394 formed by the additional loss of NH, and *m/z* 365 corresponding to the carbocation of the triply unsaturated sterol. The level of 7-dehydrocholesterol in the brain of the SLOS mouse was measured to be 316.49 ± 75.61 ng/mg (n = 4, mean ± SE) Levels of oxysterols and sterols are detailed in Table 3.1. and Figure 3.1. As is evident in Figure 4.1 A, a later eluting component appears as a shoulder to the peak corresponding to 7-dehydrocholesterol. This is identified as 8-dehydrocholesterol (cholesta-5,8(9)-dien-3β-ol) (Figure 4.1 D). The MS^3 spectrum is quite different to that of the 7-dehydrocholesterol isomer, showing far less intense peaks at *m/z* 365, 151 and 137, but a more prominent one at *m/z* 231. The level of this isomer was estimated to be 133.58 ± 33.75 ng/mg in SLOS animals. As 8-dehydrocholesterol is believed to be formed from 7-dehydrocholesterol [203], their combined abundance, 450.06 ng/mg, is representative of the immediate cholesterol precursors in the Kandutsch-Russell pathway.

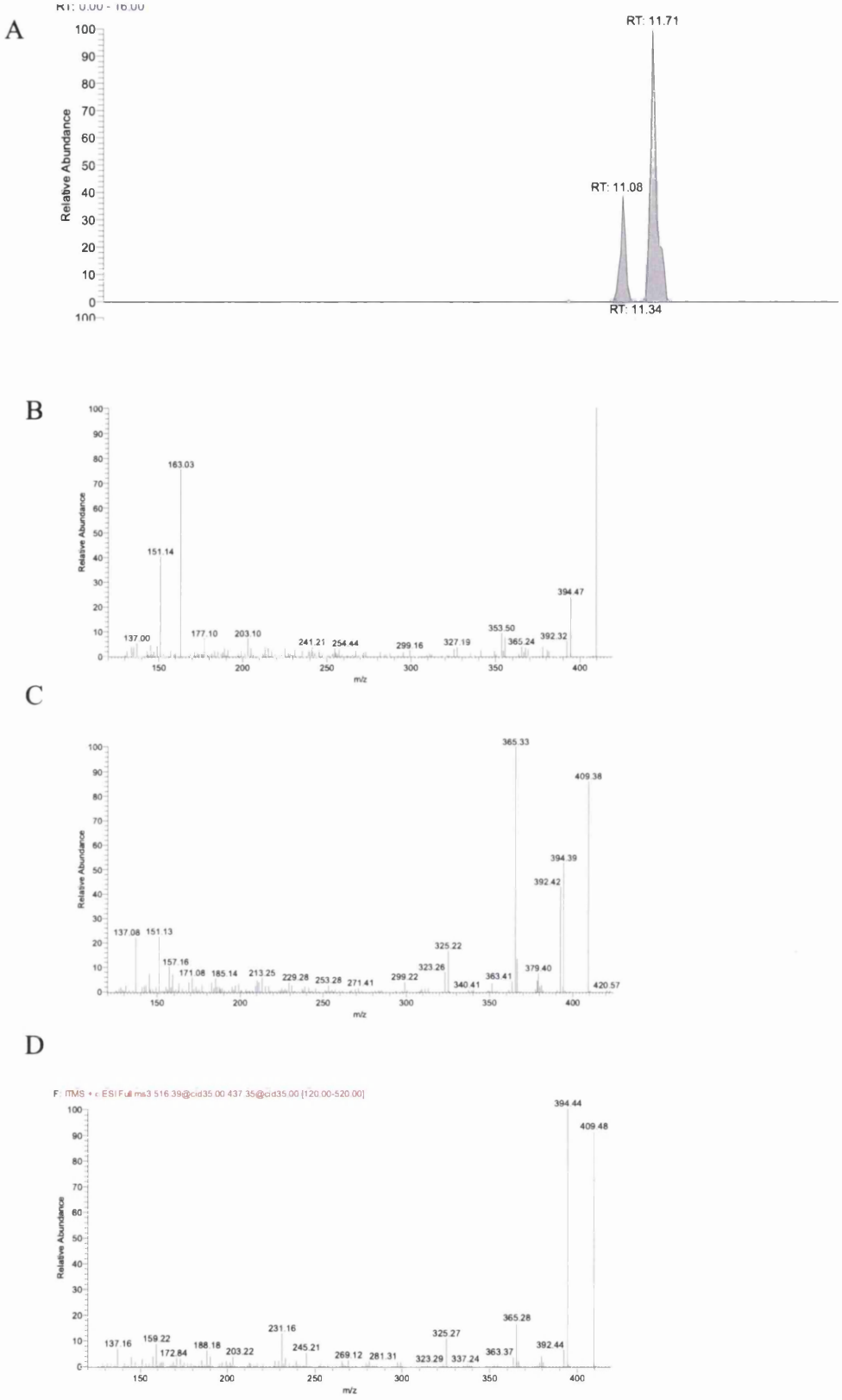

Figure 4.1 Dehydrocholesterols in SLOS mouse brain. (A) RIC of *m/z* 516.3948 ± 10 ppm generated with the short gradient. (B-D) MS^3 spectra of peaks eluting at 11.08 and 11.71 min and peak eluting as shoulder to the peak of RT 11.71 min.The MS^3 spectra correspondto GP-tagged desmosterol, 7-dehydrocholesterol and 8(14)-dehydrocholesterol respectively.

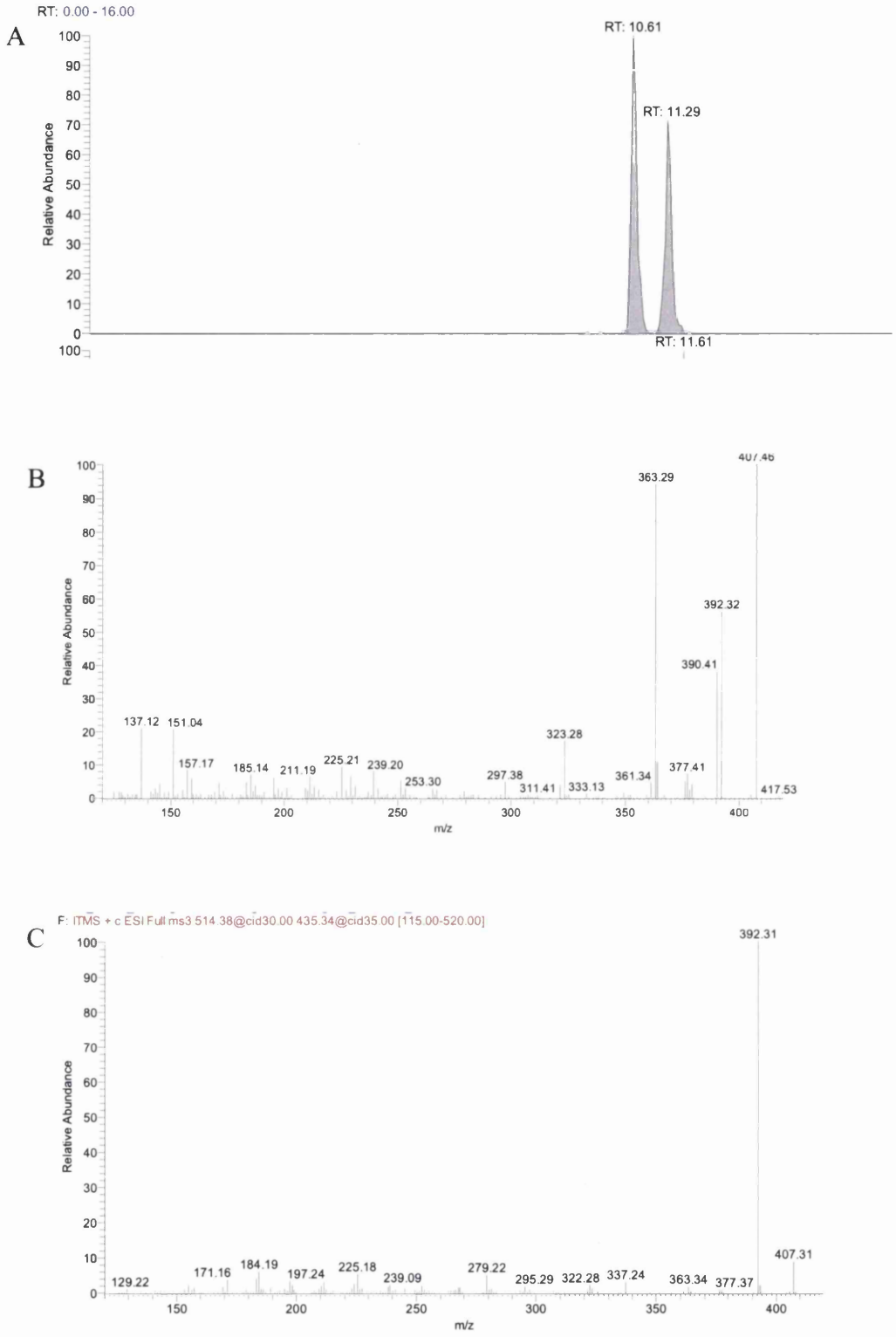

Figure 4.2 RIC for m/z 514.3792 corresponding to dehydrodesmosterols in SLOS mouse brain. (A) MS3 spectrum of peak eluting at 10.61 min corresponding to 7-dehydrodesmosterol (cholesta-5,7,24-trien-3b-ol) (B) and 11.29 min corresponding to 8-dehydrodesmosterol (cholesta-5,8(9),24-trien-3b-ol) (C).

Table 4.1 Unesterified sterol content of new born SLOS brain determined by LC-MS using the LTQ-Orbitrap

Identified structure after treatment with cholesterol oxidase	Inferred compound common name (systematic name)	$[M]^+$ of GP (*m/z*)	RT/min (Grad 1)	RT/min (Grad 2)	SLOS Brain (ng/mg)	Authentic Standard
Cholesta-4,7,24-triene-3-one 3-GP	7-Dehydrodesmosterol (Cholesta-5,7,24-trien-3βol)	514.3792	10.61		135.75 ± 30.99	No
Cholesta-4,8,24-triene-3-one 3-GP	Cholesta-5,8,24-trien-3β-ol	514.3792	11.29		79.04.76 ± 34.31	No
Cholesta-4,24-diene-3-one 3-GP	Desmosterol (Cholesta-5,24-dien-3β-ol)	516.3948	11.08		130.02 ± 30.01	Yes
Cholesta-4,7-diene-3-one 3-GP	7-Dehydroxycholesterol (Cholesta-5,7-dien-3β-ol)	516.3948	11.71		316.49 ± 75.61	Yes
Cholesta-4,8(9)-diene-3-one 3-GP	Cholesta-4,8(9)-dien-3β-ol	516.3948	11.91		133.58 ± 33.75	Yes
Cholest-4-en-3-one 3-GP	Cholesterol (Cholest-5-en-3β-ol)	518.4105	12.42		1531.48 ± 240.93	Yes
24S,25-Epoxycholest-4-en-3-one 3-GP	24S,25-Epoxycholesterol (3β-hydroxycholest-5-en-24S,25-epoxide)	532.3898	6.68 6.94	12.28 13.68	(0.024 ± 0.004	Yes
26-Hydroxycholesta-4,24(Z)-diene-3-one 3-GP	(24Z)26-Hydroxydesmosterol (Cholesta-5,24(Z)-dien-3β-ol)	532.3898	7.10	14.56	0.016	Yes
23-Hydroxycholesta-4,24-dien-3-one-3GP	23-Hydroxydesmosterol (Cholesta-5,24-dien-3β,23-diol)	532.3898	7.36	16.22	0.062 ± 0.011	No
Cholest-4-ene-3,24-dione 3-GP	24-Oxocholesterol (3β-Hydroxycholest-5-en-24-one)	532.3898	7.72	18.24	0.035 ± 0.006	Yes
Cholest-4-ene-3,22-dione 3-GP	22-Oxocholesterol (3β-hydroxycholest-5-en-22-one)	532.3898	7.98	19.78	0.118 ± 0.028	Yes
4β-Hydroxycholesta-4,7-dien-3-one 3-GP	4-Hydroxy-7-dehydrocholesterol (Cholesta-5,7-dien-3β,4-diol)	532.3898	9.64 10.10	25.18 25.93	0.168 ± 0.039	No
Cholest-4-en-3,6-dione 3-GP	6-Oxocholesterol (Cholest-4-en-3,6-dione)	532.3898	10.45	26.97	0.040 ± 0.012	Yes
22R-Hydroxycholest-4-en-3-one 3-GP	22R-Hydroxycholesterol (Cholest-5-en-3β,22R-diol)	534.4054	6.06	9.43	0.010 ± 0.002	Yes
24S-Hydroxycholest-4-en-3-one 3-GP	24S-Hydroxycholesterol (Cholest-5-en-3β,24S-diol)	534.4054	7.36 7.67	16.22 18.03	0.346 ± 0.041	Yes
25-Hydroxycholest-4-en-3-one 3-GP	25-Hydroxycholesterol (Cholest-5-en-3β,25-diol)	534.4054		17.41	0.006 ± 0.002	Yes

24R-Hydroxycholest-4-en-3-one 3-GP	24R-Hydroxycholesterol (Cholest-5-en-3β,24R-diol)	534.4054	7.84	19.22	0.048 ± 0.008	Yes
(25R)26-Hydroxycholest-4-en-3-one 3-GP	(25R)26-Hydroxycholesterol (Cholest-(25R)-5-en-3β,26-diol)	534.4054	7.99	19.59	0.025 ± 0.017	Yes
7β-Hydroxycholest-4-en-3-one 3-GP	7β-Hydroxycholesterol (Cholest-5-en-3β,7β-diol)	534.4054	9.59 10.00	24.30 25.64	0.244 ± 0.078	Yes
7α-Hydroxycholest-4-en-3-one 3-GP	7α-Hydroxycholesterol (Cholest-5-en-3β,7α-diol)	534.4054	10.16	26.06 27.30	0.132 ± 0.051	Yes
6β-Hydroxycholest-4-en-3-one 3-GP	6β-Hydroxycholesterol (Cholest-4-en-3β,6β-diol)	534.4054	10.51	26.99	0.129 ± 0.045	Yes
5α-Hydroxycholest-7-en-3,6-dione	3β,5α-Dihydroxycholest-7-en-6-one	548.3847	8.34 9.22	21.19 23.73	0.299 ± 0.042	No
5α-Hydroxycholest-7-en-3,6-dione	3β,5α-Dihydroxycholest-7-en-6-one	548.3847	9.07 9.59	22.74 24.45	1.343 ± 0.368	No
Hydroxycholestendione	Dihydroxycholestenone	548.3847	10.10	25.96	0.602 ± 0.266	No
24,25-Dihydroxycholest-4-en-3-one 3-GP	24S,25-Epoxycholesterol (3β-hydroxycholest-5-en-24S,25-epoxide)	550.4003	3.84 4.51	3.78 4.87	0.598 ± 0.128	Yes
20,22-Dihydroxycholest-4-en-3-one 3-GP	20,22-Dihydroxycholesterol (Cholest-5-en-3β,20,22-triol)	550.4003	4.30	4.51	0.024 ± 0.007	Yes
24-Hydroxy-25-methoxycholest-4-en-3-one 3-GP	24S,25-Epoxycholesterol (3β-Hydroxycholest-5-en-24S,25-epoxide)	564.4160	6.06 6.53	9.22 11.14	0.297 ± 0.103	Yes

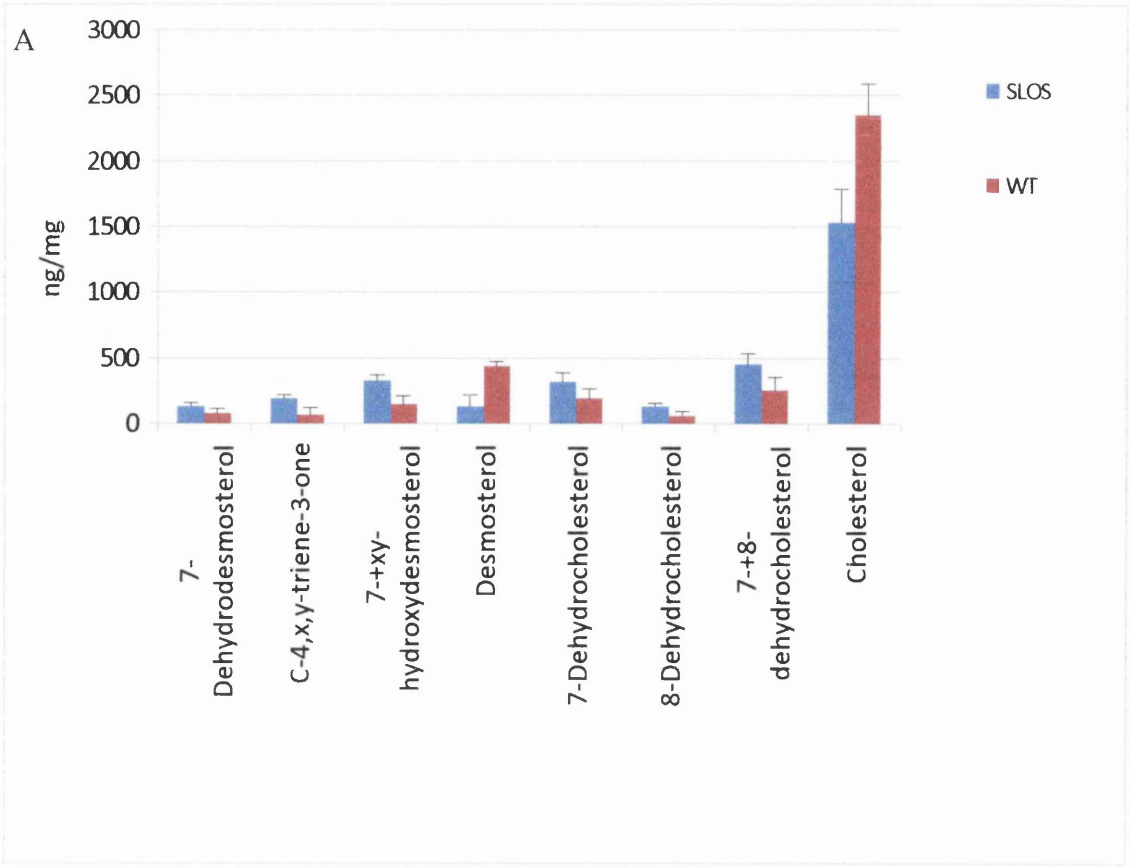

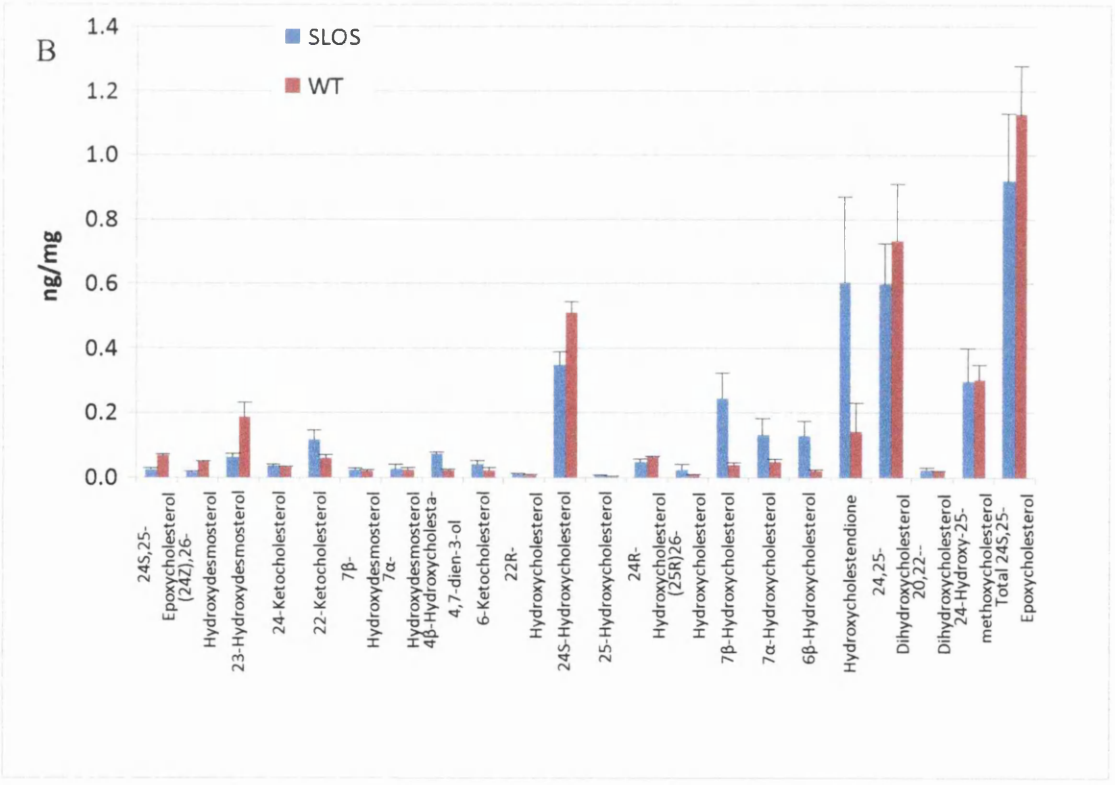

Figure 4.3 Sterols (A) and oxysterols (B) identified in SLOS and wild type mouse brains.

Unsurprisingly, in light of the requirement of the Dhcr7 enzyme to produce desmosterol via the Block pathway the desmosterol level is diminished in the SLOS mouse (130.02 ± 30.01 ng/mg) compared the wild type (439.66 ng/mg [chapter 3]). In the Block pathway the precursor of desmosterol is 7-dehydrodesmosterol. This metabolite following GP-tagging has an *m/z* of 514.3792. Two components from SLOS mouse brain elute with this *m/z* (Figure4.2A). The MS^3 spectrum of the component eluting at 10.61 min gives a spectrum similar to that of 7-dehydrocholesterol, however *m/z* values for high mass fragments ions were reduced down by two mass units (Figure 4.2B vs. Figure 4.1B). The A and B ring fragment ions are identical to those characteristic for the MS^3 spectrum of 7-dehydrocholesterol (i.e. *m/z* 137, 151) indicating that the extra unsaturation is elsewhere, hypothetically at C-24. The latter chromatographic peak eluting at 11.29 min gives an MS^3 spectrum more in line with that predicted for 8-dehydrodesmosterol (cholesta-5,8(9),24-trien-3β-ol) (Figure 4.2CC). However, authentic standards are not available for 7- and 8-dehydrodesmosterols to confirm these presumptions. The levels of these two putatively identified molecules in the SLOS mouse are 135.75 ± 30.99 ng/mg and 79.04.76 ± 34.31 ng/mg, respectively. The combined level of 7-dehydrodesmosterol and 8-dehydrodesmosterol is 327.51 ng/mg in the SLOS mouse compared to 143.70 ng/mg in the wild type. As was the case with immediate precursors of cholesterol in the Kandutsch-Rusell pathway, there is an elevation in the level of the immediate precursors of desmosterol in the Block pathway. The SLOS mouse is viable, hence retains some Dhcr7 enzymatic activity allowing the formation of cholesterol. Its level in the SLOS mouse is 1531.48 ± 240.93 ng/mg compared to 2350.69 ng/mg in the wild type mouse.

24S,25-Epoxycholesterol and cholesterol and desmosterol derived oxysterols

The availability of cholesterol in the SLOS mouse brain suggests that a normal profile of cholesterol derived oxysterols may be observed, but at lower levels than in the wild type animal. Similar to the wild type mouse, the pattern of monohydroxycholesterols in the brain of the newborn SLOS mouse is dominated by 24S-hydroxycholesterol (Figure 4.4). The chromatogram (short gradient) of GP-tagged monohydroxycholesterols (RIC *m/z* 534.4054) shows two closely eluting peaks at 7.36 and 7.67 min identified as *syn* and *anti* conformers of GP-derivatised 24S-hydroxycholesterol. Both peaks give an identical MS^3 ($[M]^+ \rightarrow [M-79]^+ \rightarrow$) spectrum showing a characteristic triad of low mass fragment ions at *m/z* 151 ($*b_1$-12), 163 ($*b_3$-C_2H_4) and 177 ($*b_2$), and a distinctive ion at 353 (Figure 4.5A). The enzyme responsible for the formation of 24S-hydroxycholesterol from cholesterol is cytochrome P450

(Cyp in mouse, CYP in human) 46a1 and is expressed in normal brain exclusively in neurons [204]. In the SLOS newborn mouse the concentration of 24S-hydroxycholesterol in brain was determined to be 0.346 ± 0.041 ng/mg. This value is about 70% that found in the wild type newborn animal (0.510 ± 0.034 ng/mg [119]). This lower level of 24S-hydroxycholesterol in SLOS brain is a reflection of a lower cholesterol concentration in the SLOS mouse brain than in the wild type. Application of the short chromatographic gradient as utilised in

Figure 4.4A does not fully separate 24S-hydroxycholesterol, 25-hydroxycholesterol and 26-hydroxycholesterol making quantification of the latter two compounds unreliable. To resolve this issue we developed a longer chromatographic gradient giving better separation of these isomers (Figure 4.4B).

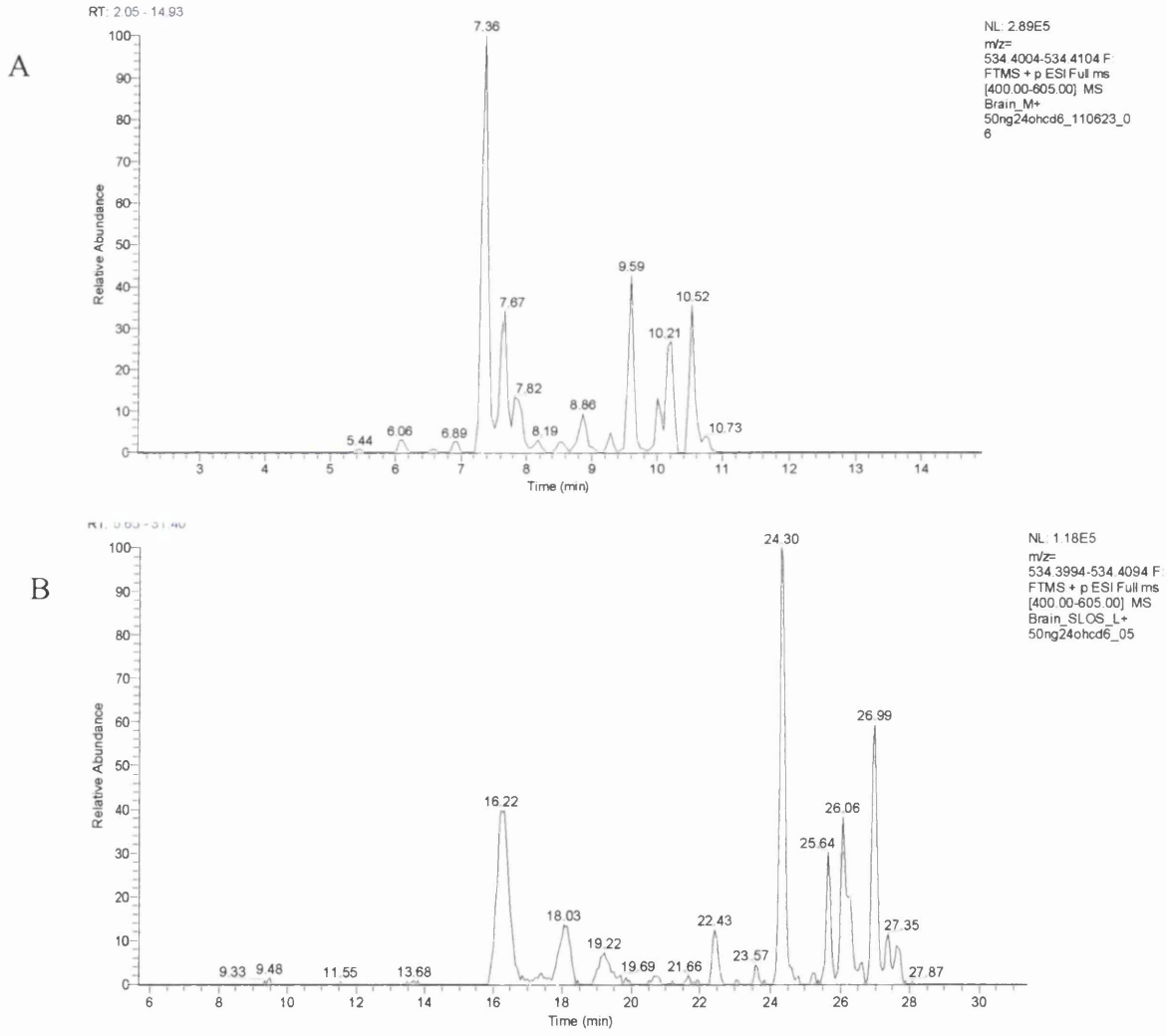

Figure 4.4 RIC of monohydroxycholesterols from newborn SLOS mouse brain following GP charge-tagging. (A) LC-MS RIC for m/z 534.4054 _ 10 ppm using the short gradient. (B) Analysis of RIC for *m/z* 534.4054 using the long gradient.

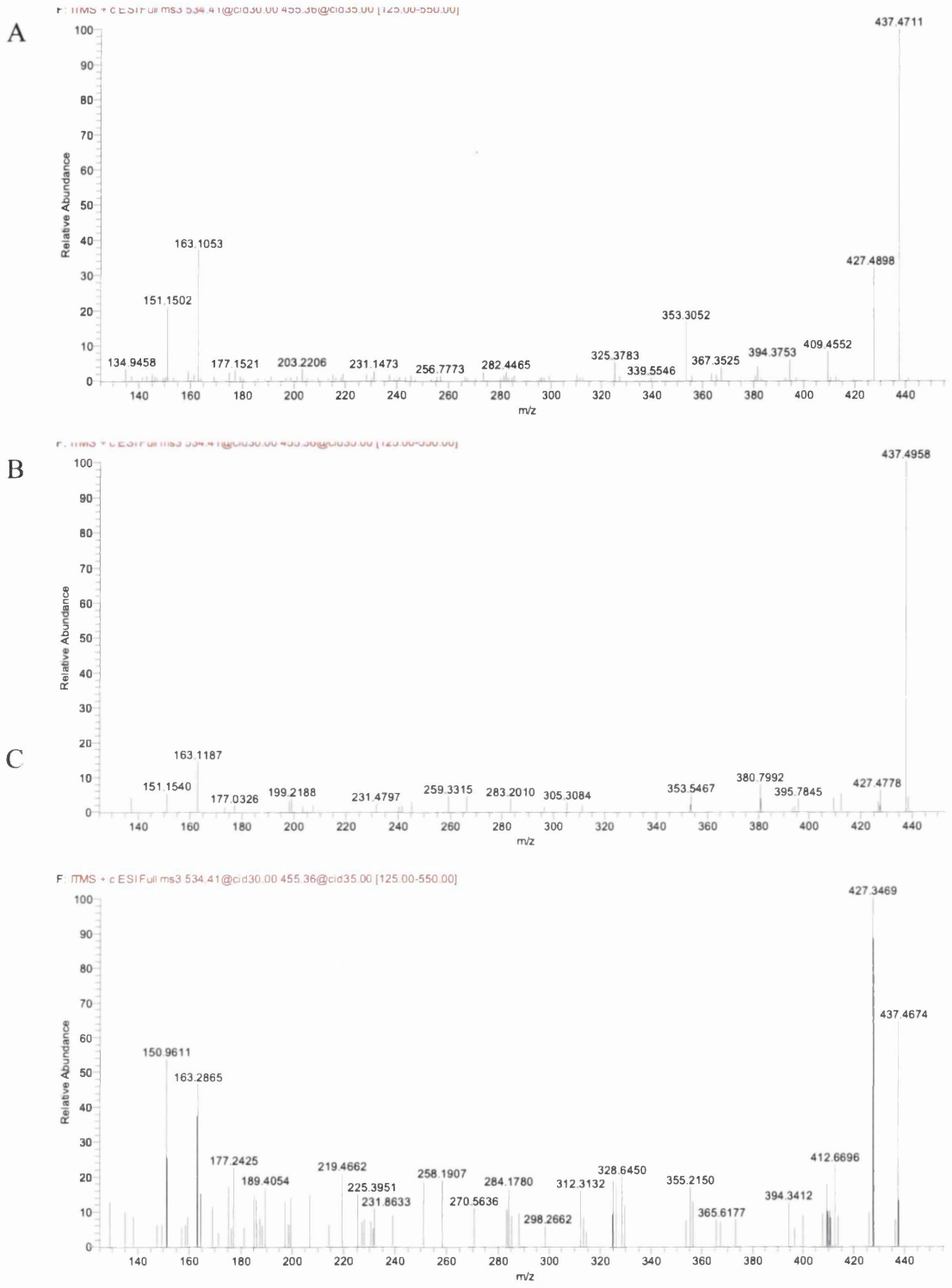

Figure 4.5 MS^3 spectra of peaks eluting in long gradient: (A) 17.41 min corresponding to 24S-hydroxycholesterol (cholest-5-ene-3b,24S-diol); (B) 17.41 min corresponding to 25-hydroxycholesterol (cholest-5-ene-3b,25-diol); (C) 19.69 min corresponding to 26-hydroxycholesterol (cholest-5-ene-3b,26-diol).

A great advantage of utilising the GP-tag with MS^3 fragmentation is that the resulting spectra allow isomer differentiation. For example, the MS^3 spectrum of 25-hydroxycholesterol (

Figure 4.5B) is completely dominated by the fragment ion at *m/z* 437 resulting from facile dehydration of the $[M-79]^+$ ion and is quite different from MS^3 spectra of the other isomers. 25-Hydroxycholesterol is formed from cholesterol either in a reaction catalysed by cholesterol 25-hydroxylase (Ch25h) [8, 29] or as a side-product of Cyp46a1 or Cyp27a1 catalysed hydroxylation of cholesterol [107, 205]. The level of 25-hydroxycholesterol in the SLOS mouse brain was at about the detection limit of our methodology (0.006 ± 0.002 ng/mg). 26-Hydroxycholesterol is formed in a Cyp27a1 catalysed reaction [17], and in SLOS mouse brain the level of this oxysterol was determined to be 0.025 ± 0.017 ng/mg (
Figure 4.5C).

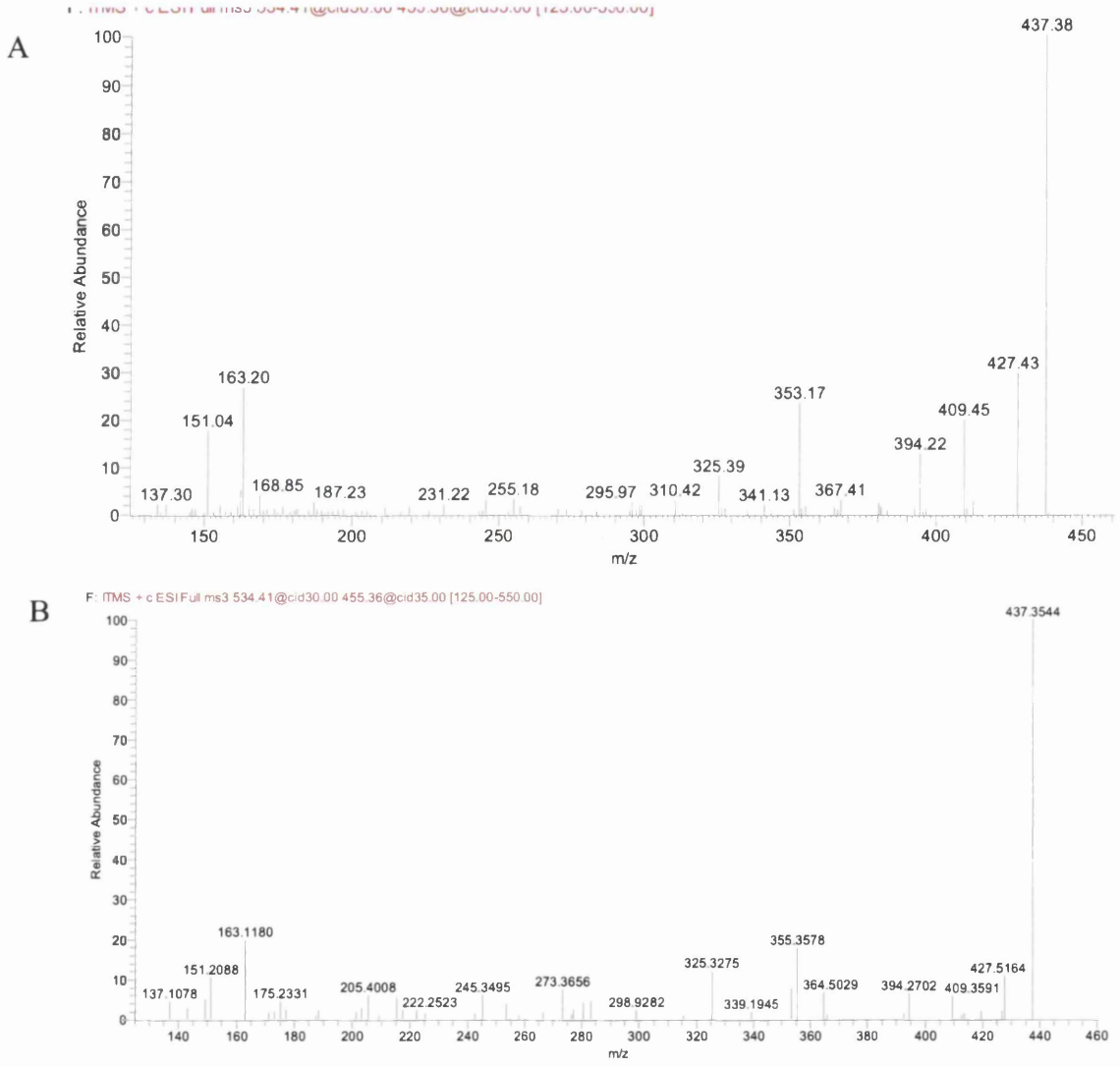

Figure 4.6 MS^3 spectra of peaks eluting in long gradient presented in Figure 4.4B: (A) 17.41 min corresponding to 24R-hydroxycholesterol (cholest-5-ene-3b,24R-diol) and in short gradient (B) 6.06 min corresponding to 22R-hydroxycholesterol (cholest-5-ene-3b,22R-diol)

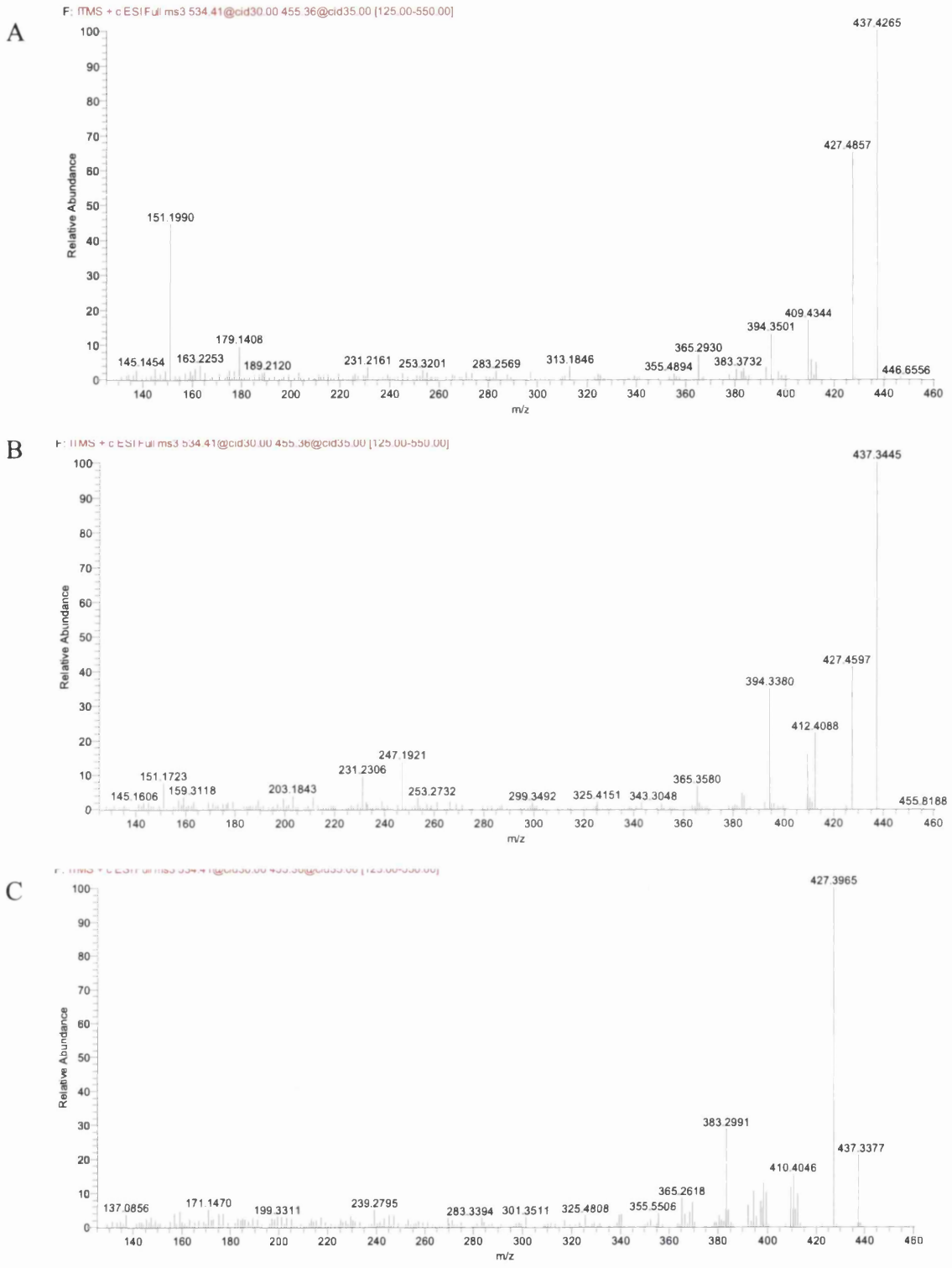

Figure 4.7 MS^3 spectra of peaks eluting in the short gradient presented in Figure 4.4A: (A) 9.59 min corresponding to 7β-hydroxycholesterol (cholest-5-ene-3 β,7β-diol), 7α-hydroxycholesterol (cholest-5-ene-3 β,7α-diol) and (C) 10.51 min corresponding to 6β-hydroxycholesterol (cholest-5-ene-3 β,6β-diol)

As well as finding 24S-hydroxycholesterol in brain, we also find low levels of the 24R-isomer (0.048 ± 0.008 ng/mg) (Figure 4.6A). We also identified low levels of 22R-hydroxycholesterol (0.010 ± 0.002 ng/mg) giving a peak eluting at 6.06 min in the short gradient (Figure 4.6B). This is generated from cholesterol via oxidation by Cyp11a1 ($P450_{SCC}$) [206]. The combined levels of the side-chain hydroxycholesterols in the SLOS mouse is 0.435 ng/mg, this compares with 0.594 ng/mg in the wide type mouse [13] i.e. about 70%.

We also identified monohydroxysterols with hydroxylation in the B-ring at positions 7β-, 7α- and 6β (0.244 ± 0.078, 0.132 ± 0.051 and 0.129 ± 0.045 ng/mg respectively, Figure 4.7 A, B and C). These are autoxidation products of cholesterol, formed during sample storage or they may be formed endogenously by reaction of cholesterol with reactive oxygen species (ROS), or alternatively they may be formed extra-cerebrally and cross the BBB from the circulation into brain. 6β-Hydroxycholesterol is a formed from 5,6-epoxycholesterol following acid hydrolysis and is a subsequent dehydration product [207]. The level of 7-oxocholesterol was below the limit of detection and no evidence of 4α- or 4β-hydroxycholesterols was found.

24S,25-Epoxycholesterol is formed in parallel to cholesterol via a shunt of the mevalonate pathway. The RIC of *m/z* 532.3898, the appropriate *m/z* of the GP-tagged 24S,25-epoxycholesterol, from SLOS mouse brain samples revealed two peaks eluting at 6.70 and 6.96 min corresponding to the *syn* and *anti* conformers of GP-tagged 24S,25-epoxycholesterol (0.024 ± 0.004 ng/mg) (Figure 4.8A). The MS^3 spectra are shown in Figure 4.8B. The peak eluting at 7.74 min was identified as GP-tagged 24-oxocholesterol (0.035 ± 0.006 ng/mg). The presence of a 24-oxo group is characterised by an abundant $[M\text{-}79\text{-}CO]^+$ ion (*m/z* 425) in the MS^3 spectrum (Figure 4.8C). 24-Oxocholesterol is formed from 24S,25-epoxycholesterol during derivatisation. Analysis of the newborn SLOS mouse brain also revealed a peak with retention time 7.99 min which gave an MS^3 spectrum corresponding to GP-tagged 22-oxocholesterol (0.118 ± 0.028 ng/mg) (Figure 4.8D). The peak in the RIC of *m/z* 532.3898 eluting at 7.37 min (0.062 ± 0.011 ng/mg) presumptively identified as to GP-tagged 23-hydroxydesmosterol [119]. The MS^3 ($[M]^+ \rightarrow [M\text{-}79]^+ \rightarrow$) spectrum being is completely dominated by the $[M\text{-}79\text{-}H_2O]^+$ ion at *m/z* 435 (Figure4.8A) and an $[M]^+ \rightarrow [M\text{-}97]^+ \rightarrow$ MS^3 spectrum indicating that the facile hydroxyl group is located α to the side-chain double bond in desmosterol.

Other compounds identified in the SLOS new born mouse brain include (24Z)26-hydroxydesmosterol eluting at 7.11 min (0.016 ± 0.003 ng/mg (Figure4.8B). Close inspection of the RIC *m/z* 532.3898 reveals further peaks at 8.62 and 9.34 min that give MS^3 spectra compatible with GP-tagged 7β- and 7α-hydroxydesmosterols, respectively (0.024 ± 0.005 ng/mg and 0.027 ± 0.013 ng/mg), although authentic standards are not available to confirm the identification. These oxysterols could possibly be formed in Cyp7a1 catalysed reactions with desmosterol as the substrate, or via ROS or autoxidation [190].

24S,25-Epoxycholesterol is unstable in acid solution and is susceptible to both hydrolysis and methanolysis during the derivatisation process [120]. The RIC of *m/z* 550.4003 (Figure 4.10A), appropriate for the hydrolysis product, revealed two peaks eluting at 3.84 min and 4.51 min identified as the *syn* and *anti* conformers of GP-tagged 24,25-dihydroxycholesterol (0.598 ± 0.128 ng/mg). The MS^3 spectra are presented in Figure 4.10B. Close inspection of the RIC for *m/z* 550.4003 shown in Figure 4.10C reveals a shoulder on the leading edge of the peak at 4.51 min.

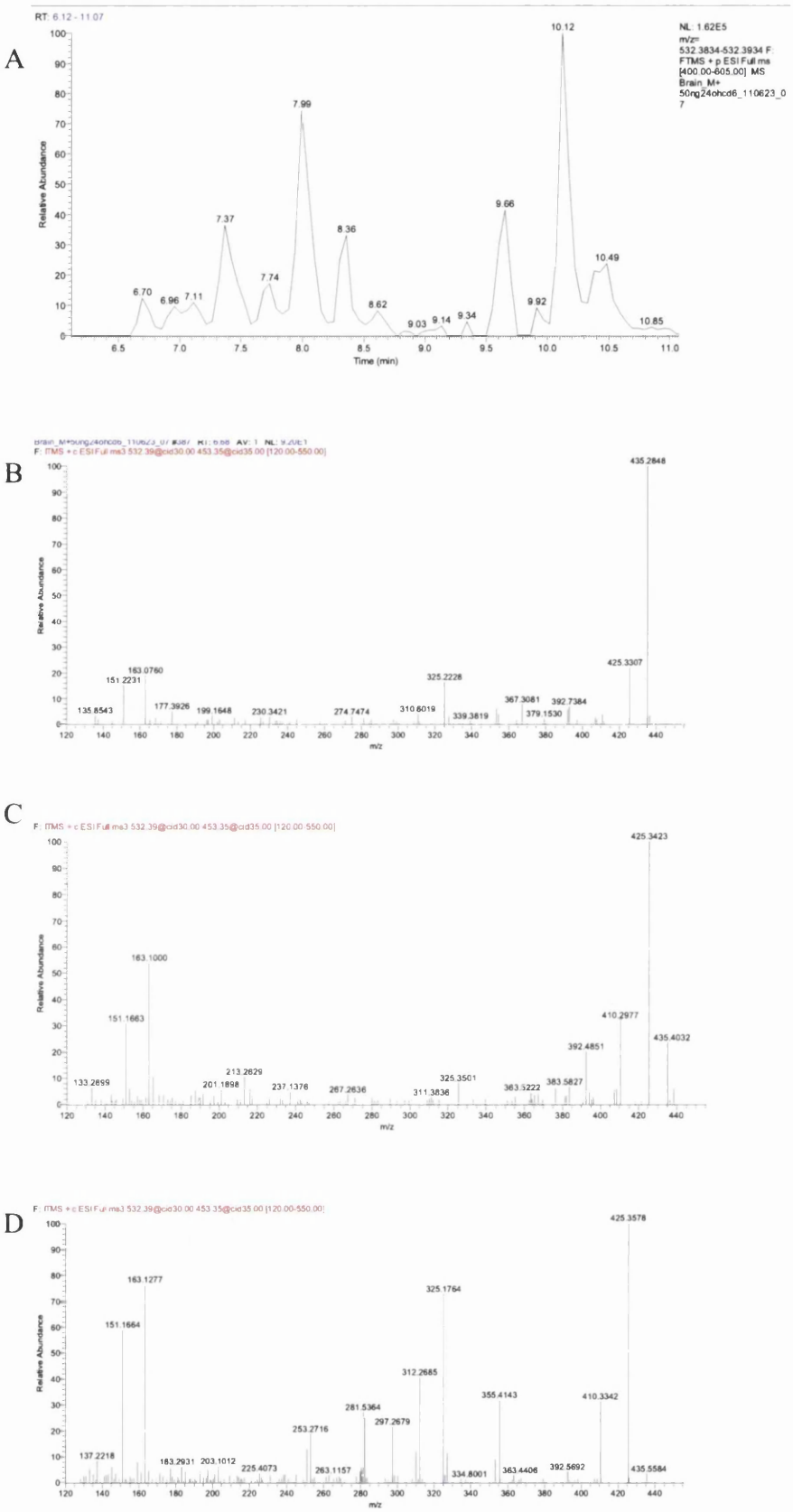

Figure 4.8 RIC for m/z 532.3898 from newborn SLOS mouse brain following GP charge-tagging using the short gradient. MS^3 spectra of peaks eluting in (A) 6.70 min corresponding to 24S,25-epoxycholesterol (24S,25-epoxycholest-5-ene-3β-ol), (B) 7.74 min corresponding to 24-oxocholesterol (24-oxocholest-5-ene-3β-ol), (B) 7.99 min corresponding to 22-oxocholesterol (22-oxocholest-5-ene-3β-ol).

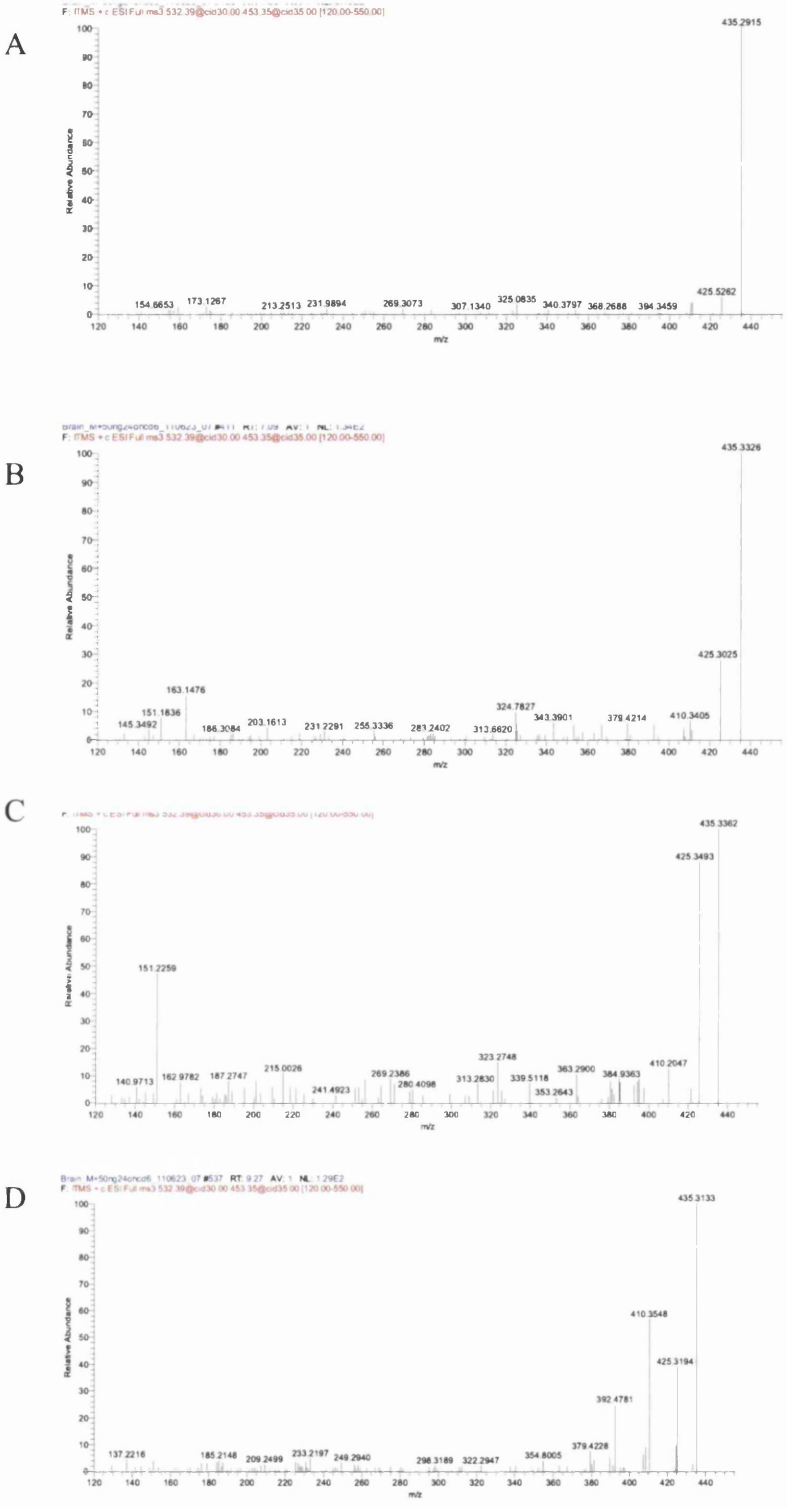

Figure 4.9 MS^3 spectra of peaks eluting in the short gradient presented in Figure 4.8A: (A) 7.37 min corresponding to 23-dehydrocholesterol (cholest-5,24-diene-3β,23-diol), (B) 7.11 min corresponding to (24Z)26-hydroxydesmosterol (cholest-5,24-diene-3β,(24Z)26-diol), (C) 8.62 min corresponding to 7β-hydroxydesmosterols (cholest-5,24-diene-3β,7β-diol) and (D) 9.34 min corresponding to 7α-hydroxydesmosterols (cholest-5,24-diene-3β,7α-diol).

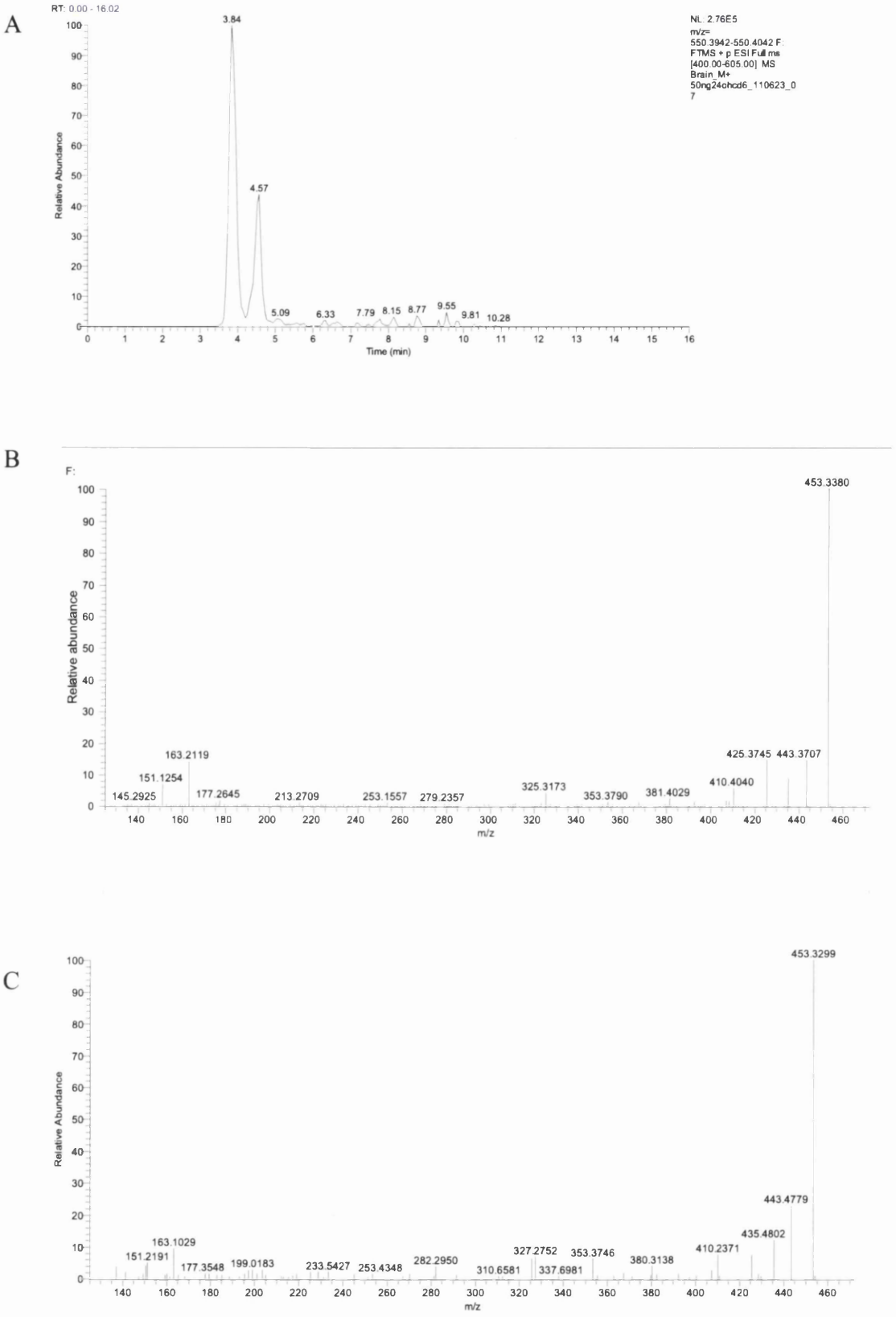

Figure 4.10 RIC for m/z 550.4005 from newborn SLOS mouse brain following GP charge-tagging using the short gradient (A). MS^3 spectra of a doublet eluting in (B) 3.84 min and 4.57 min corresponding to 24,25-dihydroxycholesterol (cholest-5-ene-3β,24,25-triol) and (C) MS^3 spectrum corresponding to 20R,22R -dihydroxycholesterol (cholest-5-ene-3β,20R,22R-triol)

The MS^3 spectrum suggests the presence of 20,22-dihydroxycholesterol (0.024 ± 0.007 ng/mg).

Analysis of the RIC of *m/z* 564.4160 showed two peaks with retention times and MS^3 fragmentation characteristic for the methanolysis product of 24S,25-epoxycholesterol. The level of the methanolysis product in SLOS brain was determined to be 0.297 ± 0.103 ng/mg. The combined concentration of native 24S,25-epoxycholesterol, its isomer 24-oxocholesterol, its hydrolysis product 24,25-dihydroxycholesterol and its methanolysis product 24-hydroxy-25-methoxycholesterol equals to 0.920 ng/mg. Considering that the level of cholesterol in the newborn SLOS mouse is only about 60% that of the wild type, it was expected that the 24S,25-epoxycholesterol ratio between the mice would give a similar percentage. In fact, the level in the SLOS mouse is about 80% of that in the wild type. One plausible explanation for the higher than expected level of 24S,25-epoxycholesterol in the SLOS mouse is the down regulation of Cyp7b1, the enzyme responsible for 24S,25-epoxycholesterol metabolism. Björkhem et al have noted down regulation of CYP7B1 in human SLOS patients [2].

7-Dehydrocholesterol derived oxysterols

Studies of developing mouse embryos from another SLOS mouse model, the *Dhcr-7*-KO reported presence of three novel monohydroxydehydrocholesterol isomers [31;32]. These were identified by high performance (HPLC) purification and NMR analysis as 4α-, 4β- and 24-hydroxy-7-dehydrocholesterols [32]. In our SLOS mouse model these three novel metabolites may account for the late eluting peaks in the of RIC *m/z* 532.3898 (Figure 4.8A). The components eluting at 9.66 and 10.12 min both give MS^3 ($[M]^+ \rightarrow [M-79]^+ \rightarrow$) spectra compatible with an A/B ring system containing two double bonds, and an extra alcohol group (besides that at C-3 oxidised here by cholesterol oxidase to a 3-oxo group), possibly the 4α- and 4β-hydroxy-7-dehydrocholesterol isomers reported by Xu et al (0.168 ± 0.039 ng/mg Figure 4.11A and B. No authentic standard is available for these isomers. The latest eluting peak (10.49 min) gives a spectrum indicative of GP-tagged cholest-4-ene-3,6-dione (0.040 ± 0.012 ng/mg, Figure 4.11C). No evidence was found for a metabolite giving MS^n spectra appropriate to 24-hydroxy-7-dehydrocholesterol.

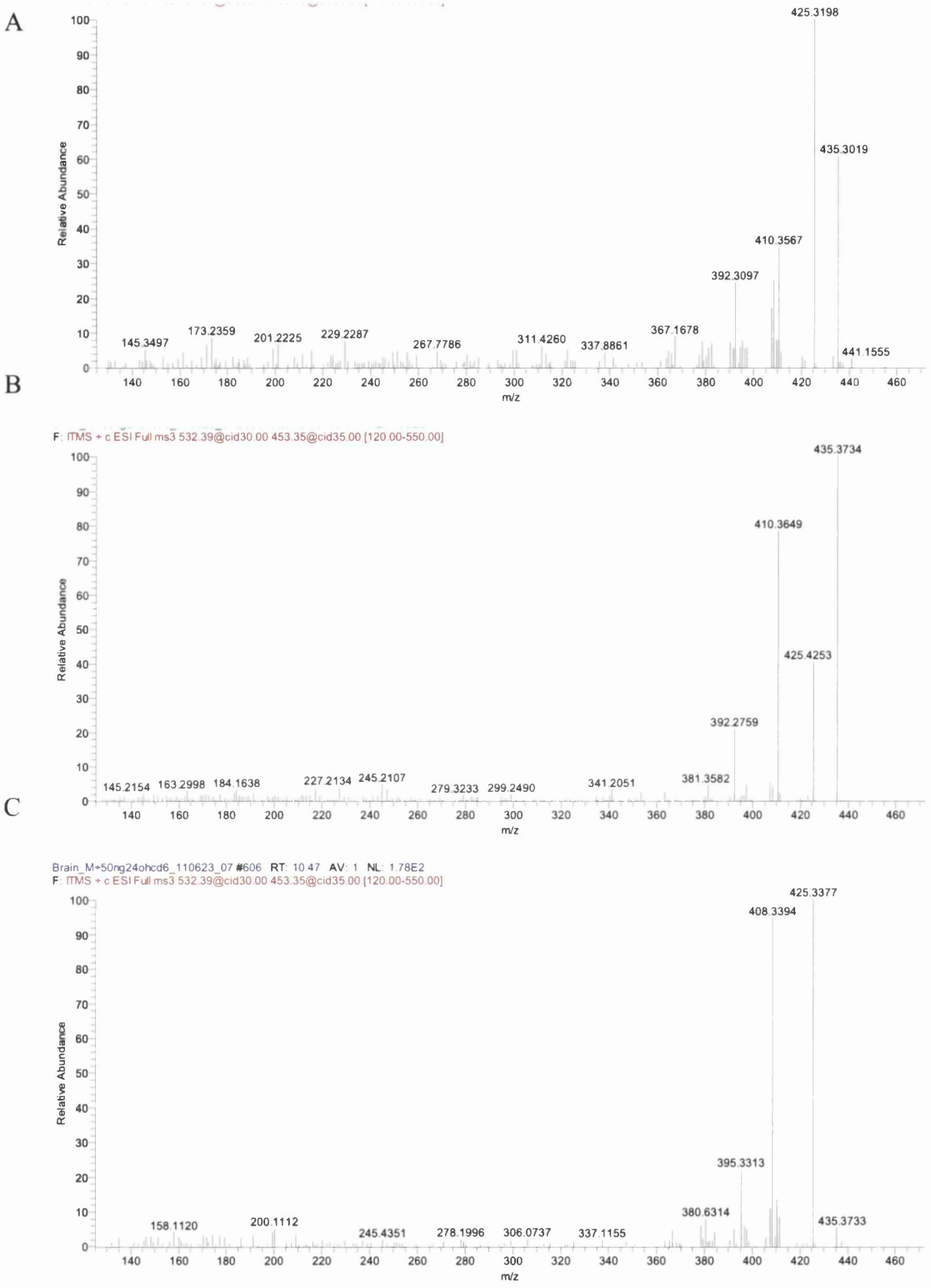

Figure 4.11 MS^3 spectra of peaks eluting in the short gradient presented in Figure 4.8A: (A) 9.66 min corresponding to 4α-hydroxy-7-dehydrocholesterol (cholest-5,7-diene-3β,4α-diol), 10.12 min corresponding to 4β-hydroxy-7-dehydrocholesterol (cholest-5,7-diene-3β,4β-diol), 10.49 min corresponding to cholest-4-ene-3,6-dione

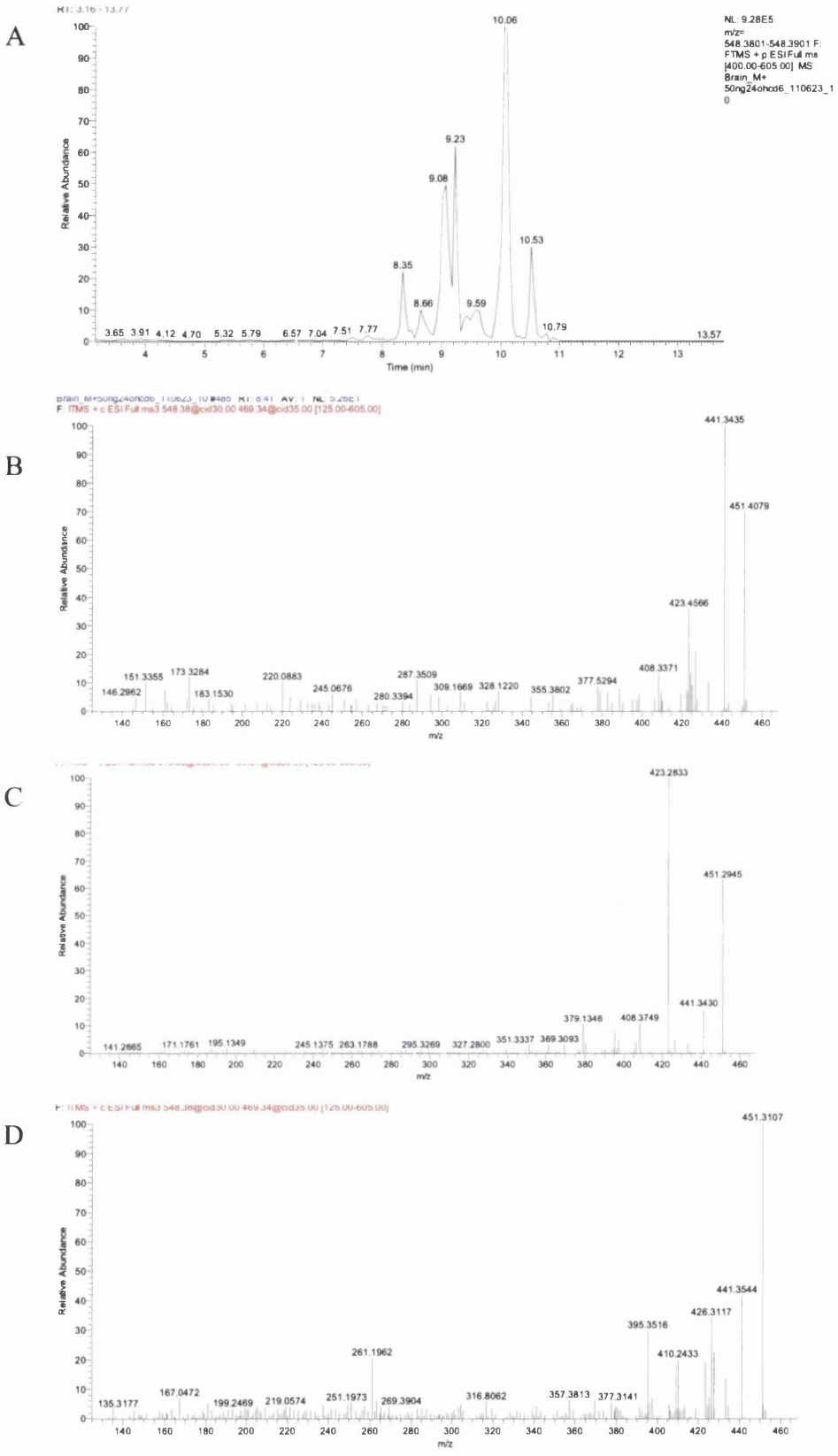

Figure 4.12 RIC for m/z 548.3847 from newborn SLOS mouse brain following GP charge-tagging using the short gradient (A). MS^3 spectra of peaks eluting at (B) 8.41 min and (C) 9.07 min possibly both corresponding to 3b,5a-dihydroxycholest-7-en-6-one and (D) 10.12

min probably corresponding to an additional dihydroxycholestenoneisomer. In the absence of authentic standards these identifications are presumptive.

Xu et al also identified 3β,5α-dihydroxycholest-7-en-6-one in the brain extract from embryonic *Dhcr-7*-KO mouse and suggested its formation was through 5α,6α-epoxycholest-7-en-3β-ol and subsequently cholest-7-en-3β,5α,6β-triol [32]. Oxidation by cholesterol oxidase and GP tagging 3β,5α-dihydroxycholest-7-en-6-one will give an $[M]^+$ ion at *m/z* 548.3847.

The RIC for this mass from brain extracts of our *Dhcr7* $^{\Delta 3\text{-}5/T93M}$ SLOS mouse is shown in Figure 4.12A. The chromatogram shows a large number of late eluting analytes. The MS^3 spectra of three distinct compounds are shown in Figure 4.12B-D. The components eluting at 8.41 (in Figure 4.12B) and 9.22 min give a similar pattern of MS^3 fragment ions dominated by successive losses of 18 Da (H_2O), 28 Da (CO) and 46 Da (H_2O+CO) from the $[M-79]^+$ ion. The pattern indicates the presence of a free hydroxy and a carbonyl group attached to the sterol skeleton. The spectra are compatible with that predicted for GP tagged 3β,5α-dihydroxycholest-7-en-6-one following treatment with cholesterol oxidase where the GP-tag is on C-6, with the two chromatographic peals corresponding to the *syn* and *anti* isomers (0.299 ± 0.042 ng/mg). Likewise, the components eluting at 9.07 (in Figure 4.12C) and 9.59 min give similar MS^3 spectra, this time dominated by the loss of 18 Da (H_2O) and 46 Da (H_2O+CO) from the $[M-79]^+$ ion, with only a minor loss of 28 Da (CO). Following treatment with cholesterol oxidase 3β,5α-dihydroxycholest-7-en-6-one is converted to 5α-hydroxycholest-7-ene-3,6-dione and this latter pair of peaks probably correspond to *syn* and *anti* confirmers of the molecules with the derivatising group at C-3 (1.343 ± 0.368 ng/mg). The final major peak at *m/z* 10.10 min gives a different MS^3 spectrum to that of the earlier isomers, but the parent structure is not immediately obvious (0.602 ± 0.266 ng/mg, in Figure 4.12D).

4.3 Discussion

Cholesterol and desmosterol levels were reduced in the SLOS mouse compared to the wild type, while their respective precursors 7-dehydrocholesterol (and 8-dehydrocholesterol) and 7-dehydrodesmosterol (and 8-dehydrodesmosterol) were increased. This findings are in a good agreement with studies by Marcos et al and Correa-Cerro et al who also observed a reduction in cholesterol and an elevation in DHC in one day old SLOS mouse brain [9;10].

It is not clear how the mutation in *DHCR7* results in the characteristic SLOS phenotype. A lack of cholesterol (or desmosterol) during development may account for the features like dysmorphia and mental retardation. It is also feasible that a decreased level of cholesterol metabolites required for normal development or a build up of toxic metabolites of 7-dehydrocholesterol (and/or 7-dehydrodesmosterol) is responsible for the formation of SLOS symptoms.

The analysis of sterolome of SLOS mouse showed a decreased the level of essentially all cholesterol-derived, enzymatically-formed oxysterols, in particular the dominating brain oxysterol 24S-hydroxycholesterol (reduced to about 70% of the wild type) (Fig. 7). This is not surprising as 24S-hydroxylation is an "exit" route for the cholesterol, and in reduced supply of this sterol its metabolism is also diminished [34]. In the SLOS mouse total amount of 24S,25-epoxycholesterol was also reduced compared to the wild type, although not to significance.

In conclusion, in newborn brain from the *Dhcr7*$^{\Delta 3\text{-}5/T93M}$ mouse model of SLOS there is a reduced level of cholesterol and desmosterol and elevated level of 7-dehydrocholesterol and 7-DHD. In concert to the reduction in cholesterol there is also a reduction of cholesterol derived oxysterols, but an elevation in 7-dehydrocholesterol derived oxysterols. It is not clear at present whether these latter oxysterols are formed by autoxidation, via ROS, or enzymatically.

Chapter 5

5 Profiling of sterol content of Cyp46a1 -/- mouse brain

5.1 Introduction

Cholesterol accounts for the 2% of the mass of mouse brain [85] making the brain the most cholesterol-rich organ in the body. Although only a fraction of this pool is physiologically active, it still requires an efficient turnover mechanism. Cholesterol cannot cross blood brain barrier, but its 24S-hydroxylated derivative is membrane permeable and readily passes to the blood stream. This hydroxylation is mainly provided by cholesterol hydroxylase Cyp46a1, an endoplasmatic enzyme which belongs to the family of cytochrome P450 monooxygenases [208]. In mouse the enzyme is predominantly expressed in the brain, and to a lesser extent, in the testis and liver [29]. Cyp46a1 preferably hydroxylase 24S position of cholesterol, but 25-hydroxylase activity is also detected [208]. In the circulation, 24S-hydroxycholesterol is a substrate for hepatic enzyme Cyp7b1, which initiates conversion of this oxysterol into bile acid, which is excreted from the body.

Apart from serving as an exit routE for cholesterol, 24S-hydoxycholesterol is involved in cell signalling as a potent ligand to Liver X Receptors (LXR) [173, 209, 210]. LXRs, both isoforms α and β, are expressed in the brain where they regulate cholesterol metabolism and trafficking [211, 212].

Transgenic mice with knockout mutation were created in the Mc Donald's laboratory by replacing a fragment of the first exon of *Cyp46a1* with a terminal sequence of bovine tau protein coupled to bacterial β-galactosidase gene [106]. Obtained mutants did not present phenotype, moreover, the weight of main organs such as liver, brain and adrenal gland was not differing from the wild type mice. Although there were no physical symptoms, the deficiency of Cyp46a1 adversely affected spatial, associative and motor learning as well as long term potential (LTP) of hippocampal neurons [213].

Basic biochemical analysis showed the absence of 24S-hydroxycholesterol with normal levels of cholesterol. The inhibition of cholesterol metabolism was compensated by decreased cholesterol synthesis reflected by reduced levels of its precursor, desmosterol.

In this work we present more comprehensive profile of cholesterol derivatives aiming to get a better understanding of the effect of the *Cyp46a1* knockout on the lipidome.

5.2 Results

Cholesterol has a relatively low polarity, therefore it elutes from the first SPE column in fraction SPE1-Fr3 and from the second column in fractions SPE2-Fr1,2,3. Upon ionisation, GP-derivatised generated a molecular ion of *m/z* 518.4105. Figure 5.1 presents chromatogram for GP-derivatised cholesterol extracted from *Cyp46a1-/-* mouse brain, the MS^3 fragmentation pattern is shown in Figure 5.2. Analysis of these sterol fractions unsurprisingly revealed a high level of cholesterol (~16 µg/mg), similar in knockout and wild type animals.

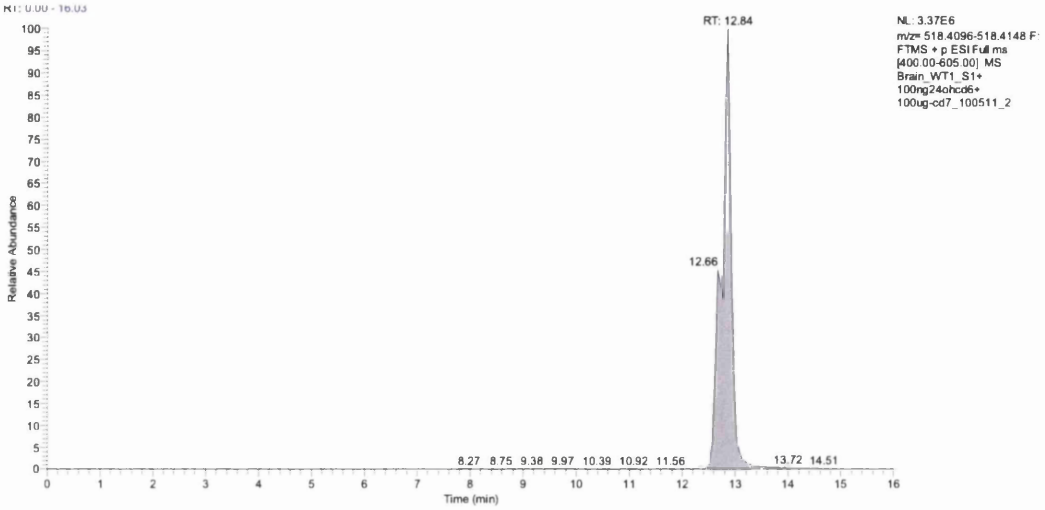

Figure 5.1.GP derivatives of cholesterol identified in brain of *Cyp46a1-/-* mouse.

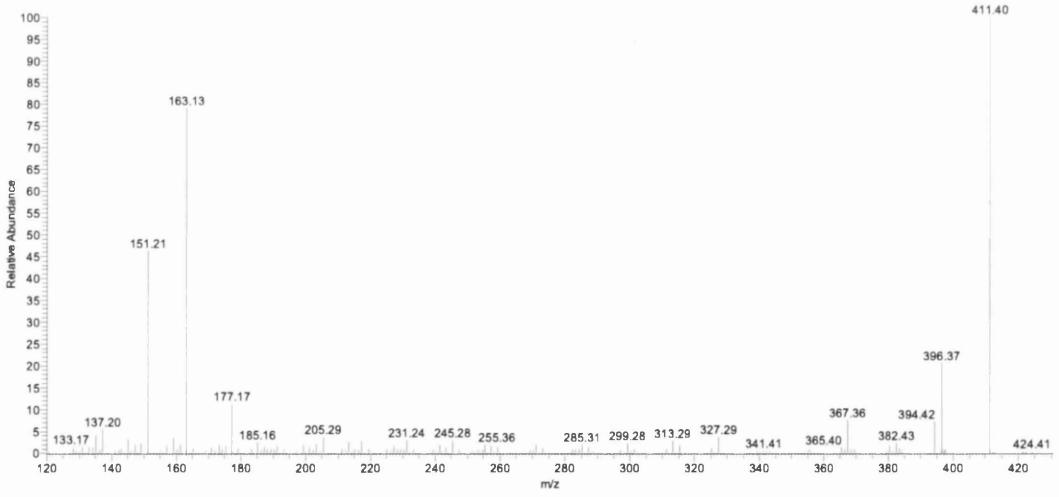

Figure 5.2. MS^3 spectrum of peak eluting at 12.85 min identified as GP-tagged cholesterol

The quantification of cholesterol precursor - desmosterol showed a variation between *Cyp46a1+/+* and *Cyp46a1-/-*, where knockout mice had reduced level by 50% (0.104 µg/mg and 0.057±0.004 µg/mg) (RIC and MS3 spectrum showed in Figure 5.4 and Figure 5.5). The detailed levels of sterols are shown in Table 5.1.

Table 5.1 Sterols identified by LC-ESI-MSn in murine brain following SPE and charge-tagging with GP-hydrazine. Two replicates of Cyp46a1$^{-/-}$ and one replicate of Cyp46a1$^{+/+}$ mice were analysed.

Identified structure after treatment with cholesterol oxidase	$[M]^+$of GP *m/z*	RT (min)	RRT	Adult wild type brain (µg/mg)	KO (ng/mg)	Inferred compound trivial name
C-4,7,24-triene-3-one	514.3792	11.00	0.996	5.647	6.583±4.09	7-Dehydrodesmosterol
C-4,24-diene-3-one	516.3948	11.52	1.003	104.286	57.3828±4.5382	Desmosterol
C-4-ene-3-one	518.4105	12.84	1.006	16026	15736±658	Cholesterol

Table 5.2 Oxysterols identified by LC-ESI-MSn in murine brain following SPE and charge-tagging with GP-hydrazine. Two replicates of Cyp46a1$^{-/-}$ and two replicates of Cyp46a1$^{+/+}$ mice were analysed.

Identified structure after treatment with cholesterol oxidase	$[M]^+$of GP *m/z*	RT	RRT	Cyp46a1+/+ (ng/mg)	Cyp46a1-/- (ng/mg)	Inferred compound trivial name
C-4-ene-3,24-dione	532.3898	7.84	1.05	0.3390±0.0216	0.0049±0.0030	24-Oxocholesterol
C-4-ene-24S,25-epoxide 3-one	532.3898	6.86	0.92	0.0260±0.0028	0.0033±0.0009	24S,25-Epoxycholesterol
C-4-ene-24,25-diol-3-one	550.4003	4.02	0.54	0.1588±0.0009	0.0781±0.0290	24S,25-Epoxycholesterol
C4-ene-24-ol,25-OMe-3-one	564.416	6.26	0.84	0.1173±0.0042	0.0372±0.0185	24S,25-Epoxycholesterol
Total epoxy				0.6411±0.0155	0.1235±0.0435	Total 24S,25-Epoxycholesterol
C-4-ene-22R-ol-3-one	534.4054	6.71	0.90	ND	0.0004±0.0005	22R-Hydroxycholesterol
C-4-ene-24S-ol-3-one	534.4054	7.49	1.01	27.9069±0.7322	0.0173±0.0025	24S-Hydroxycholesterol
C-4-ene-24R-ol-3-one	534.4054	7.98	1.07	NA	0.1598±0.0228	24R-Hydroxycholesterol
C-4-ene-25-ol-3-one	534.4054	7.60	1.00	0.7696±0.1029	0.0502±0.0094	25-Hydroxycholesterol
C-(25R)-4-ene-26-ol-3-one	534.4054	7.96	0.99	0.3342±0.1327	0.1485±0.0060	25R,26-Hydroxycholesterol
C-(25S)-4-ene-27-ol-3-one	534.4054	8.94	1.20	0.0283±0.0048	0.0302±0.0353	25S,27-Hydroxycholesterol
C-4-ene-7β-ol-3-one	534.4054	9.66	1.30	0.0433±0.0093	0.1834±0.2425	7β-Hydroxycholesterol
C-4-ene-7α-ol-3-one	534.4054	10.17	1.37	0.0055±0.0011	0.0401±0.0525	7α-Hydroxycholesterol
C-4-ene-6β-ol-3-one	534.4054	10.54	1.42	ND	0.0527±0.0690	6β-Hydroxycholesterol
C-4-ene-20,22-diol-3-one	550.4003	4.56	0.61	0.0106±0.0014	0.0295±0.0018	20,22-Dihydroxycholesterol

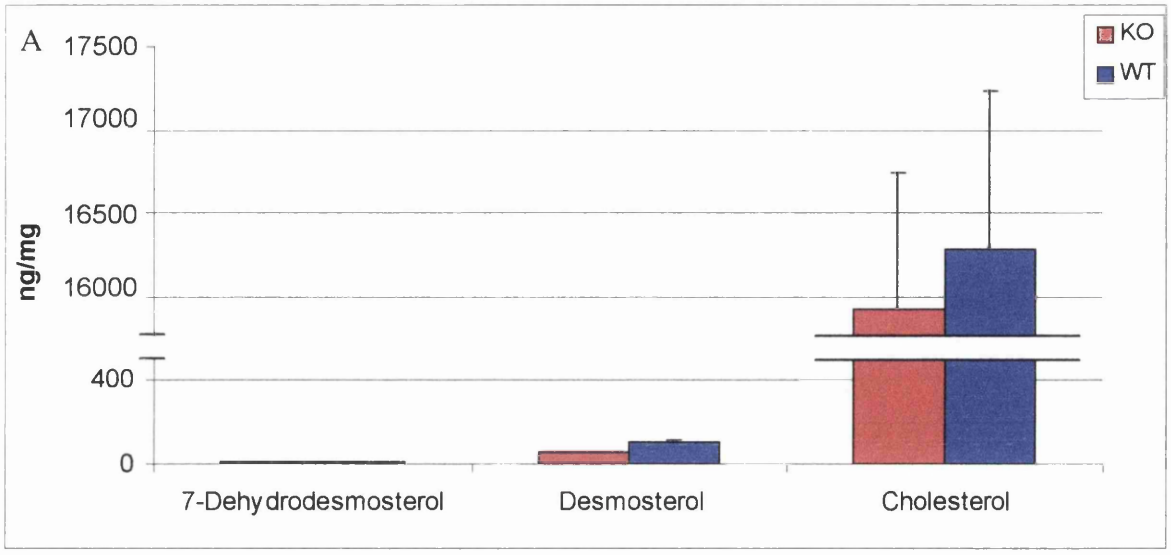

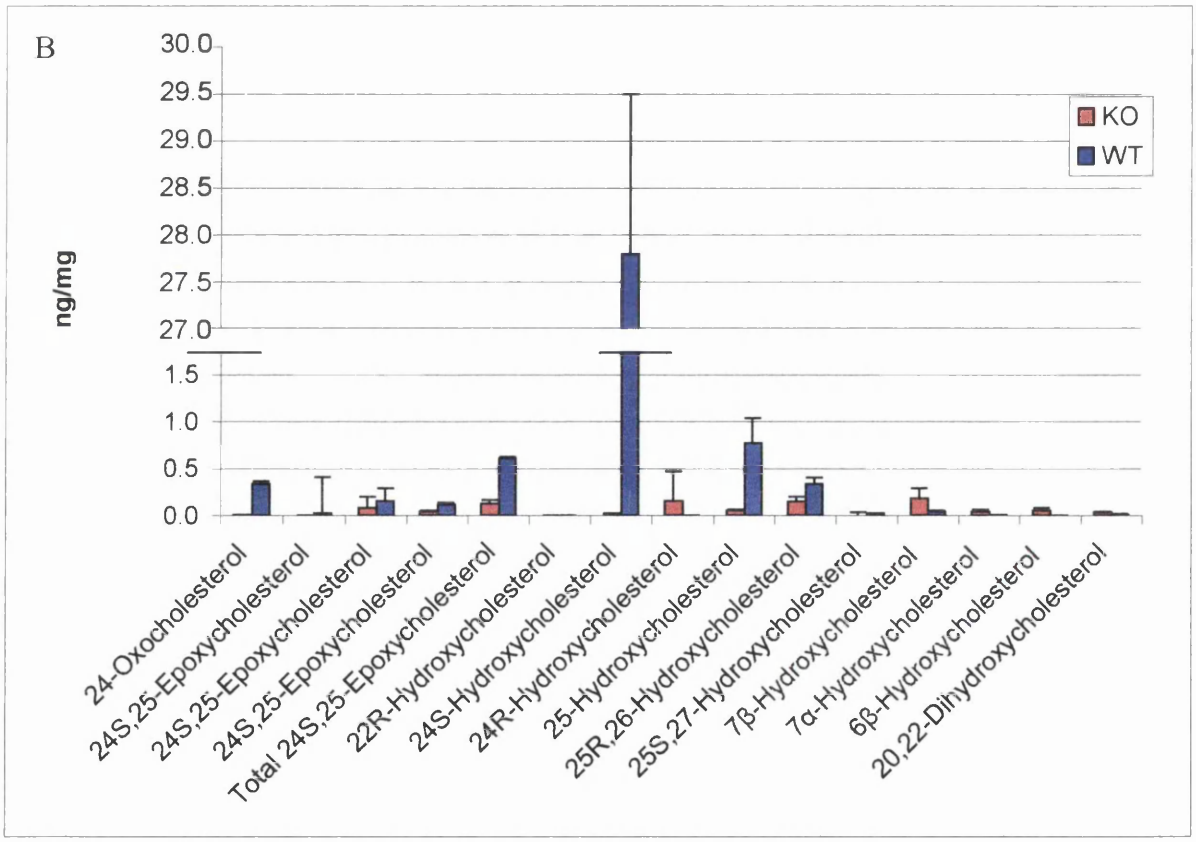

Figure 5.3 Sterols (A) and oxysterols (B) identified in Cyp46a1$^{-/-}$ and wild type mouse brains.

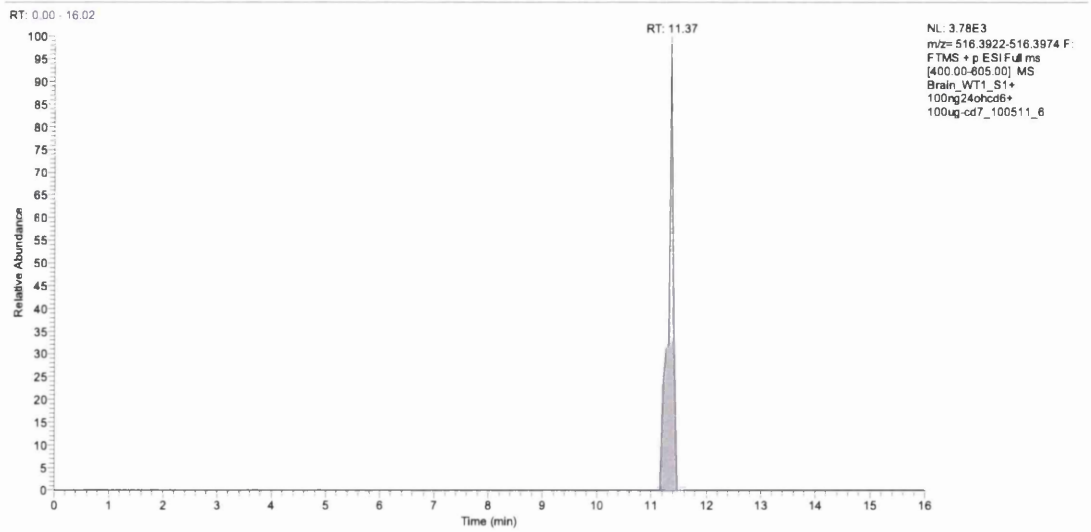

Figure 5.4. RIC 516.3948 m/z corresponding to GP-derivatised desmosterol identified in brain of *Cyp46a1*+/+ mouse.

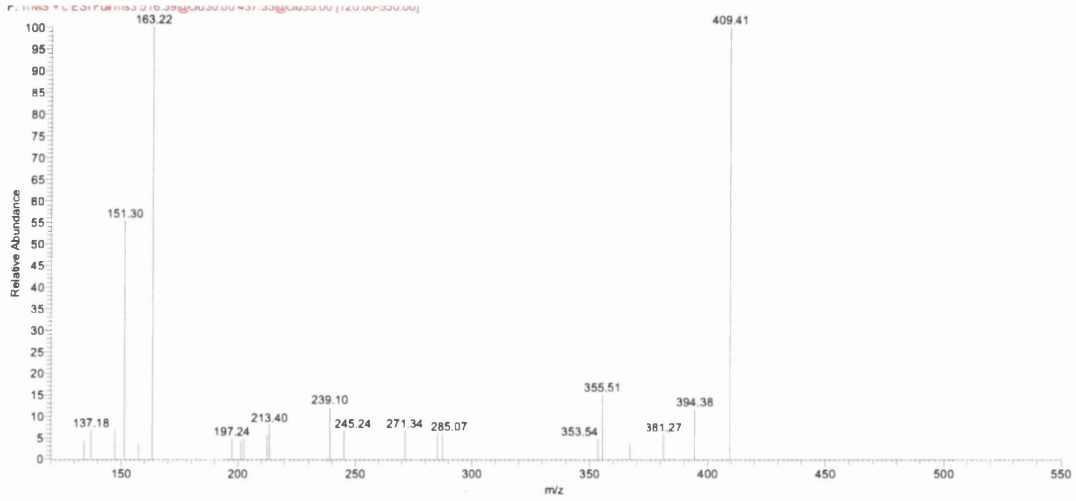

Figure 5.5. MS^3 spectrum of compound eluting at 11.33 min identified as GP-tagged desmosterol

The wild type mouse chromatogram is completely dominated by GP-tagged 24S-hydroxycholesterol (27.9069±0.7322 ng/mg, Table 5.2) which, following derivatisation, gives two peaks corresponding to the *syn* and *anti* conformers of the GP-derivative, RT 7.49 min and 7.80 min. The MS3 chromatogram is showed in Figure 5.7. In the *Cyp46a1*-/- mouse the deletion of *Cyp46a1* gene results in a great reduction in the level of 24S-hydroxycholesterol in brain (Table 5.2). The almost complete depletion of the sample from this major oxysterol allows the injection of greater amounts of material on-column without risking column overloading. As a consequence, the sensitivity of the analytical method increases from 50 pg/mg to 5 pg/mg. Interestingly, low levels of 24S-hydroxycholesterol

(0.0173±0.0025 ng/mg) are still observed in brain of the *Cyp46a1-/-* mouse as revealed in the RIC of 534.4054 for the GP-tagged hydroxycholesterols . The origin of this oxysterol may be from extracerebral synthesis or from other cholesterol hydroxylases present in brain e.g. cholesterol 27-hydroxylase, Cyp27a1 [106, 177, 182].

Murine brain also contains another isomer of 24-hydroxylated cholesterol, 24R-hydroxycholesterol (MS^3 spectrum presented in Figure 5.8). In brain of the *Cyp46a1-/-* mouse present at the level 0.1598±0.0228 ng/mg, while in wild type animal, putative 24R-hydroxycholesterol was dominated by its 24S isomer and, therefore, not reliably quantifiable. 24R-Hydroxycholesterol could conceivably be formed from desmosterol in a hydration reaction catalysed by D-bifunctional protein (DBP), a multifunctional enzyme expressed in brain, although the hydratase domain of this stereospecific enzyme usually forms (R)-hydroxy-acyl-CoA intermediates from trans-2-enoyl-CoAs [45]. Alternatively, a mouse microsomal Cyp3a enzyme has be shown to be a hepatic 24R-hydroxylase to 5β-cholestane-3α,7α,12α,25-tetrol and could have some activity towards cholesterol [214], or the source of 24R-hydroxycholesterol may be some other cholesterol hydroxylases present in brain e.g. Cyp27a1 [177]. In knockout mouse it may be expected that some other oxysterol would compensate the absence of Cyp46a1 from brain, however, in agreement with earlier studies [106] there was no matching increases in the abundance of any other oxysterol.

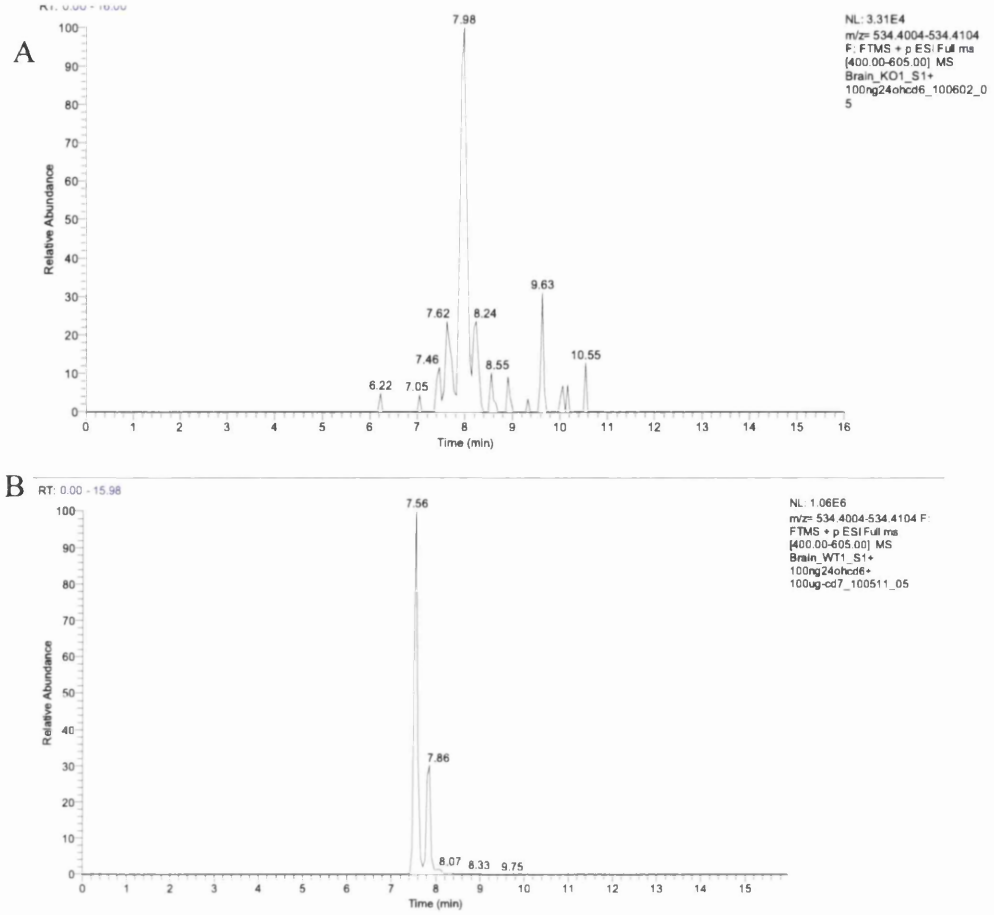

Figure 5.6. Monohydroxylated GP derivatives of cholesterol in brain of *Cyp46a1* +/+ (A) and *Cyp46a1*-/- (B) mouse brain.

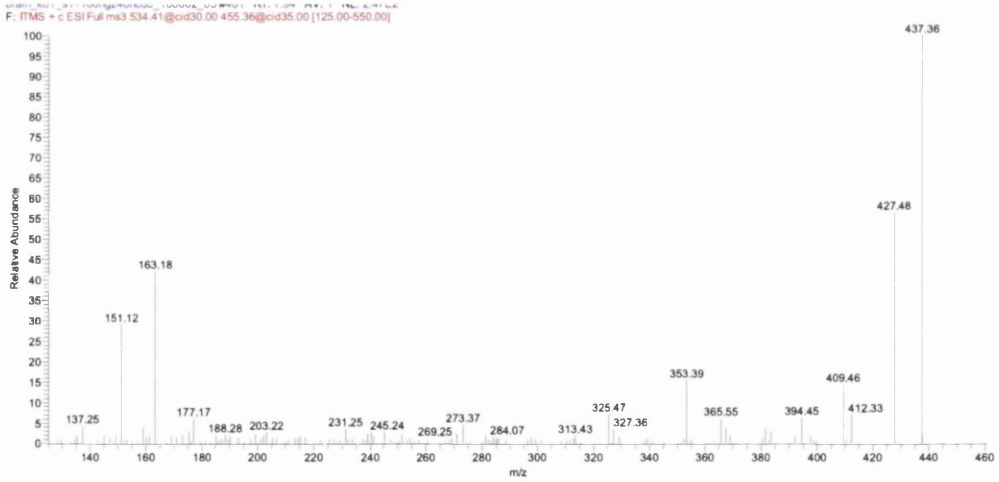

Figure 5.7. MS^3 spectrum of peak eluting at 7.49 min identified as GP-tagged 24S-hydroxycholesterol

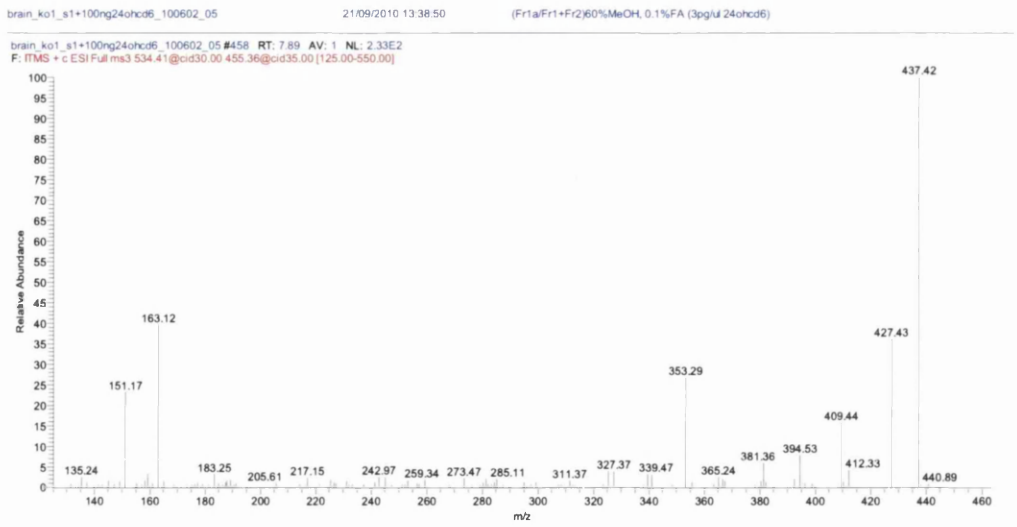

Figure 5.8. MS^3 spectrum of peak eluting at 7.49 min identified as GP-tagged 24R-hydroxycholesterol

GP-Tagged 26-hydroxycholesterol (Figure 5.9) was identified at relatively low levels of in wild type mice 0.3342±0.1327 ng/mg, while in the knockout mice these were 0.1485±0.0060 ng/mg. In the chromatogram of wild type mouse brain 27-hydroxycholesterol is eluted closely to 24S- and 24R-hydroxycholesterol, therefore the integration and quantification of 27-hydroxycholesterol peak is biased.

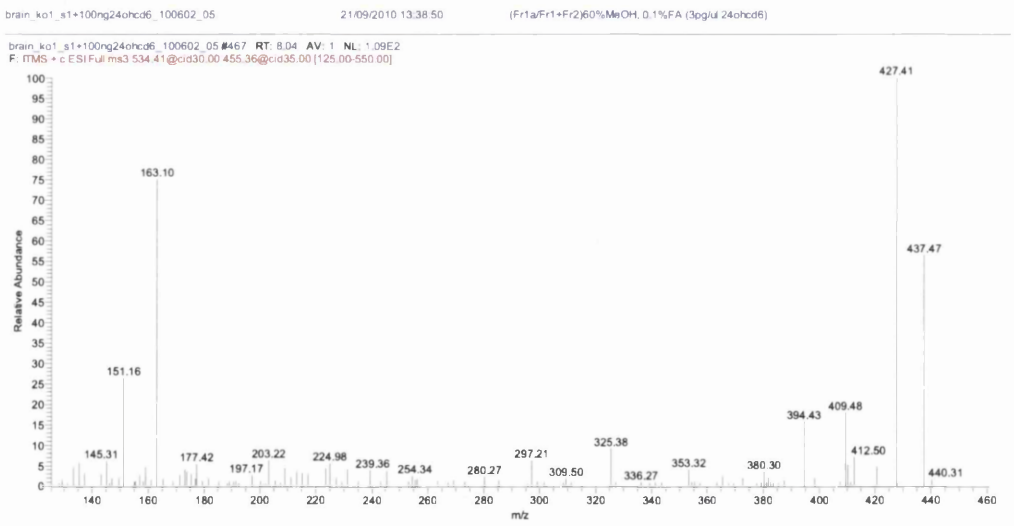

Figure 5.9. MS^3 spectrum of GP-tagged 26-hydroxycholesterol eluting as a peak of RT 8.04 min

Also trace amounts of 25-hydroxycholesterol was detected at very low level in knockout type mice: 0.0502±0.0094 ng/mg while in the wild type these were quantified at 10-

fold higher levels (0.7696±0.1029ng/mg), MS^3 spectrum presented in Figure 5.10. In the knockout chromatogram the absence of major analyte 24S-hydroxycholesterol reveals peaks belonging to the other compounds, therefore its quantification is more reliable. Cholesterol 25-hydroxylse (ch25h) and Cyp27a1 are both expressed in rodent brain and will generate 25- and 26-hydroxycholesterols respectively [108, 177].

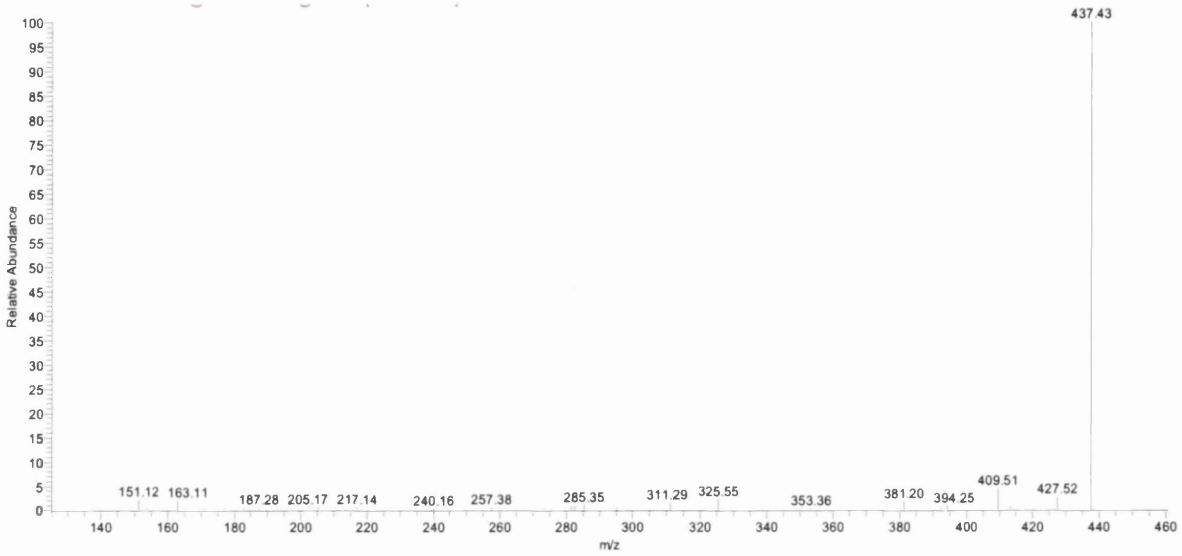

Figure 5.10. MS^3 spectrum of peak eluting at 7.63 min identified as GP-tagged 25-hydroxycholesterol

Ring-hydroxylated sterols such as 7α- and 7β-hydroxycholesterol (MS^3 spetra presented in Figure 5.11 and Figure 5.12, respectively) were detected in some analytical runs of *Cyp46a1-/-* (<0.050 ng/mg), in wild type animals the levels of 7α- and 7β-hydroxycholesterols were significantly higher (0.0401±0.0525 and 0.1834±0.2425 ng/mg, respectively). It is likely that 7α- and 7β-hydroxycholesterols are imported into brain from the bloodstream as Cyp7a1, the cholesterol 7α-hydroxylase, is liver specific, while 7β-hydroxycholesterol can be of a non-enzymatic source arising from cholesterol autoxidation [185, 215].

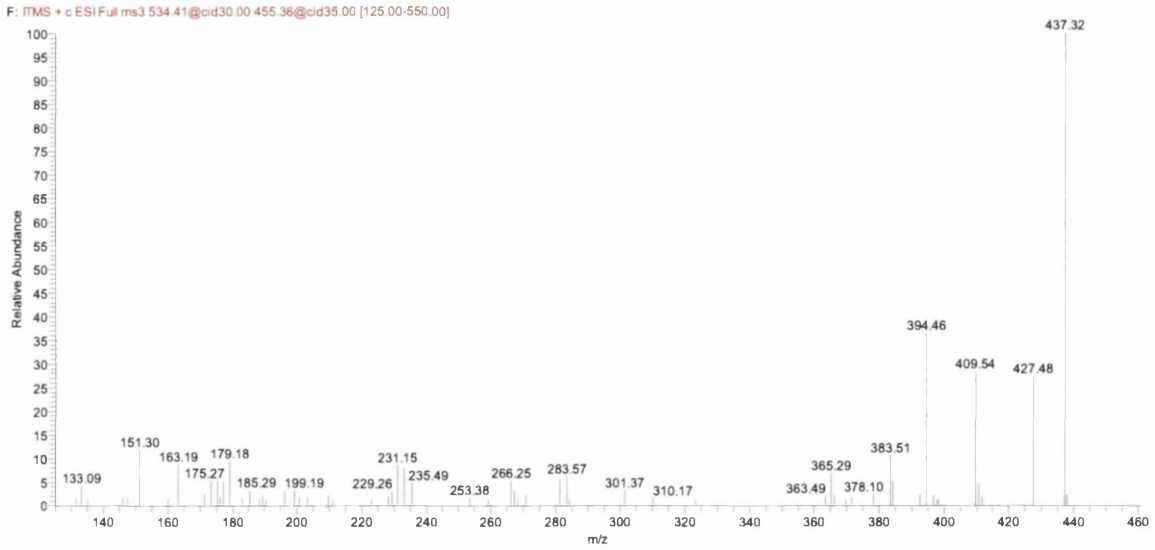

Figure 5.11. MS^3 spectrum of peak eluting at 10.18 min identified as GP-tagged 7α-hydroxycholesterol.

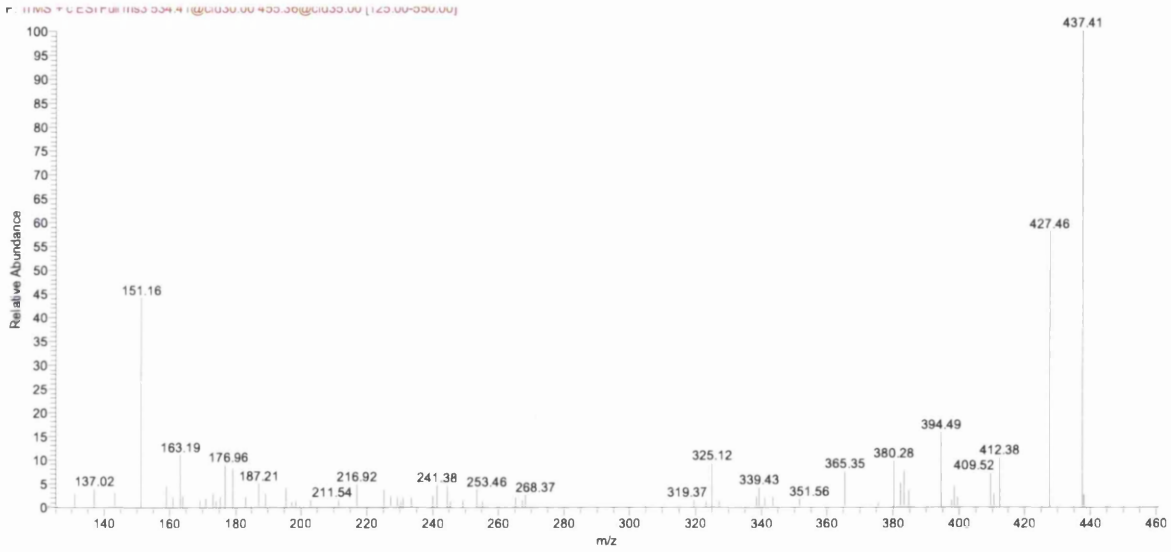

Figure 5.12. MS^3 spectrum of peak eluting at 9.59 min identified as GP-tagged 7β-hydroxycholesterol.

The final eluting oxysterol from the RIC of 534.4054 corresponds to 6β-hydroxycholesterol (MS^3 spectrum in Figure 5.13); in wild type these were below the detection level, while in *Cyp46a1-/-* animal were quantified as 0.0527±0.0690 ng/mg. This is derived from either cholestane-3β,5α,6β-triol or a 5,6-epoxycholesterol during the charge-tagging process.

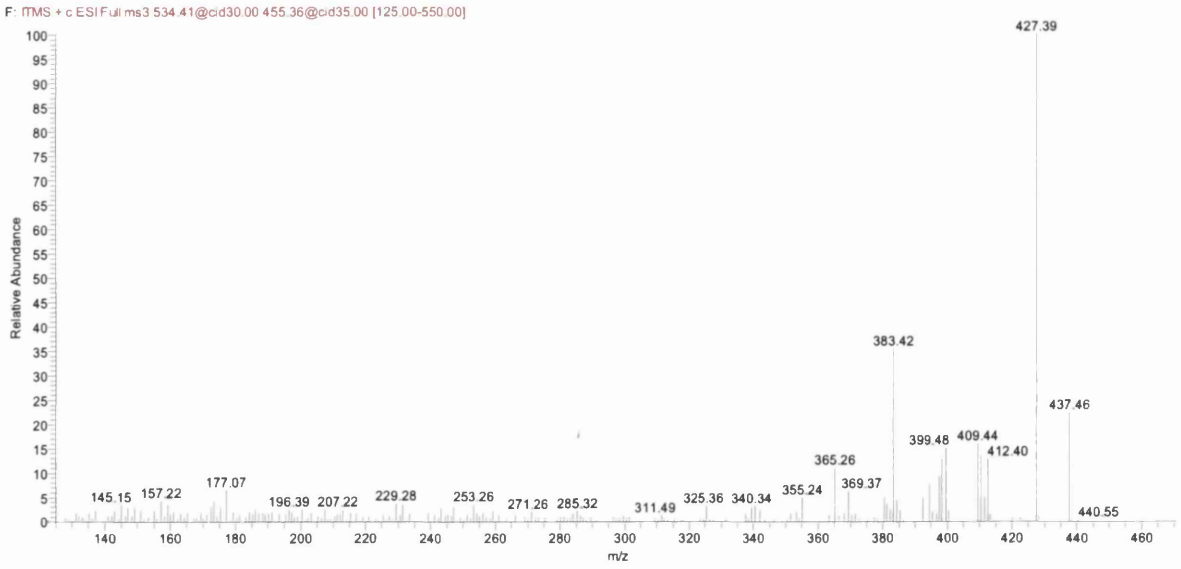

Figure 5.13. MS^3 spectrum of peak eluting at 10.53 min identified as GP-tagged 6β-hydroxycholesterol.

There are also low levels of a side-chain hydroxylated sterol, probably the 25S isomer of 26-hydroxycholesterol (0.0283±0.0048 and 0.0302±0.0353 ng/mg) present in the wild type and *Cyp46a1*$^{-/-}$ brain. There is evidence that cholest-(25S)-5-en-3β,27-diol is formed from cholesterol by a microsomal enzyme in contrast to the mitochondrial Cyp27a1 enzyme which gives the 25R isomer [216].

Table 5.2 lists the levels of detected metabolites. The identification of oxysterols was confirmed by comparison of accurate mass, retention time and MS^n spectra with authentic standards (Figure 5.14).

24S,25-Epoxycholesterol is produced as a side product of the cholesterol biosynthesis pathway. During the GP-tagging reactions the 24S,25-epoxide isomerises to the 24-ketone, is hydrolysed to the 24,25-diol and undergoes methanolysis to the 24-ol-25-methoxide and/or 24-methoxide-25-ol (Figure 5.14-Figure 5.18). Each of this products was quantified separately, the total sum of the compounds is considered as a final concentration of 24S,25-epoxycholesterol, which was higher in wild type mice (0.6411±0.0155 ng/mg and 0.1235±0.0435 ng/mg; in wild type and *Cyp46a1-/-*, respectively).

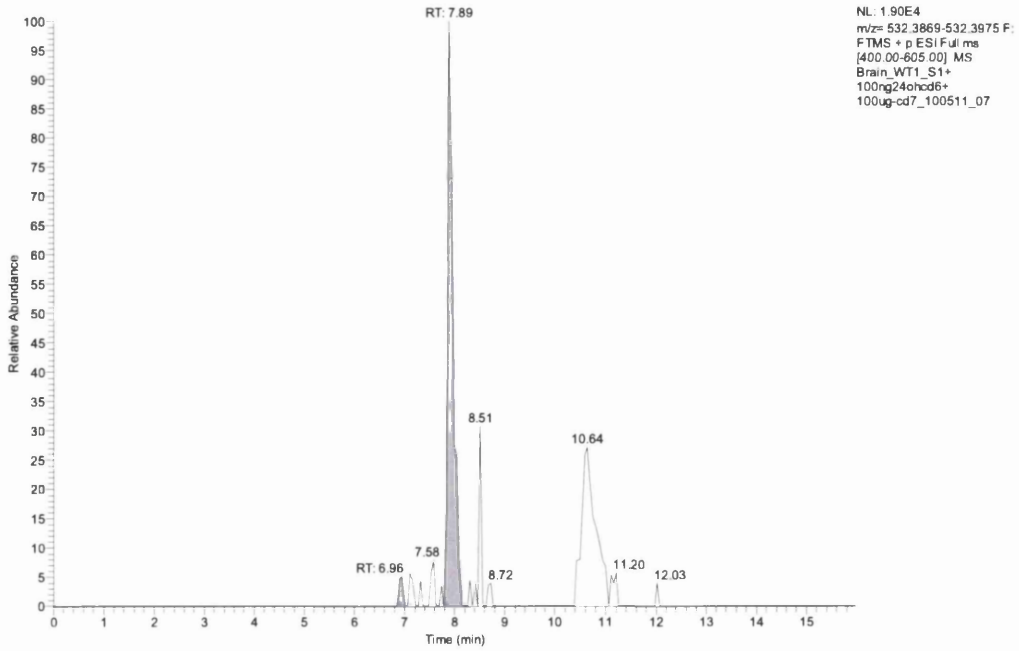

Figure 5.14. GP derivatives of 24S,25-epoxycholesterol identified in brain of *Cyp46a1*+/+ mouse.

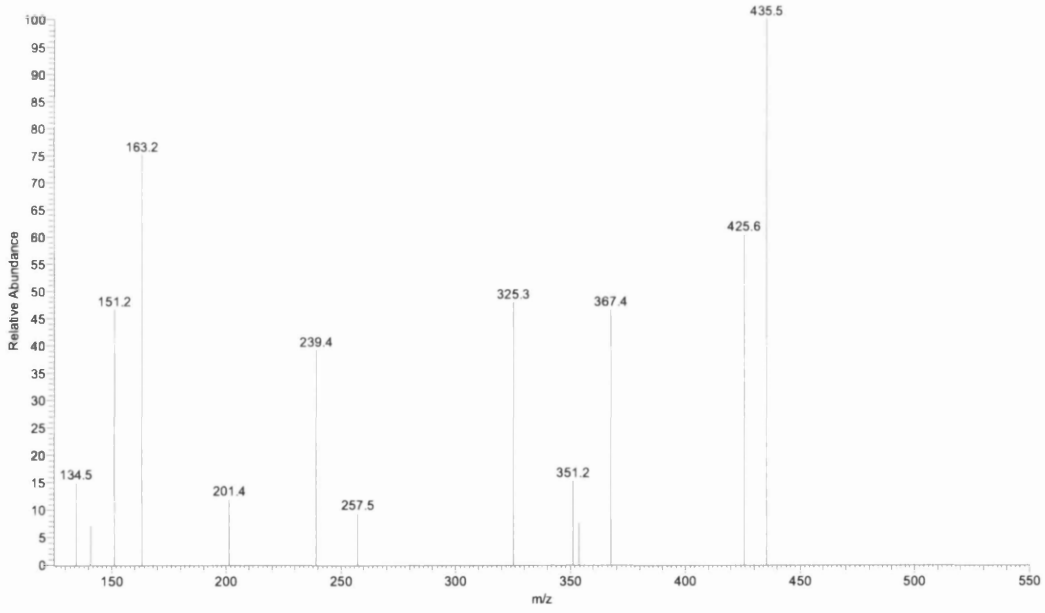

Figure 5.15. MS^3 spectrum of peak eluting at 7.97 min identified as GP-tagged 24S,25-epoxycholesterol.

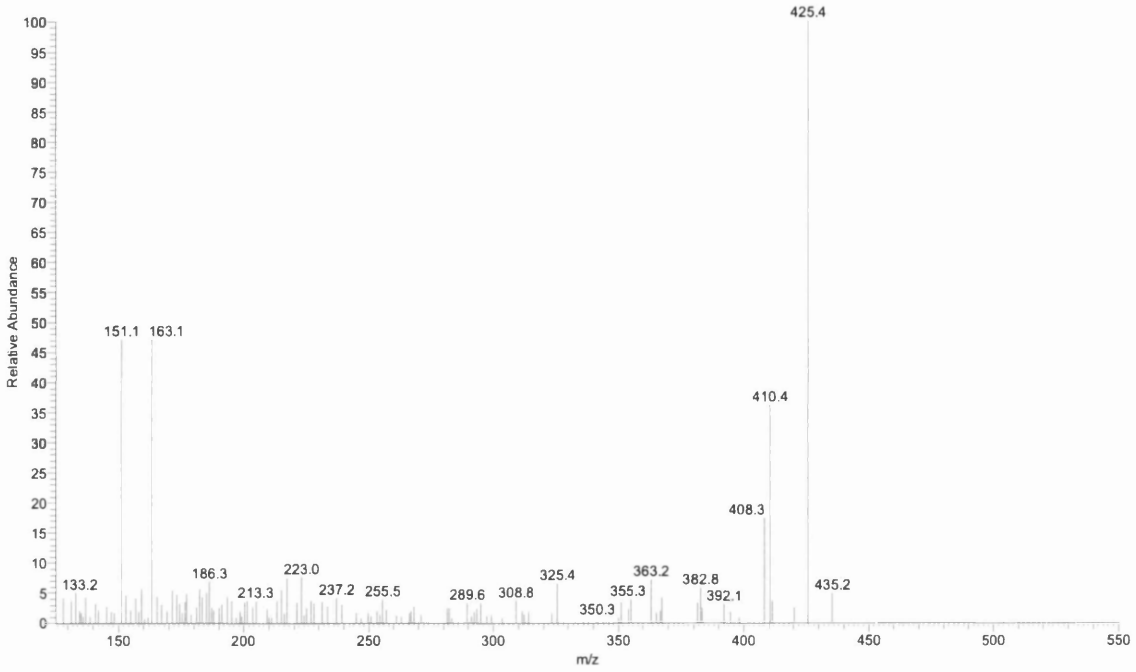

Figure 5.16. MS^3 spectrum of GP-tagged 24-ketocholesteroleluting at 7.92 min.

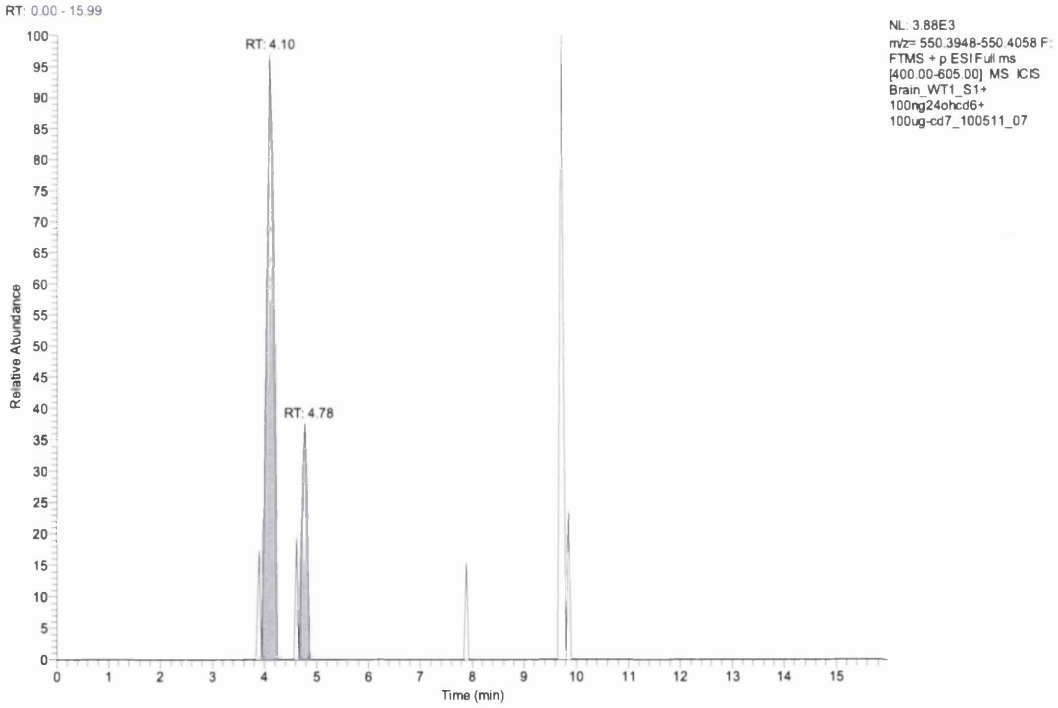

Figure 5.17. RIC of *m/z* 550.4005 showing GP derivatives of 24,25-dihydroxycholesterol in *Cyp46a1*+/+ mouse brain.

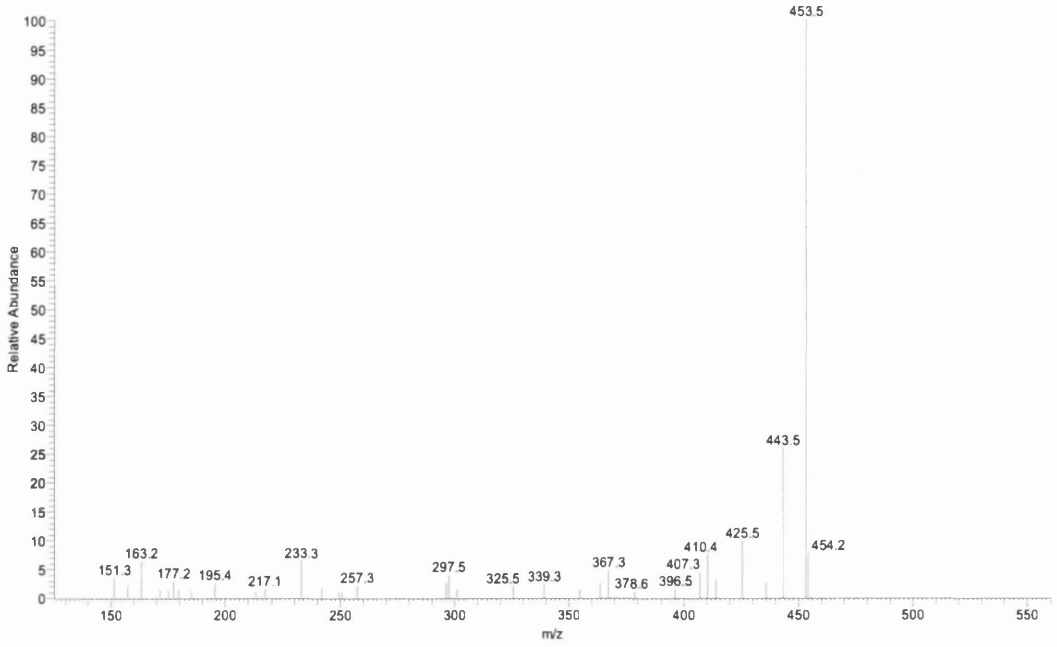

Figure 5.18. MS^3 spectrum of GP-tagged 24-ketocholesterol eluting at 7.92 min.

Cytochrome P450 11a1, also known as P450scc, is expressed in rodent brain [174, 183]. In the first step this enzyme hydroxylates cholesterol at C-22R, and then at C-20R to give the diol, followed by the cleavage of the C-20 – C-22 bond to reveal pregnenolone. Low levels of both 22R-hydroxycholesterol (1 pg/mg±0.49pg/mg) RT6.80min and 20R,22-dihydroxycholesterol (29 pg/mg) are evident in the *Cyp46a1-/-* animals. As in the wild type animal low levels of 24S,25-epoxycholesterol are found in brain from the *Cyp46a1-/-* animal appearing as the GP-tagged epoxide, its 24-oxo isomer and methanolysis and hydrolysis products (127 pg/mg) (Figure 5.16- Figure 5.18).

Despite the absence of appreciable amounts of 24S-hydroxycholesterol or of a major replacement oxysterol in the brain of *Cyp46a1-/-* mouse, the level of cholesterol is essentially identical to that of the wild-type mouse (Table 5.1, Figure 5.2). This is in agreement with earlier studies which showed that knockout of the *Cyp46a1* gene in mice does not reduce the brain cholesterol level only its rate of synthesis [106]. This hypothesis is further supported in the present study where reduction of desmosterol levels are noted in the *Cyp46a1* mouse (Figure 5.4).

5.3 Discussion

24S-Hydroxylation is the main enzyme involved in metabolism of cholesterol in the brain and in mouse accounts for about 70% of cholesterol turnover [105]. Unexpectedly, a consequence of deletion of the *Cyp46a1* gene in the cholesterol 24-hydroxylase knockout mouse was a reduction in the rate of cholesterol biosynthesis rather than an its accumulation in the brain [106]. The deletion of cholesterol 24S-hydroxylase results in removal of the most abundant metabolite unveiling less pronounced compounds which in wild type animal would be obscured by 24S-hydroxycholesterol. This aim of this study was to unveil an alternative routes of cholesterol removal in the absence of Cyp46a1. However, the sterols extracted form the brain of Cyp46a1 deficient animal did not exhibit the increase in its level which would compensate for the loss of cholesterol 24S-hydroxylase. The steady level of cholesterol is maintained via reduction of its production rather than an alternative route of exertion.

In the lipid extracts of brain *Cyp46a1-/-* mouse low levels of both 24S- and 24R-hydroxycholesterols were found (Table 5.2). The origin of these oxysterols are not defined as there are few references to the presence of 24R-hydroxycholesterol in mammals. Work of Spencer and colleagues have shown that this isomer can be formed enzymatically from 24R,25-epoxycholesterol by Dede cells and by rat liver homogenate [217]. However, 24R,25-epoxycholesterol is not the natural 24,25-epoxide formed via the shunt of the mevalonate pathway in mammals [218]. In the brain of the *Cyp46a1-/-* mouse we also detected a small quantities of (25R),26-hydroxycholesterol and of an isomer which is probably (25S),27-hydroxycholesterol. While Cyp27a1, the microsomal (25R),26-hydroxylase, is expressed in brain [177], a microsomal (25S),27-hydroxylase is expressed in mammalian liver [208]. 25-hydroxycholesterol in chromatograms acquired from the wild type brain is almost entirely dominated by closely eluting 24S-hydroxycholesterol [123, 148]. However, in the absence of the *Cyp46a1* gene the presence of 25-hydroxycholesterol (50 pg/mg) in brain is evident.

25-Hydroxycholesterol has been recently intensively studied for its function in the immune system [41, 130]. A number of reports show that it is produced and secreted by macrophages in response to TLR activation [129, 130, 135].

Cyp7a1 is a liver specific enzyme catalyzing a reaction of 7α-hydroxylation of cholesterol [215], so detected 7α-hydroxycholesterol in brain is probably a consequence of diffusion of this oxysterol across the blood brain barrier from the circulation. Cholesterol can become also oxidized on its tetracycling core forming analytes such as 7α- and 7β-hydroxycholesterols [186]. This may be arise from oxidative stress [219], or can be generated

during sample preparation [185] Similarly, the 5α and 5β isomers of 5,6-epoxycholesterol are formed from cholesterol non-enzymatically [186].

Unlike Cyp7a1, Cyp7b1, the oxysterol 7α-hydroxylase, is expressed in the brain [220, 221]. Here we obtain evidence for the presence of this enzyme in brain with the identification of 7α,26-dihydroxycholesterol, the 7α-hydroxylation product of 26-hydroxycholesterol.

Chapter 6

6 Analysis of oxysterols and sterols from Cyp27a1 -/- mouse brain

6.1 Introduction

Cerebrotendinous Xanthomatosis (CTX) is an inborn error of cholesterol metabolism resulting in an impaired synthesis of bile acids. Clinical symptoms of the disorder include accumulation of sterols in tendons and brain (xanthomas), atherosclerosis, mental retardation, ataxia and cataracts [222]. CTX was first described by van Bogaert in 1937 [2] while the genetic defect underlying the disease was identified in 1991 by Cali [223].

CTX is caused by a recessive mutation in the gene coding the mitochondrial cytochrome P450 enzyme sterol 27-hydroxylase (CYP27A1). This hydroxylase catalyses the initial step in the "alternate" bile acids biosynthesis pathway where cholesterol is hydroxylated at the C-26 position and subsequently transformed into chenodeoxycholic acid. The "classical" bile acid pathway also requires 26-hydroxylation of the intermediates to produce cholic acid. CYP27A1 is also involved in the hydroxylation of a number of other substrates such as vitamin D_3 [224-226].

The *CYP27A1* gene is located on the long arm of human chromosome 2 [223]. The genetic alterations underlying CTX include deletions, insertions, mis-sense and non-sense mutations that affect various regions of the CYP27A1 gene [227, 228].
There is a significant variation between clinical symptoms of CTX which do not correlate with the genotypes of the patients. This implies the possible role of other factors in the development of CTX [229].

Biochemical analysis of samples from CTX patients show that the general pool of bile acids is reduced in particular chenodeoxycholic acid is almost completely absent. Furthermore their blood has an increased concentration of cholestanol and normal to increased level of cholesterol [230] and altered ratios of cholesterol precursors [231]. Analysis of urine and shows abnormal multihydroxylated alcohols [232, 233].

A murine model of CTX has been constructed by replacing the 71 bp fragment of *Cyp27a1* that encodes the heme-binding region of the hydroxylase with a neomycin resistance gene cassette. This region is believed to be essential for the catalytic activity of the enzyme [234].

Unlike patients affected by CTX, the knock-out ($Cyp27a1^{-/-}$) mice, do not show the features characteristic for CTX such as xanthomas. Despite missing the main phenotypical features of human CTX, the knockout mice still develop abnormal levels of cholesterol precursors and metabolites [214, 235-237].

The deletion of *Cyp27a1* causes a compensatory increase in the expression of Cyp7a1 catalyzing the first step of the classical pathway of bile acid synthesis and Cyp3a which is responsible for side-hydroxylation of oxysterols [214]. Upregulated expression of enzymes is followed by an increase in the level of their products detected in blood and plasma. Analysis of the tissues shows a high content of 7α-hydroxycholesterol and side-chain hydroxylated sterols.

In this study we focused on a detailed analysis of the oxysterols extracted from the brains of Cyp27a1$^{-/-}$ homozygous mice. A study carried out by Ogundare et al [167] showed the presence of bile acid precursors in human cerebrospinal fluid, here is further investigated a possibility that brain has autonomous bile acid synthesis pathways. This analysis of the mouse brain lipidome aims to identify the disturbances in the oxysterol formation that may affect the formation of bile acids in this organ.

6.2 Results

Sterols

Cholesterol treated with cholesterol oxidase and subjected to GP-derivatisation yields an $[M]^+$ ion of *m/z* of 518.4105. A chromatogram obtained for the analysis of fraction 3a at *m/z* 518.4105 showed a single peak with a RT of 11.75 min (Figure 6.1A and B); this was identified as cholesterol by the comparison with the authentic standard. The deletion of 27-hydroxylase does not affect the level of cholesterol in the brain (16.90±0.29ug/mg in wild type and 16.98±0.96ug/mg in knockout, as per Table 6.1).

(A)

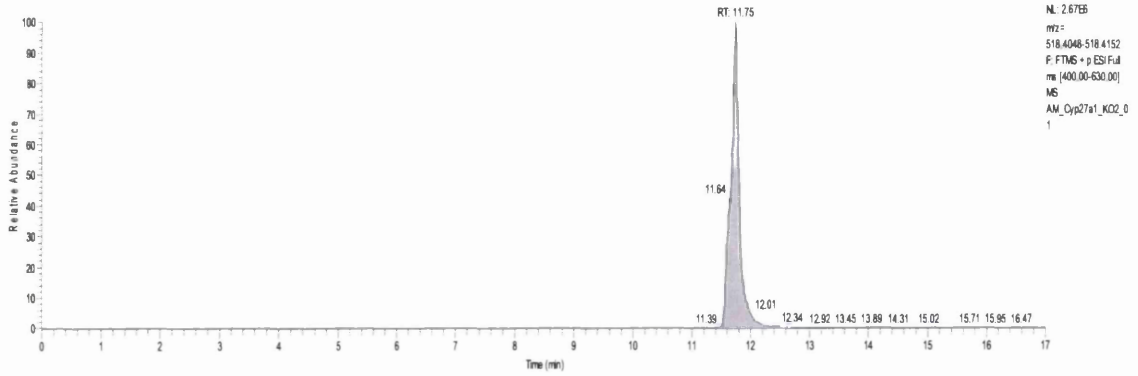

(B)

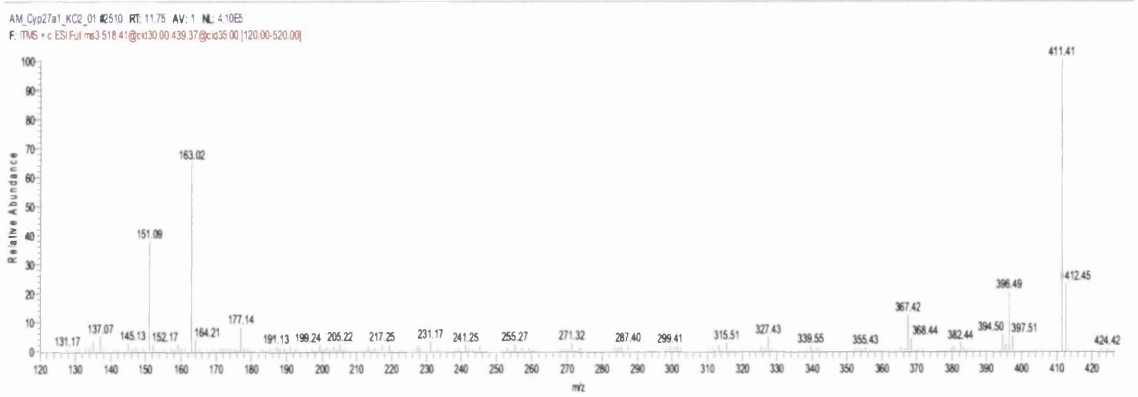

Figure 6.1 Cholesterol in brain of Cyp27a1-/- mouse.
(A) RIC of m/z 518.4105±5 ppm
(B) MS3 spectrum of peak eluting at 11.75min identified as GP-tagged cholesterol

Cholesterol can be synthesised by two pathways that use different unsaturated sterols in the finals step: either desmosterol or 7-dehydrocholesterol. Sterols with two C-C double bonds derivatised with GP give a molecular ion *m/z* 516.3948.

(A)

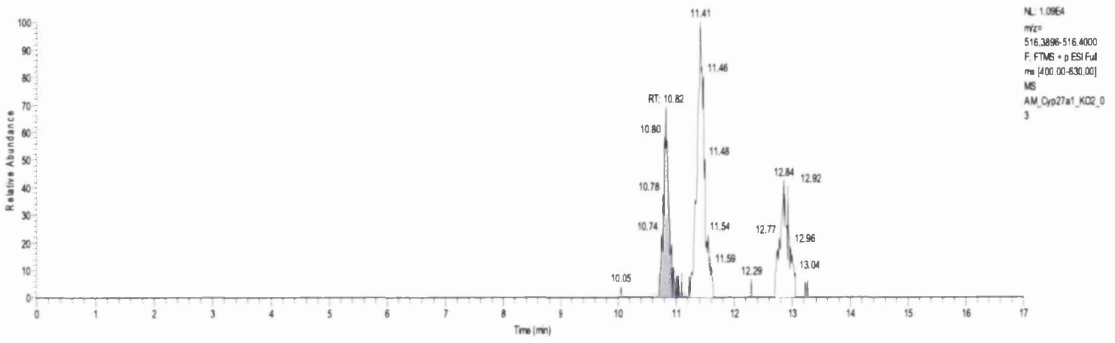

(B)

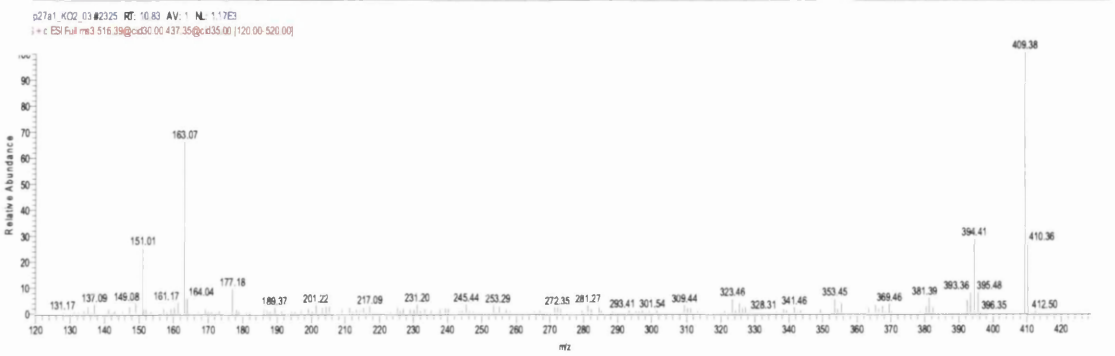

Figure 6.2 Desmosterol in brain of Cyp27a1$^{-/-}$ mouse.
(A) RIC of m/z 516.3948±5 ppm
(B) MS^3 spectrum of peak eluting at 10.82min identified as GP-tagged desmosterol

Analysis of RIC at *m/z* 516.3948 shows two peaks with RT 10.82min and 11.41min. Based on the comparison with an authentic GP-tagged standard, the peak at 10.82 min was identified as desmosterol (Figure 6.2). Level in Cyp27a1$^{-/-}$ animals was established as 0.0377±0.0012 ug/mg, in comparison, more was detected in wild type 0.0630±0.0048ug/mg.

Table 6.1 Sterols and oxysterols identified by LC-ESI-MS^n in murine brain following SPE and charge-tagging with GP-hydrazine. Samples from three Cyp27a1$^{-/-}$ and three Cyp27a1$^{+/+}$ mice were analysed.
Quantitation of sterols present in fraction 1a based on [$^2H_6$]cholest-5-ene-3β,24(R/S)-diol internal standard and GP-tagged 3-oxo-4-ene compounds giving

m/z	RT	GP Derivative Analysed Systematic name	Originating Cmpd in Fr 3a (underlined) and in Fr3b (*italics*) Common name	Mean concentration µg/mg ± SD (n = 3)			
				Cyp27a1 $^{+/+}$ mice		Cyp27a1 $^{-/-}$ mice	
				Fr 3a	Fr 3b	Fr 3a	Fr 3b
518.4105	11.75min	Cholest-4-en-3-one 3-GP	Cholesterol/ Cholest-4-en-3-one	16.90±0.29		16.98±0.96	
518.4105	11.98min	Cholest-4-en-3-one 3-GP	*Cholest-4-en-3-one*		0.1722±0.0587		1.3013±0.8154
516.3948	10.82min	Cholest-4,24-dien-3-one 3-GP	Desmosterol/ *Cholest-4,24-dien-3-one*	0.0630±0.0048	ND	0.0377±0.0012	ND
516.3948	11.41min	Cholest-4,7-dien-3-one 3-GP	7-Dehydrocholesterol/ *Cholest-4,7-dien-3-one*	0.0116±0.0012	ND	0.0543±0.0011	ND
516.3948		Total level of precursors		0.0746±0.0060	ND	0.0920±0.0013	ND
516.3948	11.60min	Cholest-4,6-dien-3-one 3-GP + Cholest-4,8(9)-dien-3-one 3-GP	*Cholesta-4,6-dien-3-one+ cholesta-4,8(9)-3-one*	NA	ND	NA	2.7910±1.7455

m/z	RT Short gradient Long gradient*	Systematic name	Common name (in Fr 1a)	Mean concentration ng/mg ± SD (n = 3)			
				Cyp27a1 $^{+/+}$ mice		Cyp27a1 $^{-/-}$ mice	
				Fr1a	Fr1b	Fr1a	Fr1b
532.3898	6.59min+6.85min	24S,25-Epoxycholest-4-en-3-one 3-GP	24S,25-Epoxycholesterol/ 24S,25-Epoxycholest-4-en-3-one	0.0348±0.0032	ND	0.0409±0.0045	ND
532.3898	7.00min	26-Hydroxycholest-4,24Z-dien-3-one 3-GP	(24Z),26-Hydroxydesmosterol/ *26-Hydroxycholest-4,24Z-dien-3-one*	0.0159±0.0016	ND	0.0197±0.0021	ND
532.3898	7.8min	Cholest-4-en-3,24-dione 3-GP	24-Oxocholesterol/ Cholest-4-en-3,24-dione	0.9691±0.0233	ND	0.5904±0.0323	ND
532.3898	8.25min	Cholest-4-en-3,22-dione 3-GP	22-Oxocholesterol/Cholest-4-en-3,22-dione	0.0071±0.0009	ND	0.0098±0.0007	ND
532.3898	9.20min	7α-Hydroxycholest-4,24Z-dien-3-one 3-GP	7α-Hydroxydesmosterol/ *7α-Hydroxycholest-4,24Z-dien-3-one*	0.0078±0.0010	ND	0.0270±0.0030	ND
532.3898	10.28min	Cholest-4-ene-3,6-dione 6-GP	6-Oxocholesterol/Cholest-4-ene-3,6-dione	ND	ND	0.0494±0.0143	ND

534.4054	7.30min 7.74	24S-Hydroxycholest-4-en-3-one 3-GP	24S-Hydroxycholesterol/ 24S-Hydroxycholest-4-en-3-one	23.5548±0.6460	ND	25.9209±1.7289	ND
534.4054	*18.18min	26-Hydroxycholest-4-en-3-one 3-GP	26-Hydroxycholesterol/ *26-Hydroxycholest-4-en-3-on*	0.0904±0.0069	ND	0.0111±0.0019	ND
534.4054	*17.96min	24R-Hydroxycholest-4-en-3-one 3-GP	24R-Hydroxycholesterol/ 24R-Hydroxycholest-4-en-3-one	0.6421±0.0227	ND	0.3096±0.0545	ND
534.4054	9.64min	3β-Hydroxycholest-4-en-7-one 7-GP	3β-Hydroxycholest-4-en-7-one/ *3β-Hydroxycholest-4-en-7-one*	0.0050±0.0011	ND	0.0415±0.0022	0.0052±0.0009
534.4054	10.07+10.40min	7α-Hydroxycholest-4-en-3-one 3-GP	7α-Hydroxycholesterol/ *7α-Hydroxycholest-4-en-3-one*	0.0358±0.0065	ND	2.4936±0.3520	0.0572±0.0070
534.4054	9.50+9.90min	7β-Hydroxycholest-4-en-3-one 3-GP	7β-Hydroxycholesterol/ *7β-Hydroxycholest-4-en-3-one*	0.0384±0.0069	ND	0.3382±0.0308	ND
534.4054	10.30+10.50min	6β-Hydroxycholest-4-en-3-one 3-GP	6β-Hydroxycholesterol/ *6β-Hydroxycholest-4-en-3-one*	0.0356±0.0031	ND	0.7092±0.1737	ND
536.4211	10.59 min	7α-Hydroxy-5α-cholestan-3-one 3-GP	5α-cholestan-3β,7α-diol/ *7α-Hydroxy-5α-cholestan-3-one*	ND	ND	0.2051±0.2061	ND
550.4003	3.45min	24S,25-Dihydroxycholest-4-en-3-one 3-GP	24,25-Dihydroxycholesterol/ 24S,25-Dihydroxycholest-4-en-3-one	0.1658±0.0290	ND	0.2004±0.0250	ND
550.4003	5.30+6.20min	7α,25-Dihydroxycholest-4-en-3-one 3-GP	7α,25-Dihydroxycholesterol/ *7α,25-Dihydroxycholest-4-en-3-one*	0.0285±0.0026	0.0022±0.0005	0.1183±0.0095	0.0392±0.0022
550.4003	5.65min	7α,27-Dihydroxycholest-4-en-3-one 3-GP	7α,27-Dihydroxycholesterol/ *7α,27-Dihydroxycholest-4-en-3-one*	ND	0.0022±0.0004	0.0429±0.0038	0.0244±0.0003
550.4003	7.10min	X,Y-Dihydroxycholest-4-en-3-one 3-GP	X,Y-Dihydroxycholesterol/ *X,Y-Dihydroxycholest-4-en-3-one*	ND	ND	0.0225±0.0025	0.0013±0.0003
550.4003	7.42min	X,Y-Dihydroxycholest-4-en-3-one 3-GP	X,Y-Dihydroxycholesterol/ *X,Y-Dihydroxycholest-4-en-3-one*	ND	ND	ND	0.0018±0.0002
550.4003	8.10min	X,Y-Dihydroxycholest-4-en-3-one 3-GP	X,Y-Dihydroxycholesterol/ *X,Y-Dihydroxycholest-4-en-3-one*	ND	ND	ND	0.0045±0.0005
550.4003	8.75+8.95min	7α,12α-Dihydroxycholest-4-en-3-one 3-GP	7α,12α-Dihydroxycholesterol/ *7α,12α-Dihydroxycholest-4-en-3-one*	0.0002±0.0001	ND	0.4971±0.1658	0.1409±0.0235
550.4003	9.65min	6β,12α -Dihydroxycholest-4-en-3-one 3-GP	6β,12α-Dihydroxycholesterol/ *6β,12α -Dihydroxycholest-4-en-3-one*	ND	ND	0.0894±0.0223	0.0066±0.0012
552.4160	8.52min	7α,12α-dihydroxy-5β-cholestan-3-one 3-GP	*7α,12α-dihydroxy-5β-cholestan-3-one*	ND	ND	ND	0.1260±0.0036
552.4160	9.14min	unknown		ND	ND	0.0870±0.0571	ND
562.3639	5.25min	unknown		ND	ND	0.0051±0.0014	0.0163±0.0099
562.3639	5.82min	unknown		0.0031±0.0015	0.0052±0.0012	0.0151±0.0038	0.0029±0.00003
564.3796	5.35min	unknown		0.0041±0.0014	ND	ND	ND
564.3796	5.60min	unknown		0.0132±0.0020	ND	ND	ND
564.4160	6.00min	unknown		0.0927±0.0155	ND	0.1149±0.0177	ND

566.3952	3.65min	7α,12α,X -Trihydroxycholest-4-en-3-one 3-GP	7α,12α,X –Trihydroxycholesterol/ *7α,12α,X -Trihydroxycholest-4-en-3-one*	ND	ND	0.2354±0.0224	0.1336±0.0154
566.3952	5.36min	X,Y,Z-Trihydroxycholest-4-en-3-one 3-GP	X,Y,Z-Trihydroxycholesterol/ *X,Y,Z-Trihydroxycholest-4-en-3-one*	ND	ND	0.0342±0.0078	ND
566.3952	8.32min	X,Y,Z-Trihydroxycholest-4-en-3-one 3-GP	X,Y,Z-Trihydroxycholesterol/ *X,Y,Z-Trihydroxycholest-4-en-3-one*	ND	ND	0.0597±0.0197	0.0056±0.0021
568.4109	4.11min	X,Y,Z-Trihydroxy-5β-cholestan-3-one 3-GP	X,Y,Z-Trihydroxy-5β-cholestan-3-one/ *X,Y,Z-Trihydroxy-5β-cholestan-3-one*	ND	ND	0.0088±0.0035	ND
568.4109	4.45min	X,Y,Z-Trihydroxy-5β-cholestan-3-one 3-GP	X,Y,Z-Trihydroxy-5β-cholestan-3-one/ *X,Y,Z-Trihydroxy-5β-cholestan-3-one*	ND	ND	0.0027±0.0006	ND
568.4109	4.95min	X,Y,Z-Trihydroxy-5β-cholestan-3-one 3-GP	X,Y,Z-Trihydroxy-5β-cholestan-3-one/ *X,Y,Z-Trihydroxy-5β-cholestan-3-one*	ND	ND	0.0043±0.0022	ND
568.4109	5.46min	X,Y,Z-Trihydroxy-5β-cholestan-3-one 3-GP	X,Y,Z-Trihydroxy-5β-cholestan-3-one/ *X,Y,Z-Trihydroxy-5β-cholestan-3-one*	ND	ND	0.0142±0.0056	ND
568.4109	6.80min	X,Y,Z-Trihydroxy-5β-cholestan-3-one 3-GP	X,Y,Z-Trihydroxy-5β-cholestan-3-one/ *X,Y,Z-Trihydroxy-5β-cholestan-3-one*	ND	ND	0.0083±0.0015	ND
568.4109	7.40min	X,Y,Z-Trihydroxy-5β-cholestan-3-one 3-GP	X,Y,Z-Trihydroxy-5β-cholestan-3-one/ *X,Y,Z-Trihydroxy-5β-cholestan-3-one*	ND	ND	0.0192±0.0011	0.0913±0.0073
568.4109	7.60min	X,Y,Z-Trihydroxy-5β-cholestan-3-one 3-GP	X,Y,Z-Trihydroxy-5β-cholestan-3-one/ *X,Y,Z-Trihydroxy-5β-cholestan-3-one*	ND	ND	0.0155±0.0014	0.0267±0.0011
568.4109	7.90min	X,Y,Z-Trihydroxy-5β-cholestan-3-one 3-GP	X,Y,Z-Trihydroxy-5β-cholestan-3-one/ *X,Y,Z-Trihydroxy-5β-cholestan-3-one*	ND	ND	0.0050±0.0013	0.0116±0.0017
568.4109	8.10min	X,Y,Z-Trihydroxy-5β-cholestan-3-one 3-GP	X,Y,Z-Trihydroxy-5β-cholestan-3-one/ *X,Y,Z-Trihydroxy-5β-cholestan-3-one*	ND	ND	0.0095±0.0016	0.0020±0.0004
			Total concentration of 24S,25-EC	1.2624±0.0711	ND	0.9466±0.0491	ND

nd – the analyte was below the detection level
na – the analyte peak cannot be confidently integrated due to complexity of the spectra
*- data obtained from the long gradient LC analysis

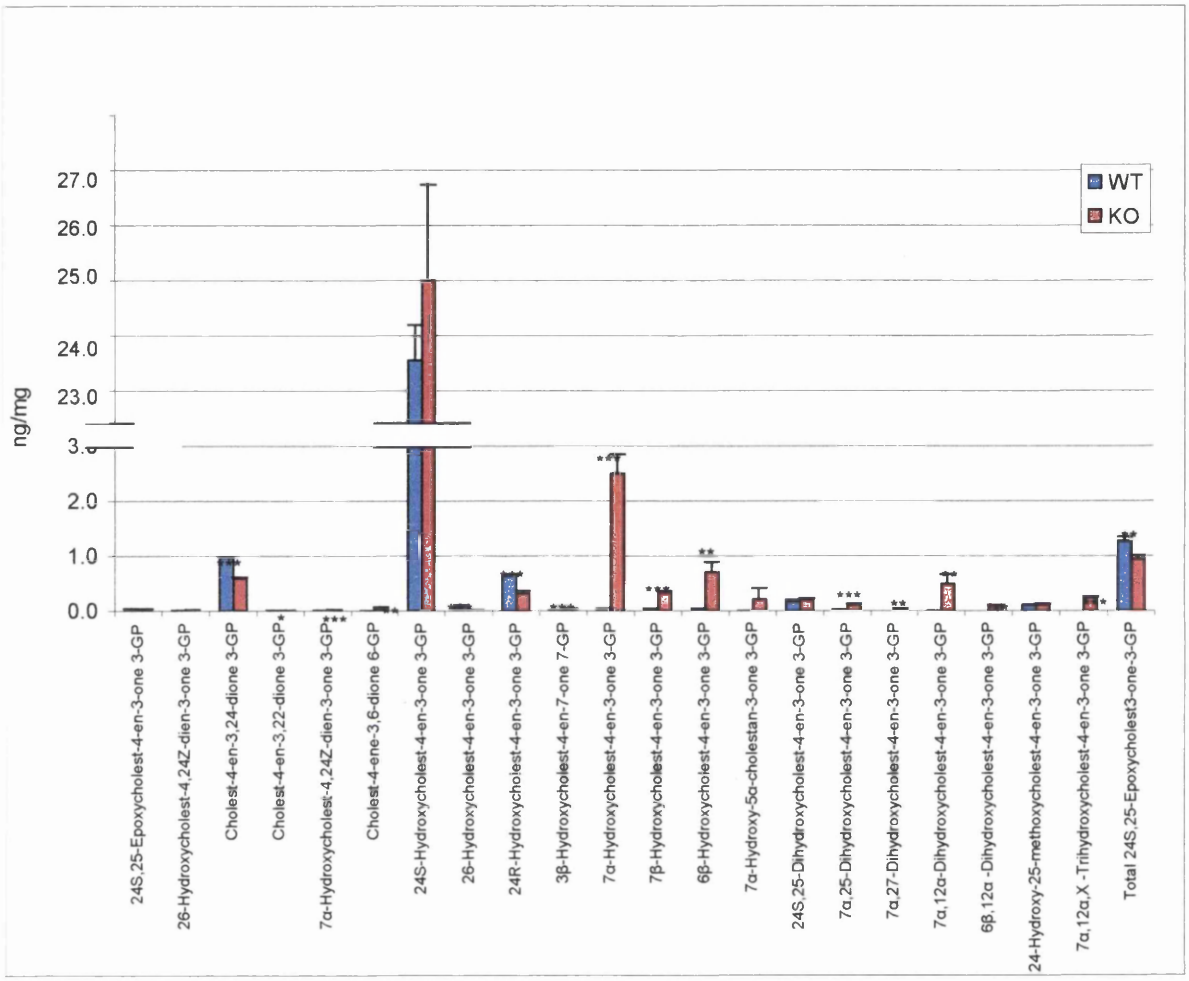

Figure 6.3 Oxysterols identified in fraction 1a of Cyp27a1$^{-/-}$ and Cyp27a1$^{+/+}$ mice brains extracts. Charge-tagged with GP-hydrazine oxysterols identified by LC-ESI-MS^n.

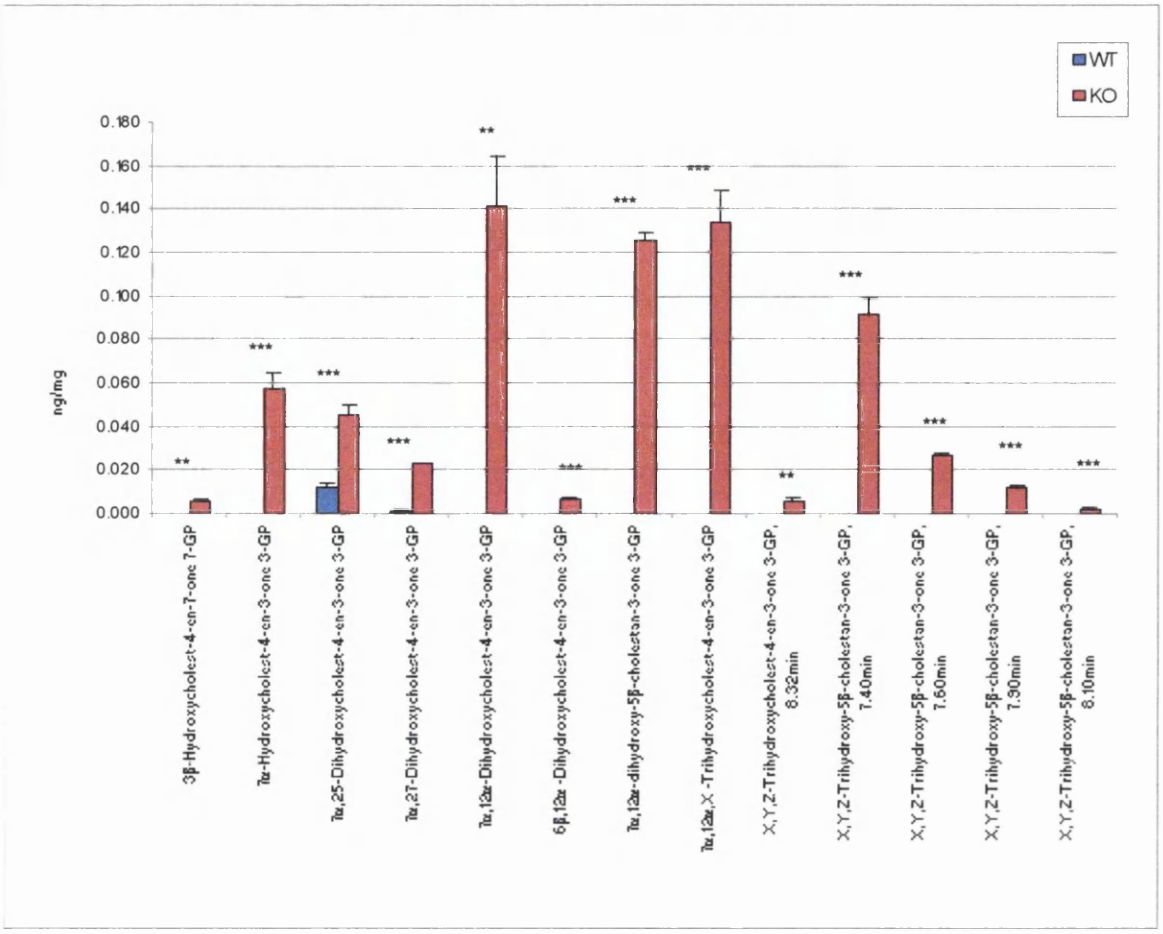

Figure 6.4 Oxysterols identified in fraction 1b of Cyp27a1$^{-/-}$ and Cyp27a1$^{+/+}$ mice brains extracts..

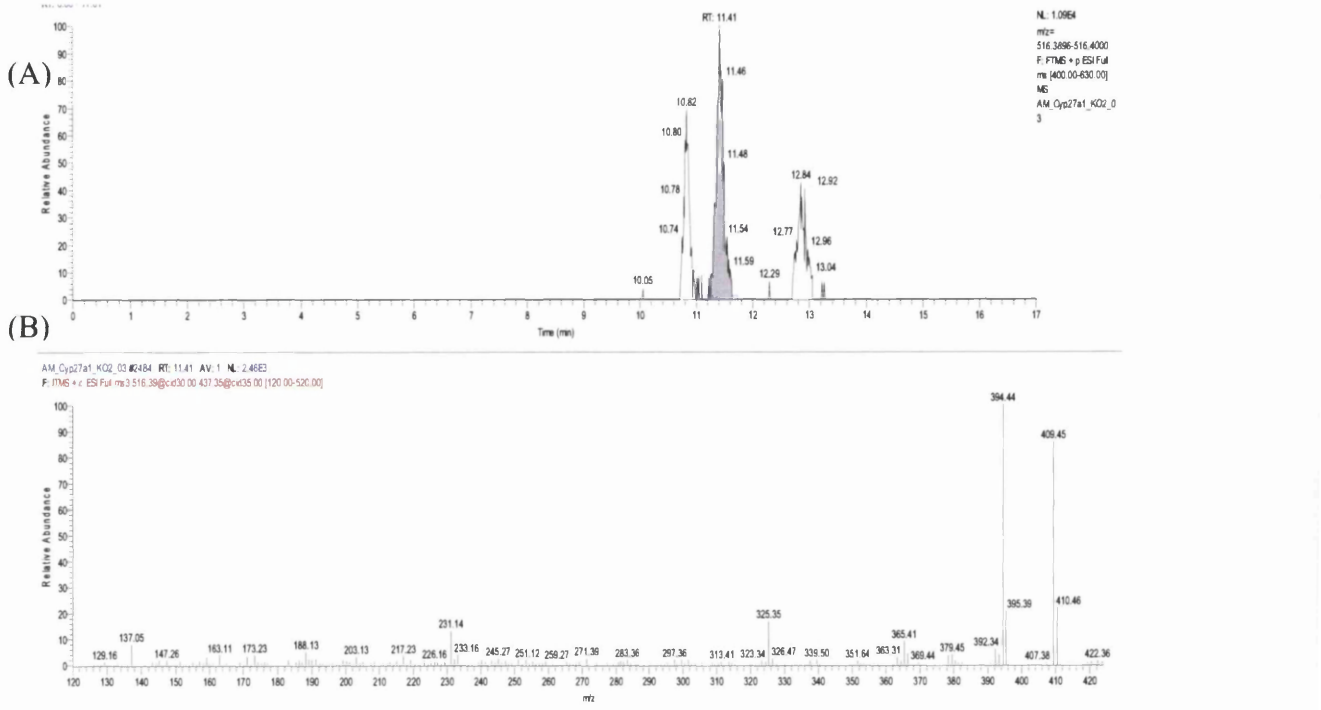

Figure 6.5 8(9)-Dehydrocholesterol in brain of Cyp27a1$^{-/-}$ mouse.
(A) RIC of m/z 516.3948±5 ppm
(B) MS^3 spectrum of peak eluting at 11.41min identified as GP-tagged 8(9)-dehydrocholesterol

The second peak in the chromatogram of *m/z* 516 eluted at RT 11.41 min (Figure 6.5). Analysis of the spectrum and comparison with an authentic standard identified this compound as 8(9)-dehydrocholesterol. In KO mice the concentration is 0.0543±0.0011 μg/mg, while in WT 0.0116±0.0012 μg/mg.

Conversely to sterols with 3β-hydroxy-5-en group which can be only detected after the treatment with Cholesterol oxidase, sterols naturally possessing an oxo group can be derivatisation in the absence of the enzyme. We analysed fraction 3b where the derivatisation was carried out without the enzymatic oxidation; RIC of *m/z* 518 showed a peak at RT 11.98 min (Figure 6.6), which we identified as cholest-4-en-3-one at concentration 1.3013±0.8154 μg/mg in the knockout and 0.1722±0.0587 μg/mg in the wild type mice. The slight retention time shift in comparison with Figure 6.1 was a consequence of analysis being performed in different analytical batches.

Sterols possessing an oxo group and two unsaturated bonds, after derivatisation with GP reagent are detected at *m/z* ratio of 516.3948. The RIC showed a peak at 11.65 min present only in Cyp27a1 deficient animals. The MS^3 spectrum of *m/z* 516 contains dominating ions of *m/z* 409 and *m/z* 394 and low intensities ions of *m/z* 137, *m/z* 231, *m/z* 247 *m/z* 325 and *m/z* 365. Comparison of MS^3 spectrum with authentic standards of cholesta-4,6-

dien-3-one and cholesta-4,8(9)-dien-3-one suggests that the analyte is a mixture of the above substances. Fragment ions of *m/z* 409 and *m/z* 394 dominate the spectra of both standards. Ions of *m/z* 247 and 365 are present in the MS^3 spectrum of cholesta-4,6-dien-3-one, while ions *m/z* 137, *m/z* 231, *m/z* 325 and *m/z* 365 are in MS^3 spectrum of cholesta-4,8(9)-dien-3-one. The standards elutes at very similar times (relative retention times 0.975 and 0.974, respectively) therefore this method is not sufficient to separate these analytes.

.

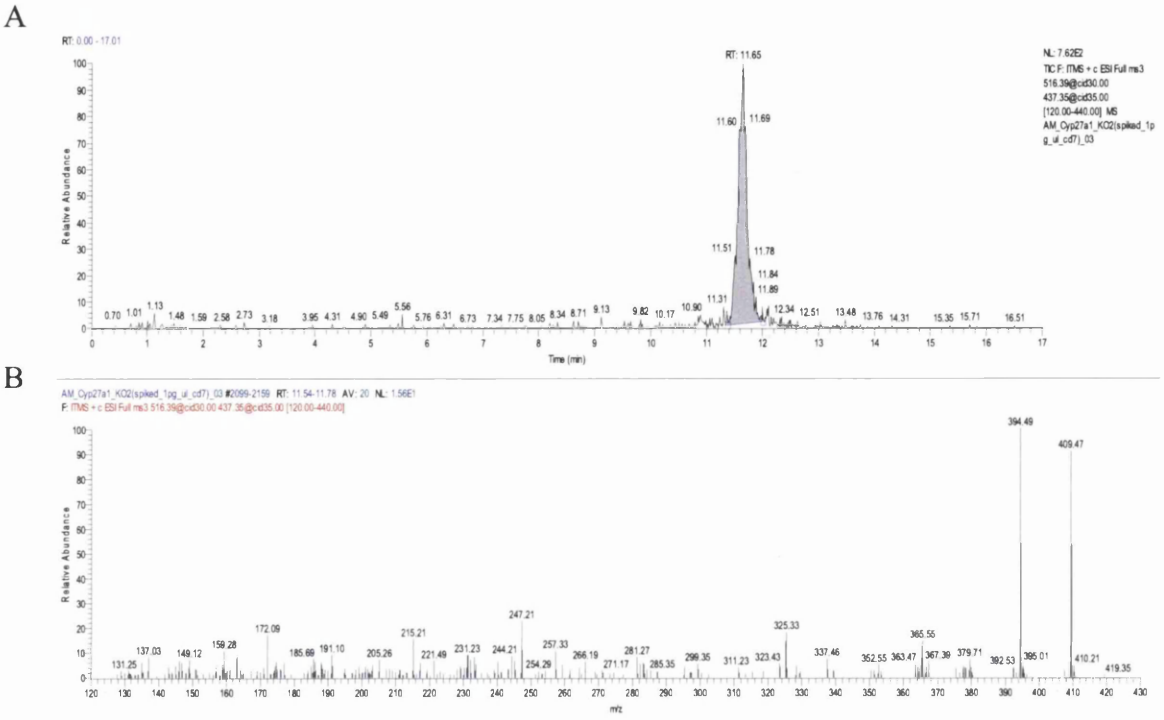

Figure 6.6 Cholestadien-3-one mixture in brain of Cyp27a1$^{-/-}$ mouse.
(A) RIC of m/z 516.3948±5 ppm
(B) MS^3 spectrum of peak eluting at 11.41min identified as a mixture of GP-tagged 7- and 8(9)-dehydrocholesterols

Oxysterols

24S,25-Epoxycholesterol is produced by the shunt pathway of cholesterol biosynthesis [218]. This oxysterol is present at a high concentration in the developing nervous tissues [120] and has been implicated the development of the brain[121].

GP derivatised 24S,25-epoxycholesterol has a *m/z* ratio 532.3898. However, due to chemical labiality this oxysterol is degraded during sample preparation and can be transformed into 24,25-dihydrocholesterol (*m/z* of GP derivatised 550.4003), 24-methoxy,25-hydroxycholesterol or 24S-hydroxy,25-methoxycholesterol (*m/z* of GP derivatised 564.4106) or 24-oxocholesterol (*m/z* of GP derivatised 532.3898) [120]. The total level of this oxysterol

was determined to be 1.2624±0.0711 ng/mg in the wild type mouse and 0.9466±0.491 ng/mg in the knockout mice (Table 6.1). RIC chromatograms and MS^n spectra are shown in Figure 6.9 -Figure 6.10.

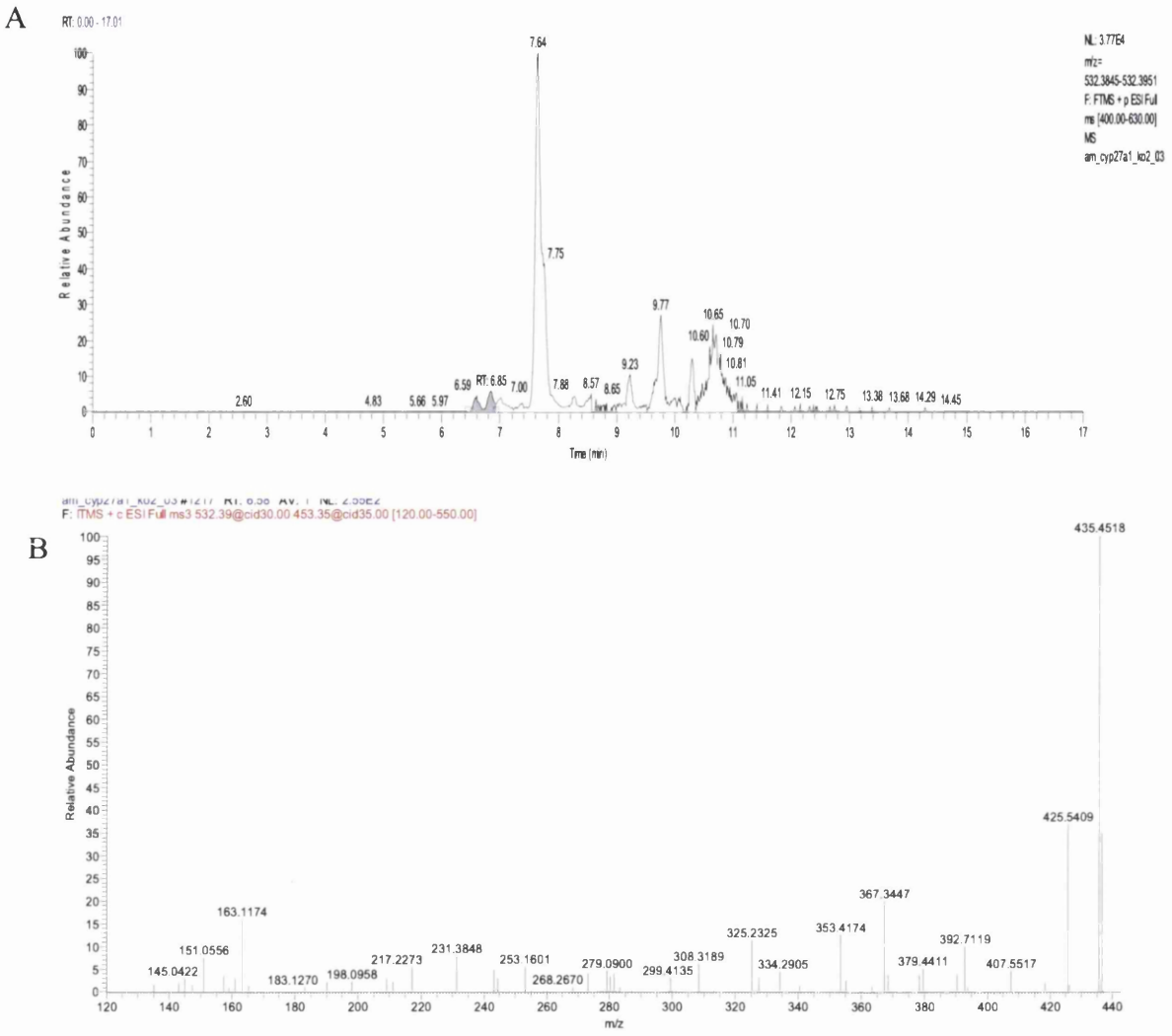

Figure 6.7 24S,25-Epoxycholesterol in brain of Cyp27a1$^{-/-}$ mouse.
(A) RIC of m/z 532.3898±5 ppm of Cyp27a1$^{-/-}$ mouse
(B) MS^3 spectrum of peak eluting at 6.59min identified as GP-tagged 24S,25-epoxycholesterol

A

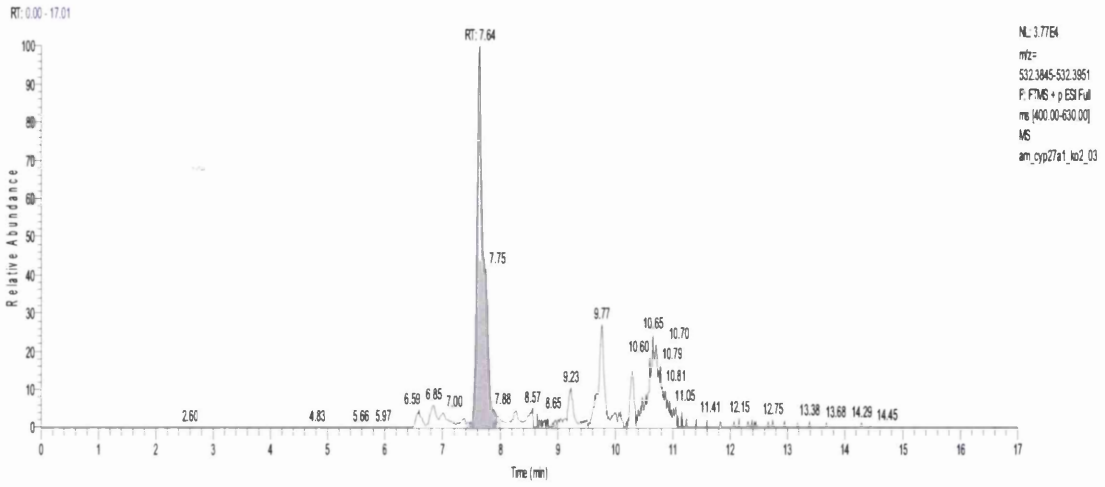

B

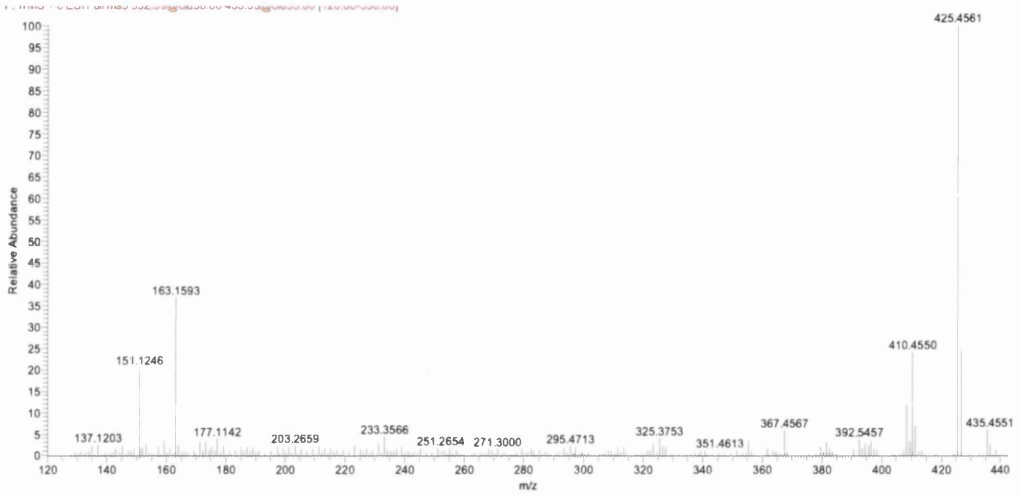

Figure 6.8. 24-Oxocholesterol from brain of Cyp27a1$^{-/-}$ mouse.
(A) RIC of m/z 532.3898±5 ppm of Cyp27a1$^{-/-}$
(B) MS^3 spectrum of peak eluting at 7.64 min identified as GP-tagged 24-oxocholesterol

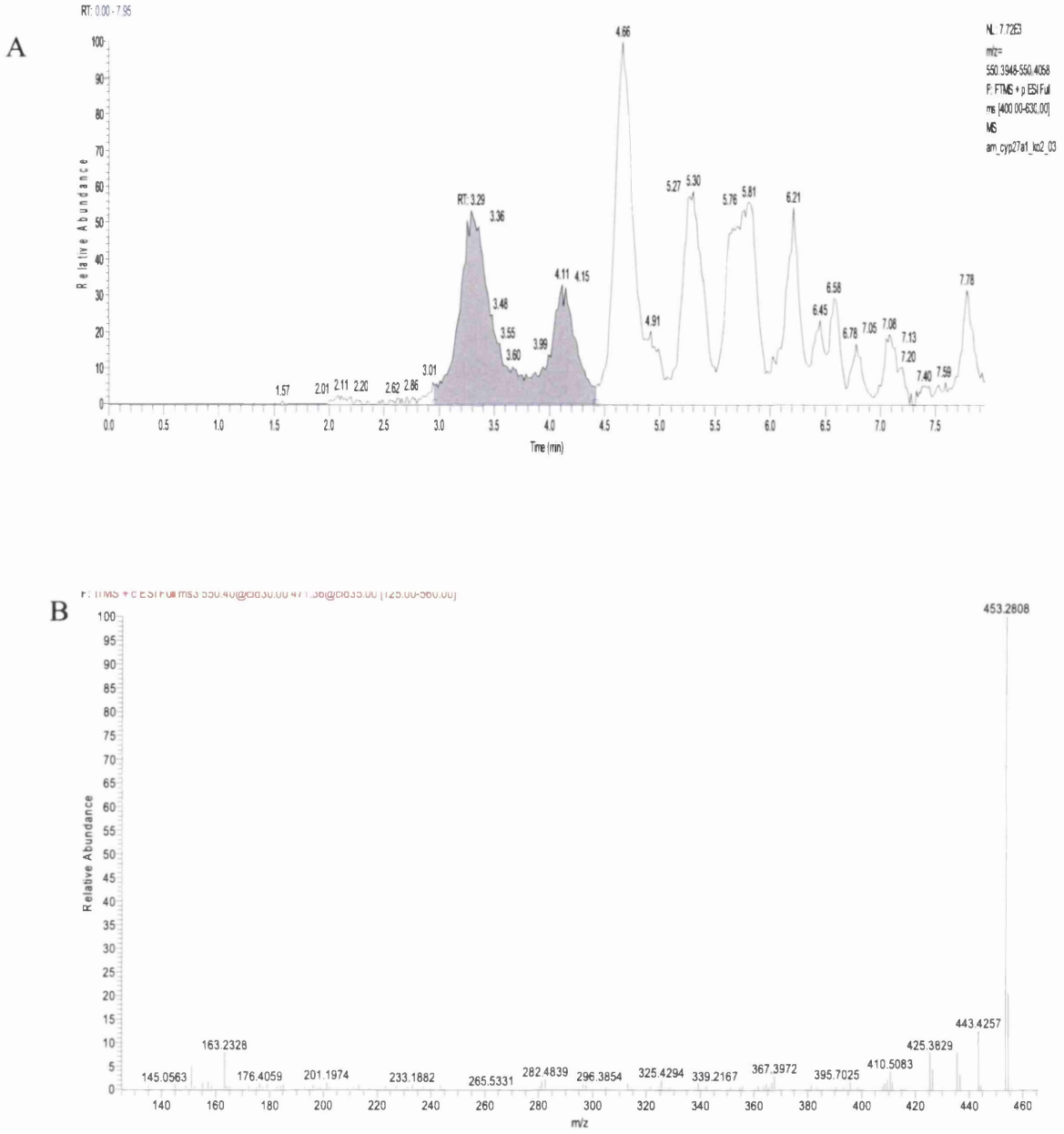

Figure 6.9 24,25-Dihydroxycholesterol from brain of Cyp27a1$^{-/-}$ mouse.
(A) RIC of m/z 550.4003±5 ppm from Cyp27a1$^{-/-}$ mouse
(B) MS^3 spectrum of peak eluting at 3.29 min identified as GP-tagged 24,25-dihydroxycholesterol

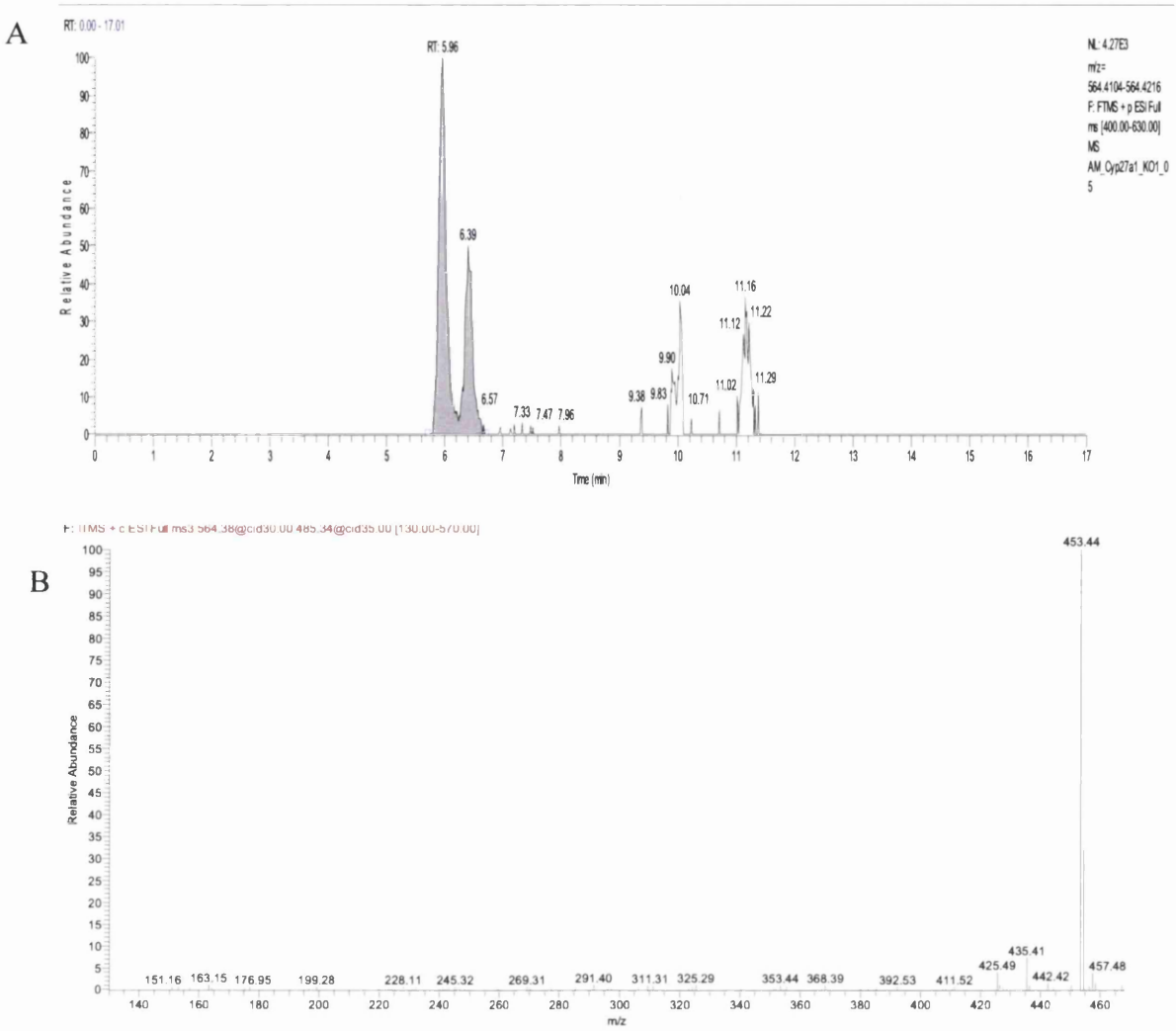

Figure 6.10 3β,24(or25)-dihydroxycholest-5-ene-25(or24)-methoxide from brain of Cyp27a1$^{-/-}$ mouse.
(A) RIC of *m/z* 564.4160±5 ppm of Cyp27a1$^{-/-}$ mouse
(B) MS^3 spectrum of peak eluting at 5.96 min identified as GP-tagged 3β,24(or25)-dihydroxycholest-5-ene-25(or24)-methoxide.

Further analysis of peaks present in RIC at *m/z* 532.3898 reveals a compound eluting at 9.20 min with an MS^3 fragmentation pattern resembling that of 7α-hydroxycholesterol but with an extra-unsaturation (Figure 6.11). The spectrum contains low mass ions *m/z* 151, *m/z* 179 and *m/z* 231, while higher mass ions have their *m/z* ratios reduced by two units compared to the 7α-hydroxycholesterol spectrum i.e. *m/z* *m/z* 392 cf. 394, 407 cf. 409, 425 cf. 427 and 435 cf 437. Based on the fragmentation profile that shows the same features as 7α-hydroxycholesterol on the level of tetracyclic core we putatively identified this compound as 7α-hydroxydesmosterol. The concentration is calculated to be 0.0078±0.0010 ng/mg in wild type and 0.0270±0.0030 ng/mg in Cyp27a1$^{-/-}$ littermates which gives almost 3.5 fold increase in knockout mice.

The studies on the "cholesterol-free mouse" which lack 24-dehydrocholesterol reductase (Ch24r) showed that 7α-hydroxydesmosterol can be formed by the action of Cyp7a1, and in vitro at a rate similar to hydroxylation of cholesterol (5% and 6% of the total amount of substrate) [190].

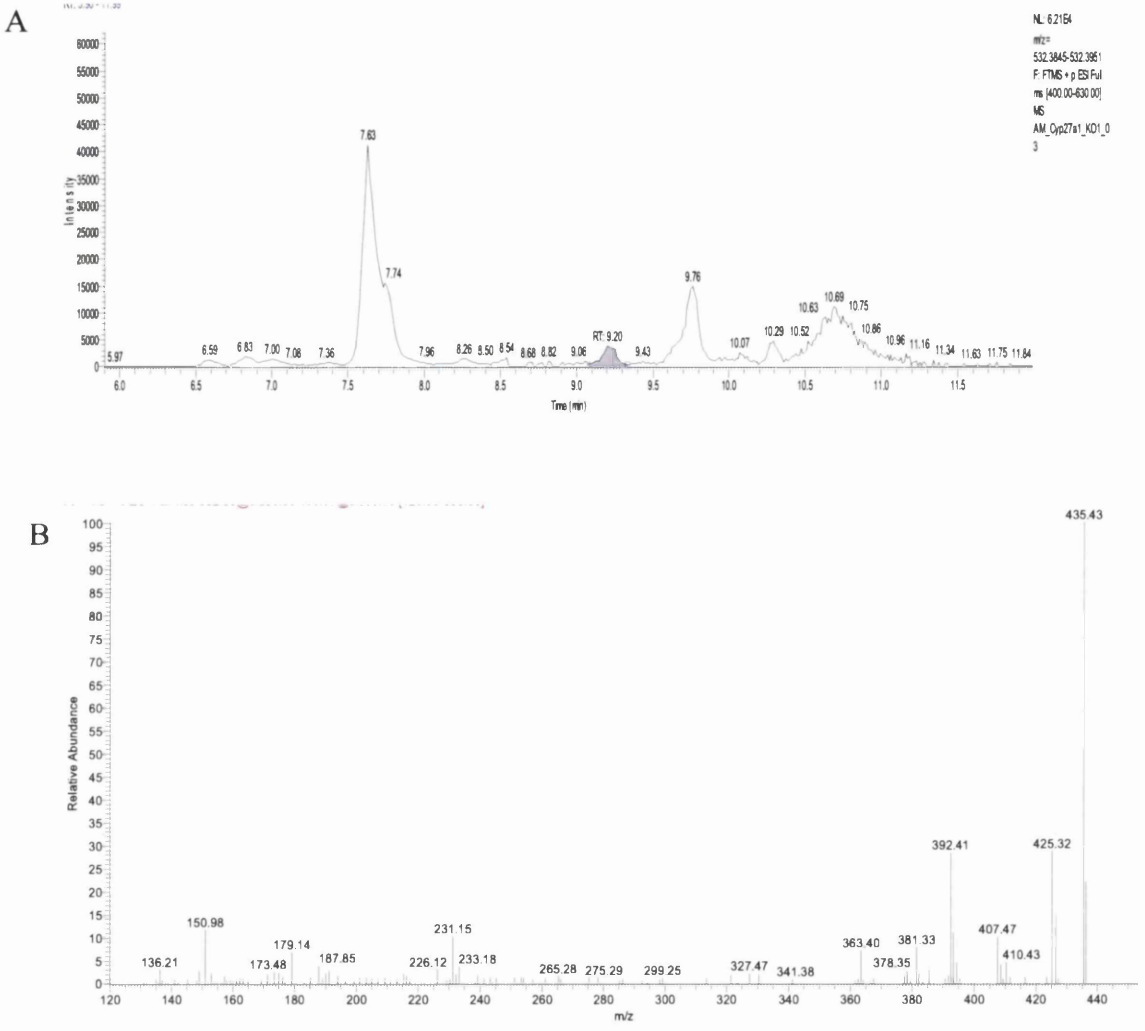

Figure 6.11 7α-Hydroxydesmosterol brain of Cyp27a1$^{-/-}$ mouse.
(A) RIC of m/z 532.3898±5 ppm from Cyp27a1$^{-/-}$.
(B) MS^3 spectrum of the peak eluting at 9.20 min identified as GP-tagged 7α-hydroxydesmosterol.

We can hypothesise that 7α-hydroxydesmosterol can be further hydroxylated at position 12α by Cyp8b1, yielding 7α,12α-dihydroxydesmosterol. This oxysterol when subjected to oxidation and derivatisation will produce a molecular ion of *m/z* 548.3847. We analysed the relevant RIC and analysed the MS^3 spectra. The peak eluting at RT 7.77 min (Figure 6.12) has a MS^3 fragmentation pattern similar to that of 7α,12α-dihydroxycholesterol with the high mass fragments reduced by two mass units. Low mass fragments consist of ions

m/z 151 and *m/z* 179 and 279 present in the spectrum of 7α,12α-dihydroxycholesterol. The concentration has been calculated as 0.0107±0.016 ng/mg in Cyp27a1$^{-/-}$ and 0.0002±0.00004 ng/mg in wild type littermates.

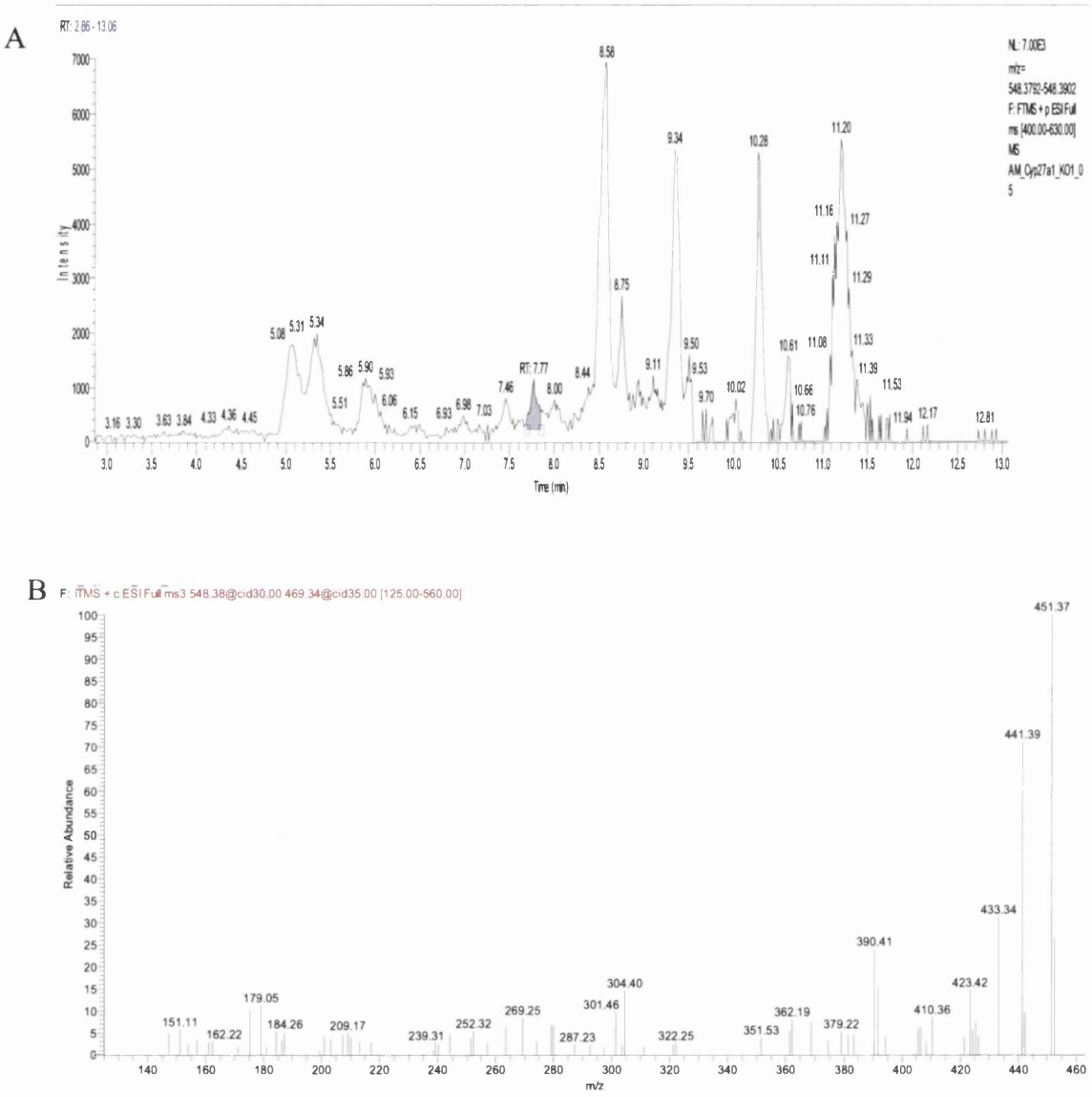

Figure 6.12 7α,12α-Dihydroxydesmosterol in brain of Cyp27a1$^{-/-}$ mouse.
(A) RIC of m/z 548.3847±5 ppm from Cyp27a1$^{-/-}$ mouse
(B) MS^3 spectrum of peak eluting at 7.77 min identified as GP-tagged 7α,12α-dihydroxydesmosterol

In fraction 1b of the knockout mice we also found a small amount of 7α,12α-dihydroxy-cholesta-4,24-dien-3-one at a level of 0.0024±0.0005ng/mg. This indicates that 7α,12α-dihydroxylated desmosterol may exist in two forms: 3β-hydroxy-5-ene and 3-oxo-4-ene,

where the metabolic conversion is catalysed by 3β-hydroxy-Δ^5-C_{27}-steroid dehydrogenase/isomerise.

A

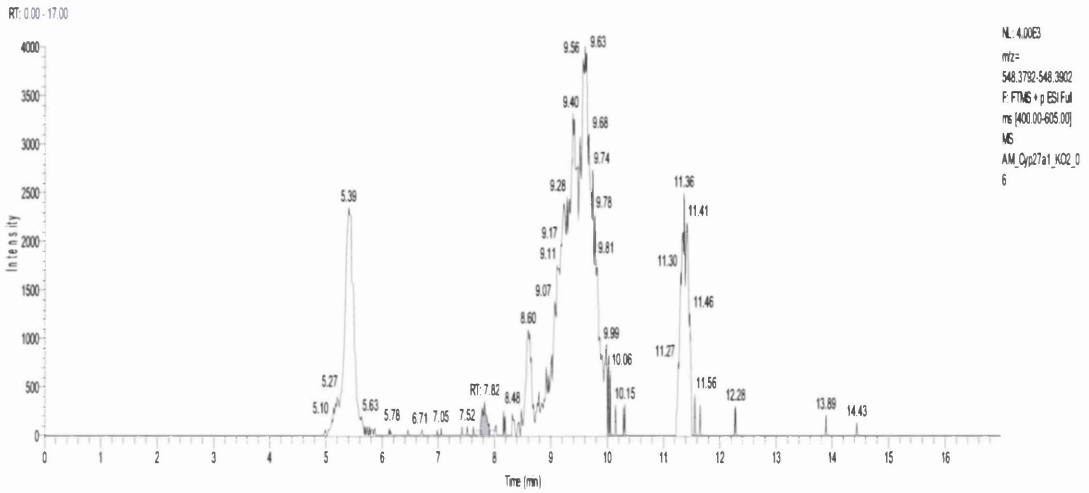

B

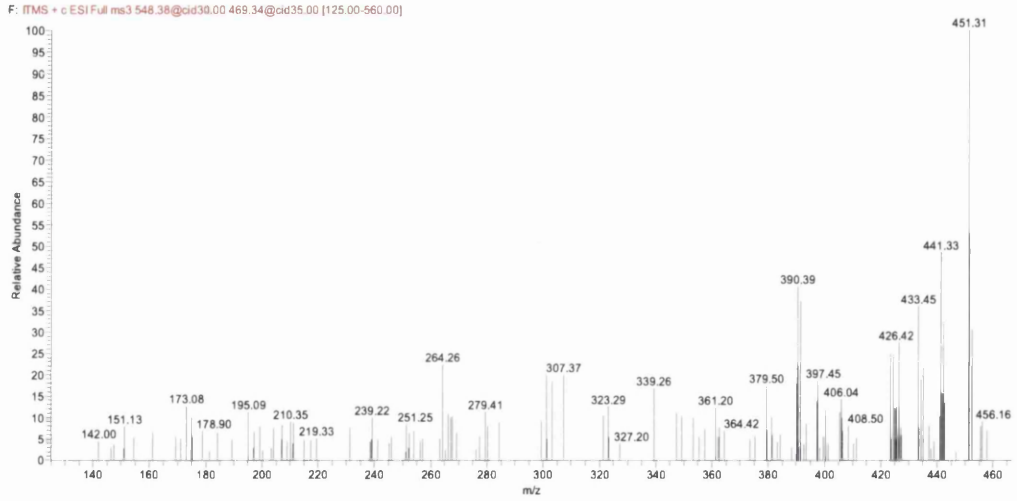

Figure 6.13 7α,12α-Dihydroxycholesta-4,24-dien-3-one in brain of Cyp27a1$^{-/-}$ mouse.
(A) RIC of m/z 548.3847±5 ppm from Cyp27a1$^{-/-}$ mouse
(B) MS^3 spectrum of peak eluting at 7.82min identified as GP-tagged 7α,12α-dihydroxycholesta-4,24-dien-3-one.

Further analysis of *m/z* 532.2898 RIC revealed peak eluting at 8.25min (Figure 6.11). The MS^n spectrum and retention time corresponds with GP-derivatised 22-oxocholesterol. The level of this analyte is elevated in knockout mice (0.0098±0.0007 ng/mg in KO and 0.0071±0.0009ng/mg in WT).

At 10.29 min elutes another compound with *m/z* 532.3898 (Figure 5.13). The fragmentation profile of the MS^n spectrum fits the characteristics of GP-derivatised cholest-4-en-3,6-dione. The levels were evaluated as 0.0494±0.0143 ng/mg in knockout mice, in wild type were

below the detection limit. Cholest-4-en-3,6-dione is usually considered to be a product of cholesterol autoxidation.

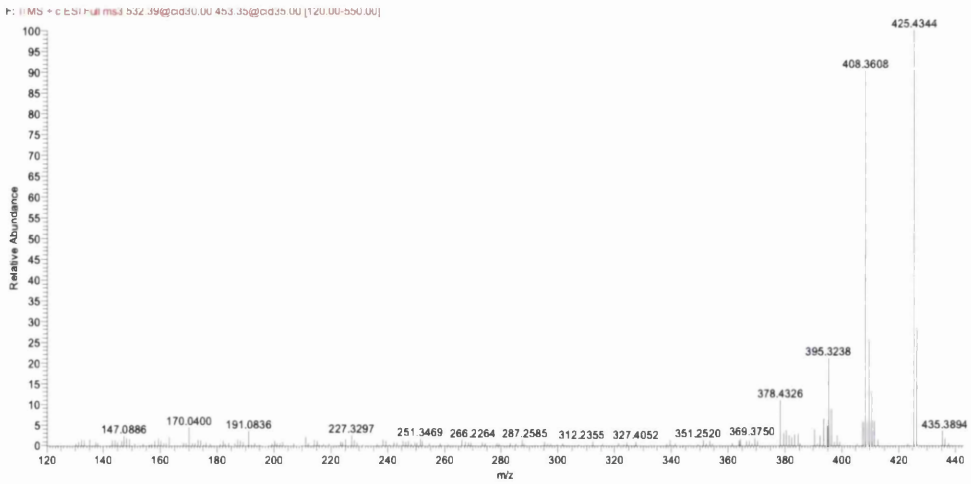

Figure 6.14 Cholest-4-en-3,6-dione in brain of Cyp27a1$^{-/-}$ mouse.
(A) RIC of m/z 532.3898±5 ppm from Cyp27a1$^{-/-}$ mouse
(B) MS^3 spectrum of peak eluting at 10.29 min identified as GP-tagged cholest-4-en-3,6-dione

The compound of m/z 532.3898 eluting at RT 9.76 does not have the features characteristic for any of the reference standards. The MS^n spectrum is dominated by fragment ion 435, which shows that the molecule easily undergoes dehydration, which occurs when a hydroxyl group is attached to the tertiary carbon atom such as C-25 or is allyl to a double bond. Low mass fragments do not exhibit the triad characteristic for the derivatised 3β-hydroxy-5-ene group, therefore the tetracyclic structure may contain a double bond at C-7 or C-8(9) position (Figure 5.14).

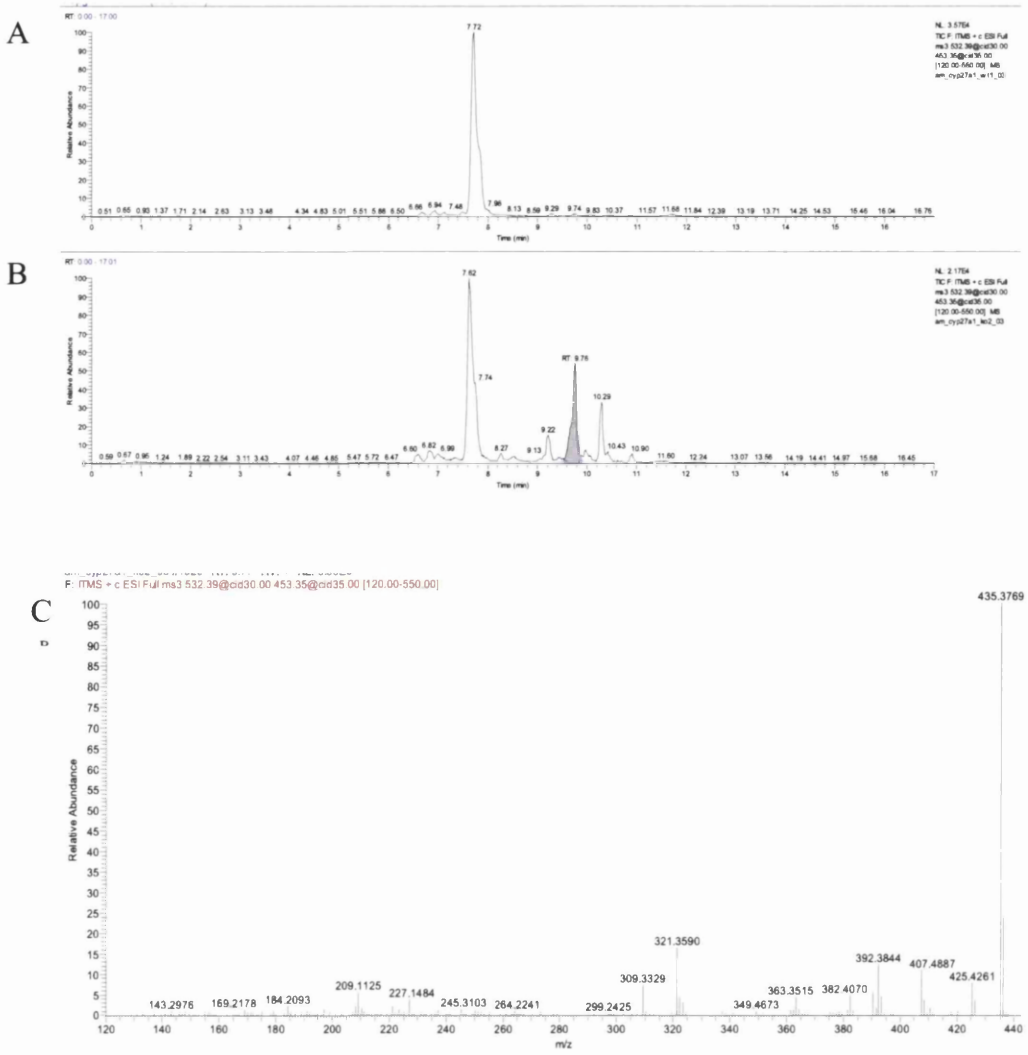

Figure 6.15 X-Hydroxydehydrocholesterol in brain of Cyp27a1$^{-/-}$ mouse. (A) RIC of m/z 532.3898±5 ppm of Cyp27a1$^{+/+}$ and Cyp27a1$^{-/-}$ (B) mouse (C) MS^3 spectrum of peak eluting at 9.76min

The chromatogram of monohydroxylated cholesterols of *m/z* 534.4054 is dominated by 24S-hydroxycholesterol in both knockout and wild type mice which elutes in the chromatogram in two peaks (RT 7.35 min and 7.66 min), identified as *syn-* and *anti-* GP modified conformers (Fig.14). 24S-Hydroxycholesterol is a product of catalytic activity of neuron-specific enzyme Cyp46a1. The total concentration of 24S-hydroxycholesterol in KO mice was determined to be 25.9209±1.7289 ng/mg and in WT mice at 25.9209±1.7289 ng/mg, respectively.

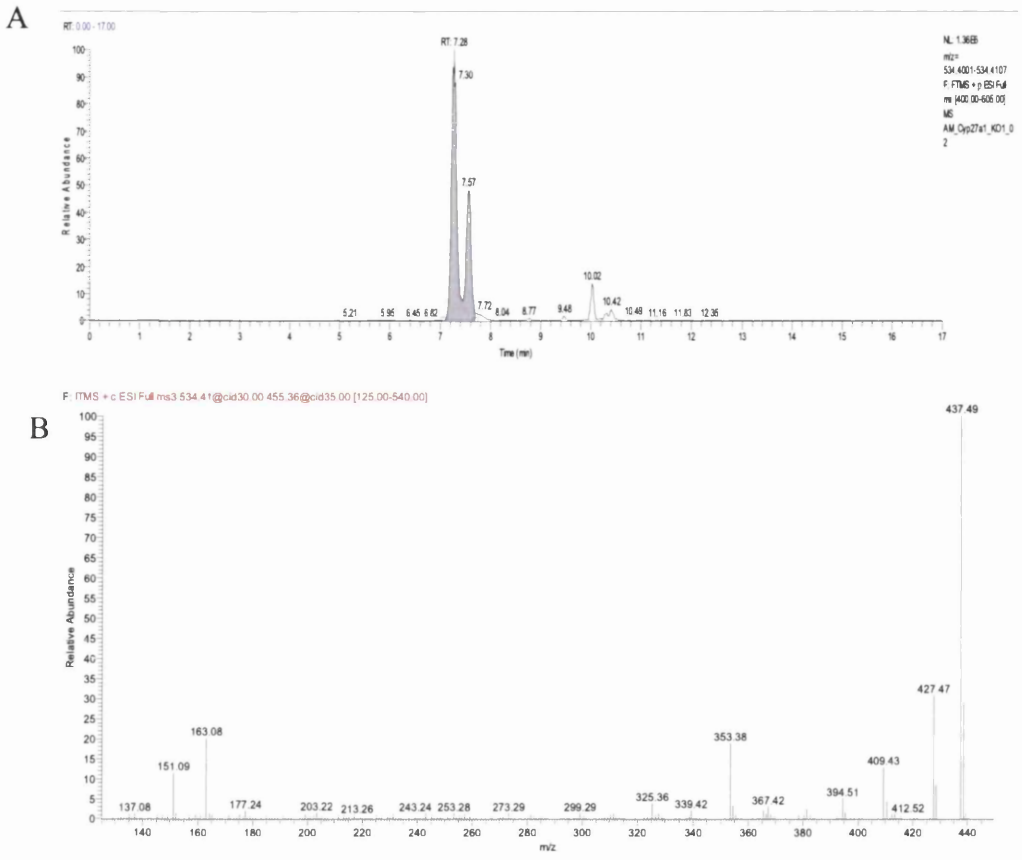

Figure 6.16 24S-Hydroxycholesterol in brain of Cyp27a1$^{-/-}$ mouse.
(A) RIC of m/z 534.4054±5 ppm of Cyp27a1$^{-/-}$mouse.
(B) MS^3 spectrum of peak eluting at 7.36 min identified as GP-tagged 24S-hydroxycholesterol

24S-Hydroxycholesterol can be metabolised by the action of Cyp39a1 which introduces the hydroxyl group at the 7α position. The same reaction was reported to be catalysed by cholesterol 7α-hydroxylase Cyp7a1 present in the liver, but not by oxysterol 7α-hydroxylase Cyp7b1 [238], which is expressed in the brain [239]. 7α,24S-Dihydroxycholesterol was identified by comparison with the standard and the level was calculated as 0.0311±0.0053 ng/mg and 0.0131±0.0037 ng/mg in the knockout and the wild type mice, respectively. Spectra are presented in Figure 6.17.

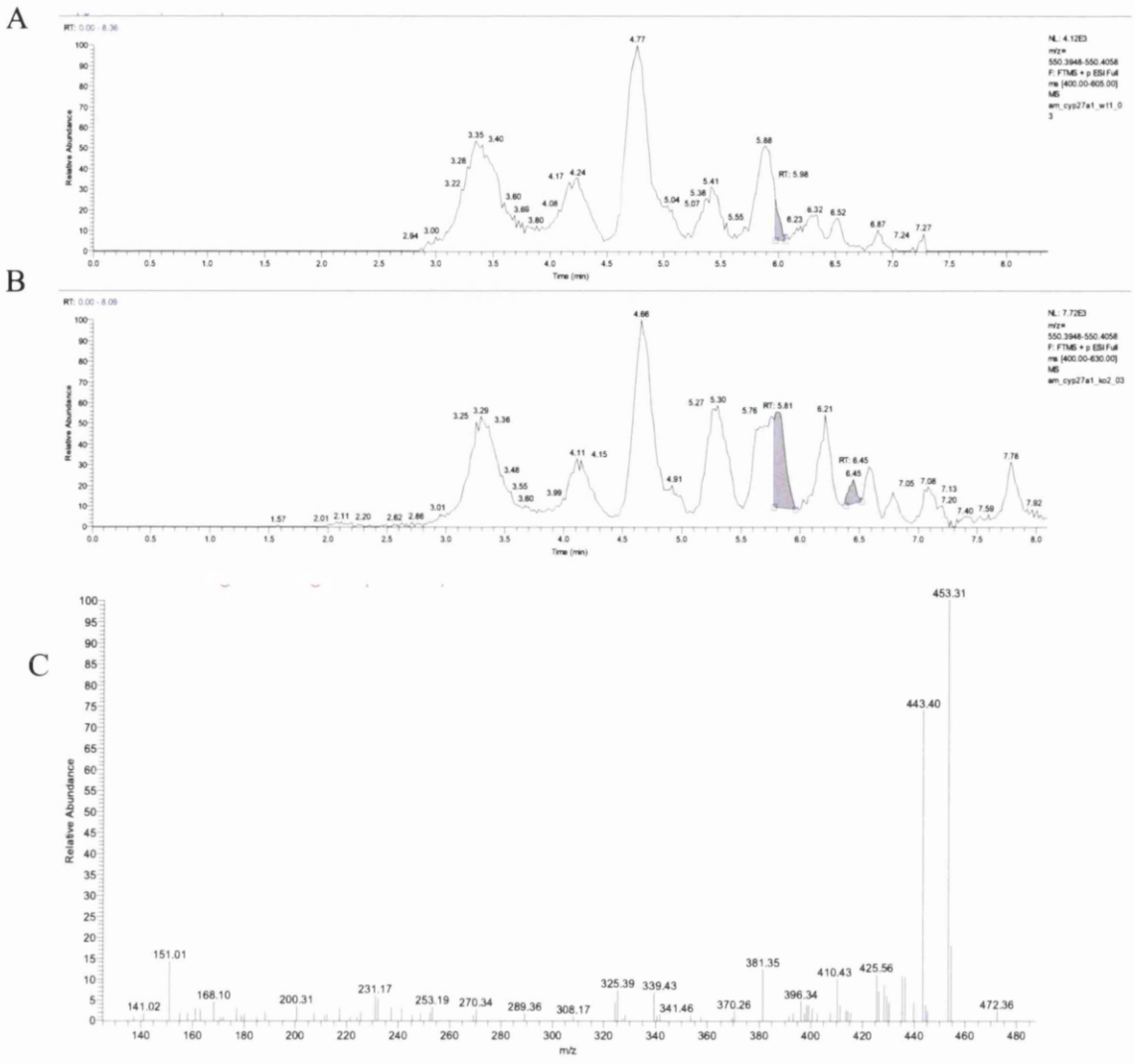

Figure 6.17 7α,24R-Dihydroxycholesterol in brain of Cyp27a1$^{-/-}$ mouse.
(A) RIC of m/z 550.4003±5 ppm of Cyp27a1$^{+/+}$ and Cyp27a1$^{-/-}$ (B) mouse (C) MS^3 spectrum of peak eluting at 5.81min identified as GP-tagged 7α,24R-dihydroxycholesterol

24R-hydroxycholesterol is the second stereoisomer of 24-hydroxylated cholesterol we identified in this study (Figure 6.18). This oxysterol elutes closely to the next compound - 27-hydroxycholesterol. To separate the above analytes we developed a different LC gradient method. The concentration of the 24R-hydroxycholesterol in the KO mice was reduced by 50% compared to the WT littermates (0.310±0.055 ug/g and 0.642±0.023 ug/g).

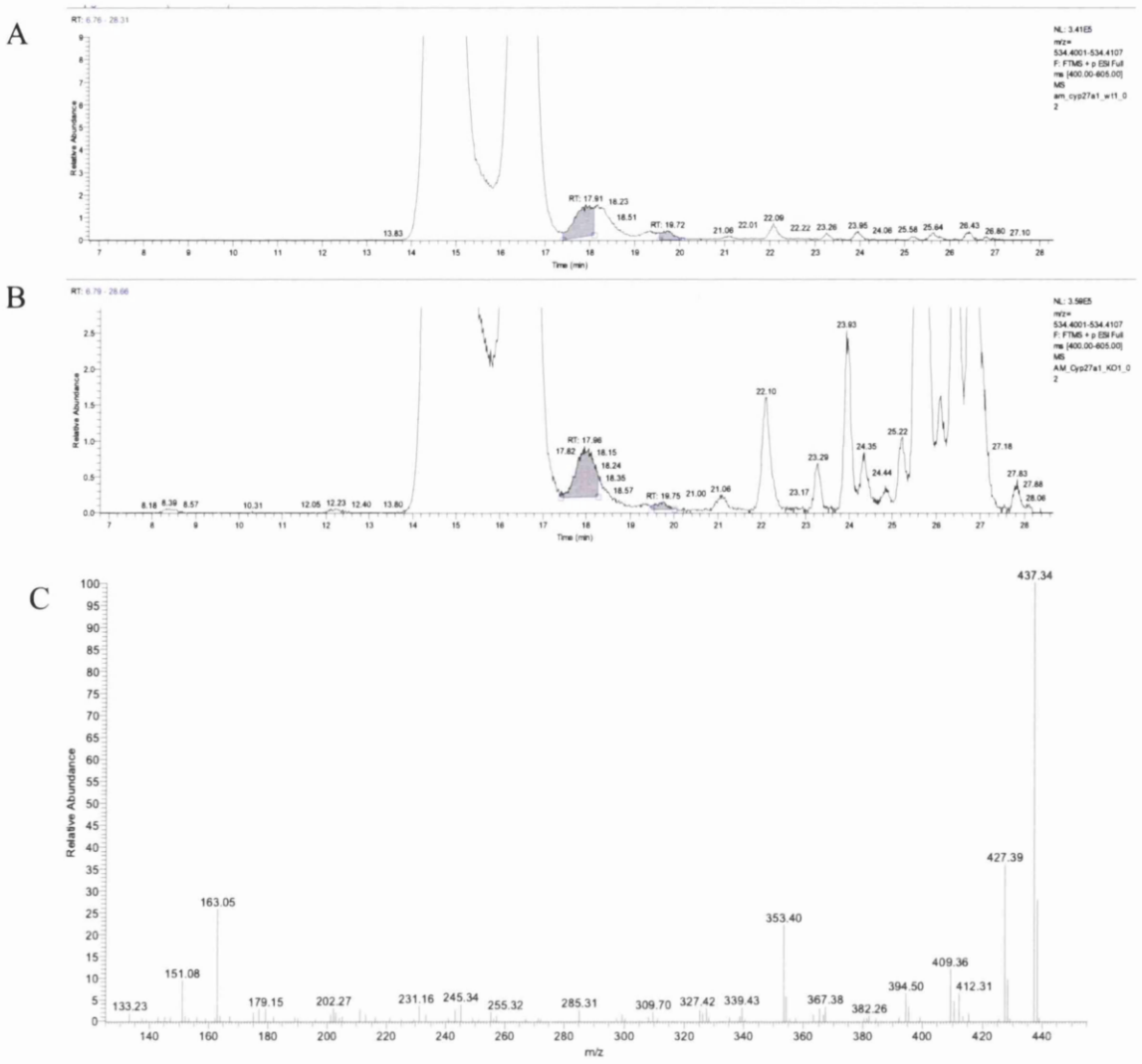

Figure 6.18 24R-Hydroxyocholesterol in brain of Cyp27a1$^{-/-}$ mouse.
(A) RIC of m/z 534.4054±5 ppm from Cyp27a1$^{-/-}$mouse (B) MS^3 spectrum of peak eluting at 17.96min identified as GP-tagged 24R-hydroxycholesterol

The amounts of 27-hydroxycholesterol in wild type mice were at level of 0.0904±0.0069 ng/mg while in knockout littermates the concentration was reduced by 90% (0.0111±0.0019 ng/mg). The residual amounts of 27-hydroxycholesterol present in Cyp27a1 deficient mice can be attributed to the activity of other enzymes with the capability of 27-hydroxylation such as Cyp46a1. The RIC chromatogram and the MS^n spectrum are shown of Figure 6.19.

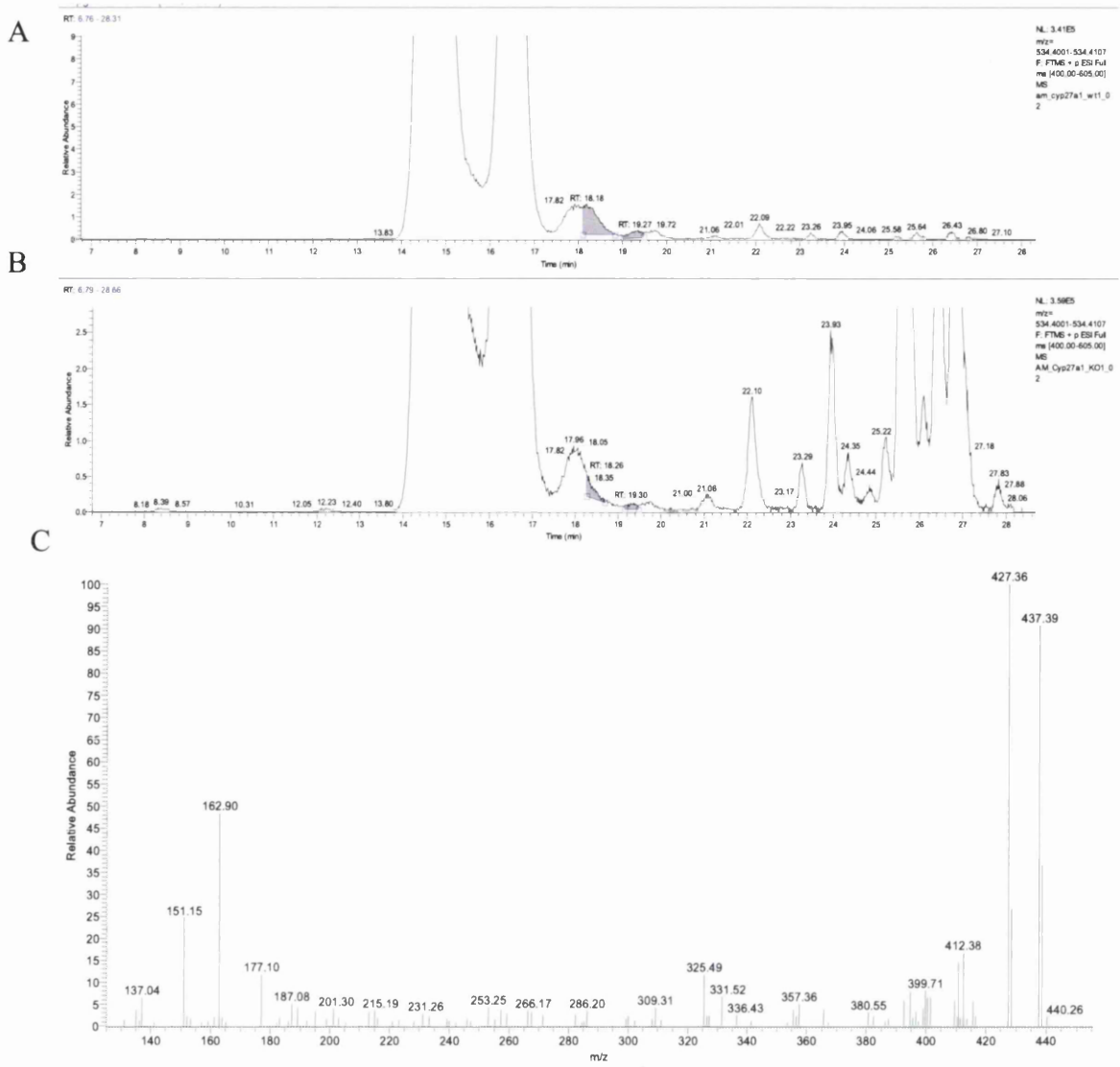

Figure 6.19 26-Hydroxydehydrocholesterol in brain of Cyp27a1$^{-/-}$ mouse.
(A) RIC of m/z 534.4054±5 ppm of Cyp27a1$^{+/+}$ and (B) Cyp27a1$^{-/-}$ mouse. (C) MS^3 spectrum of peak eluting at 18.18 min identified as GP-tagged 27-hydroxydehydrocholesterol

In Cyp27a1$^{-/-}$ mice the alternative pathway of bile acid formation is disabled, causing a compensatory up-regulation of the classical pathway [214]. In this pathway, Cyp7a1 catalyses the initial step where cholesterol is hydroxylated at the C-7 position, yielding 7α-hydroxycholesterol. Cyp7a1 is a liver specific enzyme [184], thus it is likely, that an elevated level of 7α-hydroxycholesterol is due to the influx of this oxysterol from peripheral circulation. 7α-Hydroxycholesterol was identified eluting in two peaks at 10.03 min and 10.41min (Figure 6.20). The level was 60-fold higher in the knockout mouse than in the wild type (2.4936±0.3520ng/mg and 0.0358±0.0065ng/mg).

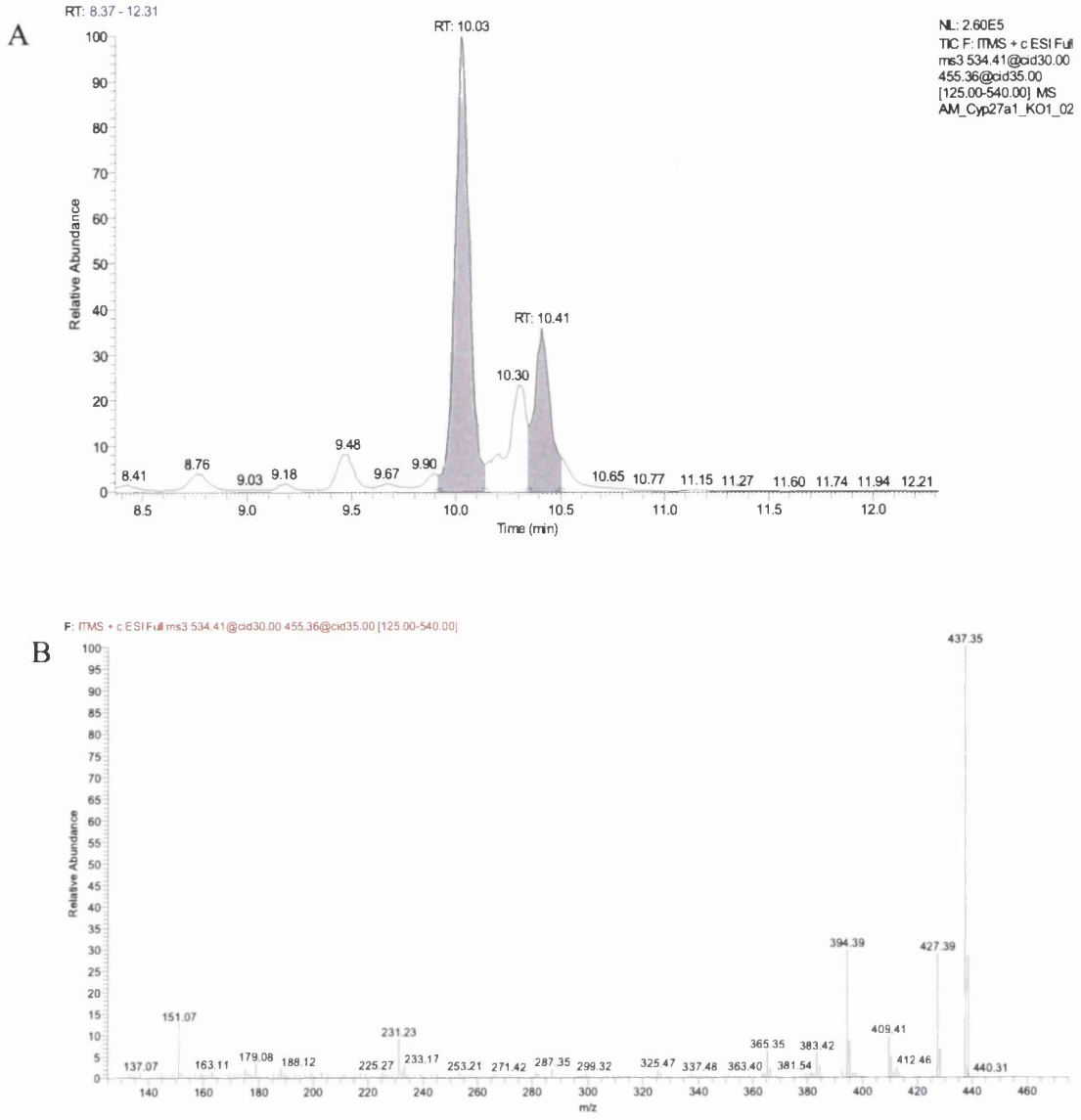

Figure 6.20 7α-Hydroxycholesterol in brain of Cyp27a1$^{-/-}$ mouse.
(A) RIC of m/z 534.4054±5 ppm of Cyp27a1$^{-/-}$ mouse
(B) MS^3 spectrum of peak eluting at 10.03 min and 10.41 min identified as GP-tagged 7α-hydroxycholesterol

We also quantified 7β-hydroxylated cholesterol which is usually considered as an autoxidation product of cholesterol. The total concentration in the knockout mice is almost 10 fold higher than in the wild type (0.3382±0.0308 ng/mg and 0.0348±0.0069 ng/mg). 7α-Hydroxycholesterol can be converted to 7-oxocholesterol by 7α-hydroxycholesterol dehydrogenase at least in hamster [240]. 7-Oxocholesterol can be quantified from fraction 1b.. The level of 7-oxocholesterol was calculated as 0.0548±0.0272 ng/mg in Cyp27a$^{-/-}$ mice while in the wild type the amounts were below the detection limit. Significantly, in mouse 11β-hydroxysteroid dehydrogenase 1 (11βHSD1) catalyses the conversion of 7-oxocholesterol to 7β-hydroxycholesterol [241]. 7-Oxocholesterol itself can be formed from 7-

dehydrocholesterol via a reaction catalysed by Cyp7b1. 8,9-Dehydrocholesterol an isomer of 7-dehydrocholesterol is present at elevated concentrations in the Cyp27a1-/- brain.

Another monohydroxycholesterol found in this study was 6β-hydroxycholesterol. The level in the knockout mice was 20-fold higher than in wild type (0.7092±0.1737 ng/mg and 0.0356±0.0031 ng/mg). This oxysterol is formed by hydrolysis of 5,6-epoxycholesterol [126], however we cannot rule out the possibility that 6β-hydroxycholesterol is the product of an autoxidation of 7- and 8(9)-dehydrocholesterols. These are elevated in the knockout mice and have been shown to be prone to autooxidation [242].

In the second step of the neutral pathway of bile acid synthesis 7α-hydroxycholesterol is oxidised at the C-3 position by an ER enzyme, 3β-hydroxy-Δ^5-steroid oxidoreductase (Hsd3b7) [243-245] with the shift of double bond from C-5-C-6 to C-4-C-5 forming 7α-hydroxycholest-4-en-3-one. It is possible that this reaction occurs in the brain as Hsd3b7 is present in the nervous tissue [108, 236]. 7α-Hydroxycholest-4-en-3-one can be also imported from periphery as this compound has been shown to be able to transverse the blood brain barrier [236].

In our method, we use cholesterol oxidise to transform a hydroxyl group at 3β position into an oxo group. As a consequence, the processed sample solution becomes a mixture of oxidised and indigenous sterols possessing the 3-oxo moiety. To distinguish between the levels of naturally occurring 3-oxo sterols from transformed compounds, we divided each of the SPE1 fractions in two aliquots and treated only one with the enzyme (fraction a). In the aliquot which was not enzymatically oxidised (fraction b), only the endogenous sterols possessing an oxo group will be derivatised with GP reagent.

The analysis of RIC at *m/z* 534.4054 in fraction b (Figure 6.21) established level of 7α-hydroxy-cholest-4-en-3-one as 0.0572±0.0070 ng/mg in knockout mice, while in wild type the levels were below the limit of detection.

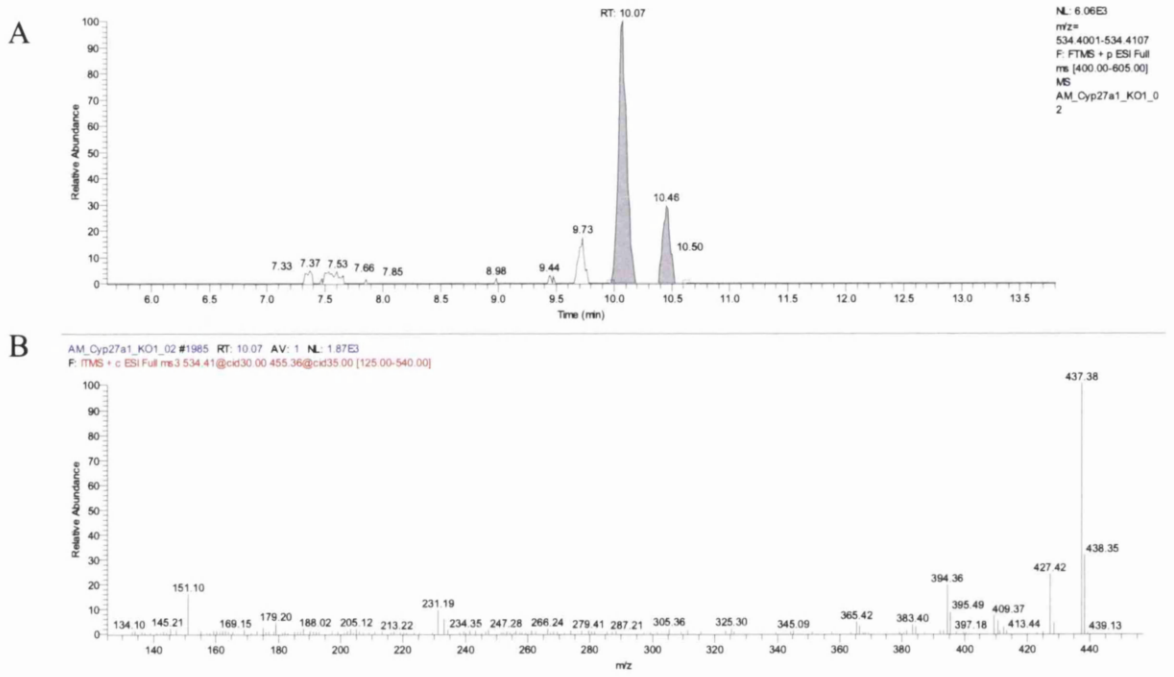

Figure 6.21 7α-Hydroxycholest-4-en-3-one in brain of Cyp27a1$^{-/-}$ mouse in fraction 1b.
(A) RIC of m/z 534.4054±5 ppm from Cyp27a1$^{-/-}$ mouse.
(B) MS^3 spectrum of peak eluting at 10.07 min identified as GP-tagged 7α-hydroxycholest-4-en-3-one.

In wild type mice, 7α-hydroxycholest-4-en-3-one during bile acid biosynthesis is subjected to further hydroxylation by Cyp27a1 at the C-27 position. The disruption of this pathway results in up-regulation of alternative routes such as C-12 hydroxylation catalysed by Cyp8b1 or dehydroxylation at C-7, reduction a C-3 and reduction of the C-4 double bond leading to formation of 5β-cholestan-3β-ol. In the neutral pathway 27-hydroxylation is required for bile acid formation after ring modifications and the malfunction of this enzyme results in accumulation of the down-stream substrates. 7α-hydroxycholest-4-en-3-one is not cleaed at a normal rate in the absence of Cyp27a1, which leads to an accumulation of this compound detected by analysis of fractions b in the knockout mice.

Double bound in 7α-hydroxycholest-4-en-3-one can be reduced forming 7α-hydroxycholestan-3-one. This oxysterol has a naturally occurring oxo moiety, therefore, it would be expected to be present in fraction 1a as well as in 1b. We were not able to identify any analytes with *m/z* ratio fitting GP derivatised 7α-hydroxycholestan-3-one in fraction 1b neither in the knockout nor in wild type mice. There is a possibility that C-3 oxo group is instantly reduced to hydroxyl moiety forming cholestan-3,7α-diol. Sterols with 3α-hydroxy or -5β-H function cannot be oxidised by the action of cholesterol oxidase and, in consequence, detected using our technique.

In fraction 1a (but not in 1b) we found a peak of *m/z* 536.4211 eluting at RT of 10.59 min (Figure 6.22). The exclusive presence of this compound in the fraction treated with cholesterol oxidase indicates that the compound possess a 3β-hydroxy-5α-hydrogen structure, which upon oxidation is converted into 3-oxo-5α-hydrogen structure and is therefore, a substrate for GP derivatisation. The *m/z* value of the compound of interest corresponds to a dihydroxylated cholestane molecule. Unfortunately at the time of writing this report the relevant standard was not available to confirm the identity of this analyte. However, in the study by DeBarber et al. [246, 247] 7α-hydroxy-5β-cholestan-3-one has been analysed by LC-MS following GP-derivatisation in the manner similar to our methodology. The MS^n spectrum presented in that work is consistent with the spectrum of the compound which we putatively identified as 5α-cholestane-3β,7α-diol. The concentration of this analyte was determined as 0.2051±0.2016 ng/mg in Cyp27a1-/- mice; conversely, in wild type this compound was below the detection limit.

The exact origin of this novel oxysterol is not known. One of the candidates is Cyp7a1 with the ability of 7α-hydroxylation, however there is no data showing cholestanol is a substrate for Cyp7a1.

There are studies reporting the presence of 7α-hydroxy-5β-cholestan-3-one in the plasma derived from $Cyp27a1^{-/-}$ mice [247]. However, we were not able to identify this substance in the brain extracts. This may be due to the reduction of peripheral 7α-hydroxy-5β-cholest-3-one [236] to 5β-cholestane-3α,7α-diol.

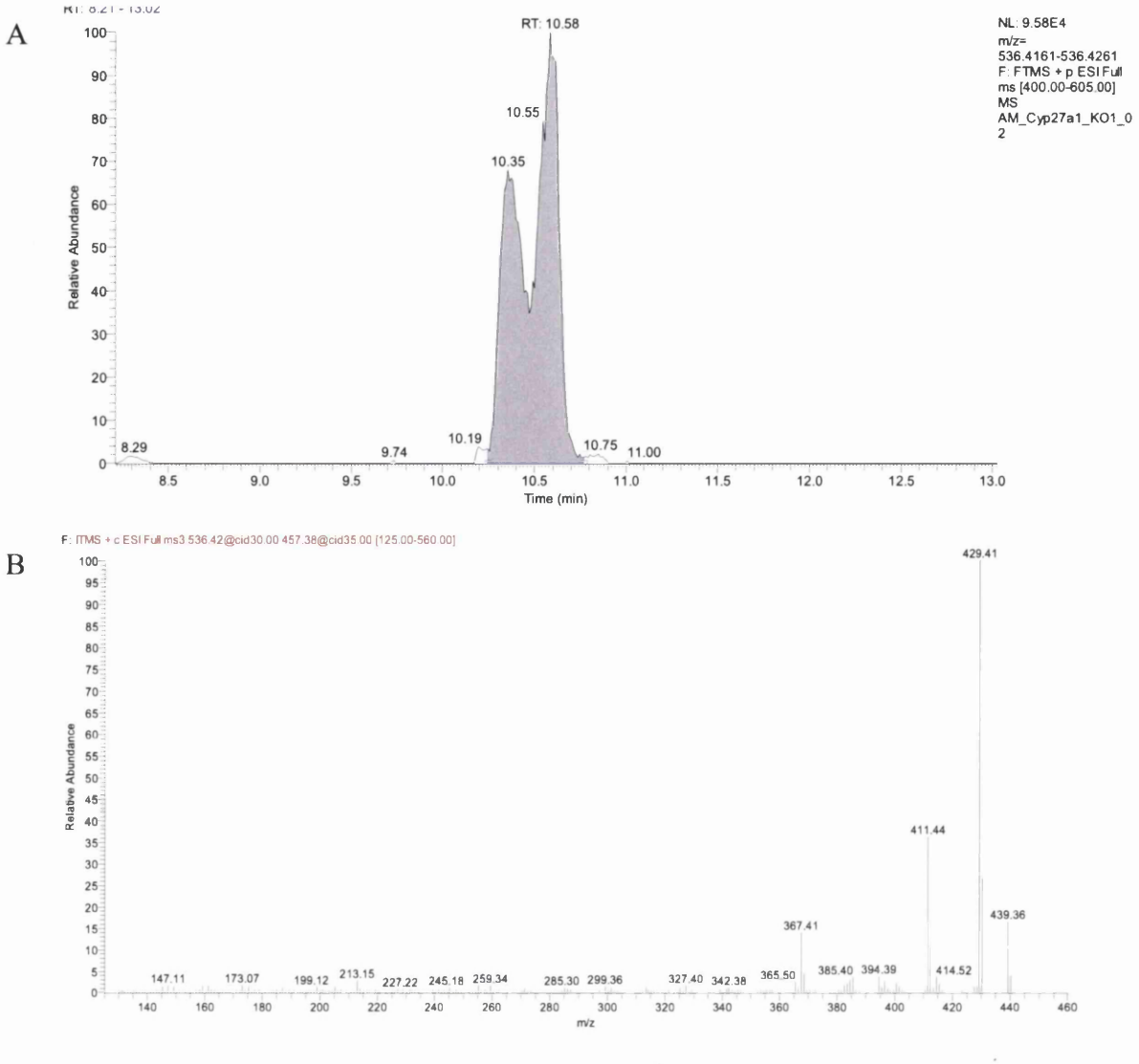

Figure 6.22. 5α-Cholestane-3β,7α-diol in brain of Cyp27a1$^{-/-}$ mouse.
(A) RIC of m/z 536.4211±5 ppm of Cyp27a1$^{-/-}$ mouse
(B) MS^3 spectrum of peak eluting at 10.02 min identified as GP-tagged 5α-Cholestane-3β,7α-diol

Other routes of the neutral pathway employs Cyp8b1 catalyzed hydroxylation at the 12α position of 7α-hydroxycholesterol and 7α-hydroxycholest-4-en-3-one. This generates 7α,12α-dihydroxycholesterol and 7α,12α-dihydroxycholest-4-en-3-one, respectively. 7α,12α-Dihydroxycholest-4-en-3-one posses an oxo moiety, therefore, it is possible to quantify this compound in fraction 1b. The analysis of RIC at *m/z* 550 in fraction b reveals a double peak (RT 8.75 min and 8.95 min), which we identified as 7α,12α-dihydroxycholest-4-en-3-one. The MS^3 spectrum (Figure 6.23) is dominated by an ion *m/z* 453 formed by the loss of water from product ion of MS^2 *m/z* 471. The ion of *m/z* 443 is a result of removal of CO group from *m/z* 471, the loss of two water molecules gives an ion of *m/z* 435. The loss of one water molecule and CO from the GP molecule will yield an ion of *m/z*425. Simultaneous double

dehydratation combined with loss of the carbonyl and NH^+ groups gives an intense ion at *m/z* 392. The complete removal of GP moiety and migration of double bond to the adjacent steroid ring of the dehydrated oxysterol molecule produces ion of *m/z* 365. The loss of the side-chain from dehydrated MS^3-parent ion generates ion of *m/z* 323 and combined with the loss of GP molecule, results in the formation of a product ion with the *m/z* 279. The doublet of ions of *m/z* 151 and 179 are the hallmark of C-7 hydroxylation and are formed during the cleavage of rings A and B of the tetracyclic steroid structure. By comparison with the internal standard we determined the level of 7α,12α-dihydroxycholest-4-en-3-one in Fr1b of the knockout mice to be 0.1409±0.0235 ng/mg, while in wild type the level was below the detection limit.

We also measured the level of 7α,12α-dihydroxycholesterol in fraction a, (chromatogram and spectrum presented in Figure 6.23) where the levels were markedly higher (0.4971±0.1658 ng/mg) in the Cyp27a1-/- mouse than the wild type (0.0002±0.0001 ng/mg). The actual amount of 7α,12α-dihydroxycholesterol in fraction a (after subtracting the amount detected in fraction b) was 0.3562 ng/mg, while in wild type the levels were evaluated as 0.0002±0.0001 ng/mg, this gives a 2500-fold difference between $Cyp27a1^{-/-}$ and control mice. This shows a major accumulation of 7α,12α-dihydroxylated cholesterol/cholestenone in the nervous tissue. Cyp27a1 utilises also 7α,12α-dihydroxycholesterol and 7α,12α-dihydroxycholest-4-en-3-one and its deletion will cause the accumulation of these oxysterols.

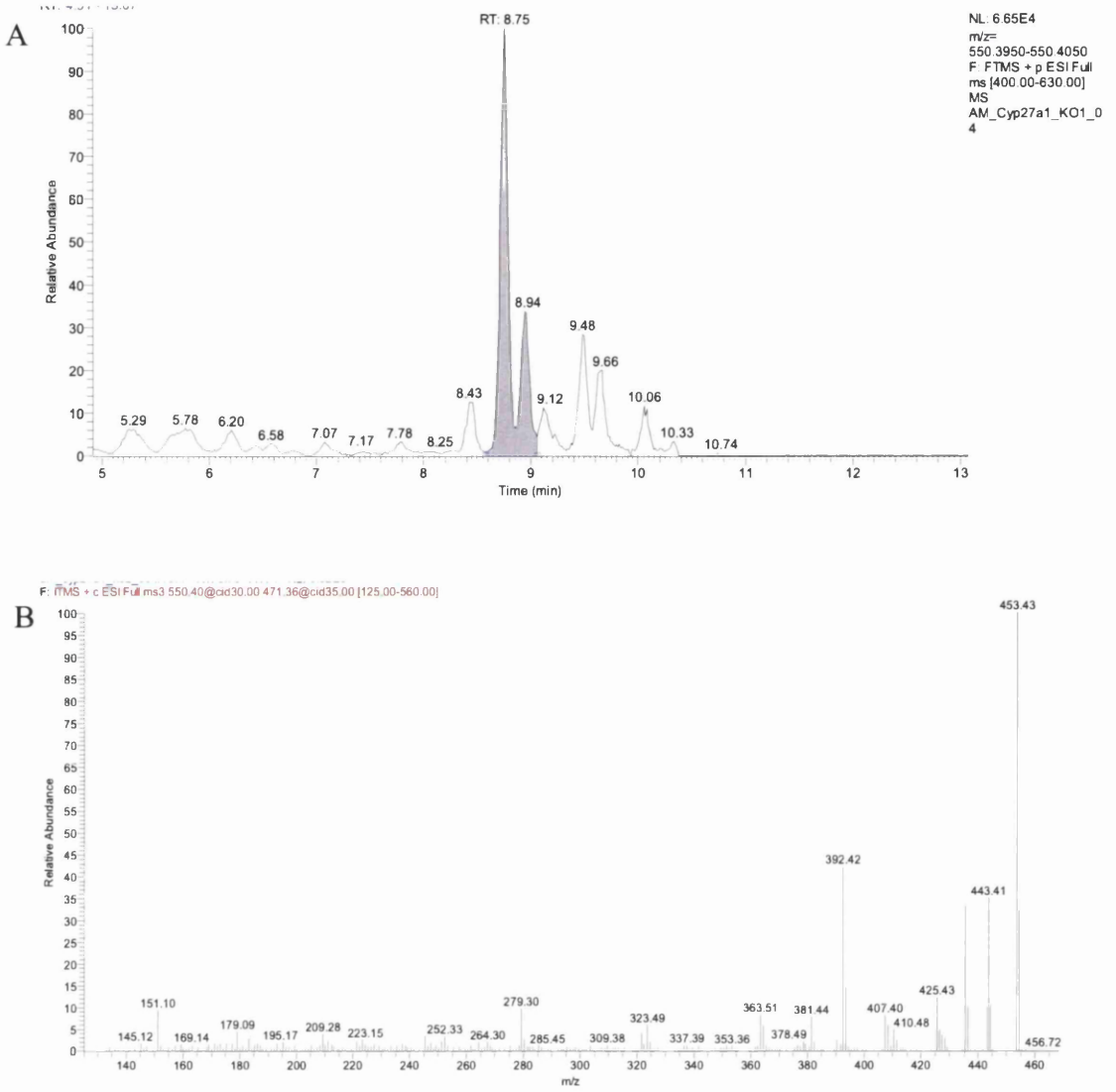

Figure 6.23. 7α,12α-Dihydroxycholesterol in brain of Cyp27a1$^{-/-}$ mouse.
(A) RIC of m/z 550.4005±5 ppm of Cyp27a1$^{+/+}$
(B) MS^3 spectrum of peak eluting at 8.75min identified as GP-tagged 7α,12α-dihydroxycholesterol

The next step of bile acid biosynthesis from 7α,12α-dihydroxycholest-4-en-3-one is reduction to 7α,12α-dihydroxy-5β-cholestan-3-one. This compound also possesses a readily derivatiseable oxo group allowing for its detection in the fraction b. GP modification of this compound should yield a derivative of *m/z* 552.4160, the analysis of relevant RIC of fraction b showed two major peaks which we identified as a doublet belonging to one analyte.

The peak exhibits a very "low" profile of fragments which is usually characteristic for oxysterols hydroxylated at the C-25 position (Figure 6.24). This compound was only detected in knockout mice at the levels of 0.1260±0.0036 ng/mg.

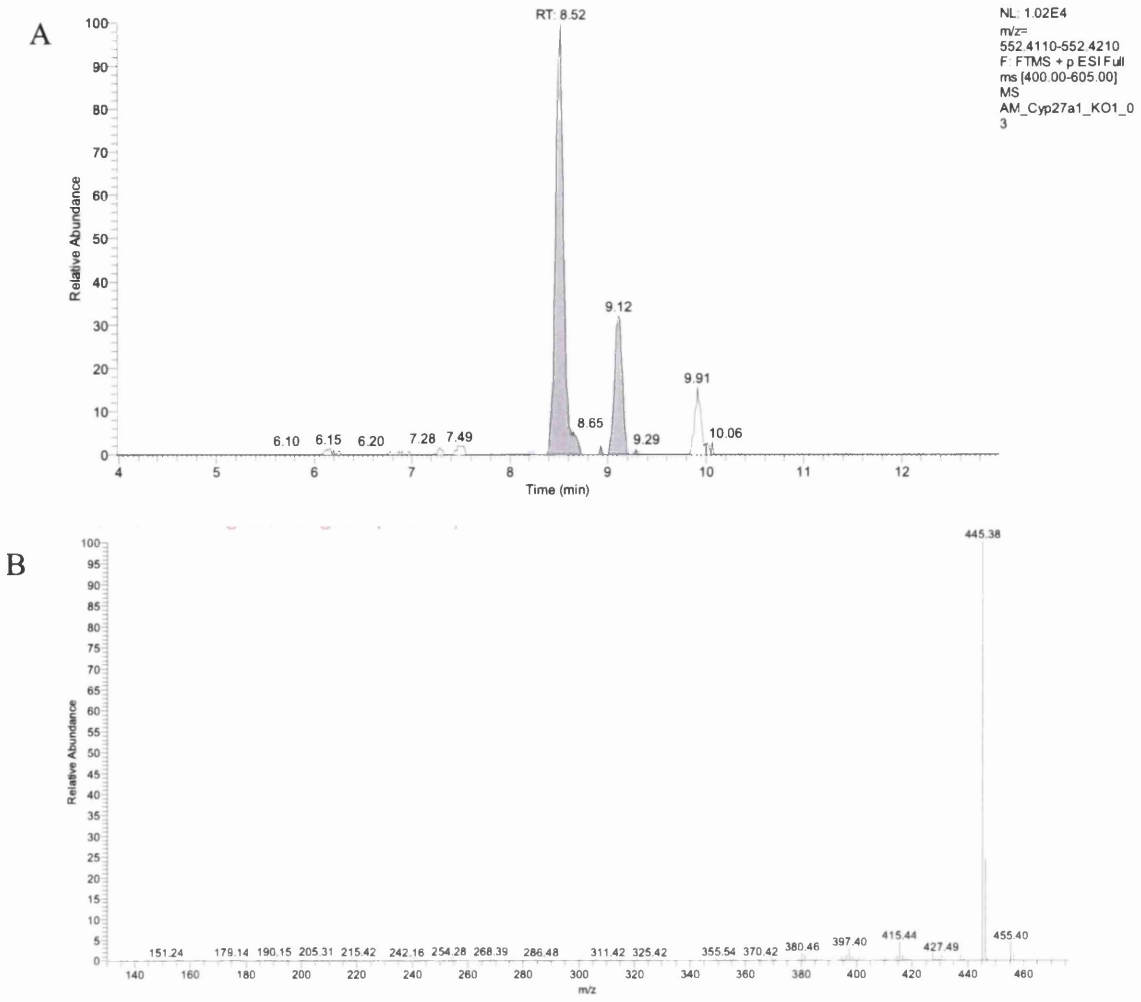

Figure 6.24. Unidentified sterol in brain of Cyp27a1$^{-/-}$ mouse in fraction 1b.
(A) RIC of m/z 552.4160±5 ppm of Cyp27a1$^{+/+}$
(B) MS^3 spectrum of peak eluting at 8.52 min

However, the above spectrum does not agree with the MS^3 spectrum of 7α,12α-dihydroxy-5β-cholestan-3-one presented in the study published by DeBarber et al. [247].
We analysed the RIC of m/z 552.4160 of metabolites obtained in the fraction 1a; the spectrum shows a number of analytes, which are present exclusively in knockout mice. The dominating peak is eluted at RT 8.52 min. The MS^3 spectrum presents a prominent ion *m/z* 445, produced by the loss of CO group from [M-79]$^+$ ion of *m/z* 473. The ion of *m/z* 365 is formed by the loss of GP moiety combined with removal of both hydroxyl groups. This analyte was absent in wild type mice; in the Cyp27a1$^{-/-}$ mice its concentration equals to 0.0870±0.0571 ng/mg.

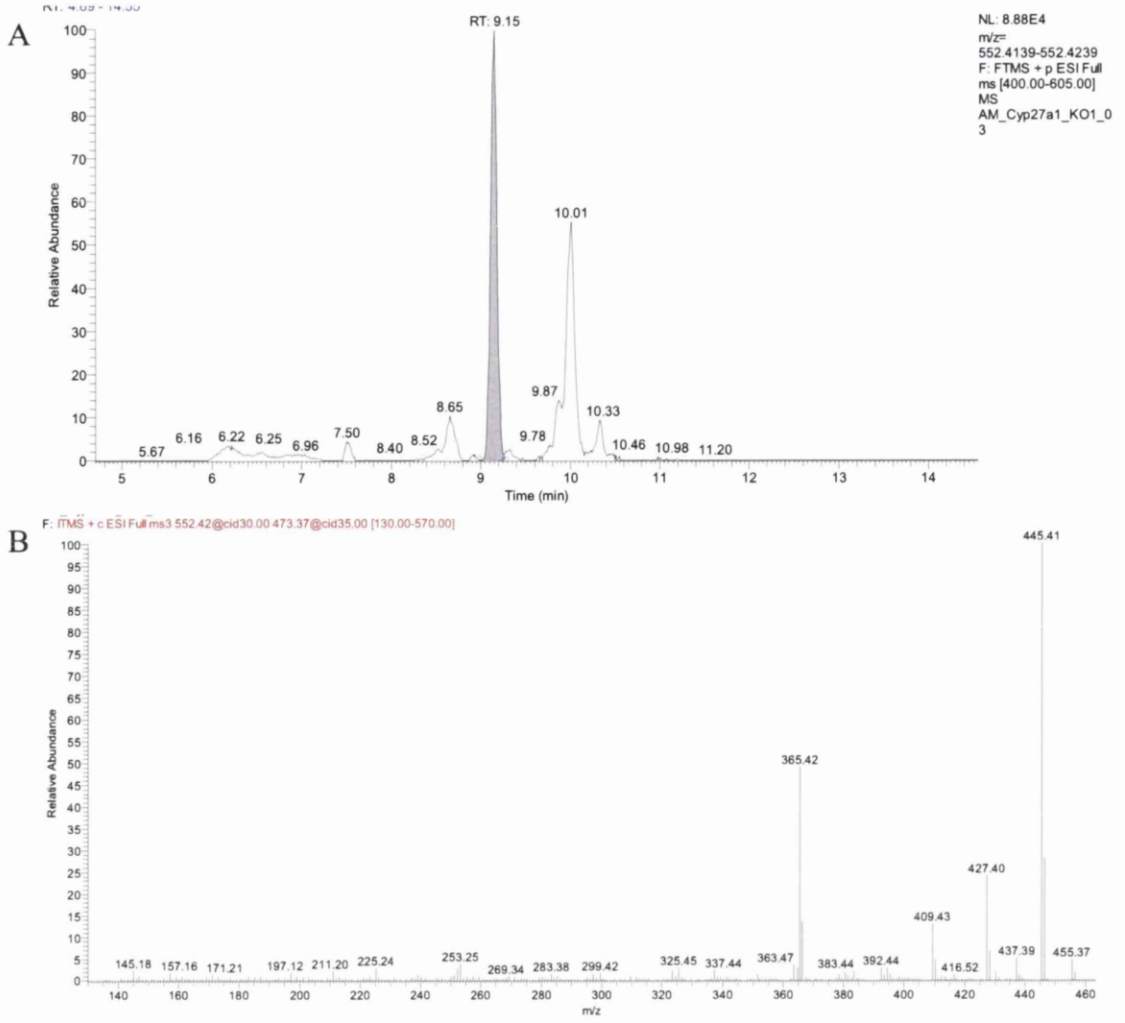

Figure 6.25. Unidentified sterol in brain of Cyp27a1$^{-/-}$ mouse in fraction 1a.
(A) RIC of m/z 552.4160±5 ppm from Cyp27a1$^{+/+}$
(B) MS^3 spectrum of peak eluting at 9.14min

The presence of doubly-hydroxylated derivatives of cholesterol is not limited to 7α,12α-hydroxylated compounds. The RIC obtained at *m/z* 550.4003 shows a large number of compounds (Figure 6.23). We identified 7α,25-hydroxycholesterol at concentration markedly increased in knockout mice as opposed to wild type (0.1183±0.0095 ng/mg and 0.0285±0.0026 ng/mg) and 7α,25-hydroxycholest-4-en-3-one (0.0392±0.0022 ng/mg and 0.0022±0.0005 ng/mg). Increased concentration in the knockout mice is not surprising as both enzymes responsible for 7α- and 25 hydroxylation are up-regulated in Cyp27a1$^{-/-}$ mice. The other compounds we putatively identified are: 6,24S-dihydroxycholesterol (0.1477±0.0094ng/mg in KO and 0.1237±0.0245 ng/mg in WT), present only in the knockouts: 6β,12α-dihydroxycholesterol (0.0894±0.0223ng/mg) and 6β,12α-Dihydroxycholest-4-en-3-one (0.0066±0.0012 ng/mg).

7α,12α-Dihydroxylated analogues of cholesterol, that contain functions of 3-oxo or 3β-hydroxy-5α-cholestan may be subjected to further hydroxylation. It was showed that microsomal enzyme CYP3A4 has the catalytic activity of 25- and 27-hydroxylase towards 3α,7α,12α-trihydroxy-5β-cholestane [214]. After derivatisation, such a compound would have m/z ratio of 566.3952 (for analytes containing unsaturated bond by 4 or 5 position) or 568.4106 (for cholestanol based sterols). The chromatograms *of m/z* 566.3952 and *m/z* 568.4109 from knockout mice showed an accumulation of analytes, which were absent in the wild type extracts (Figure 6.26 and Figure 6.27).

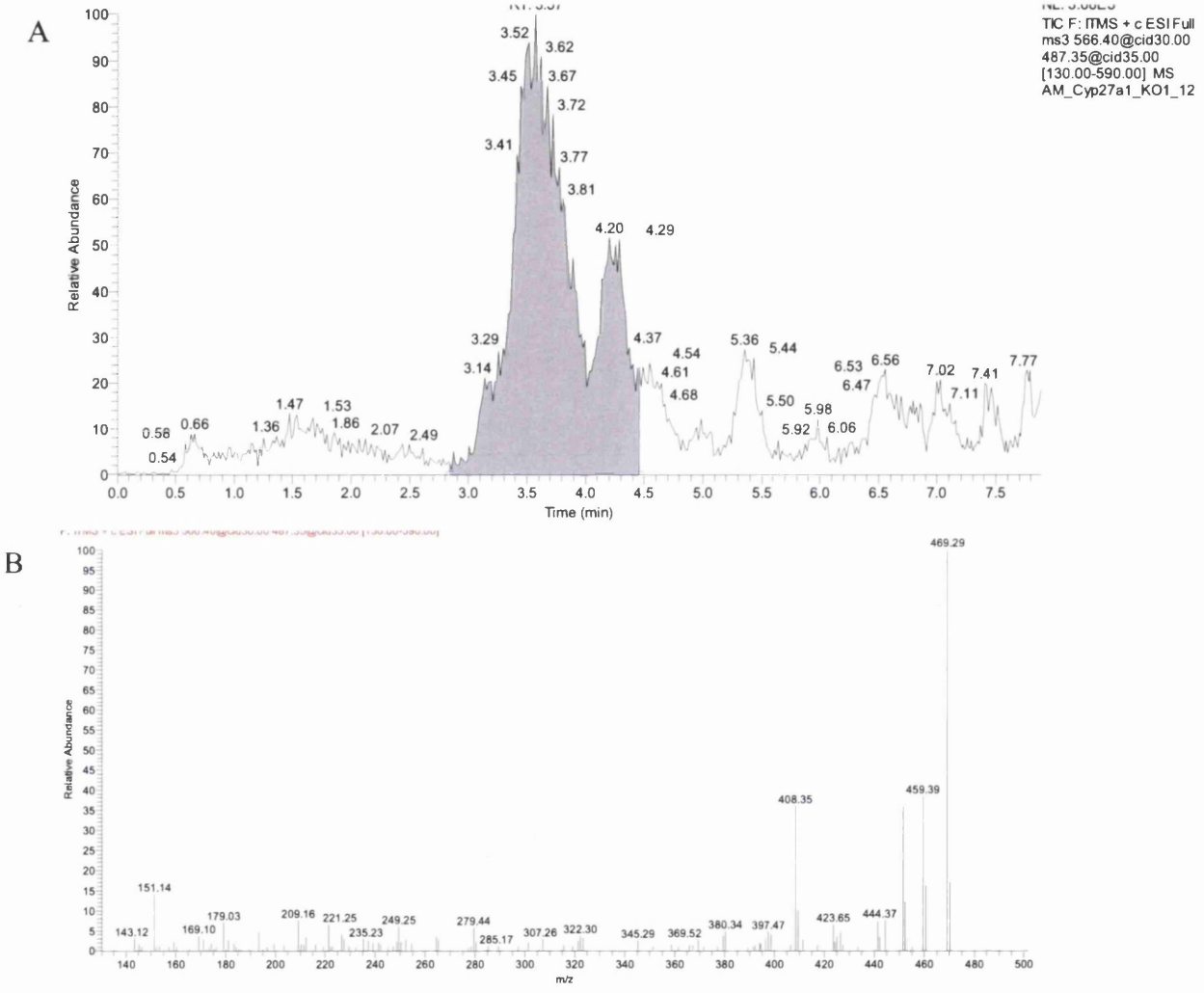

Figure 6.26. 7α,12α,X-Trihydroxycholesterol in brain of Cyp27a1$^{-/-}$ mouse in fraction 1a.
(A) RIC of m/z 566.3952±5 ppm of Cyp27a1$^{+/+}$
(B) MS^3 spectrum of peak eluting at 3.62min

RIC of *m/z* 566.3952 shows a major peak at RT 3.65min (Figure 6.26). The MS^3 spectrum has features characteristic for cholesterol hydroxylated at 7α and 12α positions. 7α Hydroxylation gives ions of *m/z* 151 and 179, while high mass fragments give similar profile to 7α,12α-dihydroxycholesterol with the masses increased by 18 units of hydroxyl group. It is

not clear where the third hydroxyl group is positioned, the fact that the fragmentation has not altered low mass fragments suggest that it was hydroxylated the side chain. According to Honda et al. [214], CYP3A4 can hydroxylate 5β-cholestane-3α,7α,12α-triol at positions 25 and 26, with the preference towards C25 hydroxylation. The concentration of this compound was calculated in the knockout mice as 0.1018ng/mg in a fraction 1a and 0.1336±0.0154 ng/mg in fraction 1b. The presence of this oxysterol in both fractions a and b suggest that it is present in two forms - 3β-hydroxy and 3-oxo containing function groups.

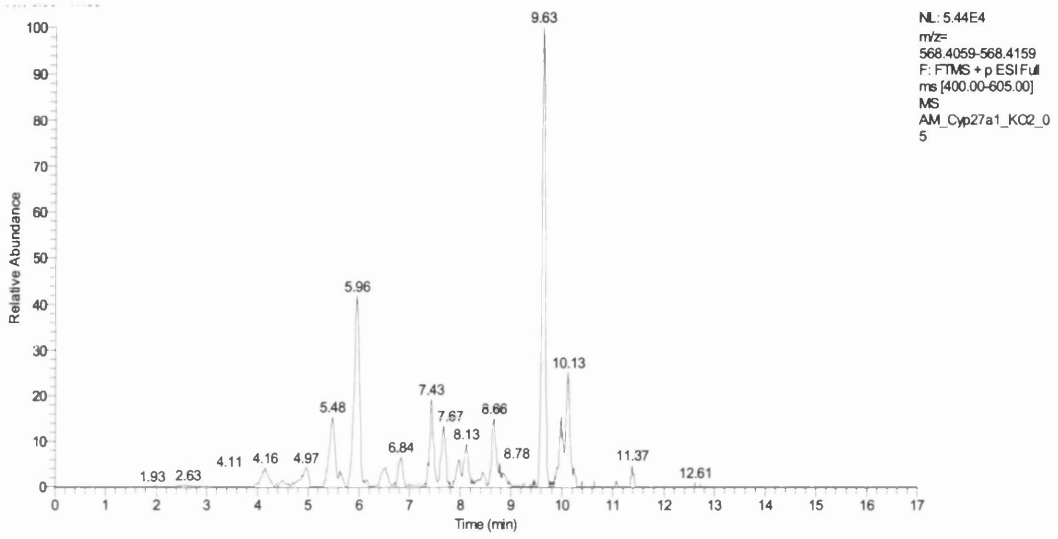

Figure 6.27. Trihydroxycholesterols in brain of Cyp27a1$^{-/-}$ mouse in fraction 1a.
(A) RIC of m/z 568.4109±5 ppm and Cyp27a1$^{-/-}$ (B) mouse

RIC of *m/z* 566.3952 shows a number of analytes unique for knockout mice (Figure 6.27), which suggest multihydroxylation of sterols with 3β-hydroxylate-5α-cholestane group. This is consistent with the observations of multi-hydroxylations of the sterol side chain reported by Honda et al [214].

6.3 Discussion

The deletion of Cyp27a1 resulted in an elevated activity of a neutral bile acid pathway, which is initiated by 7α-hydroxylation provided by Cyp7a1. This enzyme catalyses the formation of 7α-hydroxycholesterol, which in Cyp27a1-/- mice is largely accumulated. The increased activity of this enzyme is presumably responsible for 7α-hydroxylation of desmosterol, the presence of 7α-hydroxydesmosterol has been already reported in "cholesterol-free" mouse [190]. Contrary to Cyp27a1, Cyp7a1, is specific found in liver [215], so presumably the presence of its 7α-hydroxylated products in brain is possible due to

diffusion of this oxysterols across the blood brain barrier from the circulation. The mechanism by which 7α-hydroxycholestrol could pass BBB and enter the brain is not entirely clear. It is widely accepted that oxysterols can transverse the barrier in passive diffusion [30, 248] which requires the gradient of compounds, however there are reports showing active transport aiding oxysterols efflux [249]. In healthy human brain the flux of two main oxysterols from and into the brain occurs at levels 6-7mg for 24-hydroxycholesterol [171] and 5mg for 27-hydroxycholesterol [250], respectively. It is possible that in the absence of 27-hydroxycholesterol, 7α-hydroxycholesterol passes thought the BBB at increased rate which leads to its accumulation in the CNS.

Accumulated 7α-hydroxydesmosterol is probably further hydroxylated at 12α position yielding 7α,12α-dihydroxydesmosterol, which was detected in biological system for the first time. These two reaction of 7α- and 12α-hydroxylations in regard to desmosterol can implicate the existence of new metabolic pathway.

Cyp27a1 catalyses two reactions involving cholesterol. One is hydroxylation at C-26 position of cholesterol, and the second one involves the cleavage and further oxidation of the sterol side chain leading to formation of bile acids [181]. Unsurprisingly, the deficiency of this changes the oxysterol profile with an accumulation of compounds with multiple hydroxylations of the side chain. Cyp27a1-/- mouse has a largely elevated level of di- and trihydroxycholesterols. Among these oxysterols is 7α,25-dihydroxycholesterol largely studied for its function in modulation of cellular immune response. Enhanced 25-hydroxylation is not surprising as increased activity of Cyp3a, which can introduce a hydroxyl group at C-25 position, was reported [26].

Chapter 7

7 Sterol profiling of brain of the Cyp7b1-/- mouse

7.1 Introduction

In the course of the "acidic" bile acid biosynthesis pathway hydroxylation of the cholesterol side-chain at the 26 position is followed by hydroxylation of the ring structure at position 7α. This reaction is catalysed by the microsomal monooxygense Cytochrome P450 (Cyp) 7b1.

Cyp7b1 is widely distributed in various tissues; the highest expression is reported in brain, however, this enzyme is also present in liver, kidneys, ovaries, testis and the adrenal glands. In rat brain it is mainly detected in the hippocampus [220]. The analysis of mice adrenal glands showed a sexual dimorphism for the presence of Cyp7b1, with the higher level found in the males [251]. In humans the mRNA transcripts of CYP7B1 are most abundant in kidneys and brain [252]. Cyp7b1 participates in bile acid biosynthesis via the "acidic" pathway by 7α-hydroxylation of 27-hydroxycholesterol. Deficiency of this enzyme leads to accumulation of 27-hydroxycholesterol and a compensatory up-regulation of the classical pathway resulting in an increased level of cholic acid.

Another substrate of Cyp7b1 is 25-hydroxycholesterol. This oxysterol recently emerged as a part of the body's defence system as it is produced by stimulated murine macrophages. The product of 7α-hydroxylation of 25-hydroxycholesterol has been reported as a chemotactic factor directing B-cells in the lymphoid tissue required during the immunological response [132].

Oxysterol 7α-hydroxylase in also implicated in neuroprotection as its metabolites 7α-hydroxy-dehydroepiandrogene and 7α-hydroxyepiandrosterone prevent neuronal damage [253, 254].

The mutations of *CYP7B1* in humans are associated with two disorders: liver failure in children [23, 25] and hereditary spastic paraplegia type 5 in adults [24]. The first disorder has been described in four infants. The main symptoms included cholestasis, cirrhosis and elevated level of bile acid precursors in the urine. MS analysis of the patient's urine showed a large increase in the concentration of monohydroxycholenoates conjugated with sulphuric acid, glycine and taurine; hydrolysis of the sample revealed that major cholenoate was 3β-hydroxychol-5-enoic acid. The bile profile of the serum was remarkably similar to that of urine, the main compounds were identified as 3β-hydroxychol-5-enoic acid and its 27 carbon

atom analogue. Analysis of neutral sterols showed an accumulation of 27- and 24-hydroxycholesterol in the urine and serum.

The neurological importance of CYP7B1 has been revealed by analysis of the genome of patients suffering from hereditary impairment of motor functions. Hereditary spastic paraplegia type 5 (HSP5) is a neurological disorder characterised by spasticity and weakness of lower limbs. There are also reported white matter lesions in affected individuals [255]. The deficiency of CYP7B1 has been directly linked to HSP5, a number of mutations have been identified including missense and nonsense [24]. The exact dependency between the gene deficiency and the neurological symptoms are not known.

To gain a better understanding of these disorders, an animal model was constructed using a mouse with disrupted *Cyp7b1* locus. Cyp7b1 deficient mice have no physical phenotype, however, analysis of the lipidome showed alteration in the steroid profile. The most striking feature of the chemical phenotype was an accumulation of 25- and 27-hydroxycholesterol which led to the conclusion that these oxysterols are main substrates of murine Cyp7b1. on the contrary, the level of cholesterol and triglycerides was not affected in these animals. In our work we focus for the first time on the analysis of brain of Cyp7b1 knockout animals.

7.2 Results

Sterols

Cholesterol upon oxidation with cholesterol oxidase and GP-derivatisation produces an $[M]^+$ ion of *m/z* of 518.4105. We quantified a compound which presented as a single peak in the RIC of *m/z* 518.4105 with the RT 11.47 min (Figure 7.2A and Figure 7.2B) whose MS^3 spectrum was identical to the authentic standard of cholesterol. Data was obtained by the analysis four wild type and four knockout animals of 13 months and, three wild type and three knockout of 23 months. The levels of sterols are presented in Table 7.1. The levels of brain cholesterol were not affected by the presence of the Cyp7b1 mutation. The concentration was measured as 10.60±1.43 μg/mg in the wild type and 10.33±2.02 μg/mg in the knockout mice of 13 months and 15.81±0.65 μg/mg 16.85±0.59 μg/mg in 23 month mice (Table 7.1).

Table 7.1 Sterols identified by LC-ESI-MSn in murine brain following SPE and charge-tagging with GP-hydrazine. Three samples of 12 months old and four samples of 23 months old $Cyp7b1^{-/-}$ and $Cyp7b1^{+/+}$ mice were analysed. Dehydrocholesterols were quantified for one sample from 13 month old animal. An asterix indicated the long gradient.

M/z	RT min	Systematic name	Common name	$Cyp7b1^{+/+}$ µg/mg		$Cyp7b1^{-/-}$ µg/mg		TT	TT
				13 months	23 months	13 months	23 months	13	23
518.4105	11.75	Cholest-4-en-3-one 3-GP	Cholesterol	10.60±1.43	15.81±0.65	10.33±2.02	16.85±0.59	nd	***
516.3847	10.66	Cholest-4,24-dien-3-one 3-GP	Desmosterol	0.0688		0.0060		*	
516.3847	10.90	Cholest-4,8(9)-dien-3-one 3-GP	8(9)-Dehydrocholesterol	0.0089		0.0021			
516.3847	11.17	Unknown	Unknown	0.0116		0.0013		*	

M/z	RT min	Systematic name	Common name	$Cyp7b1^{+/+}$ ng/mg		$Cyp7b1^{-/-}$ ng/mg		TT	TT
				13 months	23 months	13 months	23 months	13	23
532.3898	6.68	24S,25-Epoxycholest-4-en-3-one 3-GP	24S,25-Epoxycholesterol	0.0045±0.0014	0.0120±0.0024	0.0084±0.0038	0.0218±0.0006	nd	***
532.3898	7.11	26-Hydroxycholest-4,24Z-dien-3-one 3-GP	(24Z),26-Hydroxydesmosterol	0.0029±0.0008	0.0094±0.0016	0.0096±0.0040	0.0252±0.0009	*	**
532.3898	7.49	26-Hydroxycholest-4,24E-dien-3-one 3-GP	(24E),26-Hydroxydesmosterol	0.0028±0.0004	0.0089±0.0034	0.0187±0.0064	0.0383±0.0037	*	***
532.3898	7.74	Cholest-4-en-3,24-dione 3-GP	24-Oxocholesterol	0.9160±0.2662	1.3834±0.2982	3.5534±1.2725	2.0680±0.1838	*	**
534.4054	7.48	24S-Hydroxycholest-4-en-3-one 3-GP	24S-Hydroxycholesterol	16.8211±2.5529	24.8063±2.5754	18.2565±4.2880	24.0204±1.2117	nd	nd
534.4054	17.72*	24R-Hydroxycholest-4-en-3-one 3-GP	24R-Hydroxycholesterol	0.1995±0.0890*	0.3020±0.0306*	0.1356±0.0222*	0.3590±0.0660*	nd	nd
534.4054	15.86*	25-Hydroxycholest-4-en-3-one 3-GP	25-Hydroxycholesterol	ND	ND	0.8892±0.1422*	2.0906±0.4461*	***	***
534.4054	18.58*	27-Hydroxycholest-4-en-3-one 3-GP	27-Hydroxycholesterol	0.2766±0.1340*	0.2976±0.1204 *	3.0686±0.8612*	3.7181±0.3911*	**	***
534.4054	10.23	7α-Hydroxycholest-4-en-3-one 3-GP	7α-Hydroxycholesterol	0.0095±0.0046	0.0095±0.0046	0.0071±0.0036	0.0192±0.0035	nd	*
534.4054	9.64	7β-Hydroxycholest-4-en-3-one 3-GP	7β-Hydroxycholesterol	0.0302±0.0086	0.0153±0.0026	0.0338±0.0066	0.0281±0.0073	nd	*
534.4054	10.50	6β-Hydroxycholest-4-en-3-one 3-GP	6β-Hydroxycholesterol	0.0501±0.0246	0.0155±0.0053	0.0282±0.0080	0.0819±0.0406	nd	*
548.3847	7.57		3b-hydroxy-5-cholestenoic acid	0.0089±0.0023	0.0145±0.0047	0.1175±0.0250	0.1509±0.0081	***	***
550.4003	3.47	24S,25-Dihydroxycholest-4-en-3-one 3-GP	24S,25-Dihydroxycholesterol	0.0265±0.0292	0.0858±0.0276	0.0334±0.0226	0.3009±0.0477	nd	***
550.4003	5.58	7α,25-Dihydroxycholest-4-en-3-one 3-GP	7α,25-Dihydroxycholesterol	0.0114±0.0050	0.0197±0.0037	0.0009±0.0001	0.0131±0.0026	***	*
550.4003	5.92	7α,27-Dihydroxycholest-4-en-3-one 3-GP	7α,27-Dihydroxycholesterol	0.0206±0.0105	0.0339±0.0099	0.0124±0.0024	0.0451±0.0056	nd	nd
564.4160	6.07		24-methoxy,25-hydroxy-cholesterol	0.0007±0.0003	0.0504±0.0160	0.0018±0.0002	0.1698±0.0308	nd	
			Epoxy total	0.9593±0.2390	1.5063±0.3006	3.6109±0.2160	2.5765±0.1460	***	**

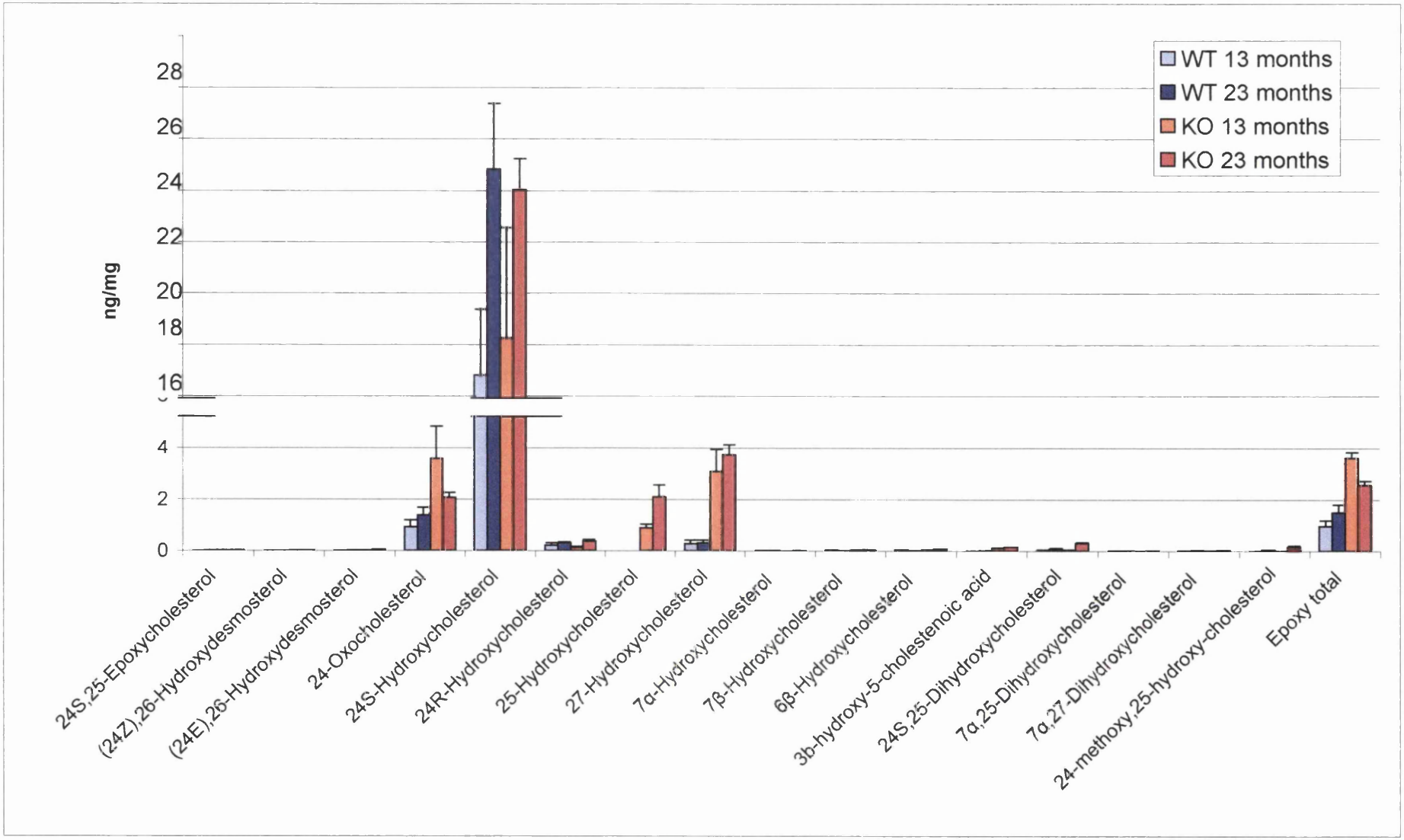

Figure 7.1 Oxysterols extracted from fraction 1a identified in Cyp7b1$^{-/-}$ and Cyp7b1$^{+/+}$ mice brains

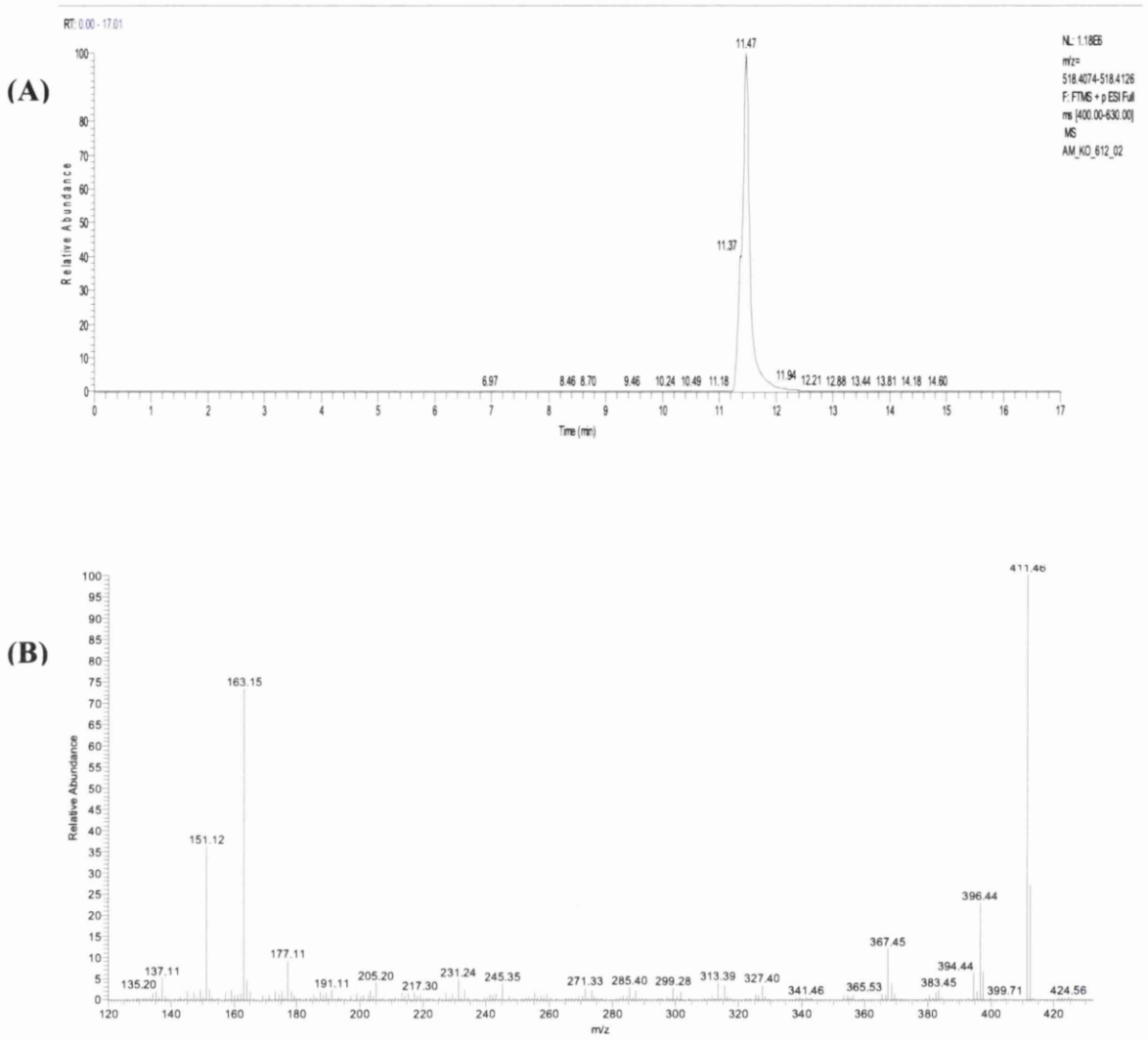

Figure 7.2. Cholesterol in mouse brain. (A) RIC of *m/z* 518.4105±5 ppm of Cyp7b1$^{-/-}$ mouse. (B) MS^3 spectrum of peak eluting at 11.75 min identified as GP-tagged cholesterol from the the Cyp7b1$^{+/+}$ mouse.

Cholesterol precursors include sterols containing an additional double bond either in the side chain (desmosterol) on within the cyclic core. Both dehydrocholesterol molecules upon oxidation and GP-derivatisation will be detected as ions of *m/z* 516.3948. The analysis of brain samples carried out under routine analytical conditions did not provide a MS signal sufficient for the quantification of cholesterol precursors. To get an insight into the levels of the precursors we analysed one knockout and one wild type brain from 13 month animals by injecting much higher amounts of brain extract in to the LC-MS system than under routine

conditions. The chromatogram of both the wild type and knockout mouse shows three peaks with RT: 10.66 min, 10.90 min and 11.17 min (Figure 7.4A and Figure 7.4B). The MS^n spectra of these analytes are shown in Figure 7.4C, Figure 7.4D and Figure 7.4E.

Based on the information obtained from the analysis of authentic standards we identified the first peak as desmosterol and the peak with RT 11.17 min as 8(9)-dehydrocholesterol. The identity of the peak with RT 10.90 min is unknown. The level of desmosterol was lower in the knock out brain compared to the wild type (0.0060 μg/mg and 0.0688 μg/mg, respectively). The amount of 8(9)-dehydrocholesterol was also reduced in the knockout animals (0.0021 μg/mg in the knockout and 0.0089 μg/mg in the wild type). The third, unidentified, compound is present in the knockout brain also at reduced concentration (0.0013 μg/mg in the knockout and 0.0116 μg/mg in the wild type).

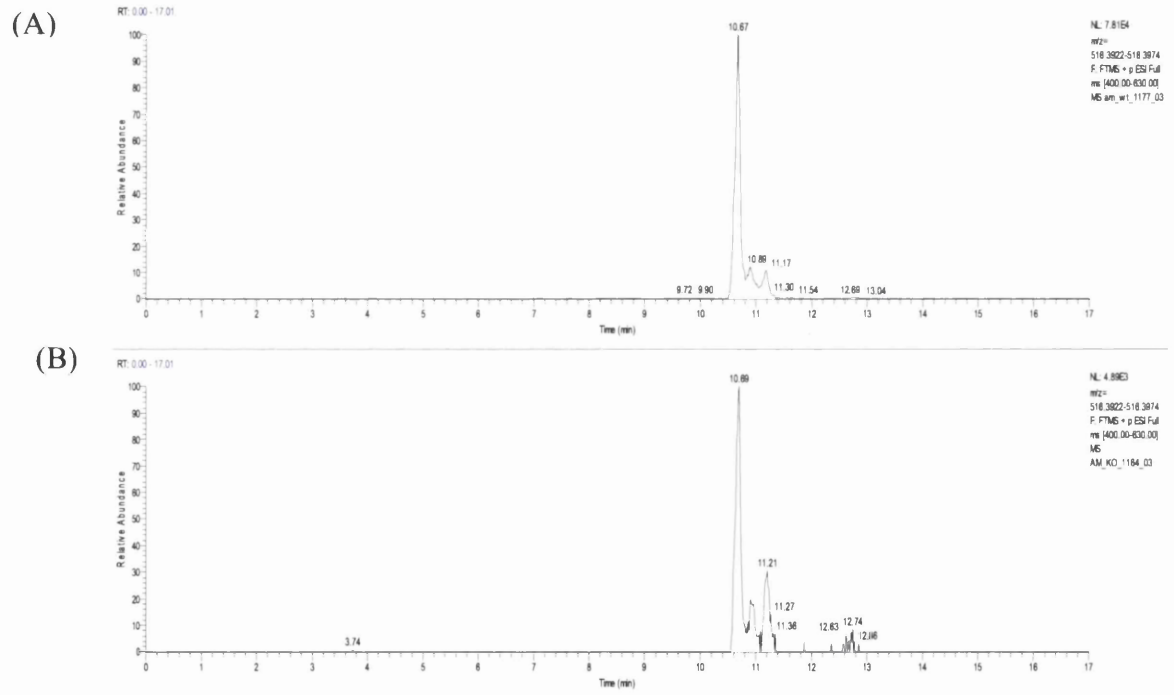

Figure 7.3 Cholesterol precursors in mouse brain. RIC of *m/z* 516.3948±5 ppm in brain of the $Cyp7b1^{+/+}$ (A) and $Cyp7b1^{-/-}$ (B)

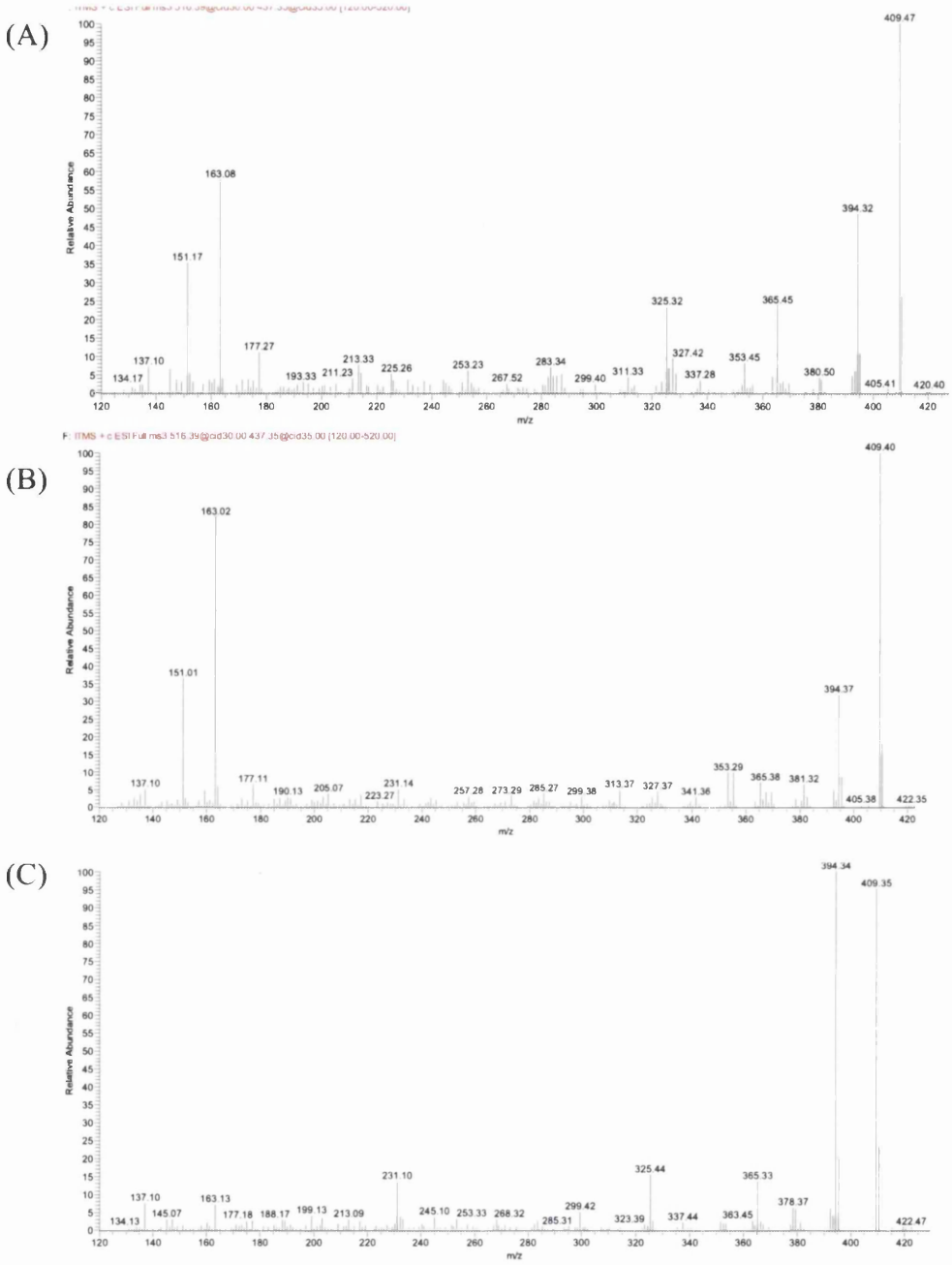

Figure 7.4 Cholesterol precursors in mouse brain.
RIC of *m/z* 516.3948±5 ppm in brain of the Cyp7b1$^{-/-}$ and respective spectra
(A) MS^3 spectrum of GP-tagged desmosterol eluting at 10.67 min
(B) MS^3 spectrum of unidentified compound eluting at 10.82 min
(C) MS^3 spectrum of peak eluting at 11.21 min identified as GP-tagged 8(9)-dehydrocholesterol

The level of precursors is reduced although the amount of cholesterol is maintained which suggest that the rate of the cholesterol biosynthesis has been diminished. The unchanged level of cholesterol is agrees with the findings of Li-Hawkins et al. where cholesterol was assessed in a wide array of murine tissues.

Oxysterols

Cholesterol with an epoxy function between the 24S and 25 positions is a side-product of the mevalonate pathway [218]. It is implicated in neurogenesis [121] and high levels were identified in developing brain [120]. GP modified 24S,25-epoxycholesterol produces a molecular ion of a *m/z* ratio 532.3898. Chemical instability is responsible for transformation of this compound into its isomer (24-ketocholesterol, GP derivatised *m/z* 532.3898), a hydrated (24S,25-dihydroxycholesterol, GP derivatised *m/z* 550.4003) and methanol-modified (24-hydroxy-25-methoxycholesterol or the 24-hydroxy-25-methoxy isomers, GP derivatised *m/z* 564.4160) form [120]. The levels of these analytes were combined to give the total concentration of 24S,25-epoxycholesterol, which is significantly higher in the knockout mice. In 13 months old mice the levels were 0.9593±0.2390 ng/mg and 3.6109±0.2160 ng/mg for wild type and knockout animals respectively, and for the 23 month old animals 1.5063±0.3006ng/mg and 2.5765±0.1460ng/mg, respectively. RIC chromatograms and MSn spectra are shown in Figure 7.5-
Figure 7.7. As the level of cholesterol precursors decreased implying a reduced cholesterol biosyntesis, the elevated level of 24S,25-epoxycholesterol can be a consequence of the absence of Cyp7b1. This also suggests that 24S,25-epoxycholesterol can be a substrate for Cyp7b (data in the Table 7.1).

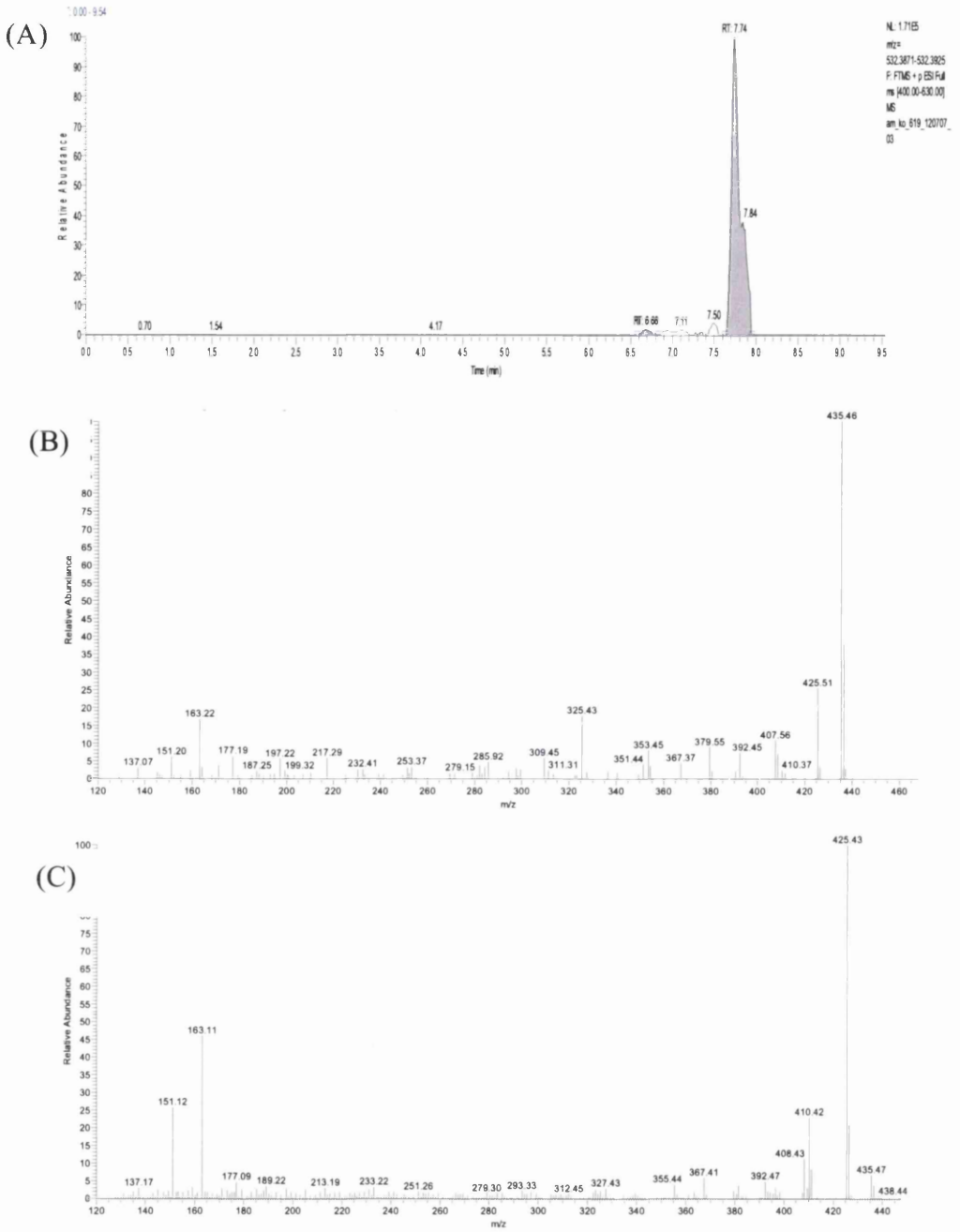

Figure 7.5. 24S,25-Epoxycholesterol and 24-ketocholesterol in brain of 23 month old Cyp7ba1$^{+/+}$ and Cyp7ba1$^{-/-}$ mice. The spectrum comes from the short HPLC elution.
(A) RIC of m/z 532.3898±5 ppm of Cyp7ba1$^{+/+}$ and Cyp7ba1$^{-/-}$ mice
(B) MS^3 spectrum of peak eluting at 6.68 min identified as GP-tagged 24S,25-epoxycholesterol
(C) MS^3 spectrum of peak eluting at 7.74 min identified as GP-tagged 24-ketocholesterol

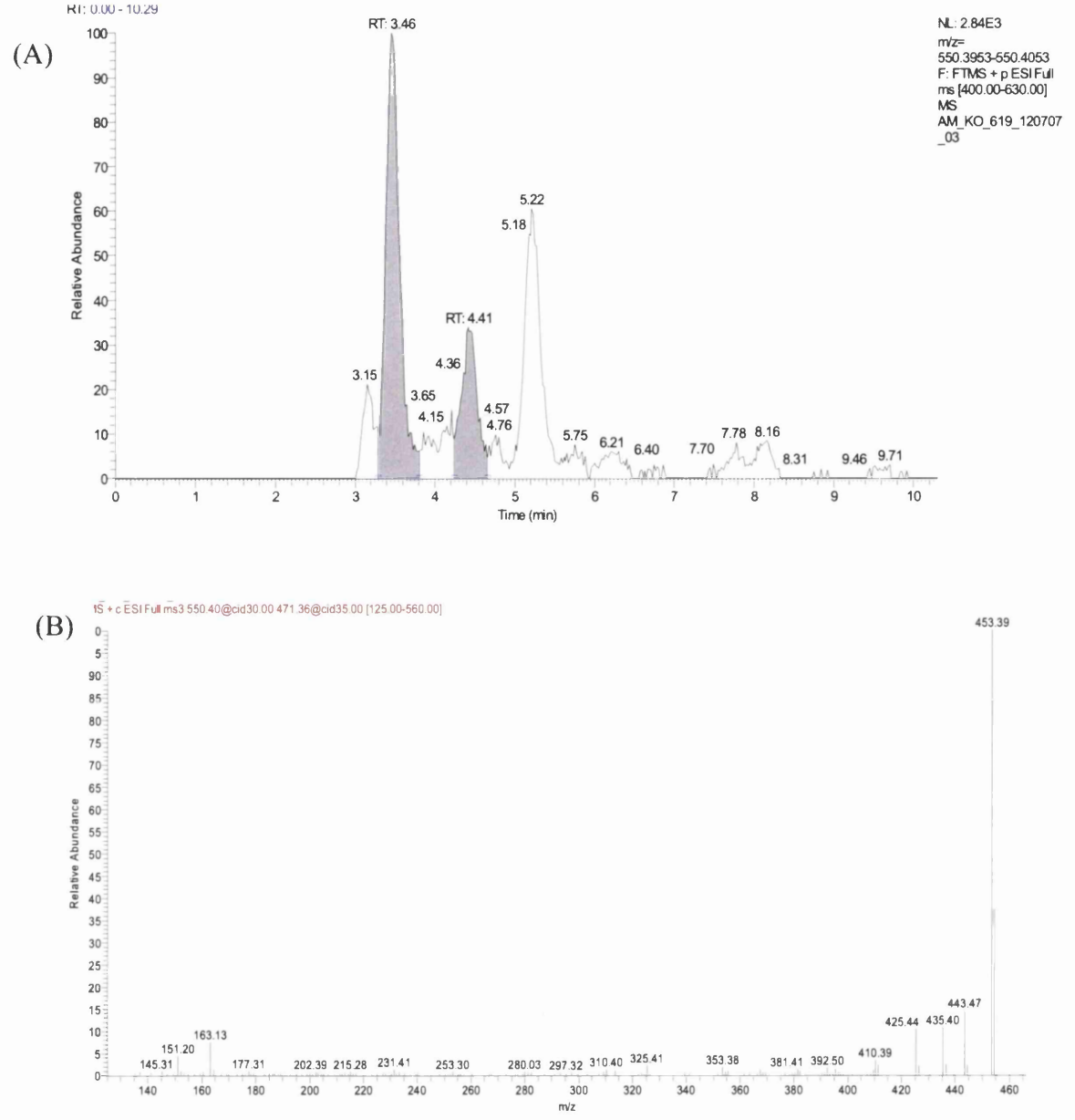

Figure 7.6. 24,25-Dihydroxycholesterol in brain of 23 month old Cyp7ba1$^{+/+}$ and Cyp7ba1$^{-/-}$ mice. The spectrum received from the short HPLC gradient.
(A) RIC of m/z 550.4003±5 ppm of Cyp7ba1$^{+/+}$ and Cyp7ba1$^{-/-}$ mice
(B) MS^3 spectrum of peak eluting at 3.48 min identified as GP-tagged 24,25-dihydroxycholesterol

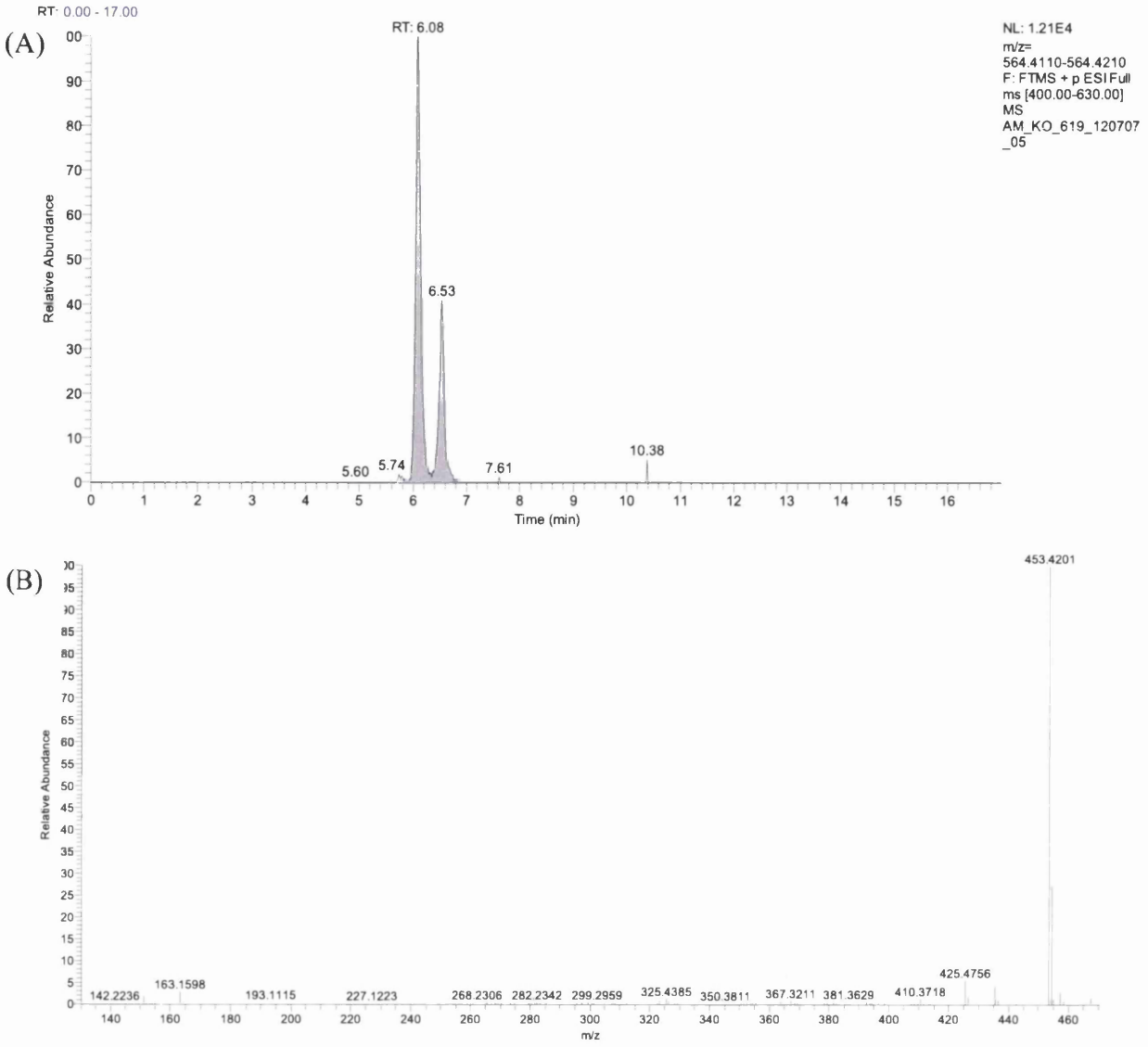

Figure 7.7. 24-hydroxy-25-methoxy- or 24-hydroxy-25-methoxycholesterol from brain of 23 month old Cyp7ba1$^{-/-}$ mice. The spectrum recorded from the short HPLC gradient.
(A) RIC of *m/z* 564.4160±5 ppm of Cyp7ba1$^{-/-}$ mice
(B) MS^3 spectrum of peak eluting at 6.07 min identified as GP-tagged 24-hydroxy-25-methoxy- or 24-hydroxy-25-methoxycholesterol .

Further peaks in RIC of *m/z* 532.3898 eluting at RT 7.11 min and 7.50 min were identified as (24Z) and (24E) isomers of 26-hydroxydesmosterol. The levels of both of these oxysterols were markedly higher in the Cyp7b1 deficient animals. MS^n spectra are illustrated in Figure 7.8. (24Z)-26-Hydroxydesmosterol concentrations in 13 months old mice were 0.0029±0.0008 ng/mg in the wild type and 0.0096±0.0040 ng/mg in the knockout, for 23 month-old mice the levels were 0.0094±0.0016 ng/mg and 0.0252±0.0009 ng/mg. The amounts of (24E)-26-hydroxydesmosterol in 13 months old mice were estimated as

0.0028±0.0004 ng/mg and 0.0187±0.0064 ng/mg in the wild type and knockout, respectively; in 23 months old mice this analyte was found at the levels of 0.0089±0.0034 ng/mg and 0.0383±0.0037 ng/mg.

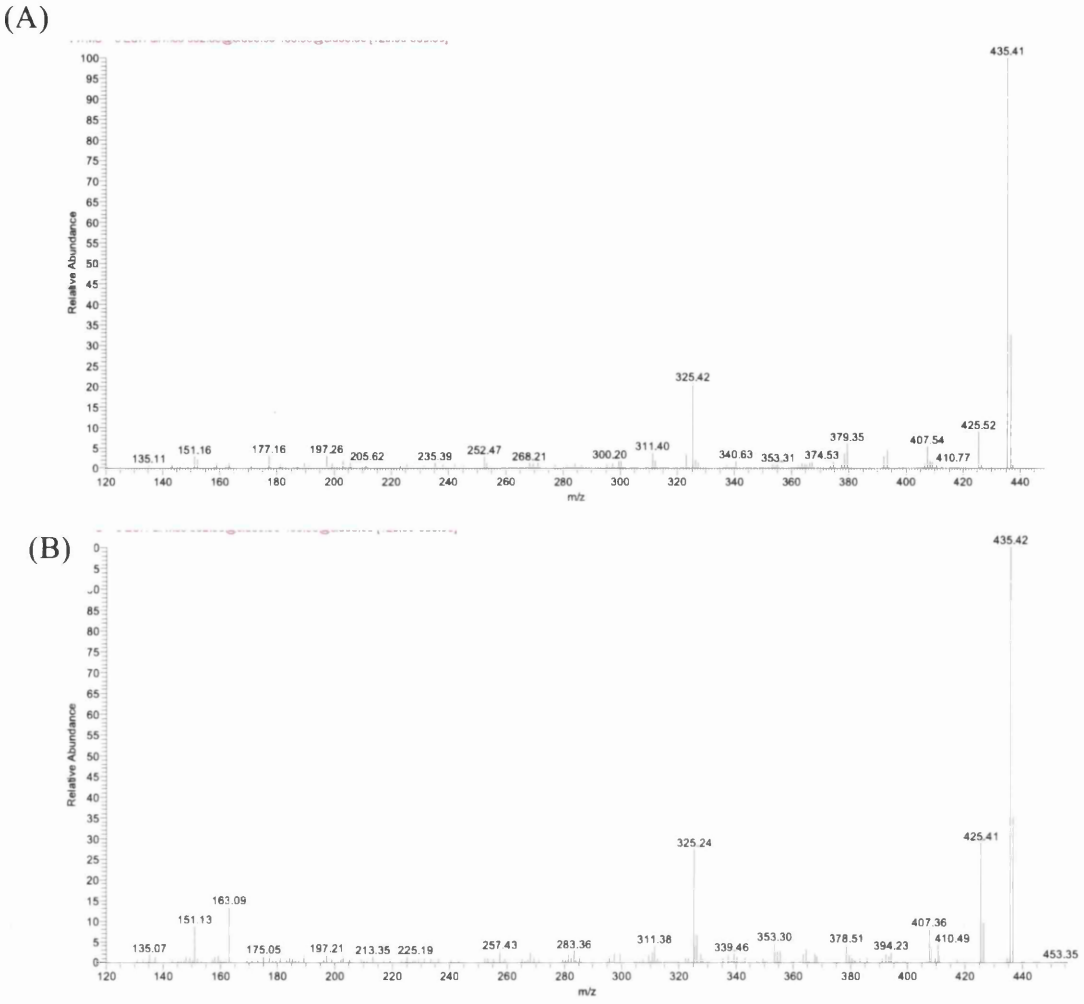

Figure 7.8 (24Z)-26-Hydroxydesmosterol and (24E)-26-hydroxydesmosterol from brain 23 month old Cyp7ba1$^{-/-}$ mice. The spectrum from the short HPLC elution.
(A) MS^3 spectrum of peak eluting at 7.11 min identified as GP-tagged (24Z)-26-hydroxydesmosterol.
(B) MS^3 spectrum of peak eluting at 7.50 min identified as GP-tagged (24E)-26-hydroxydesmosterol.

At 10.45 min elutes another compound with *m/z* 532.3898 (Figure 7.9). The fragmentation profile of the MS^n spectrum fits the characteristics of GP-derivatised cholest-4-en-3,6-dione. The levels were evaluated as 0.0494±0.0143 ng/mg in knockout mice, but in wild type mice were below the detection limit. The origin of cholest-4-en-3,6-dione is not known, it could be generated during an autoxidation of cholesterol.

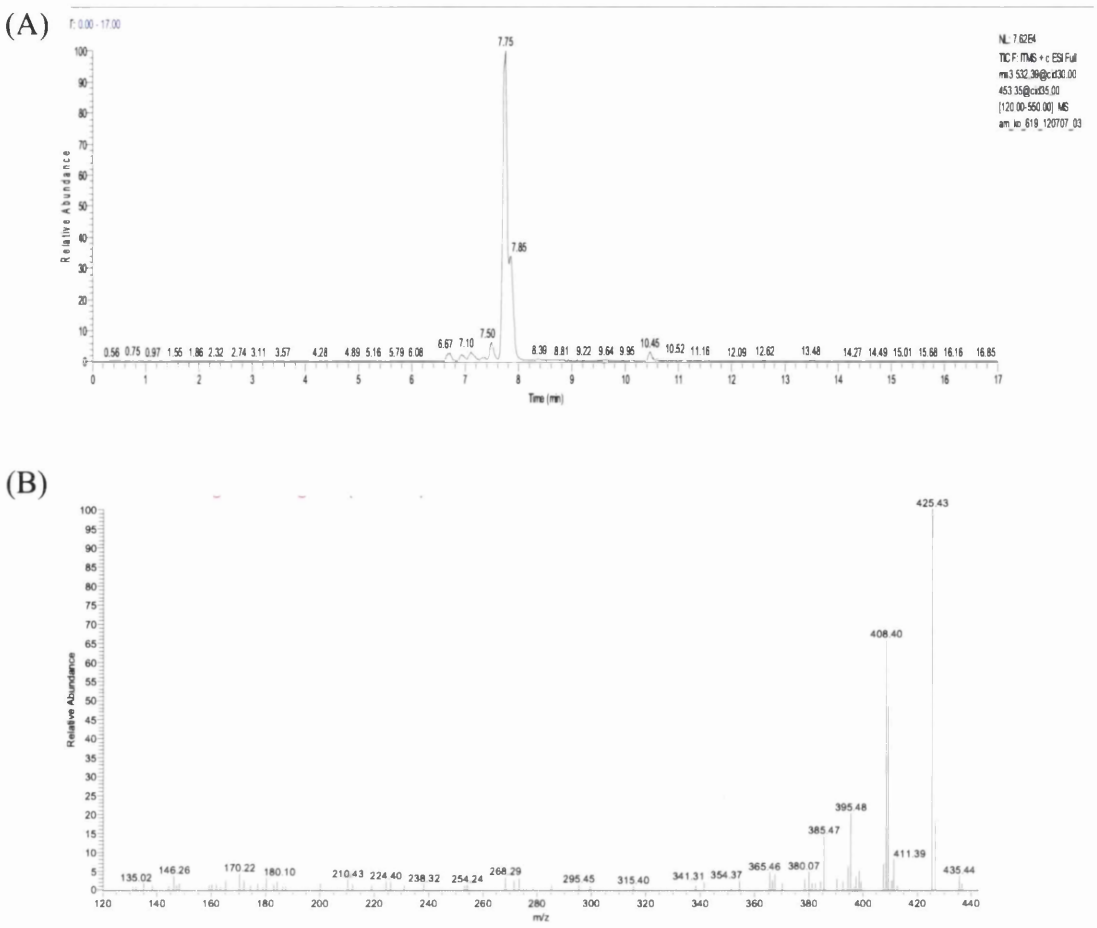

Figure 7.9 Cholest-4-en-3,6-dione in brain of 23 months old Cyp7b1$^{-/-}$ mouse. The spectrum received from the short HPLC gradient.
(A) RIC of m/z 532.3898±5 ppm from Cyp7b1$^{-/-}$ mouse
(B) MS^3 spectrum of peak eluting at 10.45 min identified as GP-tagged cholest-4-en-3,6-dione.

The most abundant monohydroxylated sterol in brain is 24S-hydroxycholesterol [256]. 24S-Hydroxylation provides as an exit route for brain-derived cholesterol in a reaction catalysed by the brain-specific enzyme Cyp46a1. GP-modified 24S-hydroxycholesterol has *m/z* ratio 534.4054 and in our LC method *syn-* and *anti-* isomers elute separately at RT 7.48 min and 7.79 min. RIC and MS^n spectra are shown in Figure 7.10.

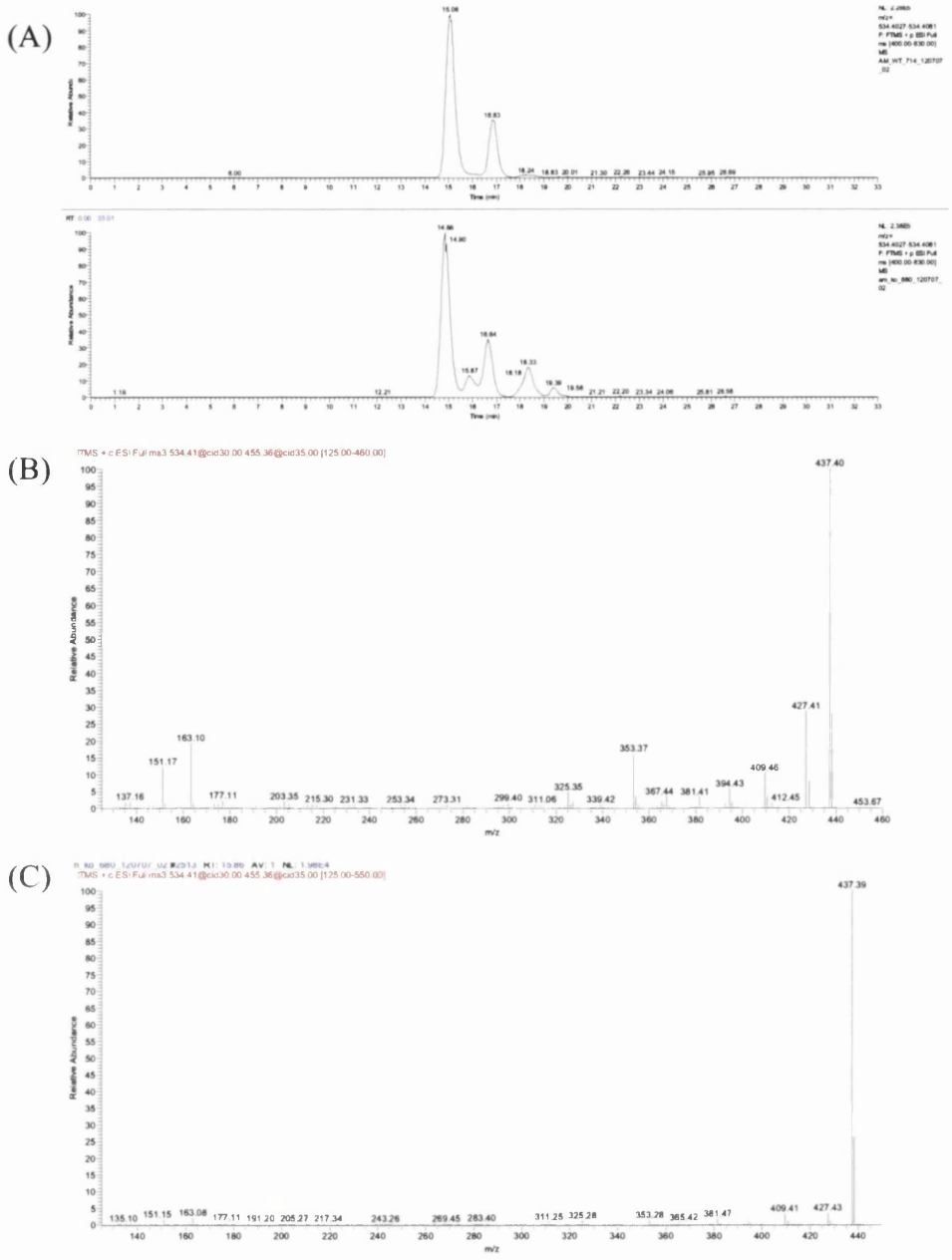

Figure 7.10 24S-Hydroxycholesterol in brain of Cyp7b1$^{+/+}$ and Cyp7b1$^{-/-}$ 23months old mice. The spectrum recorded using an extended HPLC gradient, described in detail in Chapter 3.
(A) RIC of m/z 534.4054±5 ppm of Cyp7b1$^{+/+}$ and Cyp7b1$^{-/-}$ 23 months old mice.
(B) MS^3 spectrum of peak eluting at 14.86 min identified as GP-tagged 24S-hydroxycholesterol.
(C) MS^3 spectrum of peak eluting at 15.87 min identified as GP-tagged 25-hydroxycholesterol

The total concentration of 24S-hydroxycholesterol in wild type 13 months old mice was determined to be 16.8211±2.5529 ng/mg and in knockout mice at 18.2565±4.2880 ng/mg, in 23 months old animals the levels were 25.9581±3.0040 and 25.3367±1.4027, respectively. There was no statistical difference in the amount of 24S-hydroxycholesterol between the wild

type and knockout mice which suggests that Cyp7b1 is not involved in the metabolism of 24S-hydroxylated cholesterol. On the contrary, the deletion of Cyp7b1 caused a substantial accumulation of both 25- and 26-hydroxycholesterol, as also reported by Li-Hawkins [103] for other tissues. In our work both oxysterols were quantified using chromatograms developed in the long gradient LC analysis, where these compounds elutes at RT 15.87 min and 18.33 min, respectively. 25-Hydroxycholesterol is a catalytic product of the enzyme cholesterol 25-hydroxylase, however it can be also generated by Cyp3a [26], Cyp27a1 [182, 257] and Cyp46a1 [29]. While in wild type animals 25-hydroxycholesterol was not detected, in the knockout animals this compound was easily integrated and quantified as 0.8892±0.1422 ng/mg in 13 months old and 2.0906±0.4461 ng/mg in 23 months old mice (Figure 7.10). 25-Hydroxycholesterol is subject to 7α-hydroxylation catalysed by Cyp7b1; therefore we also measured the level of its products. 7α,25-Dihydroxycholesterol in the knockout mice had markedly reduced level (0.0009±0.0001 ng/mg 0.0131±0.0026 ng/mg in 13 and 23-month old mice, respectively) compared to the wild type, 0.0114±0.0050 ng/mg 0.0197±0.0037 ng/mg.

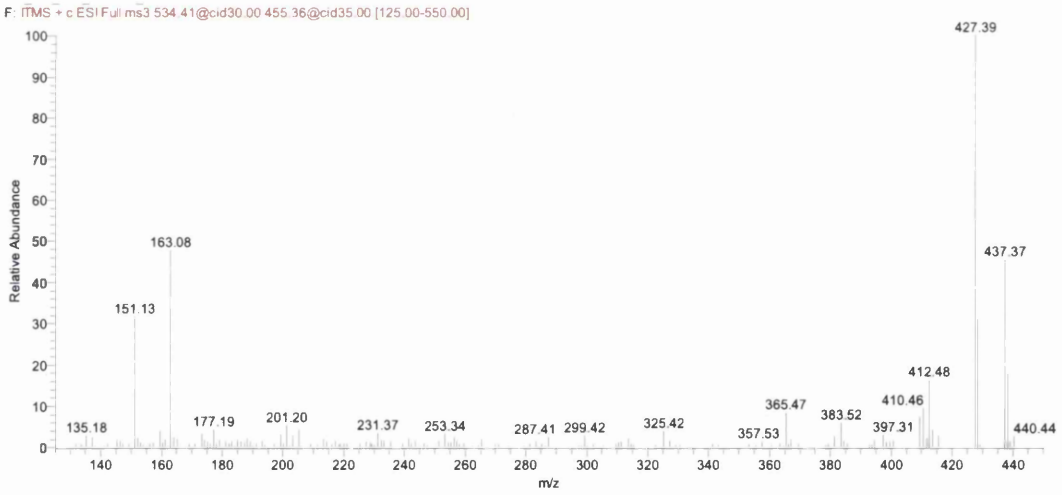

Figure 7.11 26-Hydroxycholesterol in brain of Cyp7b1$^{-/-}$ 23months old mouse. MS^3 spectrum of peak eluting at 18.33 min identified as GP-tagged 25-hydroxycholesterol. The spectrum recorded for a long HPLC gradient.

We also quantified the product of 7α-hydroxylation of 27-hydroxycholesterol. Surprisingly, the amounts of 7α,27-dihydroxycholesterol in the wild type and knockout mice did not show a statistical difference. In the wild type mice these were 0.0206±0.0105 ng/mg and 0.0339±0.0099 ng/mg in 13 and 23 month-old mice, while in its knockout counterparts were 0.0124±0.0024 ng/mg and 0.0451±0.0056 ng/mg.

A variant of the acidic pathway of bile acid biosynthesis is initiated by 27-hydroxylation of cholesterol followed by 27-carbonylation and ultimately carboxylation all catalysed by Cyp27a1, this is followed by 7α-hydroxylation by Cyp7b1. In the wild type animals the levels of 27-hydroxycholesterol are relatively low and were established as 0.2766±0.1340 ng/mg and 0.2976±0.1204 ng/mg in 13 and 23 month-old animals, while in the knockouts the amounts were increased roughly 15-fold (3.0686±0.8612 ng/mg and 3.7181±0.3911 ng/mg, respectively). The MS3 spectrum from Cyp7b1-/- animal is presented in

Figure 7.11. 27-Hydroxycholesterol is a substrate for 7α-hydroxylation catalysed by Cyp7b1 [245, 251, 258] and in mice the deletion of Cyp7b1 causes a major accumulation of 27-hydroxycholesterol.

Carboxylation of cholesterol at C-27 position yields 3β-hydroxycholest-5-enoic acid, which upon GP derivatisation produces an ion of *m/z* 548.3847 (Figure 7.12). In the "acidic" pathway 3β-hydroxycholest-5-enoic acid is further hydroxylated at the 7α position by Cyp7b1, thus dysfunction of this enzyme leads to an accumulation of its substrate. In the wild type mice the concentration of this compound was low (0.0089±0.0023 ng/mg in 13 month old and 0.0145±0.0047 ng/mg in 23 month old) while in the knockouts these were 10 to 13-fold increased (0.1175±0.0250 ng/mg in 13 month old and 0.1509±0.0081 ng/mg in 23 month old).

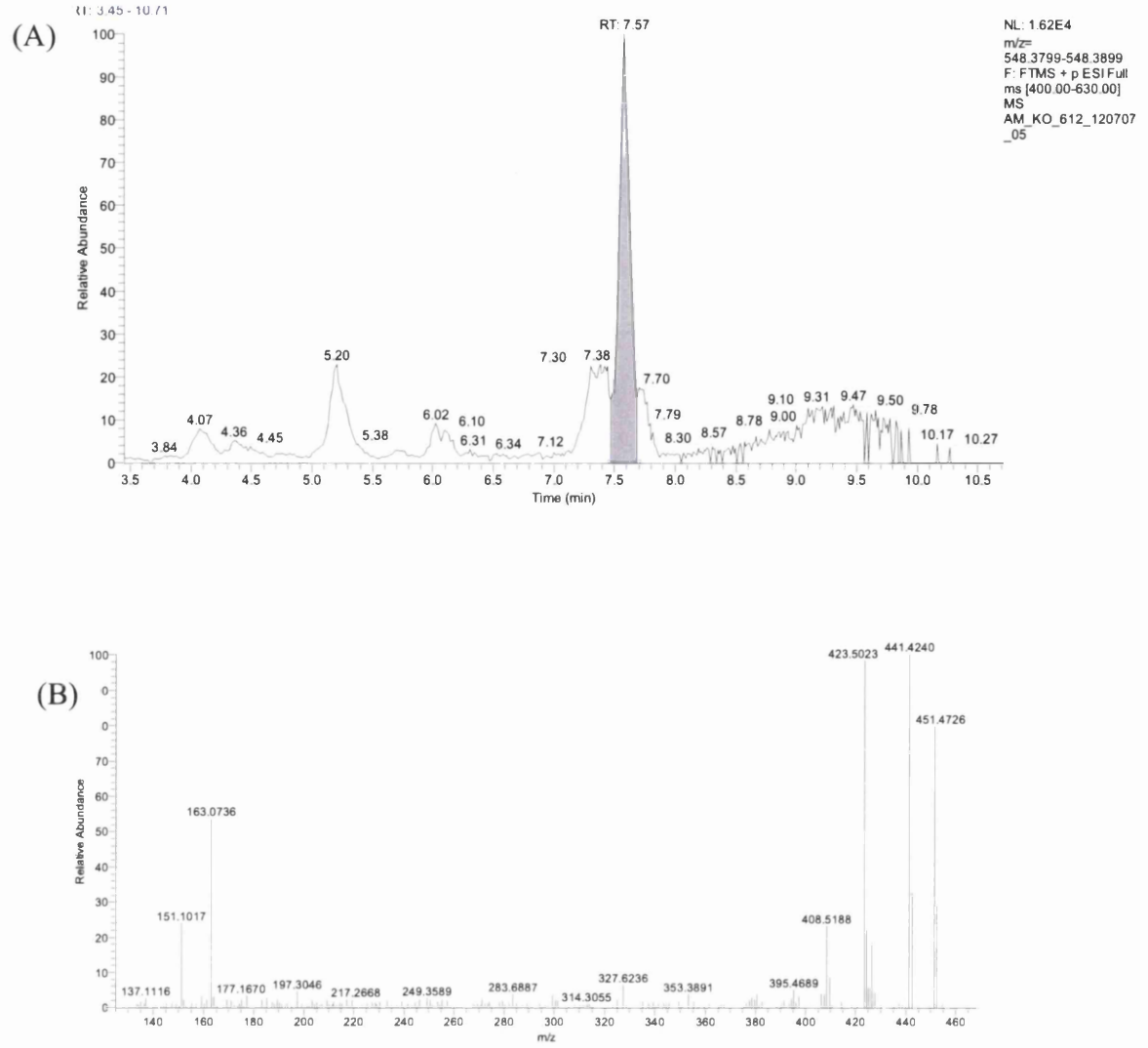

Figure 7.12 3β-Hydroxycholest-5-enoic acid in brain of Cyp7b1$^{-/-}$ and Cyp7b1$^{+/+}$ 23months old mouse. The spectrum recorded for a SHORT HPLC gradient.
(A) RIC of m/z 548.3849±5 ppm of Cyp7b1$^{-/-}$ and Cyp7b1$^{+/+}$ mouse.
(B) MS^3 spectrum of peak eluting at 7.58 min identified as GP-tagged 3β-Hydroxycholest-5-enoic acid

24R-Hydroxycholesterol is a diastereoisomer of 24S-hydroxycholesterol eluting later than its S isomer. With this long LC gradient method 24R-hydroxycholesterol appears as shoulders to 26-hydroxycholesterol, with retention times 17.72 min and 19.74 min (Figure 7.10), and the MS^3 fragmentation profile resembles that of 24S- isomer (Figure 7.12). The concentration of the 24R-hydroxycholesterol in the wild type and the knockout mice did not differ significantly in both age groups (13 months: WT 0.1995±0.0890 ug/g and KO 0.1356±0.0222 ng/mg 23 months: WT 0.3020±0.0306 ug/g and KO 0.3590±0.0660 ug/g).

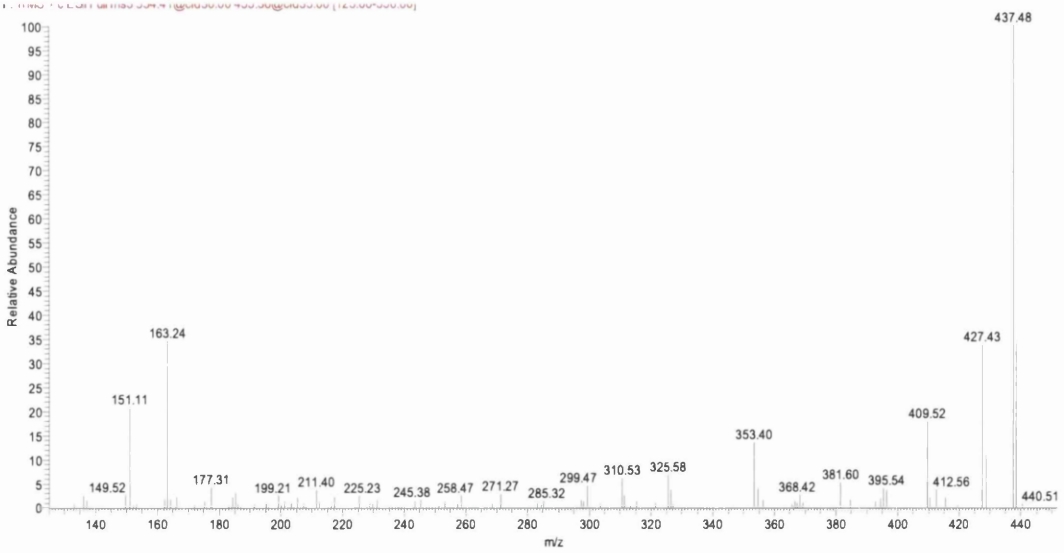

Figure 7.13 24R-Hydroxyocholesterol in brain of Cyp7b1$^{+/+}$ 23months old mouse. MS^3 spectrum of peak eluting on the shoulder of a dominating peak at 17.72 min) identified as GP-tagged 24R-hydroxycholesterol. The spectrum recorded for a long HPLC gradient.

The late eluting compounds on the in the chromatogram of *m/z* 534.4054 are products of cholesterol ring hydroxylations: 7α, 7β- and 6β-hydroxycholesterol. The amounts of these compounds in 13-month old group do not differ between Cyp7b1 deficient and wild type mice, for elder group there is a marked increase in the levels of all three compounds in the Cyp7b1-/- animals (Table 7.1). 7α-Hydroxycholesterol is the first intermediate in the "classical" bile acid biosynthesis pathway, where is synthesised by Cyp7a1, however it can be also a product of cholesterol autoxidation. The concentration of this compound in the mature 23 month wild type was established as 0.0095±0.0046 ng/mg while in the knockouts this was 0.0192±0.0035 ng/mg. This result is consistent with Li-Hawkins et all (44) who reported a 30-40% increase in the level of Cyp7a1 protein in Cyp 7b1$^{-/-}$ mouse liver. This pattern was not observed in younger animals, however this may be due to insufficient accumulation of metabolites.

The origin of 6β- and 7β-hydroxycholesterol is not clear, they are mainly considered as a cholesterol autoxidation products. Both compounds are significantly more concentrated in 23 months old knockouts.

7.3 Discussion

In humans dysfunction of CYP7B1 is implicated in two different disorders: spastic paraplegia type 5 and lethal neonatal liver disease [221], [259]. The mechanisms behind the development of two separate syndromes arising from the mutations in the same gene remain unknown.

In this study we analysed sterol content of Cyp7b1 deficient mice. Although the absence of this enzyme in mice does not have the deleterious effect observed in humans [103], it still provide an insight into metabolic pathways affected by the absence of Cyp7b1 the analysis of oxysterols and sterols form Cyp7b1-/- brain allowed to target the putative substrates of this enzyme. Cyp7b1 is expressed in the brain tissue brain oxysterol hydroxylase [220, 221] well characterised as 7α-hydroxylase for 25- and 26-hydroxycholesterols. The current study confirmed this activity of Cyp7b1 by showing a major accumulation of these two oxysterols. The Cyp7b1-/- mice had also an elevated level of cholesterol biosynthesis by-product: 24S,25-epoxycholesterol. In the light of reduced levels of cholesterol precursors, the increased level of 24S,25-epoxycholesterol suggests that this oxysterol can be metabolised by Cyp7b1 under normal physiological conditions. In the light of neurodegenerative disorder spastic paraplegia type 5 arising form mutation in CYP7B1, this finding is particularly interesting. 24S,25-Epoxycholesterol is important for neuronal development and disruption of its metabolism may be implicated in the neuronal impairment.

Analysis of hydroxylated desmosterols identified two compounds, namely (24Z),26-hydroxydesmosterol and (24E),26-hydroxydesmosterol. Biological origins of these compounds are not defined, however it has been reported that human recombinant of CYP27A1 used desmosterol as a substrate [191]. Increased level of (24Z),26- and (24E),26-hydroxydesmosterols in mutated mice points at possible mechanism of metabolism of this oxysterols by the catalytical activity of Cyp7b1. The biological activity of these sterols remains to be assessed. Neither of hydroxydesmosterols is a ligand to Liver X Receptor α or β, as opposed to desmosterol – a potent activator of LXRs [119].

Chapter 8

8 Macrophages

8.1 Introduction

25-Hydroxycholesterol was initially considered as a product of cholesterol autoxidation generated during sample processing [260, 261], however later studies reported the enzymatic origin of 25-hydroxycholesterol, catalysed by an enzyme cholesterol 25-hydroxylase [8]. The role of 25-hydroxycholesterol in cholesterol homeostasis emerged for the first time in 1975. The work of Kandutsch and others [262, 263] showed that 25-hydroxycholesterol, among other oxygenated derivatives of cholesterol, can suppress activity of the mevalonate pathway. Oxysterols reduced the activity of HMG CoA reductase - the rate-limiting enzyme in cholesterol biosynthesis pathway. Since then numerous studies characterised 25-hydroxycholesterol as a potent regulatory agent capable to moderate many aspects of cholesterol metabolism [104, 264, 265].

Cholesterol 25-hydroxylase is a microsomal glycoprotein [8], which does not belong to the cytochrom P450 family of cholesterol hydroxylases. It is detected across the whole body [8], however, challenge with TLR ligands such as LPS selectively induces the gene in the heart, brain, muscle, kidney, lung and liver [130].

Inhibition of the mevalonate pathway is through the regulatory protein INSIG (insulin induced gene), which upon binding to 25-hydroxycholesterol binds to SCAP (SREBP cleavage-activating protein) and prevents SREBP (sterol regulatory element binding protein) being transported to the Golgi for processing to its active form which regulates cholesterol biosynthesis [68]. Moreover, this oxysterol is also a potent ligand of LXR, which is involved in cholesterol metabolism and cellular trafficking [51, 209, 210].

The last five years have brought important findings regarding the role of 25-hydroxycholesterol in immunity. Microarray data showed upregulation of the cholesterol 25-hydroxylase gene upon treatment with LPS in vitro, moreover the level of 25-hydroxycholesterol increased in blood of human volunteers who received an injection of LPS [129]. In 2010 Park et al showed that the induction of cholesterol 25-hydroxylase is also possible by type I interferons and that upregulation involved the STAT1 signalling pathway [266].

25-Hydroxycholesterol can by further hydroxylated by Cyp7b1 forming 7α,25-dihydroxycholesterol. In 2011 two groups reported the role of this oxysterol in directing B cells required for humoral response. 7α,25-Dihydroxycholesterol has been defined as a

ligand for a chemotactic receptor EBI2, directing B cells for the maturation in lymphoid tissue [132, 137, 267].

In the following study we investigated the impact of interferon β (IFNβ), interferon γ (IFNγ) and murine cytomegalovirus (mCMV) on the synthesis of 25-hydroxycholesterol in bone marrow derived murine macrophages (BMDM).

8.2 Results

Bone derived murine macrophages were cultured in full media, and subjected to the following treatments for 12 hours: interferon β, interferon γ, murine cytomegalovirus and control. Interferon challenge was performed at concentration 25 U/ml. Each experiment was performed in triplicate in Edinburgh University and then biological material was shipped to Swansea.

25-Hydroxycholesterol

In the first round of experiments we focused exclusively on 25-hydroxycholesterol and its dependency on interferon or virus treatment. The chromatogram of GP derivatised 25-hydroxycholesterol derived from treated BMDM consists of one peak eluting at 7.59 min and is showed in Figure 8.1, the identity of the compound was confirmed by the MS^3 spectrum presented in Figure 8.2.

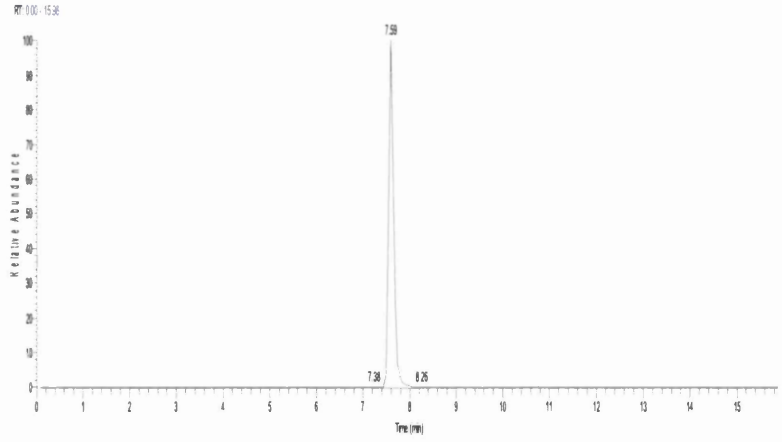

Figure 8.1. RIC of *m/z* 534.4054±5 ppm corresponding to 25-hydroxycholesterol extracted frommurine bone marrow derived macrophages.

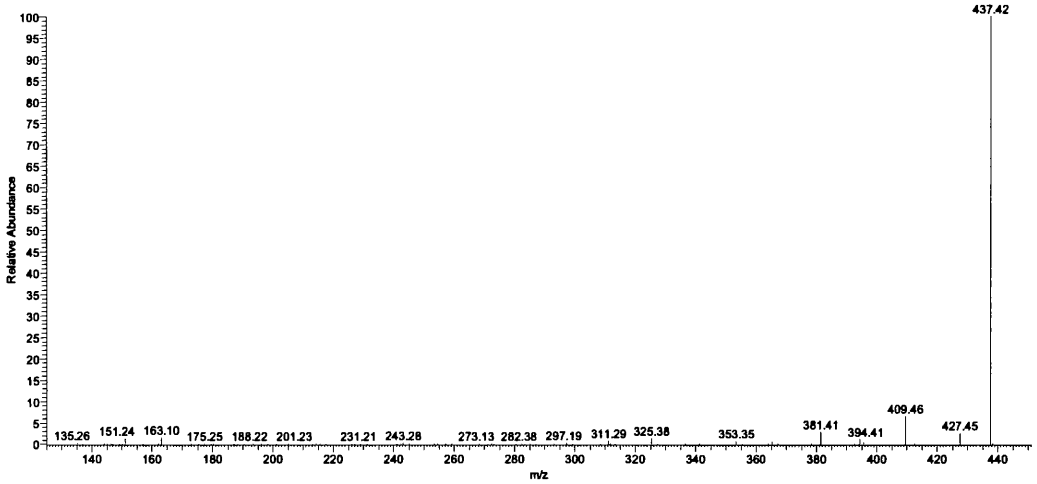

Figure 8.2. MS^3 spectrum of peak eluting at 7.59 min identified as GP-tagged 25-hydroxycholesterol.

In untreated cells the level of 25-hydroxycholesterol was evaluated as 11.20±2.57 ng/plate, in samples treated with interferon γ and mCMV the concentrations were 64.27±0.72 ng/plate and 58.98±9.05 ng/plate which gives 5.5-fold increase. Cells challenged with interferon β also had an elevated concentration of this oxysterol which was quantified as 19.68±1.74 ng/plate (Figure 8.3A). The levels of 25-hydroxycholesterol measured in the cell media (Figure 8.3B) closely reassemble the pattern established in the cells, where the highest increase was found in samples treated with interferon γ and MCMV. In the media of untreated cells the level equals 54.39±1.44 ng/ml while in interferon γ and mCMV these were 195.19±12.71 ng/ml 202.54±2.68 ng/ml, in interferon β treated sample the concentration was only moderately increased to 87.83±6.47 ng/ml. The fold-difference between the untreated cell media and interferon γ or mCMV treated cell media was about 3 fold. The reduced relative increase in the concentration of 25-hydroxycholesterol in media compared to cells can be attributed to the relatively short incubation time, where the cell may require more than 12 hours to excrete the oxysterol to the external matrix. The results are presented in .

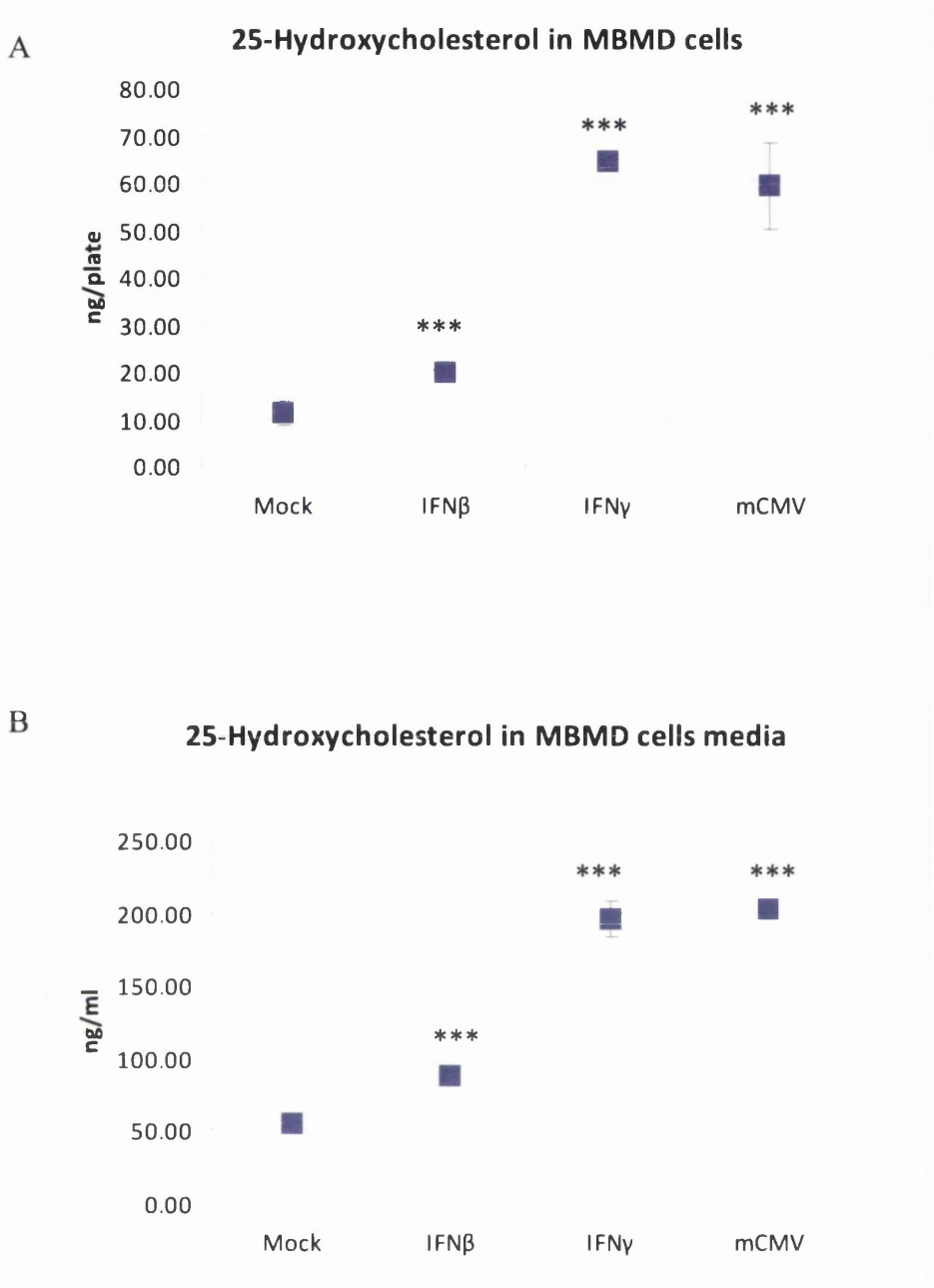

Figure 8.3. Concentrations of 25-hydroxycholesterol extracted from BMDM cells expressed as ng/plate (A) or cell media expressed as ng/ml (B) following mCMV infection, IFNβ (25 U/ml), IFNγ (25 U/ml) stimulation for 12 hours. Error bars show SE for data obtained from 3 independent biological replicates.

To assess the impact of 25-hydroxycholesterol on the mevalonate pathway we measured the concentration of cholesterol and its precursor desmosterol. As 25-hydroxycholesterol is a potent INSIG ligand we expect that an increased level of this oxysterol would adversely affect the synthesis of cholesterol. Surprisingly the concentration of cholesterol is higher in interferon γ and mCMV treated macrophages. The increase in interferon β treated samples is smaller but still statistically significant ($p<0.01$,Figure 8.4). This trend applies only to cholesterol analysed in the cells, in the media the level is steady as cholesterol in present in the bovine serum supplementing the media. The increased concentration of cholesterol may reflect either an import from extracellular matrix or enhanced rate of synthesis. To investigate the origin of the cellular cholesterol we measured the level of its precursor desmosterol. The level of this compound is around 100 times lower than cholesterol therefore the quantification is less robust. We recorded the statistically significant increase in the level of desmosterol in mCMV treated samples (Figure 8.5), which suggest that the viral treatment in this experiment encouraged the synthesis of cholesterol.

Unlike the situation with 25-hydroxycholesterol where there were fold changes between treated and untreated samples, the changes in levels of cholesterol and desmosterol were much less drastic. These changes may be a consequence in small changes in the number of cells per plate.

A

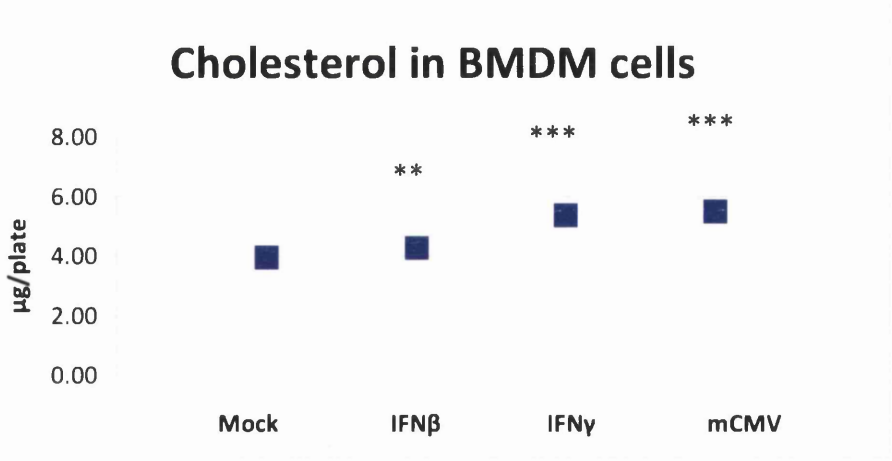

B

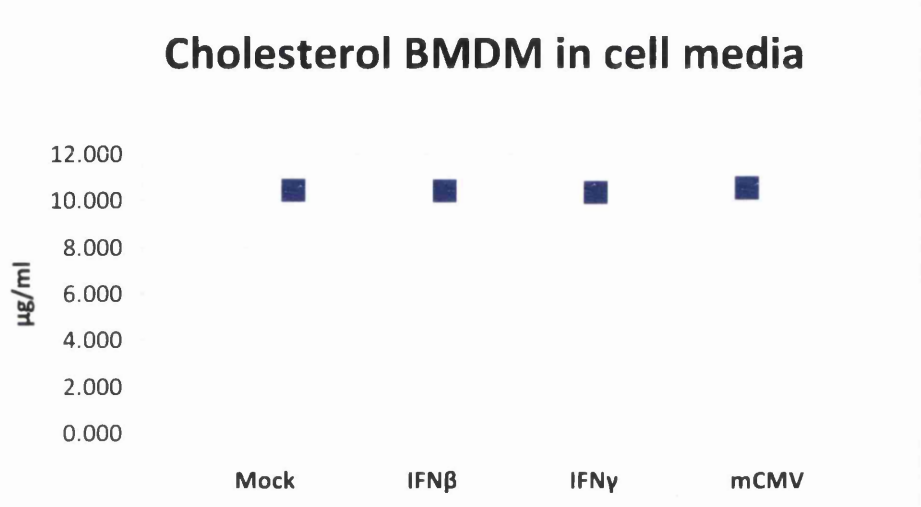

Figure 8.4. Concentrations of cholesterol extracted from BMDM expressed as µg/plate (A) or cell media expressed as µg/ml (B) following IFNβ (25 U/ml), IFNγ (25 U/ml) stimulation and mCMV infection for 12 hours. Data are the mean of 3 biological replicates, error bars represent SD, ***P≤0.001, **p≤0.01

A

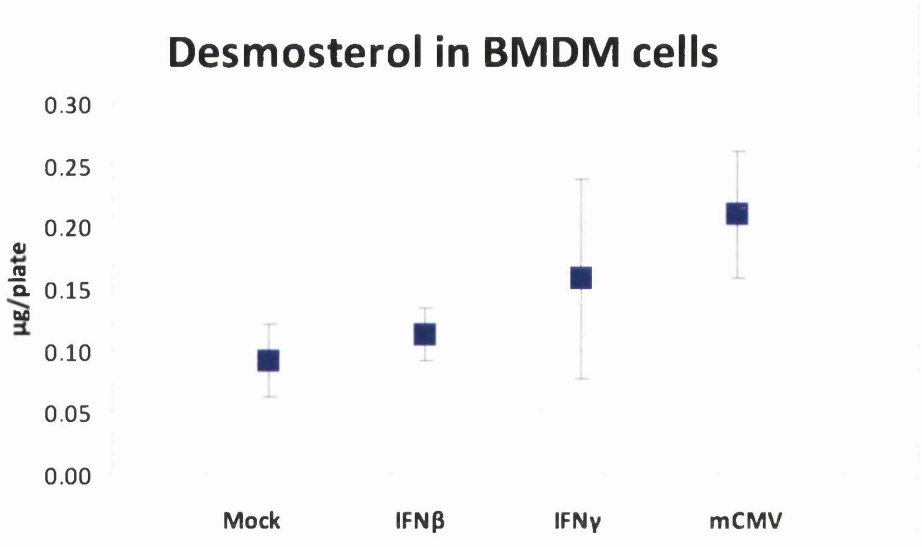

B

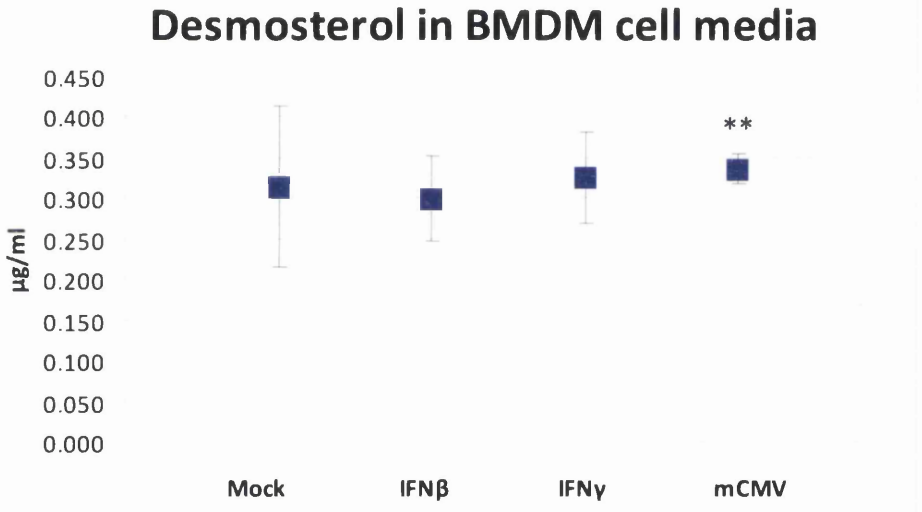

Figure 8.5 Concentrations of desmosterol extracted from BMDM media expressed as µg/plate (A) or cell media expressed as µg/ml (B) following IFNβ (25 U/ml), IFNγ (25 U/ml) stimulation and mCMV infection for 12 hours. Data are the mean of 3 biological replicates, error bars represent SD, **$p \leq 0.01$

Sterol depleted medium

In the following experiments we investigated the time-dependant change in the concentration of sterols produced in response to the interferon or virus stimuli. In this study the macrophages were incubated during the treatments in a sterol-depleted medium to avoid the bias provided by cholesterol and oxysterols present in the medium.

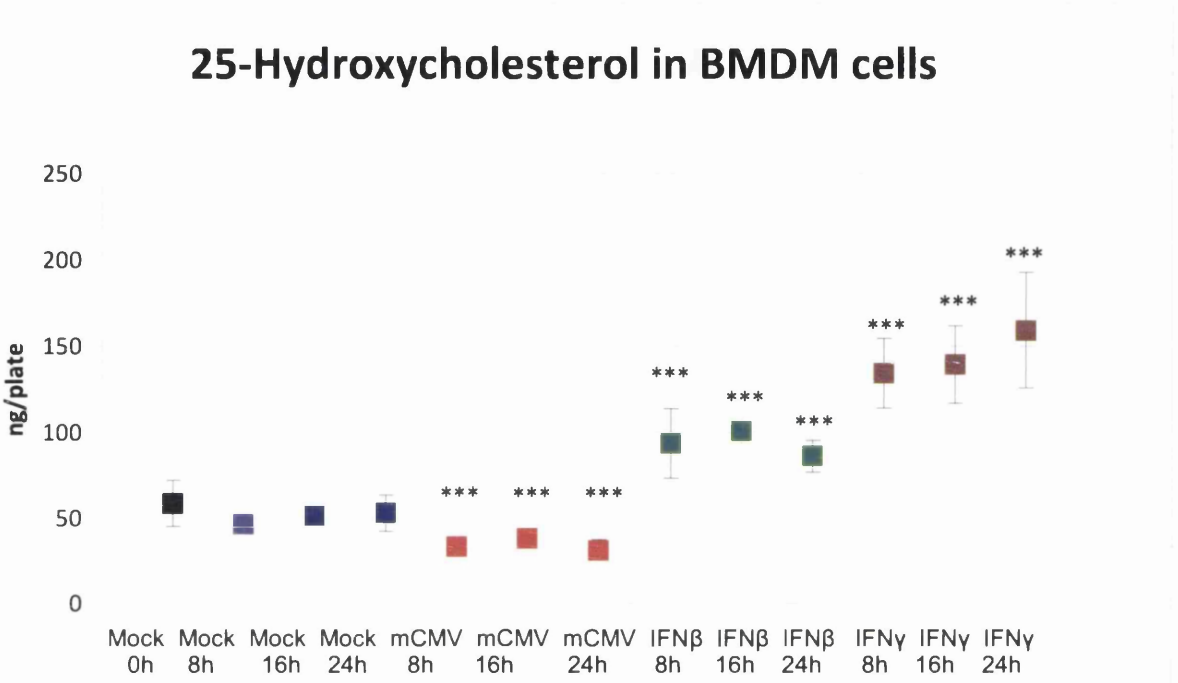

Figure 8.6. Concentrations of intra-cellular 25-hydroxycholesterol expressed as ng/plate in BMDM following MCMV infection, IFNβ (10 U/ml), IFNγ (10 U/ml) stimulation for 8, 16 and 24 hours. Error bars show SE for data obtained from 3 independent biological replicates, *** $p<0.001$.

The increase in the concentration of 25-hydroxycholesterol was triggered by interferon β and interferon γ. Treatment with interferon β increased the concentration 2-fold, while with interferon γ almost 3-fold. The elongated time of incubation did not affect the level of 25-hydroxycholesterol in a statistically significant degree, suggesting that the activation occurs within the first 8 hours of treatment and is maintained for at least another 16 hours (Figure 8.6).

Surprisingly, in this experiment the treatment with MCMV did not alter the concentration of 25-hydroxycholesterol. The study by Haspot et al. [268] points at the depletion of cholesterol as the factor inhibiting viral entry into a host cell, therefore it is feasible that culturing the macrophages in serum free media abolished the antiviral response.

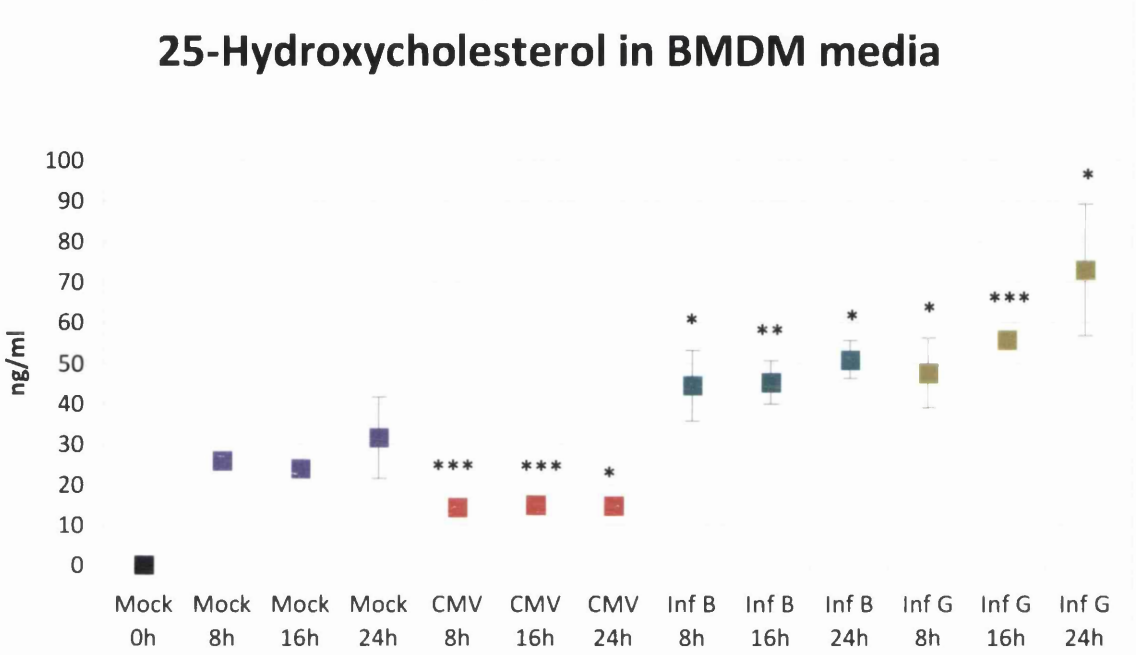

Figure 8.7. Concentrations of 25-hydroxycholesterol extracted from BMDM media expressed as ng/ml following MCMV infection, IFNβ (10 U/ml), IFNγ (10 U/ml) treatment for 8, 16 and 24 hours. Error bars show SE for data obtained from 3 independent biological replicates; * $<0.001 p<0.05$,** $0.01<p<0.01$,*** $p<0.001$.

Even more pronounced trend was observed in the levels of 25-hydroxycholesterol measured in the cell media [Figure 8.7]. The stimulation with mCMV did not increase the concentration of 25-hydroxycholesterol, confirming the results in the cells. The media of the cells treated with interferon β contained on average 2 times more 25-hydroxycholesterol, while in the interferon γ challenged samples the level of this oxysterol rose 3-fold on average. The analysis of the levels at 8, 16 and 24 hours shows a time wise rise in the levels of the oxysterol. An increase of the metabolite is a result of an accumulation of 25-hydroxycholesterol in the cellular media.

Other oxysterols

We also quantified other monohydroxylated derivatives of cholesterol in cells and secreted to the medium: 7β-hydroxycholesterol, 7-ketocholesterol, 7α-hydroxycholesterol and 6-hydroxycholesterol. The levels of these oxysterols do not show a dependence on the applied treatments and are no more than a few of percent of the abundance of 25-hydroxycholesterol.

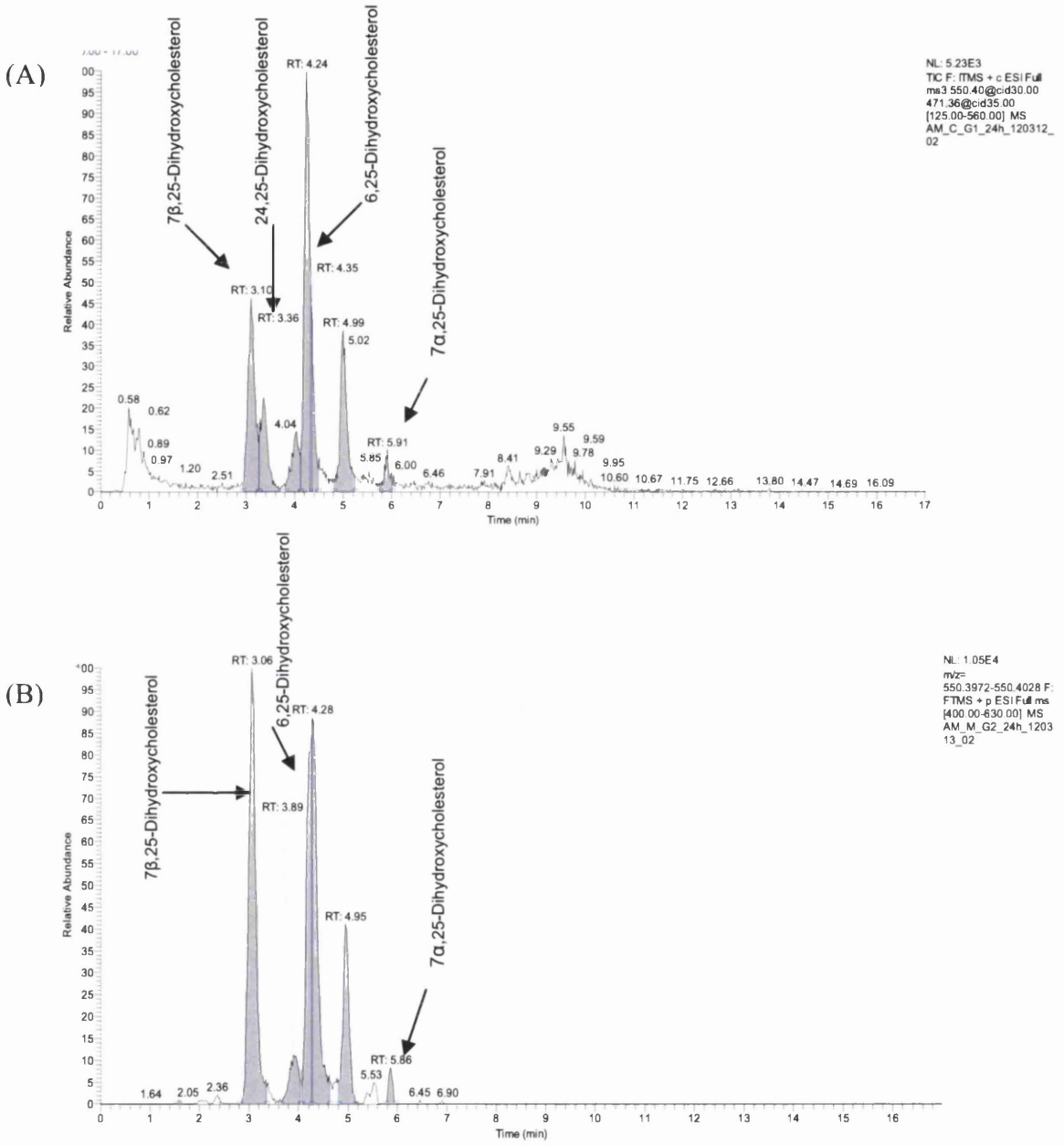

Figure 8.8. Doubly hydroxylated cholesterol derivatives in murine bone marrow derived macrophages. RIC of *m/z* 550.4003±5 ppm obtained from the analysis of from IFNγ treated cells (A) and cell media (B).

Table 8.1. Sterols identified by LC-ESI-MSn in murine bone marrow derived macrophages following SPE and charge-tagging with GP-hydrazine. MCMV, interferon β, interferon γ and control samples (nine replicates) were analysed. The colours indicate the statistical significance of differences between control samples and relevant treatments. (Transparent: $p>0.05$, orange: $0.01<p<0.05$, yellow $0.001<p<0.01$, red: $p<0.001$)

m/z	RT min	Systematic name	Common name	Mean concentration ng/plate ± SD (n = 9)			
				Control	mCMV	IFN B	IFN G
534.4054	7.00	25-Hydroxycholest-4-en-3-one 3-GP	25-hydroxycholesterol	50.19±7.35	34.14±6.04	93.46±13.14	144.45±25.24
534.4054	9.13	7β-Hydroxycholest-4-en-3-one 3-GP	7β-hydroxycholesterol	0.9020±0.3455	0.9942±0.7794	0.8834±0.3785	0.8154±0.2243
534.4054	9.36	3β-Hydroxycholest-4-en-7-one 3-GP	7-ketocholesterol	0.2640±0.1110	0.2888±0.1614	0.2487±0.1123	0.2796±0.1430
534.4054	9.57	7β-Hydroxycholest-4-en-3-one 3-GP	7β-hydroxycholesterol	0.2838±0.1230	0.3032±0.2714	0.2661±0.1416	0.2424±0.0724
534.4054	9.73	7α-Hydroxycholest-4-en-3-one 3-GP	7α-hydroxycholesterol	0.0495±0.0343	0.0568±0.0867	0.0455±0.0398	0.0493±0.0204
534.4054	10.03	6-Hydroxycholest-4-en-3-one 3-GP	6-hydroxycholesterol	0.1106±0.1049	0.1980±0.3296	0.1994±0.1891	0.2109±0.1002
532.3898	6.57	25-Hydroxycholest-4,X-dien-3-one 3-GP (?)	25-hydroxy-X-dehydrocholesterol (?)	0.0769±0.0142	0.0702±0.0156	0.1806±0.0336	0.2894±0.0444
548.3847	4.78	unknown		0.0267±0.0114	0.0210±0.0083	0.0444±0.0134	0.0721±0.0255
548.3847	5.66	unknown		0.0292±0.0163	0.0144±0.0146	0.0553±0.0261	0.0801±0.0299
550.4003	3.10	7β,25-Dihydroxycholest-4-en-3-one 3-GP	7β,25- dihydroxycholesterol (total)	0.5369±0.1611	0.4369±0.1460	1.1933±0.3757	1.9902±0.5096
550.4003	3.36	24,25-Dihydroxycholest-4-en-3-one 3-GP	24,25-dihydroxycholesterol total	0.5462±0.2630	0.5418±0.2525	0.5120±0.2258	0.6175±0.3415
550.4003	3.84	unknown		0.1443±0.0443	0.0906±0.0181	0.0873±0.0377	0.0901±0.0311
550.4003	4.01	unknown		0.2411±0.1050	0.2153±0.0892	0.2096±0.0757	0.2566±0.1224
550.4003	4.08	unknown		1.0423±0.4001	0.7173±0.3106	2.0438±0.8827	3.1399±1.0759
550.4003	4.24	6,25-Dihydroxycholest-4-en-3-one 3-GP (?)	6,25- dihydroxycholesterol (?)	1.3934±0.4565	0.2032±.00954	2.5904±1.0507	3.9206±1.2911
550.4003	4.99	unknown		0.3910±0.1020	0.2796±0.0502	0.6859±0.2679	0.9687±0.3104
550.4003	5.91	7α,25-Dihydroxycholest-4-en-3-one 3-GP	7α,25- dihydroxycholesterol (1st peak)	0.0136±0.0183	0.0133±0.0118	0.0598±0.0824	0.1077±0.0687
550.4003	5.91	7α,25-Dihydroxycholest-4-en-3-one 3-GP	7α,25- dihydroxycholesterol (1st peak) MSMS	0.0306±0.0242	0.0545±0.0227	0.1012±0.0701	0.1660±0.0639
564.3796	5.65	unknown		0.0340±0.0347	0.0163±0.0155	0.0554±0.0231	0.1295±0.0728

Table 8.2. Sterols identified by LC-ESI-MSn in media retained after incubation of murine bone marrow derived macrophages. Compounds were separated with SPE and charge-tagged with GP-hydrazine. MCMV, interferon β, interferon γ and control samples (nine replicates) were analysed. The colours indicate the statistical significance of differences between control samples and relevant treatments. (Transparent: $p>0.05$, orange: $0.01<p<0.05$, yellow $0.001<p<0.01$, red: $p<0.001$)

m/z	RT min	Systematic name	Common name	Mean concentration ng/plate ± SD (n = 9)			
				Control	MCMV	IFN B	IFN G
534.405	7.00	25-Hydroxycholest-4-en-3-one 3-GP	25-hydroxycholesterol	27.16±6.17	14.72±1.14	46.88±6.45	58.82±14.54
534.405	9.13	7β-Hydroxycholest-4-en-3-one 3-GP	7β-hydroxycholesterol	0.2363±0.1820	0.0589±0.0536	0.1238±0.1012	0.1129±0.0911
534.405	9.36	3β-Hydroxycholest-4-en-7-one 3-GP	7-ketocholesterol	0.1311±0.1279	0.0682±.00517	0.0679±0.0720	0.0470±0.0335
534.405	9.57	7β-Hydroxycholest-4-en-3-one 3-GP	7β-hydroxycholesterol	0.0670±0.0582	0.0130±0.0162	0.0254±0.0236	0.0204±0.0211
534.405	9.73	7α-Hydroxycholest-4-en-3-one 3-GP	7α-hydroxycholesterol	0.0115±0.0183	0.0004±0.0007	0.0040±0.0051	0.0055±0.0071
534.405	10.03	6-Hydroxycholest-4-en-3-one 3-GP	6-hydroxycholesterol	0.0744±0.1212	0.0023±0.0061	0.0286±0.0372	0.0255±0.0339
532.389	6.57	25-Hydroxycholest-4,X-dien-3-one 3-GP	25-hydroxy-X-dehydrocholesterol	0.1677±0.0469	0.1473±0.0457	0.5661±0.1475	0.8063±0.2228
548.384	3.64	unknown		0.2099±0.0724	0.1548±0.0824	0.2832±0.1131	0.1903±0.0931
548.384	7.07	unknown		0.3011±0.0984	0.2296±0.0578	0.2461±0.0702	0.2256±0.0635
550.400	3.06	7β,25-Dihydroxycholest-4-en-3-one 3-GP	7β,25-dihydroxycholesterol (1st peak)	0.6309±0.2845	0.5085±0.2537	2.4763±0.8468	3.4944±1.3363
550.400	3.89	unknown		0.4118±0.1778	0.1802±0.0562	0.4085±0.1722	0.3606±0.1451
550.400	4.23	6,25-Dihydroxycholest-4-en-3-one 3-GP (?)	6,25- dihydroxycholesterol	0.3655±0.1143	0.2537±0.0712	0.9931±0.3843	1.3811±0.5215
550.400	4.28	unknown		1.1427±0.4753	0.5543±0.2137	1.8214±0.3521	2.0414±0.6550
550.400	4.95	unknown		0.4118±0.1058	0.2645±0.0852	0.9370±0.2632	1.0845±0.4186
550.400	5.86	7α,25-Dihydroxycholest-4-en-3-one 3-GP	7α,25-dihydroxycholesterol (1st peak)	0.0131±0.0112	0.0055±0.0067	0.1214±0.0674	0.1848±0.0819
564.379	1.47	unknown		0.3302±0.1030	0.2995±0.0981	0.3281±0.0614	0.3245±0.0922
564.379	3.41	unknown		1.7286±1.0502	1.0002±0.6268	0.5670±0.4730	0.4004±0.2645
564.379	4.43	unknown		0.4224±0.2738	0.2650±0.1544	0.1985±0.1473	0.1595±0.0900
564.379	4.62	unknown		0.8585±0.6871	0.4532±0.3117	0.2564±0.2227	0.1698±0.1050
564.379	5.19	unknown		3.4160±1.6362	2.2246±0.6809	1.9160±1.2514	1.1685±0.5764
564.379	5.24	unknown		3.4088±1.6316	2.2273±0.6754	1.9106±1.2468	1.1652±0.5738
564.379	6.01	7α-hydroxy-3-oxo-cholest-5-en-27-oic acid 3-GP	3β,7α-dihydroxycholest-5-en-27-oic acid	1.3163±0.7432	0.7865±0.2680	0.6576±0.4499	0.3883±0.1655
566.395	1.22	unknown		1.6058±0.5824	1.1609±0.4243	1.7624±0.7267	1.6845±0.7790
566.395	1.76	unknown		0.6225±0.2803	0.4176±0.2204	0.5883±0.3802	0.5679±0.2895
566.395	2.20	unknown		0.8047±0.3544	0.7509±0.3701	1.1391±0.4390	0.8938±0.4070
566.395	3.28	unknown		0.1616±0.0739	0.1500±0.0761	0.2478±0.0984	0.1704±0.0728

We analysed the products of a double hydroxylation of cholesterol, which, following the derivatisation, produce a molecular ion of *m/z* 550.4003. The RICs of *m/z* 550.4003 obtained from IFNγ treated macrophages and relevant media are shown in Figure 8.8B and Figure 8.8B. The first eluting compound, with retention time 3.10 min was identified as 7β,25-dihydroxycholesterol, the MS^3 spectrum is presented in

Figure 8.9. An authentic standard of 7β,25-dihydroxycholesterol elutes as a doublet, with the second peak eluting about 1.2 min later than the first one. In our analysis we identified the second peak of 7β,25-dihydroxycholesterol as a shoulder to a dominating peak and eluting at 4.35 min (Figure 8.8a). The quantification of 7β,25-dihydroxycholesterol was based on the combined area of its two peaks which showed a significantly increased concentration in interferon treated samples. As there was no statistical difference between the different time points, the data presented below were averaged concentrations calculated for replicates in each of 8, 16 and 24 hour treatments. The average level in the control samples was assessed as 0.5369±0.1611 ng/plate and in MCMV treated 0.4369±0.1460 ng/plate. In interferon treated macrophages the level of 7β,25-dihydroxycholesterol was significantly elevated: in interferon β challenged samples the concentration was 1.1933±0.3757ng/plate and in interferon γ 1.9902±0.5096ng/plate (Table 8.1).

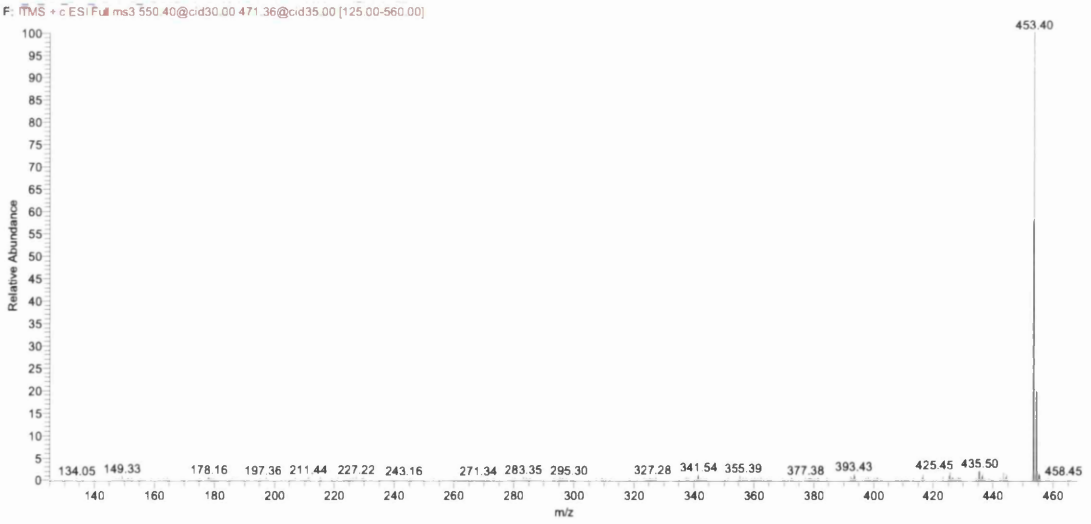

Figure 8.9. MS^3 spectrum of peak eluting at 3.10 min identified as GP-tagged 7β,25-dihydroxycholesterol from IFNγ treated cells.

In the media retained after incubation of the macrophages a similar trend was observed, however, it was only possible to integrate the first peak belonging to 7β,25-dihydroxycholesterol, as the second part of the doublet was dominated by unknown eluent. Due to this underestimation of the peak area, the result can be only used as indication of the fold difference between control and treated samples, rather than an absolute quantification. The level of 7β,25-dihydroxycholesterol in media retained after incubation of control samples and MCMV treated cells was estimated 0.6309±0.2845 ng/ml and 0.5085±0.2537 ng/ml, while in samples where the interferon was applied, the levels were markedly increased 4- and 5-fold for interferons β and γ, respectively.

The pattern of changes in the levels of 7β,25-dihydroxycholesterol closely follows those of 25-hydroxycholesterol. It is established that 7β-hydroxylation of cholesterol occurs in an autoxidation process [185], it is likely that a similar transformation applies to 25-hydroxycholesterol, resulting in generation of 7β,25-dihydroxycholesterol.

25-Hydroxycholesterol can be also hydroxylated at the 7α-position by the catalytic action of ER enzyme oxysterol 7α-hydroxylase, Cyp7b1. By the comparison of the cell extract RIC of *m/z* 550.4003 with the authentic standard we identified the peak eluting at RT 5.91 min (Figure 8.8A) as 7α,25-dihydroxycholesterol, however for the evaluation of the levels we used MS^3 TIC due to high baseline interferences in the mass RIC, the MS^3 spectrum is shown in Figure 8.10. The levels of this oxysterol were similar in control and MCMV treated macrophages (0.0306±0.0242 ng/plate and 0.0545±0.0227 ng/plate, Table 4), while the treatment of the macrophages with interferon β and γ resulted in an increase in these levels 3- and 5-fold (0.1012±0.0701 ng/plate and 0.1660±0.0639ng/plate) respectively. 7α,25-Dihydroxycholesterol was also identified in the cell media separated from the macrophages (Table 8.2). In the untreated and MCMV treated cell media the levels were 0.0131±0.0112 ng/ml and 0.0055±0.0067 ng/ml, while in the interferon β and γ treated macrophages media these were increased to 0.1214±0.0674 ng/ml and 0.1848±0.0819 ng/ml. It is worth noting that both hydroxylations: at position C-7 and C-25 were reported as an autoxidation process .

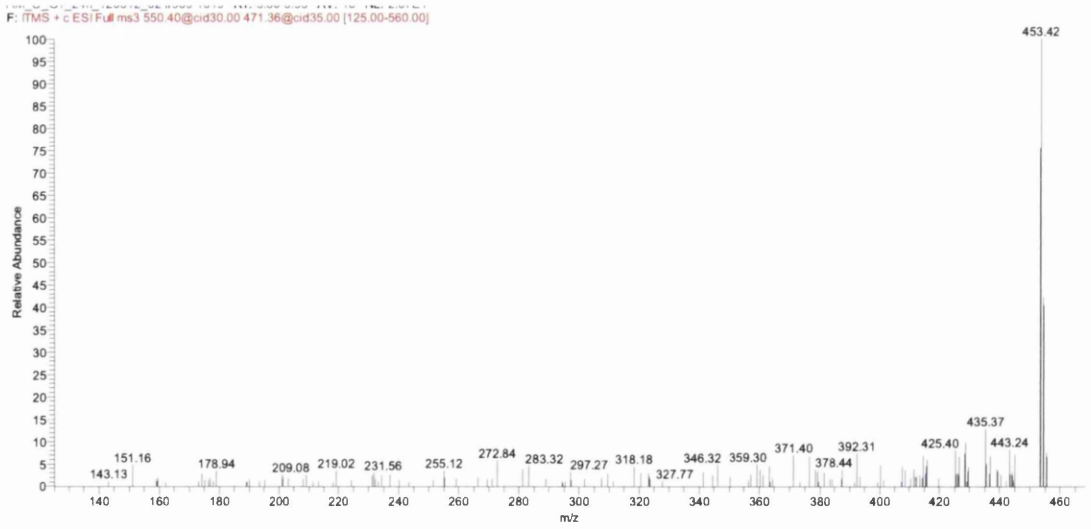

Figure 8.10. MS3 spectrum of peak eluting at 5.91 min identified as GP-tagged 7α,25-dihydroxycholesterol from IFNγ treated cells.

Further analysis of the cell extract chromatogram revealed the peak eluting at RT 3.36 min, which we identified as 24S,25-dihydroxycholesterol (MS^3 spectrum presented in Figure 8.11). This oxysterol can be produced as a result of hydrolysis of 24S,25-epoxycholesterol, however this process is usually accompanied by other products generated during the derivatisation reaction such as 24-ketocholesterol and 24-hydroxy,25-methoxy (or 24-methoxy,25-hydroxy)cholesterol. As we could not identify these products, it is viable that this doubly hydroxylated cholesterol is an authentic product present in the cells. The standard of 24S,25-dihydroxycholesterol is eluted as a doublet, in our sample the second peak is masked by a closely eluting large peak of an unidentified compound, causing integration of the second peak unreliable. The level of 24S,25-dihydroxycholesterol (only the first peak used for quantification) was steady across all the treatments: in control and MCMV treated samples was evaluated as 0.5462±0.2630 ng/plate and 0.5418±0.2525 ng/plate, and in interferon β and γ treated samples these were 0.5120±0.2258 ng/plate and 0.6175±0.3415 ng/plate, respectively. In the cell media we could not integrate the peak belonging to 24S,25-dihydroxycholesterol due to the presence of the dominating peak of 7β,25-dihydroxycholesterol.

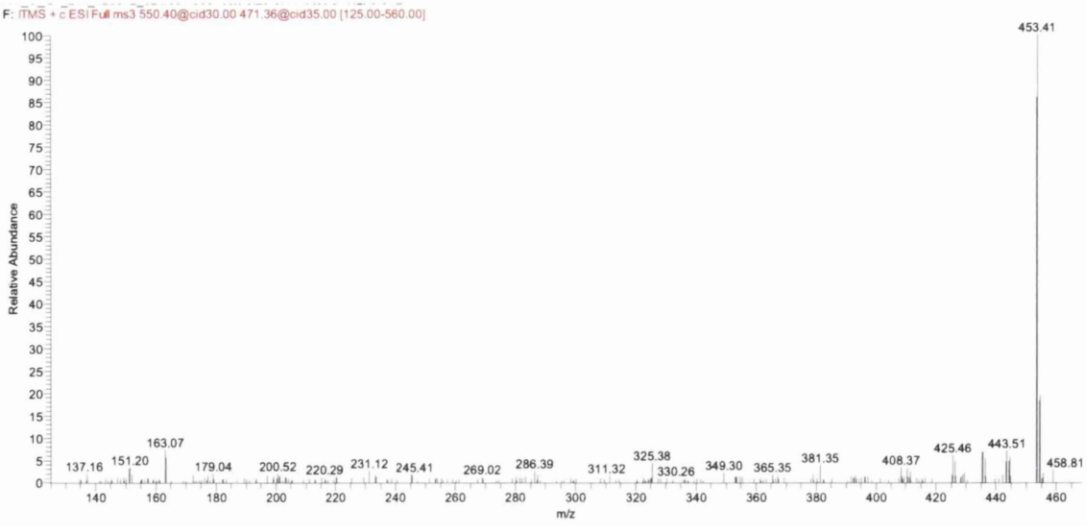

Figure 8.11. MS3 spectrum of peak eluting at 3.36 min identified as GP-tagged 24S,25-dihydroxycholesterol from IFNγ treated cells.

The dominating peak of RIC 550.4003 appears in the chromatogram of cells is at 4.24 min. The analysis of the MS^3 spectrum (Figure 12) showed a number of similar fragments to those observed in the spectrum of 6,24S-hydroxycholesterol [148]. The main difference between the spectra is the ratio between fragment ions *m/z* 453 (M-79-H_2O) and *m/z* 443 (M-79-CO). This is possibly because hydroxylation at the 25 instead of 24S position, as a hydroxyl group at 25 carbon atom tends to produce a more prominent ion 453 in the MS^3 spectra of GP-derivatised dihydroxycholesterols. The quantification of this substance showed a differences between untreated or MCMV infected cells and interferon activated macrophages. In control samples the concentration was assessed as 1.3934±0.4565 ng/plate, in MCMV these were significantly decreased to 0.2032±.00954 ng/plate. In interferon β and γ treated samples the level were 2.5904±1.0507 ng/plate and 3.9206±1.2911 ng/plate, respectively. In the cell media these levels showed a similar dependency with the concentrations in untreated and MCMV treated macrophage media evaluated as 0.3025 ng/ml and 0.2278 ng/ml in controls and MCMV treated samples, while the incubation with the interferons lead to an increase in the levels: 0.7468ng/ml and 1.1882 ng/ml in interferon β and γ, respectively.

The changes in the levels of this analyte were similar to those of 25-hydroxycholesterol, suggesting that this compound either the product of autoxidation of 25-hydroxycholesterol or unknown product of metabolism, supporting the hypothesis that this is 6,25-dihydroxycholesterol. It worth mentioning that 6β-

hydroxylation of bile acid precursors is catalysed by Cyp3a11. This enzyme hydroxylases C-6 position of litocholic and taurochenodeoxycholic acids, transforming it into less toxic bile acids. It is not known whether this enzyme is capable of 6-hydroxylation of 25-hydroxycholesterol molecule.

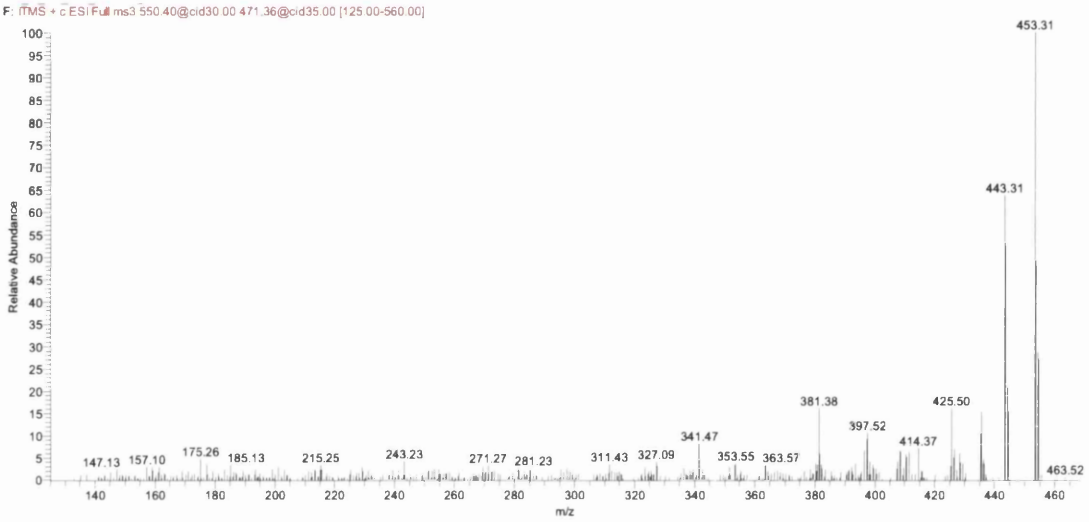

Figure 8.12. MS^3 spectrum of peak eluting at 4.24 min identified as GP-tagged 6,25-hydroxycholesterol from IFNγ treated cells.

The peak eluting at 4.98 min was not identified, however the quantification of this compound showed the increased level in the interferon treated macrophages. In untreated and MCMV incubated macrophages the levels were 0.3910 ng/plate and 0.2796 ng/plate, in interferon β and γ treated cell the concentrations were 0.6859 ng/plate and 0.9687 ng/plate, respectively.

The levels evaluated in the media showed the same pattern with the concentrations: 0.3620 ng/ml and 0.2313 ng/ml in control and MCMV treated cells, while in interferon β and γ incubations the levels were 0.7749 ng/ml and 0.9421 ng/ml, respectively.

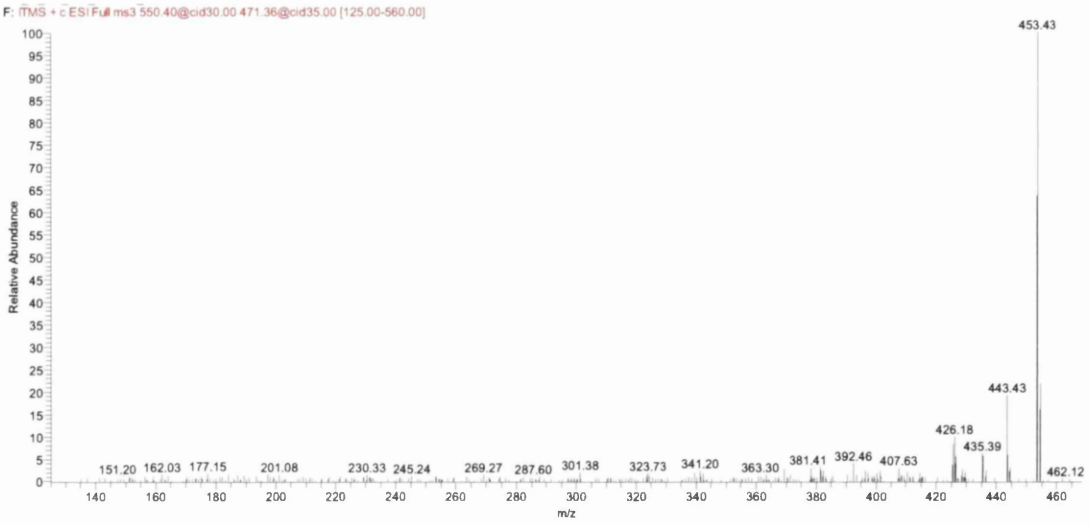

Figure 8.13. MS^3 spectrum of an unknown compound of *m/z* 550.4003 eluting at 4.98 min from IFNγ treated macrophages.

We also analysed the RIC of *m/z* value 532.3898, presenting a single dominating peak eluting at 6.63 min (Figure 14). Although MS^3 spectrum does not resemble any known standard (Figure 15), we noticed that the same compound appearing during the analysis of synthetic standards of 7α,25-dihydroxycholesterol and 7β,25-dihydroxycholesterol at an approximate level of 2% of the synthetic standards. Interestingly, this peak is absent in the analogous standards where the 25-hydroxyl is replaced by 27-hydroxyl group. A molecular ion of *m/z* 532.3898 can be produced from GP-derivatised monohydroxylated cholesterol molecule possessing one, additional unsaturated bond. 25-Hydroxy-7-dehydrocholesterol is a molecule with this structure, although in the absence of a standard it is not possible to reliably identify the analyte.

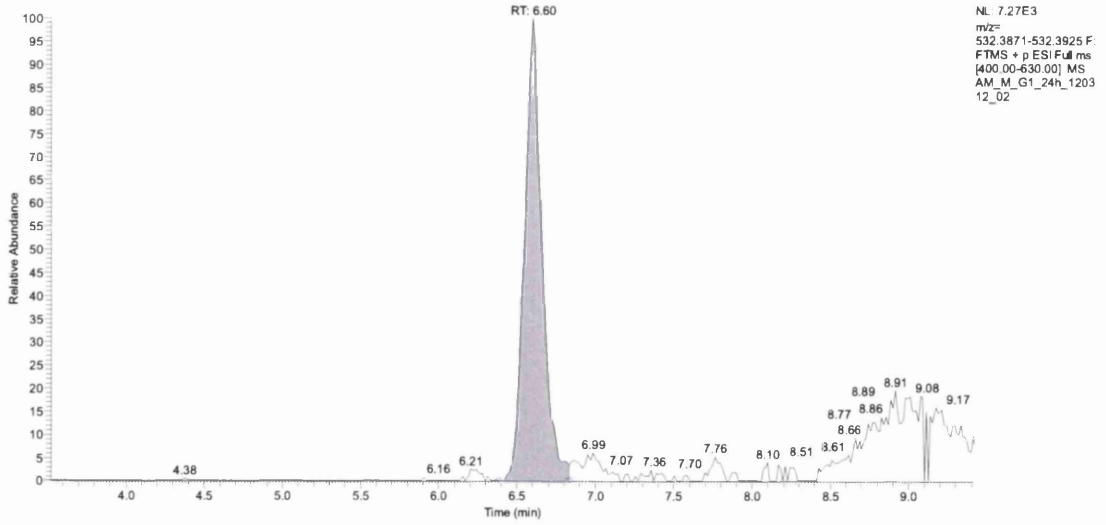

Figure 8.14. Hypothesised monohydroxylated unsaturated cholesterol derivatives in murine bone marrow derived macrophages. RIC of *m/z* 532.3898±5 ppm obtained from IFNγ treated cells.

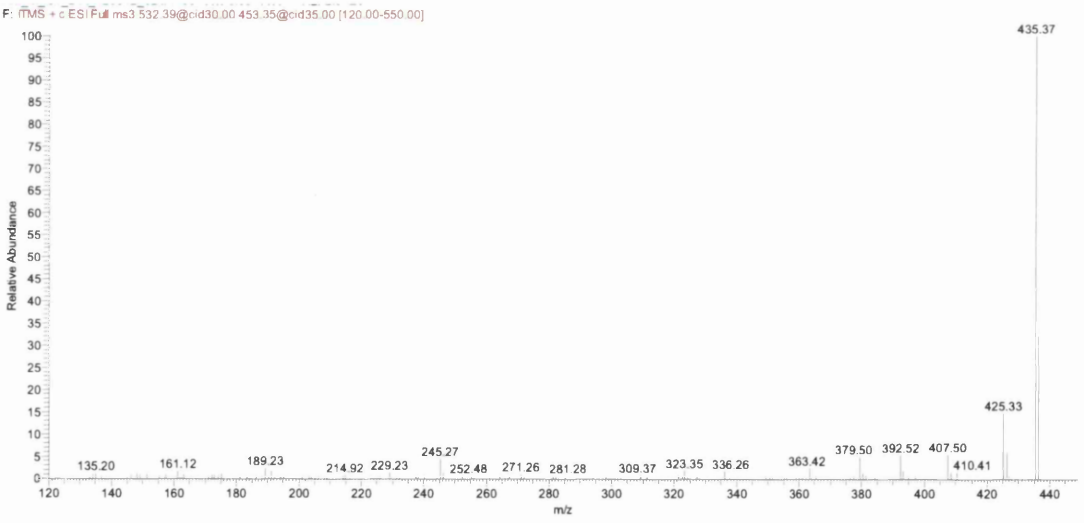

Figure 8.15. MS^3 spectrum of peak eluting at 6.59 min putatively labeled as GP-tagged 25-hydroxy-7-dehydrocholesterol from IFNγ treated cells.

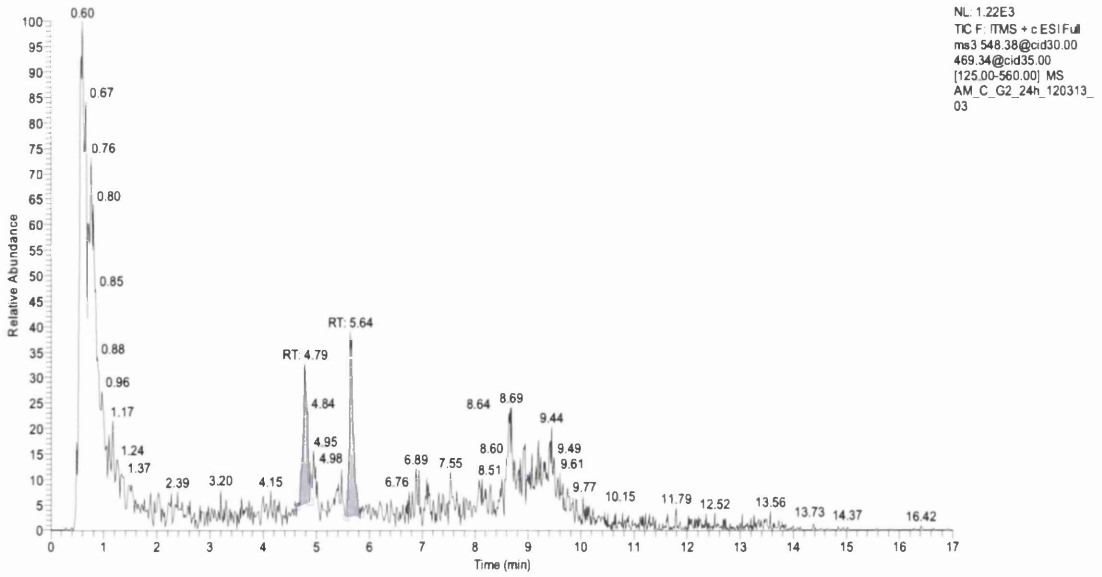

Figure 8.16. RIC of *m/z* 548.3847±5 ppm obtained from the analysis of IFNγ treated cells.

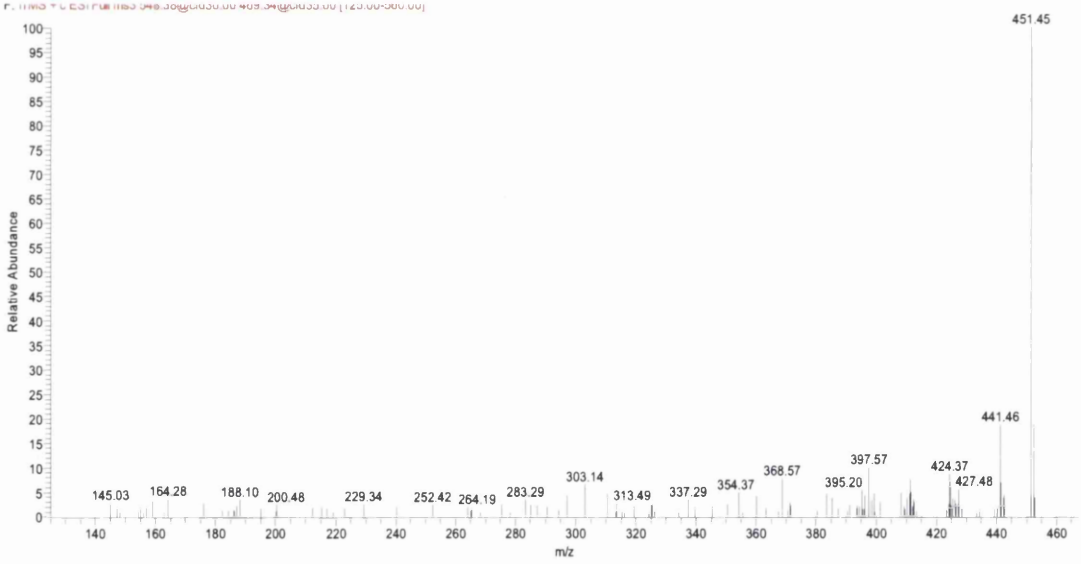

Figure 8.17. MS^3 spectrum of unknown eluent of m/z 548.3847 eluting at 4.79 min from IFNγ treated cells.

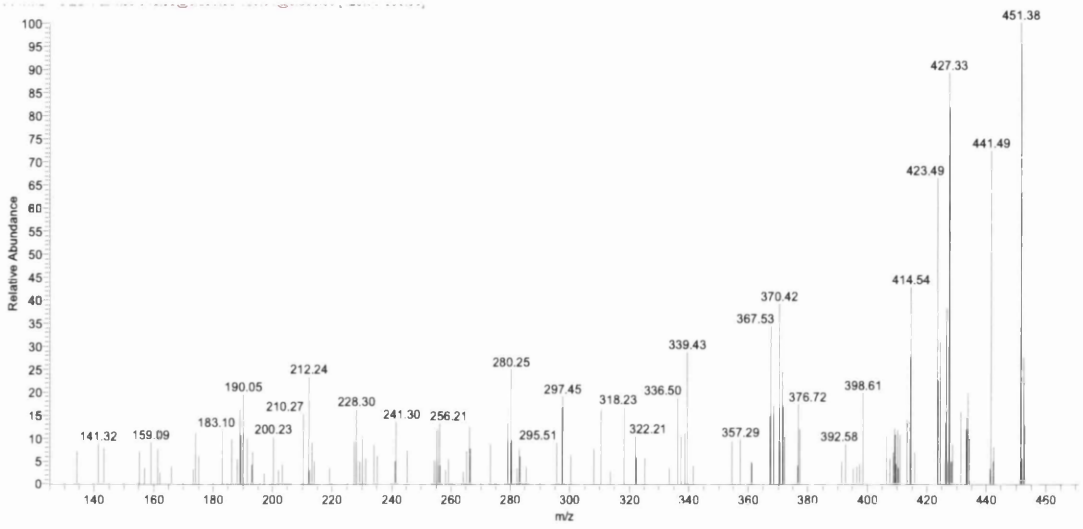

Figure 8.18. MS^3 spectrum of unknown eluent of m/z 548.3847 eluting at 4.79 min

The analysis of the cell extract in chromatograms acquired at *m/z* 548.3847 revealed two peaks (Figure 16, 17 and 18), whose intensities following the changes observed in 25-hydroxycholesterol. Due to low intensities, the estimation of the concentration was carried out based on the MS^3 chromatogram, therefore it was only used as a comparison of the folds change between the experiments. The difference between the control samples and interferon β and γ treated cell shows a strong statistical significance ($p<0.001$). The MS^3 spectra did not match any of these seen in the authentic standards; therefore the identity of these compounds is yet to be revealed.

RIC obtained at *m/z* ratio 564.3796 presented a number of compounds in the cell media (Table 5), the analytes eluting with retention times 3.41 min, 4.43 min, 4.62 min, 5.19 min, 5.24 min and 6.01 min were of a particular interest as their concentration was in a statistically significant manner lower in the interferon treated cell media than in controls (Table 8.2). This may indicate that the change in metabolism initiated by incubation with the interferons leads either to reduced synthesis or an increased uptake from the media. In the cell extract these compounds were below the level of detection.

As 25-hydroxycholesterol is a ligand to INSIG, we would be expected that alterations in the level of this oxysterol should be followed by the alterations in the levels of mevalonate pathway intermediates and its final product - cholesterol.

Sterols

Cholesterol is less polar compared to oxysterols, and is eluted from the first Sep-Pak in 100% ethanol in fraction 3. The molecular ion formed following oxidation and derivatisation steps has an *m/z* 518.4105. The RIC of *m/z* 518.4105 showed a single peak eluting at 11.66 (Figure 8.19) min with MS^3 characteristics matching the authentic standard of cholesterol (Figure 8.20). The levels of cholesterol were the highest in control and MCMV infected samples (34.84±2.64 μg/plate and 35.17±3.59 μg/plate), while in the interferon β and γ treated macrophages the concentration of cholesterol was lowered by 6% and 9% (31.64±3.99 μg/plate 32.77±3.46 μg/plate), respectively (Figure 8.21).

Desmosterol (RIC in Figure 8.22 and MS^3 in Figure 8.23), one of the cholesterol precursors, shows an analogous trend to cholesterol with a reduction of desmosterol levels by 11% and 13% in the interferon treated samples, however not to statistical significance (Figure 8.24). Although the changes in average concentrations of cholesterol and its precursors mirror in a inverse manner the concentrations of 25-hydroxycholesterol, these changes do no reach the statistical significance. However, for this evaluation we used a T Student Test, which is designed for a large representation groups and may not be sensitive enough to detect small differences between the cohorts of nine replicates.

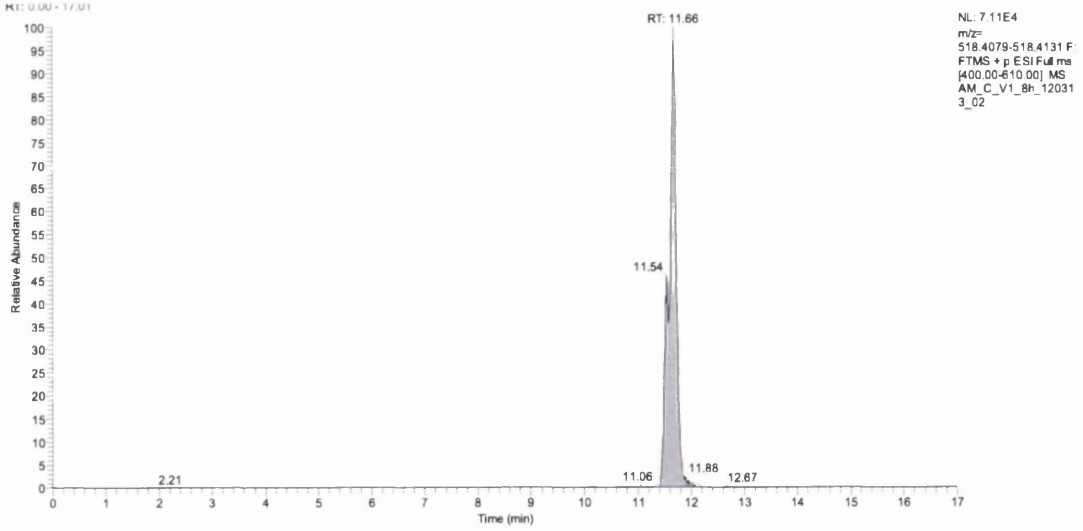

Figure 8.19. Cholesterol in murine bone marrow derived macrophages. RIC of *m/z* 518.4105±5 ppm obtained from the analysis of IFNγ treated macrophages.

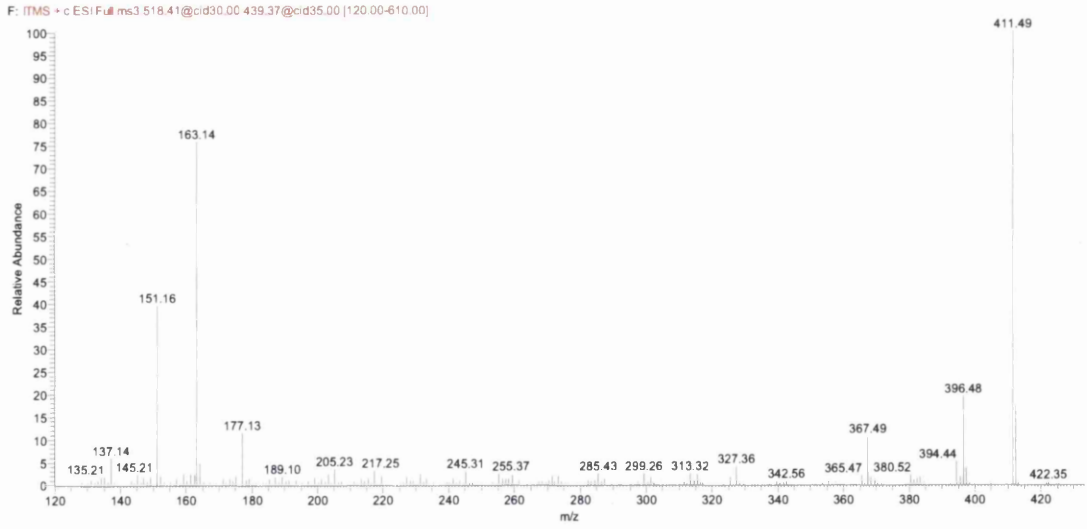

Figure 8.20. MS^3 spectrum of cholesterol, m/z 518.4105 eluting at 11.67 min from macrophages incubated with mCMV.

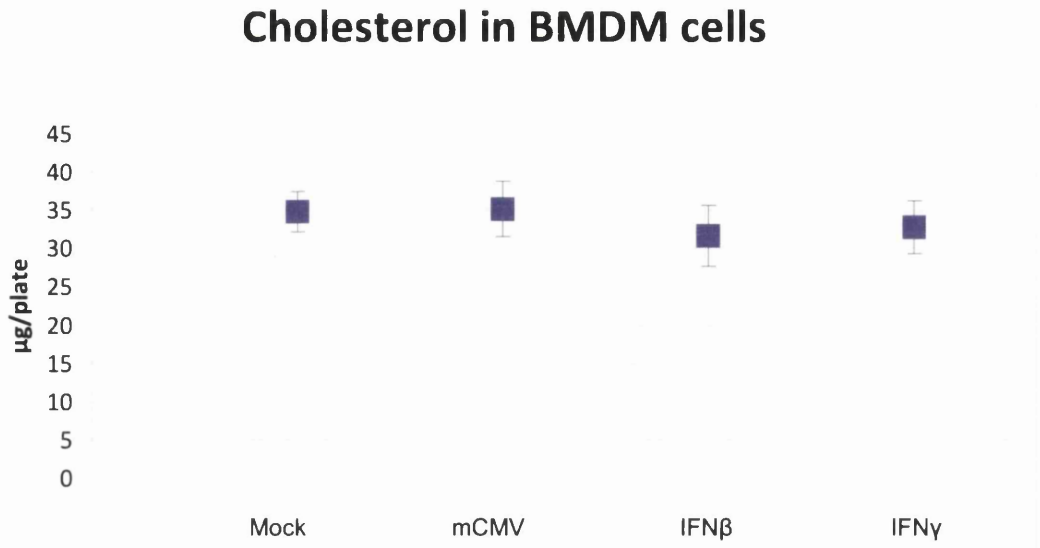

Figure 8.21. Concentrations of intra-cellular cholesterol calculated as ng/plate in BMDM control and treated by MCMV, IFNβ (10 U/ml), IFNγ (10U/ml). The bars representing an average concentration from data obtained from 3 replicates in each time point (8,16 and 24 hours). Error bars show SE 9 biological replicates.

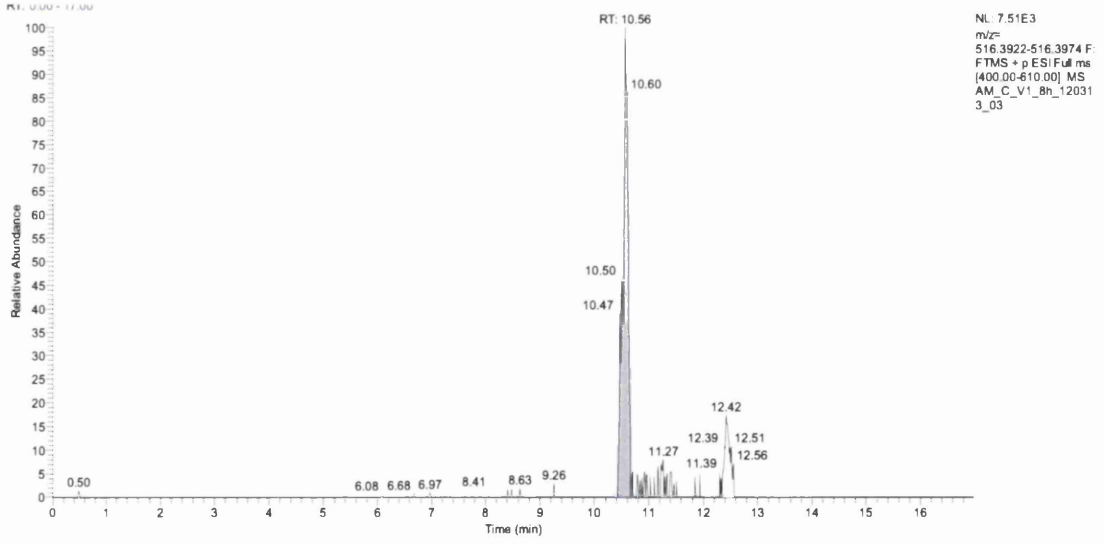

Figure 8.22. Desmosterol in murine bone marrow derived macrophages. RIC of *m/z* 516.3948±5 ppm obtained from macrophages incubated with mCMV.

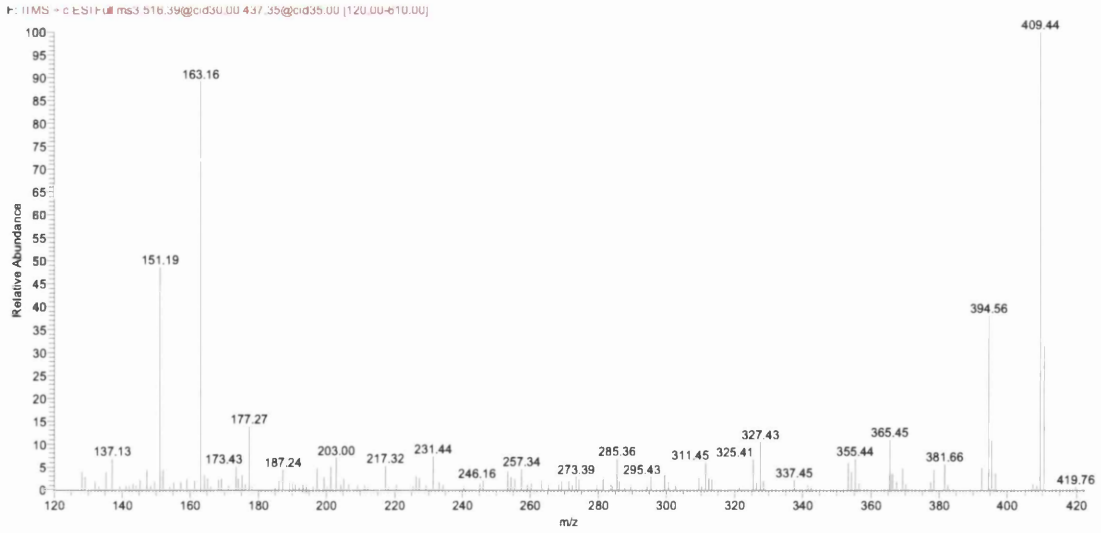

Figure 8.23. MS^3 spectrum of desmosterol, m/z 516.3948 eluting at 10.56 min. Chromatogram recorded from cells treated with mCMV.

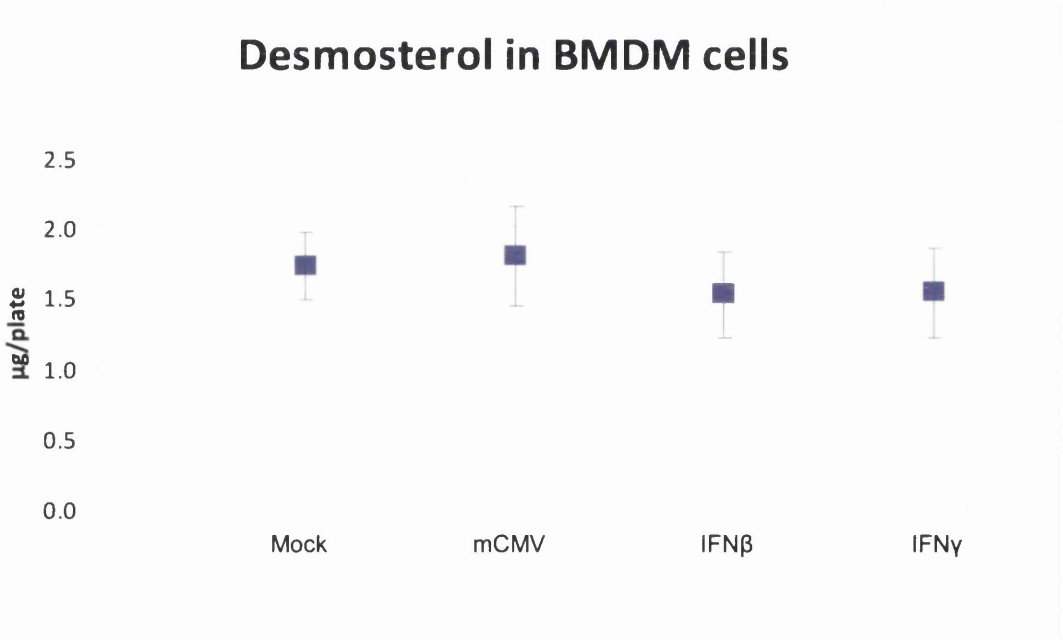

Figure 8.24. Concentrations of intra-cellular desmosterol calculated as ng/plate in BMDM control and treated by MCMV, IFNβ (10 U/ml), IFNγ (10U/ml). The bars representing an average concentration from data obtained from 3 replicates in each time point (8,16 and 24 hours). Error bars show SE 9 biological replicates.

The impact of interferon treatment on the mevalonate pathway is particularly interesting in regards to conflicting results from the first and second experiment. In the initial study the treatment increased the level of cholesterol, while in the second work this increase is not observed, moreover, averaged levels point at a decrease in the concentrations of the sterols. In the first experiment the cells were cultured in full media, therefore the sterols might have been imported into the cell, leading to an increased cellular level which was detected. In the second investigation the media used to culture the cells were not enriched with cholesterol containing serum. In this case an uptake of sterols was not possible; therefore the level of cholesterol was solely regulated by intra-cellular mechanisms. A modest down-regulation of cholesterol synthesis in interferon β and interferon γ treated samples can be attributed to an inhibition of mevalonate pathway by 25-hydroxycholesterol.

8.3 Discussion

This study showed that 25-hydroxycholesterol is excreted by macrophages in response to pathogens. Incubation with interferon type I (interferon β) as well as interferon γ were acting as inducers of cholesterol 25-hydroxylase. The level of 25-hydroxycholesterol increases both intracellulary and in the cell media.

25-Hydroxycholesterol is a potent regulator of cell metabolism as LXR ligand and as SREBP activator. SREBP regulates the synthesis of cholesterol by transcriptional control of the key enzyme in mevalonate pathway – HMG-CoA reductase. The removal of cholesterol from the cell is regulated by proteins belonging to the family of ABC transporters , expressed under control of LXR. Blanc et al showed that reduction in the activity of cholesterol biosynthetic pathway can be a part of cellular antiviral response[133]. Increased concentration of 25-hydroxycholesterol adversely affects viral growth [135]. It is not defined how this oxysterol inhibits viral propagation. Apart from decreasing the cholesterol level, 25-hydroxycholesterol can hypothetically interfere with viral cell entry by altering the properties of the membranes such as fluidity.

The cell signalling study reported by Blanc and colleagues shows that activation of cholesterol 25-hydroxylase by interferons in transduced by STAT1 protein [135]. Interferon β and Interferon γ activates respectively receptors INFAR1 and INFGR which induce its target proteins STAT 1 and 2. STAT 1 directly binds to cholesterol 25-hydroxylase promoter, thus controlling its transcriptional activity.

Chapter 9

9 Conclusions

9.1 Summary

Mass spectrometry serves as a highly sensitive and accurate tool for analysis of metabolites. The detection of compounds is based on accurate mass and structural features such as distribution of functional groups. The limitation of mass spectrometry defined by the requirement of electrical charge carried by the analyte can be solved by introduction of the derivatisation technique. With this approach even molecules with weak ionisation capacity can be subjected to mass spectroscopic analysis. This is of a particular importance for electrically neutral oxysterols.

Oxysterols exert a broad range of cellular functions, for example enable the trafficing of cholesterol, and they are precursors to steroid hormones and bile acids. Oxysterols were also recognised as ligands to "orphan" receptors such Liver X Receptor.

In our methodology oxysterols possessing 3β-hydroxy-5-ene or 3β-hydroxy-5α -hydrogen moieties are oxidised by the bacterial enzyme Cholesterol oxidase to form 3-oxo-4-ene and 3-oxo groups, respectively. The formation of an oxo group is crucial for the derivatisation step as Girard P reagent can form hydrazones with sterols possessing an oxo function. The introduction of the Girard P tag to the oxysterol provides a quaternary nitrogen carrying a positive charge. This "charge-tagging" procedure improves the MS detection by a factor of up to 10^3.

Derivatised molecules analysed by mass spectrometer can be subjected to collision with an inert gas, resulting in formation fragments ions. This was used for the determination of the structure of the analysed sterols. We applied a multistage fragmentation technique where the ions were fragmented in two steps. In the first one analytes derivatised with Girard P gave a neutral loss of 79 Da corresponding to the loss of the pyridine ring from the Girard reagent. The second collision cycle was applied only to these ions giving a neutral loss of 79 Da from the first step. This approach increased the selectivity of the method as only derivatised compounds were selected in the second cycle.

Oxysterols are generated by oxidation of cholesterol and some of the resulting molecules may be structural isomers with identical molecular mass. These can be separated prior to MS analysis by a Liquid Chromatography system. Dissolved

analytes were passed under high pressure through a C_{18} column. To improve chromatographic separation we modified an existing gradient into a curved transition between the mobile phases. This enhanced the separation of oxysterols present in nervous tissue.

In brain oxysterols are dominated by a high background of cholesterol (10^3-10^6 more abundant). Such a wide range of concentrations cannot be analysed in a single analytical run due to a limited dynamic range of the instrument. Besides, cholesterol is vulnerable to autoxidation and sterols generated in this process can obscure the analysis of endogenous metabolites. This was avoided by separating cholesterol from oxysterols at the earliest possible stage of sample preparation. We used a SPE cartridge and exploited the difference in polarities between sterols and oxysterols.

In chapter 3 we describe the analysis of sterols and oxysterols derived from newborn mouse brain. Brain is unique in the isolation of its mevalonate pathway from the peripheral organs. The blood brain barrier is impermeable to cholesterol which can not be neither imported in or exported from the brain *per se*. 24S-Hydroxylation of cholesterol provides an exit rout for brain cholesterol and 24S-hydroxycholesterol is the main oxysterol in the brain.

Due to incompleted myelination of neurons in neonatal brain, the cholesterol content is relatively low, consequently the amounts of cholesterol's main metabolite, 24S-hydroxycholesterol, is also reduced compared to an adult brain. This facilitates the analysis of other monohydroxycholesterols, otherwise obscured by 24S-hydroxycholesterol. Thus, we quantified 22R-, 25-, 26-, 7α, 7β, 6β-hydroxycholesterols. 25-Hydroxycholesterol is synthesised by the widely expressed cholesterol 25-hydroxylse, and is particularly important for an antiviral immune response. 26- and 7α-hydroxycholesterol initiate two different pathways of bile acid biosynthesis. This is interesting as bile acids can be ligands to LXRβ which has been implicated in neurogenesis. We also quantified 24S,25-epoxycholesterol, another LXR and Insig ligand. The level of desmosterol, a cholesterol precursor, in developing brain is relatively high which reflects a high rate of cholesterol synthesis. Desmosterol can become hydroxylated and we quantified 7α- and 26-hydroxydesmosterols. This is the first study reporting the presence of hydroxylated desmosterols in the brain.

Smith-Lemli-Opitz syndrome (SLOS) arises from the malfunction of dehydrocholesterol reductase converting 7-dehydrocholesterol into cholesterol. We analysed the lipidome of a mouse model of SLOS to evaluate whether the dysfunction of cholesterol biosynthesis is accompanied by formation of other compounds which could account for neuronal symptoms of SLOS. The sterol profile showed an altered level of cholesterol precursors with increased concentration of 7- and 8-dehydrocholesterols accompanied by reduced levels of desmosterol and cholesterol. The general level of oxysterols was reduced, which is a probable consequence of lower availability of cholesterol.

Next we moved to analysis of an adult brain derived from Cyp46a1 deficient mice. Cyp46a1 is almost exclusively expressed in brain where it catalyses 24S-hydroxylation of cholesterol. In this project we investigated if disabling of Cyp46a1 will reveal any other mechanisms of cholesterol removal form brain. The analysis of sterols showed a reduction in cholesterol synthesis reflected by a diminished amount of cholesterol precursors, while the concentration of cholesterol remained unaltered. The oxysterol profile remained generally unaltered, however an absence of 24S-hydroxycholesterol allowed the observation a number oxysterols allowing for their precise quantification.

In chapter 6 we profiled the sterol content of Cyp27a1$^{-/-}$ mouse brain. In humans this deficiency results in CTX, which main diagnostic features include accumulation of sterols in tendons and brain and unusual bile alcohols present in body fluids. The knock out of Cyp27a1 disables the "acetic" pathway of bile acid synthesis. The oxysterol profile revealed a high concentration of 7α-hydroxylated cholesterol and desmosterol, as well as the products of further 12α-hydroxylation of these analytes accompanied by unusually high ratio of its 3-oxo analogues. The Cyp27a1-/- brain had a high number of tri- and tetra-hydroxycholesterol isomers not observed in wild type. This may be a consequence of upregulation of Cyp3a, responsible for hydroxylation of the cholesterol side chain.

In chapter 7 we analysed sterols and oxysterols isolated from Cyp7b1$^{-/-}$ mouse brain, people affected by mutations in this gene can suffer from two different disorders: neonatal liver disease and spastic paraplegia. The levels of 25- and 26-hydroxycholesterols were largely increased due to the absence of Cyp7b1 metabolising these oxysterol under normal conditions. Concentrations of 24S,25-

epoxycholesterol, (24Z) and (24E)26-hydroxydesmosterols was also increased suggesting that this analytes can be also metabolised by Cyp7b1.

The last experimentalal chapter was concentrates on the analysis of oxysterols in challenged murine macrophages. The incubation of bone derived murine macrophages with interferon β and interferon γ led to increased production and excretion of 25-hydroxycholesterol. We also observed a rise in putative products of 25-hydroxycholesterol metabolism such as 7α,25-dihydroxycholesterol. Both are strongly involved in mechanisms of immune response.

In this work we provided a comprehensive study of oxysterols and sterols present in murine brain. W analysed brains at an early stage of development in pursuit of compounds associated with neurogenesis. We also looked into brains derived form animals carrying mutations in enzymes involved in cholesterol and sterol metabolism, in order to delve into sterol metabolic pathways subjected to constraints imposed by the mutations.

9.2 Future directions

The analysis of brain tissue and macrophages revealed an array of compounds, a number of which have been identified in vivo for the first time. The biological significance of these analytes still remains to be understood and more work is required to unveil their physiological roles.

1. Yeagle, P.L., *Cholesterol and the cell membrane.* Biochim Biophys Acta, 1985. **822**(3-4): p. 267-87.
2. Alberts B., B.D., Lewis J., Roberts K., Watson J.D. , *The molecular biology of the cell.* Garland Publishing, 1983. **New York**.
3. J.P., S., Biochemistry, 1992. **31**: p. 5472-5477.
4. RB, G., *Biomembranes, molecular structure and function.* New York: Springer Verlag,, 1989: p. 73-4.
5. Shepherd, J., *The role of the exogenous pathway in hypercholesterolaemia.* European Heart Journal Supplements, 2001. **3**(suppl E): p. E2-E5.
6. Clayton, P.T., *Disorders of cholesterol biosynthesis.* Arch Dis Child, 1998. **78**(2): p. 185-9.
7. Wentworth, P., Jr., et al., *Evidence for antibody-catalyzed ozone formation in bacterial killing and inflammation.* Science, 2002. **298**(5601): p. 2195-9.
8. Lund, E.G., et al., *cDNA cloning of mouse and human cholesterol 25-hydroxylases, polytopic membrane proteins that synthesize a potent oxysterol regulator of lipid metabolism.* J Biol Chem, 1998. **273**(51): p. 34316-27.
9. Khatri, Y., et al., *The CYPome of Sorangium cellulosum So ce56 and identification of CYP109D1 as a new fatty acid hydroxylase.* Chem Biol, 2010. **17**(12): p. 1295-305.
10. Lamb, D.C., et al., *The cytochrome P450 complement (CYPome) of Streptomyces coelicolor A3(2).* J Biol Chem, 2002. **277**(27): p. 24000-5.
11. Kelly, S.L. and D.E. Kelly, *Microbial cytochromes P450: biodiversity and biotechnology. Where do cytochromes P450 come from, what do they do and what can they do for us?* Philos Trans R Soc Lond B Biol Sci, 2013. **368**(1612): p. 20120476.
12. Jackson, C.J., et al., *Mutations in Saccharomyces cerevisiae sterol C5-desaturase conferring resistance to the CYP51 inhibitor fluconazole.* Biochem Biophys Res Commun, 2003. **309**(4): p. 999-1004.
13. Hargrove, T.Y., et al., *CYP51 structures and structure-based development of novel, pathogen-specific inhibitory scaffolds.* Int J Parasitol Drugs Drug Resist, 2012. **2**: p. 178-186.
14. Mullins, J.G., et al., *Molecular modelling of the emergence of azole resistance in Mycosphaerella graminicola.* PLoS One, 2011. **6**(6): p. e20973.
15. Cools, H.J., et al., *Impact of recently emerged sterol 14{alpha}-demethylase (CYP51) variants of Mycosphaerella graminicola on azole fungicide sensitivity.* Appl Environ Microbiol, 2011. **77**(11): p. 3830-7.
16. Fahy, E., et al., *A comprehensive classification system for lipids.* J Lipid Res, 2005. **46**(5): p. 839-61.
17. Andersson, S., et al., *Cloning, structure, and expression of the mitochondrial cytochrome P-450 sterol 26-hydroxylase, a bile acid biosynthetic enzyme.* J Biol Chem, 1989. **264**(14): p. 8222-9.
18. Brown, J., 3rd, et al., *Differential expression of cholesterol hydroxylases in Alzheimer's disease.* J Biol Chem, 2004. **279**(33): p. 34674-81.
19. Gilardi, F., et al., *Expression of sterol 27-hydroxylase in glial cells and its regulation by liver X receptor signaling.* Neuroscience, 2009. **164**(2): p. 530-40.
20. Milagre, I., et al., *Marked change in the balance between CYP27A1 and CYP46A1 mediated elimination of cholesterol during differentiation of human neuronal cells.* Neurochem Int, 2012. **60**(2): p. 192-8.

21. Oftebro, H., et al., *Cerebrotendinous xanthomatosis: a defect in mitochondrial 26-hydroxylation required for normal biosynthesis of cholic acid.* J Clin Invest, 1980. **65**(6): p. 1418-30.
22. Griffiths, W.J., *Metabolomics, Metabonomics and Metabolite Profiling.* RSC Biomolecular Sciences, 2008.
23. Setchell, K.D., et al., *Identification of a new inborn error in bile acid synthesis: mutation of the oxysterol 7alpha-hydroxylase gene causes severe neonatal liver disease.* J Clin Invest, 1998. **102**(9): p. 1690-703.
24. Tsaousidou, M.K., et al., *Sequence alterations within CYP7B1 implicate defective cholesterol homeostasis in motor-neuron degeneration.* Am J Hum Genet, 2008. **82**(2): p. 510-5.
25. Ueki, I., et al., *Neonatal cholestatic liver disease in an Asian patient with a homozygous mutation in the oxysterol 7alpha-hydroxylase gene.* J Pediatr Gastroenterol Nutr, 2008. **46**(4): p. 465-9.
26. Honda, A., et al., *Cholesterol 25-hydroxylation activity of CYP3A.* J Lipid Res, 2011. **52**(8): p. 1509-16.
27. Fayer JL, P.D., Ring BJ, Wrighton SA, Ruterbories KJ, *A novel testosterone 6 beta-hydroxylase activity assay for the study of CYP3A-mediated metabolism, inhibition, and induction in vitro.* J Pharmacol Toxicol Methods., 2001. **46**(2): p. 117-23.
28. Mast, N., et al., *Structural basis for three-step sequential catalysis by the cholesterol side chain cleavage enzyme CYP11A1.* J Biol Chem, 2011. **286**(7): p. 5607-13.
29. Lund, E.G., J.M. Guileyardo, and D.W. Russell, *cDNA cloning of cholesterol 24-hydroxylase, a mediator of cholesterol homeostasis in the brain.* Proc Natl Acad Sci U S A, 1999. **96**(13): p. 7238-43.
30. Russell, D.W., et al., *Cholesterol 24-hydroxylase: an enzyme of cholesterol turnover in the brain.* Annu Rev Biochem, 2009. **78**: p. 1017-40.
31. Brown, M.S. and J.L. Goldstein, *Suppression of 3-hydroxy-3-methylglutaryl coenzyme A reductase activity and inhibition of growth of human fibroblasts by 7-ketocholesterol.* J Biol Chem, 1974. **249**(22): p. 7306-14.
32. Brown, M.S. and J.L. Goldstein, *Cholesterol feedback: from Schoenheimer's bottle to Scap's MELADL.* J Lipid Res, 2009. **50 Suppl**: p. S15-27.
33. Bensinger, S.J., et al., *LXR signaling couples sterol metabolism to proliferation in the acquired immune response.* Cell, 2008. **134**(1): p. 97-111.
34. Joseph, S.B., et al., *LXR-dependent gene expression is important for macrophage survival and the innate immune response.* Cell, 2004. **119**(2): p. 299-309.
35. Joseph, S.B., et al., *Reciprocal regulation of inflammation and lipid metabolism by liver X receptors.* Nat Med, 2003. **9**(2): p. 213-9.
36. N, A.G., et al., *Apoptotic cells promote their own clearance and immune tolerance through activation of the nuclear receptor LXR.* Immunity, 2009. **31**(2): p. 245-58.
37. Uno, S., et al., *Suppression of β-catenin signaling by liver X receptor ligands.* Biochemical Pharmacology, 2009. **77**(2): p. 186-195.
38. Cruz P, T.C., Ramírez ME, Epuñán MJ, Valladares LE, Sierralta WD., *Proliferation of human mammary cancer cells exposed to 27-hydroxycholesterol.* Exp Ther Med, 2010. **1**(3): p. 531-536.
39. Nelson ER, W.S., Jasper JS, Park S, Suchindran S, Howe MK, Carver NJ, Pillai RV, Sullivan PM, Sondhi V, Umetani M, Geradts J, McDonnell DP, *27-*

hydroxycholesterol links hypercholesterolemia and breast cancer pathophysiology. Science, 2013. **342**(6162): p. 1094-8.
40. Mohler, J., *Requirements for hedgehog, a segmental polarity gene, in patterning larval and adult cuticle of Drosophila.* Genetics, 1988. **120**(4): p. 1061-72.
41. McDonald JG, R.D., *Editorial: 25-Hydroxycholesterol: a new life in immunology.* J Leukoc Biol, 2010. **88**(6): p. 1071-2.
42. Kandutsch AA, C.H., Heiniger HJ, *Biological activity of some oxygenated sterols.* Science., 1978 **201**(4355): p. 498-501.
43. RA., D.-B., *Feedback regulation of cholesterol synthesis: sterol-accelerated ubiquitination and degradation of HMG CoA reductase.* Cell Res., 2008. **18**(6): p. 609-21.
44. Waltl S, P.J., Fauler G, Nusshold C, Ullen A, Eibinger G, Wintersperger A, Kratky D, Malle E, Sattler W, *25-Hydroxycholesterol regulates cholesterol homeostasis in the murine CATH.a neuronal cell line.* Neurosci Lett, 2013 **539**: p. 16-21.
45. Itoh, M., et al., *Developmental and pathological expression of peroxisomal enzymes: their relationship of D-bifunctional protein deficiency and Zellweger syndrome.* Brain Res, 2000. **858**(1): p. 40-7.
46. Sacchetti, P., et al., *Liver X Receptors and Oxysterols Promote Ventral Midbrain Neurogenesis In Vivo and in Human Embryonic Stem Cells.* Cell stem cell, 2009. **5**(4): p. 409-419.
47. Hong, C. and P. Tontonoz, *Coordination of inflammation and metabolism by PPAR and LXR nuclear receptors.* Current Opinion in Genetics & Development, 2008. **18**(5): p. 461-467.
48. Endo-Umeda, K., et al., *7-Dehydrocholesterol metabolites produced by sterol 27-hydroxylase (CYP27A1) modulate liver X receptor activity.* The Journal of Steroid Biochemistry and Molecular Biology, 2014. **140**(0): p. 7-16.
49. Chiang, J.Y.L., R. Kimmel, and D. Stroup, *Regulation of cholesterol 7α-hydroxylase gene (CYP7A1) transcription by the liver orphan receptor (LXRα).* Gene, 2001. **262**(1–2): p. 257-265.
50. Kennedy, M.A., et al., *Characterization of the Human ABCG1 Gene: LIVER X RECEPTOR ACTIVATES AN INTERNAL PROMOTER THAT PRODUCES A NOVEL TRANSCRIPT ENCODING AN ALTERNATIVE FORM OF THE PROTEIN.* Journal of Biological Chemistry, 2001. **276**(42): p. 39438-39447.
51. Venkateswaran, A., et al., *Control of cellular cholesterol efflux by the nuclear oxysterol receptor LXRα.* Proceedings of the National Academy of Sciences, 2000. **97**(22): p. 12097-12102.
52. Laffitte, B.A., et al., *LXRs control lipid-inducible expression of the apolipoprotein E gene in macrophages and adipocytes.* Proceedings of the National Academy of Sciences, 2001. **98**(2): p. 507-512.
53. Wang, M.L., et al., *Identification of Surface Residues on Niemann-Pick C2 Essential for Hydrophobic Handoff of Cholesterol to NPC1 in Lysosomes.* Cell metabolism, 2010. **12**(2): p. 166-173.
54. Hornykiewicz, O., *Biochemical aspects of Parkinson's disease.* Neurology, 1998. **51**(2 Suppl 2): p. S2-9.
55. Rothlin, C.V., et al., *TAM receptors are pleiotropic inhibitors of the innate immune response.* Cell, 2007. **131**(6): p. 1124-36.

56. Spann, N.J., et al., *Regulated accumulation of desmosterol integrates macrophage lipid metabolism and inflammatory responses.* Cell, 2012. **151**(1): p. 138-52.
57. Qin, Y., et al., *Regulation of hepatic fatty acid elongase 5 by LXRalpha-SREBP-1c.* Biochim Biophys Acta, 2009. **1791**(2): p. 140-7.
58. Glass, C.K. and K. Saijo, *Nuclear receptor transrepression pathways that regulate inflammation in macrophages and T cells.* Nat Rev Immunol, 2010. **10**(5): p. 365-76.
59. Dai, Y.B., et al., *Liver X receptor beta protects dopaminergic neurons in a mouse model of Parkinson disease.* Proc Natl Acad Sci U S A, 2012. **109**(32): p. 13112-7.
60. Zelcer, N., et al., *Attenuation of neuroinflammation and Alzheimer's disease pathology by liver x receptors.* Proc Natl Acad Sci U S A, 2007. **104**(25): p. 10601-6.
61. Brown, M.S. and J.L. Goldstein, *The SREBP pathway: regulation of cholesterol metabolism by proteolysis of a membrane-bound transcription factor.* Cell, 1997. **89**(3): p. 331-40.
62. Horton, J.D., et al., *Activation of cholesterol synthesis in preference to fatty acid synthesis in liver and adipose tissue of transgenic mice overproducing sterol regulatory element-binding protein-2.* J Clin Invest, 1998. **101**(11): p. 2331-9.
63. Shimano, H., et al., *Overproduction of cholesterol and fatty acids causes massive liver enlargement in transgenic mice expressing truncated SREBP-1a.* J Clin Invest, 1996. **98**(7): p. 1575-84.
64. Radhakrishnan, A., et al., *Direct binding of cholesterol to the purified membrane region of SCAP: mechanism for a sterol-sensing domain.* Mol Cell, 2004. **15**(2): p. 259-68.
65. Brown, M.S. and J.L. Goldstein, *A proteolytic pathway that controls the cholesterol content of membranes, cells, and blood.* Proc Natl Acad Sci U S A, 1999. **96**(20): p. 11041-8.
66. Matsuda, M., et al., *SREBP cleavage-activating protein (SCAP) is required for increased lipid synthesis in liver induced by cholesterol deprivation and insulin elevation.* Genes Dev, 2001. **15**(10): p. 1206-16.
67. Yabe, D., M.S. Brown, and J.L. Goldstein, *Insig-2, a second endoplasmic reticulum protein that binds SCAP and blocks export of sterol regulatory element-binding proteins.* Proc Natl Acad Sci U S A, 2002. **99**(20): p. 12753-8.
68. Radhakrishnan, A., et al., *Sterol-regulated transport of SREBPs from endoplasmic reticulum to Golgi: oxysterols block transport by binding to Insig.* Proc Natl Acad Sci U S A, 2007. **104**(16): p. 6511-8.
69. Streicher, R., et al., *SREBP-1 mediates activation of the low density lipoprotein receptor promoter by insulin and insulin-like growth factor-I.* J Biol Chem, 1996. **271**(12): p. 7128-33.
70. Kwon, H.J., et al., *Structure of N-terminal domain of NPC1 reveals distinct subdomains for binding and transfer of cholesterol.* Cell, 2009. **137**(7): p. 1213-24.
71. Liu, J.P., *New functions of cholesterol binding proteins.* Mol Cell Endocrinol, 2009. **303**(1-2): p. 1-6.

72. Zhang, J.R., et al., *Niemann-Pick C1 protects against atherosclerosis in mice via regulation of macrophage intracellular cholesterol trafficking.* J Clin Invest, 2008. **118**(6): p. 2281-90.
73. Cohen, M.M., Jr., *Hedgehog signaling update.* Am J Med Genet A, 2010. **152a**(8): p. 1875-914.
74. Corcoran, R.B. and M.P. Scott, *Oxysterols stimulate Sonic hedgehog signal transduction and proliferation of medulloblastoma cells.* Proc Natl Acad Sci U S A, 2006. **103**(22): p. 8408-13.
75. Kalderon, D., *Transducing the hedgehog signal.* Cell, 2000. **103**(3): p. 371-4.
76. Goodrich, L.V., et al., *Conservation of the hedgehog/patched signaling pathway from flies to mice: induction of a mouse patched gene by Hedgehog.* Genes Dev, 1996. **10**(3): p. 301-12.
77. Marigo, V., et al., *Sonic hedgehog differentially regulates expression of GLI and GLI3 during limb development.* Dev Biol, 1996. **180**(1): p. 273-83.
78. Nachtergaele, S., et al., *Oxysterols are allosteric activators of the oncoprotein Smoothened.* Nat Chem Biol, 2012. **8**(2): p. 211-20.
79. Rohatgi, R., L. Milenkovic, and M.P. Scott, *Patched1 regulates hedgehog signaling at the primary cilium.* Science, 2007. **317**(5836): p. 372-6.
80. Waubant, E., *Biomarkers indicative of blood-brain barrier disruption in multiple sclerosis.* Dis Markers, 2006. **22**(4): p. 235-44.
81. Oby, E. and D. Janigro, *The blood-brain barrier and epilepsy.* Epilepsia, 2006. **47**(11): p. 1761-74.
82. Zipser, B.D., et al., *Microvascular injury and blood-brain barrier leakage in Alzheimer's disease.* Neurobiol Aging, 2007. **28**(7): p. 977-86.
83. Raza, M.W., et al., *Penetration and activity of antibiotics in brain abscess.* J Coll Physicians Surg Pak, 2005. **15**(3): p. 165-7.
84. Pentreath, V.W., P.J. Baugh, and D.R. Lavin, *Sleeping sickness and the central nervous system.* Onderstepoort J Vet Res, 1994. **61**(4): p. 369-77.
85. Osono, Y., et al., *Role of the low density lipoprotein receptor in the flux of cholesterol through the plasma and across the tissues of the mouse.* J Clin Invest, 1995. **95**(3): p. 1124-32.
86. Burg, V.K., et al., *Plant sterols the better cholesterol in Alzheimer's disease? A mechanistical study.* J Neurosci, 2013. **33**(41): p. 16072-87.
87. Vanmierlo, T., et al., *Dietary intake of plant sterols stably increases plant sterol levels in the murine brain.* J Lipid Res, 2012. **53**(4): p. 726-35.
88. Dietschy, J.M. and S.D. Turley, *Thematic review series: brain Lipids. Cholesterol metabolism in the central nervous system during early development and in the mature animal.* J Lipid Res, 2004. **45**(8): p. 1375-97.
89. Davison, A.N. and M. Wajda, *Cerebral lipids in multiple sclerosis.* J Neurochem, 1962. **9**: p. 427-32.
90. Davison, A.N., *Brain sterol metabolism.* Adv Lipid Res, 1965. **3**: p. 171-96.
91. Jurevics, H. and P. Morell, *Cholesterol for synthesis of myelin is made locally, not imported into brain.* J Neurochem, 1995. **64**(2): p. 895-901.
92. Kabara, J.J., *A critical review of brain cholesterol metabolism.* Prog Brain Res, 1973. **40**(0): p. 363-82.
93. Mengler, L., et al., *Brain maturation of the adolescent rat cortex and striatum: Changes in volume and myelination.* Neuroimage, 2014. **84**: p. 35-44.

94. Quan, G., et al., *Ontogenesis and regulation of cholesterol metabolism in the central nervous system of the mouse.* Brain Res Dev Brain Res, 2003. **146**(1-2): p. 87-98.
95. Turley, S.D., D.K. Burns, and J.M. Dietschy, *Preferential utilization of newly synthesized cholesterol for brain growth in neonatal lambs.* Am J Physiol, 1998. **274**(6 Pt 1): p. E1099-105.
96. Bjorkhem, I., *Crossing the barrier: oxysterols as cholesterol transporters and metabolic modulators in the brain.* J Intern Med, 2006. **260**(6): p. 493-508.
97. Bjorkhem, I., *Rediscovery of cerebrosterol.* Lipids, 2007. **42**(1): p. 5-14.
98. Bjorkhem, I., et al., *Importance of a novel oxidative mechanism for elimination of brain cholesterol. Turnover of cholesterol and 24(S)-hydroxycholesterol in rat brain as measured with 18O2 techniques in vivo and in vitro.* J Biol Chem, 1997. **272**(48): p. 30178-84.
99. Bjorkhem, I., et al., *Cholesterol homeostasis in human brain: turnover of 24S-hydroxycholesterol and evidence for a cerebral origin of most of this oxysterol in the circulation.* J Lipid Res, 1998. **39**(8): p. 1594-600.
100. de Chaves, E.I., et al., *Role of lipoproteins in the delivery of lipids to axons during axonal regeneration.* J Biol Chem, 1997. **272**(49): p. 30766-73.
101. Hayashi, H., et al., *Glial lipoproteins stimulate axon growth of central nervous system neurons in compartmented cultures.* J Biol Chem, 2004. **279**(14): p. 14009-15.
102. Posse De Chaves, E.I., et al., *Uptake of lipoproteins for axonal growth of sympathetic neurons.* J Biol Chem, 2000. **275**(26): p. 19883-90.
103. Li-Hawkins, J., et al., *Expression cloning of an oxysterol 7alpha-hydroxylase selective for 24-hydroxycholesterol.* J Biol Chem, 2000. **275**(22): p. 16543-9.
104. Russell, D.W., *Oxysterol biosynthetic enzymes.* Biochim Biophys Acta, 2000. **1529**(1-3): p. 126-35.
105. Xie, C., et al., *Quantitation of two pathways for cholesterol excretion from the brain in normal mice and mice with neurodegeneration.* J Lipid Res, 2003. **44**(9): p. 1780-9.
106. Lund, E.G., et al., *Knockout of the cholesterol 24-hydroxylase gene in mice reveals a brain-specific mechanism of cholesterol turnover.* J Biol Chem, 2003. **278**(25): p. 22980-8.
107. Mast, N., et al., *Broad substrate specificity of human cytochrome P450 46A1 which initiates cholesterol degradation in the brain.* Biochemistry, 2003. **42**(48): p. 14284-92.
108. Zhang, J., et al., *Metabolism of 27-, 25- and 24-hydroxycholesterol in rat glial cells and neurons.* Biochem J, 1997. **322 (Pt 1)**: p. 175-84.
109. Janowski, B.A., et al., *Structural requirements of ligands for the oxysterol liver X receptors LXRalpha and LXRbeta.* Proc Natl Acad Sci U S A, 1999. **96**(1): p. 266-71.
110. Lu, R., et al., *FGF-1 induces expression of LXRalpha and production of 25-hydroxycholesterol to upregulate the apoE gene in rat astrocytes.* J Lipid Res, 2009. **50**(6): p. 1156-64.
111. Lin, Y.Y., M. Welch, and S. Lieberman, *The detection of 20S-hydroxycholesterol in extracts of rat brains and human placenta by a gas chromatograph/mass spectrometry technique.* J Steroid Biochem Mol Biol, 2003. **85**(1): p. 57-61.
112. Kohchi, C., K. Ukena, and K. Tsutsui, *Age- and region-specific expressions of the messenger RNAs encoding for steroidogenic enzymes p450scc, P450c17*

and 3beta-HSD in the postnatal rat brain. Brain Res, 1998. **801**(1-2): p. 233-8.
113. Sanne, J.L. and K.E. Krueger, *Expression of cytochrome P450 side-chain cleavage enzyme and 3 beta-hydroxysteroid dehydrogenase in the rat central nervous system: a study by polymerase chain reaction and in situ hybridization.* J Neurochem, 1995. **65**(2): p. 528-36.
114. Tsutsui, K., et al., *Neurosteroid biosynthesis in vertebrate brains.* Comp Biochem Physiol C Pharmacol Toxicol Endocrinol, 1999. **124**(2): p. 121-9.
115. Boutaud, O., D. Dolis, and F. Schuber, *Preferential cyclization of 2,3(S):22(S),23-dioxidosqualene by mammalian 2,3-oxidosqualene-lanosterol cyclase.* Biochem Biophys Res Commun, 1992. **188**(2): p. 898-904.
116. Dollis, D. and F. Schuber, *Effects of a 2,3-oxidosqualene-lanosterol cyclase inhibitor 2,3:22,23-dioxidosqualene and 24,25-epoxycholesterol on the regulation of cholesterol biosynthesis in human hepatoma cell line HepG2.* Biochem Pharmacol, 1994. **48**(1): p. 49-57.
117. Eisele, B., et al., *Effects of a novel 2,3-oxidosqualene cyclase inhibitor on cholesterol biosynthesis and lipid metabolism in vivo.* J Lipid Res, 1997. **38**(3): p. 564-75.
118. Wong, J., et al., *Endogenous 24(S),25-epoxycholesterol fine-tunes acute control of cellular cholesterol homeostasis.* J Biol Chem, 2008. **283**(2): p. 700-7.
119. Meljon, A., et al., *Analysis of bioactive oxysterols in newborn mouse brain by LC/MS.* J Lipid Res, 2012. **53**(11): p. 2469-83.
120. Wang, Y., et al., *Targeted lipidomic analysis of oxysterols in the embryonic central nervous system.* Mol Biosyst, 2009. **5**(5): p. 529-41.
121. Theofilopoulos, S., et al., *Brain endogenous liver X receptor ligands selectively promote midbrain neurogenesis.* Nat Chem Biol, 2013. **9**(2): p. 126-33.
122. Wong, J., C.M. Quinn, and A.J. Brown, *Synthesis of the oxysterol, 24(S), 25-epoxycholesterol, parallels cholesterol production and may protect against cellular accumulation of newly-synthesized cholesterol.* Lipids Health Dis, 2007. **6**: p. 10.
123. McDonald, J.G., et al., *Extraction and analysis of sterols in biological matrices by high performance liquid chromatography electrospray ionization mass spectrometry.* Methods Enzymol, 2007. **432**: p. 145-70.
124. Bodin, K., et al., *Metabolism of 4 beta -hydroxycholesterol in humans.* J Biol Chem, 2002. **277**(35): p. 31534-40.
125. Woodland, C., et al., *Expression, activity and regulation of CYP3A in human and rodent brain.* Drug Metab Rev, 2008. **40**(1): p. 149-68.
126. Sevanian, A. and L.L. McLeod, *Cholesterol autoxidation in phospholipid membrane bilayers.* Lipids, 1987. **22**(9): p. 627-36.
127. O'Callaghan, Y.C., J.A. Woods, and N.M. O'Brien, *Comparative study of the cytotoxicity and apoptosis-inducing potential of commonly occurring oxysterols.* Cell Biol Toxicol, 2001. **17**(2): p. 127-37.
128. Sevanian, A., J. Berliner, and H. Peterson, *Uptake, metabolism, and cytotoxicity of isomeric cholesterol-5,6-epoxides in rabbit aortic endothelial cells.* J Lipid Res, 1991. **32**(1): p. 147-55.
129. Diczfalusy, U., et al., *Marked upregulation of cholesterol 25-hydroxylase expression by lipopolysaccharide.* J Lipid Res, 2009. **50**(11): p. 2258-64.

130. Bauman, D.R., et al., *25-Hydroxycholesterol secreted by macrophages in response to Toll-like receptor activation suppresses immunoglobulin A production.* Proc Natl Acad Sci U S A, 2009. **106**(39): p. 16764-9.
131. Im, S.S., et al., *Linking lipid metabolism to the innate immune response in macrophages through sterol regulatory element binding protein-1a.* Cell Metab, 2011. **13**(5): p. 540-9.
132. Liu, C., et al., *Oxysterols direct B-cell migration through EBI2.* Nature, 2011. **475**(7357): p. 519-23.
133. Blanc, M., et al., *Host defense against viral infection involves interferon mediated down-regulation of sterol biosynthesis.* PLoS Biol, 2011. **9**(3): p. e1000598.
134. Cui, G., et al., *Liver X receptor (LXR) mediates negative regulation of mouse and human Th17 differentiation.* J Clin Invest, 2011. **121**(2): p. 658-70.
135. Blanc, M., et al., *The transcription factor STAT-1 couples macrophage synthesis of 25-hydroxycholesterol to the interferon antiviral response.* Immunity, 2013. **38**(1): p. 106-18.
136. Liu, S.Y., et al., *Interferon-inducible cholesterol-25-hydroxylase broadly inhibits viral entry by production of 25-hydroxycholesterol.* Immunity, 2013. **38**(1): p. 92-105.
137. Hannedouche, S., et al., *Oxysterols direct immune cell migration via EBI2.* Nature, 2011. **475**(7357): p. 524-7.
138. Shapiro-Shelef, M. and K. Calame, *Regulation of plasma-cell development.* Nat Rev Immunol, 2005. **5**(3): p. 230-42.
139. Yi, T., et al., *Oxysterol gradient generation by lymphoid stromal cells guides activated B cell movement during humoral responses.* Immunity, 2012. **37**(3): p. 535-48.
140. Hindinger, C., et al., *Liver X receptor activation decreases the severity of experimental autoimmune encephalomyelitis.* J Neurosci Res, 2006. **84**(6): p. 1225-34.
141. Tyers, M. and M. Mann, *From genomics to proteomics.* Nature, 2003. **422**(6928): p. 193-7.
142. Griffiths, W.J., et al., *Metabolomics and metabolite profiling: past heroes and future developments.* Eur J Mass Spectrom (Chichester, Eng), 2007. **13**(1): p. 45-50.
143. Folch, J., M. Lees, and G.H. Sloane Stanley, *A simple method for the isolation and purification of total lipides from animal tissues.* J Biol Chem, 1957. **226**(1): p. 497-509.
144. Bligh, E.G. and W.J. Dyer, *A rapid method of total lipid extraction and purification.* Can J Biochem Physiol, 1959. **37**(8): p. 911-7.
145. Lucas, C.C.R., J.H., Prog. Chem. Fats other Lipids, 1970. **10**: p. 1-150.
146. De Hoffamnn E., S.V., Mass Spectrometry. Principles and applicatons, 2007. **John Viley&Sons**: p. 15-79.
147. Turley, S.D., et al., *Gender-related differences in bile acid and sterol metabolism in outbred CD-1 mice fed low- and high-cholesterol diets.* Hepatology, 1998. **28**(4): p. 1088-94.
148. Karu, K., et al., *Liquid chromatography-mass spectrometry utilizing multi-stage fragmentation for the identification of oxysterols.* J Lipid Res, 2007. **48**(4): p. 976-87.

149. Liere, P., et al., *Novel lipoidal derivatives of pregnenolone and dehydroepiandrosterone and absence of their sulfated counterparts in rodent brain.* J Lipid Res, 2004. **45**(12): p. 2287-302.
150. Olsen, J.V., et al., *A Dual Pressure Linear Ion Trap Orbitrap Instrument with Very High Sequencing Speed.* Molecular & Cellular Proteomics, 2009. **8**(12): p. 2759-2769.
151. Olsen, J.V., et al., *A dual pressure linear ion trap Orbitrap instrument with very high sequencing speed.* Mol Cell Proteomics, 2009. **8**(12): p. 2759-69.
152. Michalski, A., et al., *Ultra high resolution linear ion trap Orbitrap mass spectrometer (Orbitrap Elite) facilitates top down LC MS/MS and versatile peptide fragmentation modes.* Mol Cell Proteomics, 2012. **11**(3): p. O111.013698.
153. Breuer, O., et al., *The oxysterols cholest-5-ene-3 beta,4 alpha-diol, cholest-5-ene-3 beta,4 beta-diol and cholestane-3 beta,5 alpha,6 alpha-triol are formed during in vitro oxidation of low density lipoprotein, and are present in human atherosclerotic plaques.* Biochim Biophys Acta, 1996. **1302**(2): p. 145-52.
154. Dzeletovic, S., et al., *Determination of cholesterol oxidation products in human plasma by isotope dilution-mass spectrometry.* Anal Biochem, 1995. **225**(1): p. 73-80.
155. Honda, A., et al., *Highly sensitive quantification of 7alpha-hydroxy-4-cholesten-3-one in human serum by LC-ESI-MS/MS.* J Lipid Res, 2007. **48**(2): p. 458-64.
156. Wheeler, O.H. and O. Rosado-Lojo, *Kinetics of formation and hydrolysis of steroid Girard-T hydrazones.* Tetrahedron, 1962. **18**(4): p. 477-482.
157. Toya, K., *[Study of profile analysis on urinary free steroids using high performance liquid chromatography with spectrophotometric scanning by photodiode array--application of Girard reagent T for sample preparation].* Nihon Naibunpi Gakkai Zasshi, 1988. **64**(4): p. 310-27.
158. Griffiths, W.J., et al., *Derivatisation for the characterisation of neutral oxosteroids by electrospray and matrix-assisted laser desorption/ionisation tandem mass spectrometry: the Girard P derivative.* Rapid Commun Mass Spectrom, 2003. **17**(9): p. 924-35.
159. Griffiths, W.J., et al., *High-energy collision-induced dissociation of oxosteroids derivatised to Girard hydrazones.* Eur J Mass Spectrom (Chichester, Eng), 2004. **10**(1): p. 63-88.
160. Shackleton, C.H., et al., *Electrospray mass spectrometry of testosterone esters: potential for use in doping control.* Steroids, 1997. **62**(7): p. 523-9.
161. Brooks, C.J., et al., *Selective reactions in the analytical characterisation of steroids by gas chromatography-mass spectrometry.* J Steroid Biochem, 1983. **19**(1a): p. 189-201.
162. Griffiths, W.J., et al., *Analysis of oxysterols by electrospray tandem mass spectrometry.* J Am Soc Mass Spectrom, 2006. **17**(3): p. 341-62.
163. Wang, Y., et al., *Matrix-assisted laser desorption/ionization high-energy collision-induced dissociation of steroids: analysis of oxysterols in rat brain.* Anal Chem, 2006. **78**(1): p. 164-73.
164. Khan, M.A., et al., *Analysis of derivatised steroids by matrix-assisted laser desorption/ionisation and post-source decay mass spectrometry.* Steroids, 2006. **71**(1): p. 42-53.

165. Griffiths, W.J., et al., *Potential of sterol analysis by liquid chromatography-tandem mass spectrometry for the prenatal diagnosis of Smith-Lemli-Opitz syndrome.* Clin Chem, 2008. **54**(8): p. 1317-24.
166. Wang, Y., K. Karu, and W.J. Griffiths, *Analysis of neurosterols and neurosteroids by mass spectrometry.* Biochimie, 2007. **89**(2): p. 182-91.
167. Ogundare, M., et al., *Cerebrospinal fluid steroidomics: are bioactive bile acids present in brain?* J Biol Chem, 2010. **285**(7): p. 4666-79.
168. Griffiths, W.J., et al., *Discovering oxysterols in plasma: a window on the metabolome.* J Proteome Res, 2008. **7**(8): p. 3602-12.
169. Angulo, A., P. Ghazal, and M. Messerle, *The major immediate-early gene ie3 of mouse cytomegalovirus is essential for viral growth.* J Virol, 2000. **74**(23): p. 11129-36.
170. Tint, G.S., et al., *The use of the Dhcr7 knockout mouse to accurately determine the origin of fetal sterols.* J Lipid Res, 2006. **47**(7): p. 1535-41.
171. Lutjohann, D., et al., *Cholesterol homeostasis in human brain: evidence for an age-dependent flux of 24S-hydroxycholesterol from the brain into the circulation.* Proc Natl Acad Sci U S A, 1996. **93**(18): p. 9799-804.
172. Ohyama, Y., et al., *Studies on the transcriptional regulation of cholesterol 24-hydroxylase (CYP46A1): marked insensitivity toward different regulatory axes.* J Biol Chem, 2006. **281**(7): p. 3810-20.
173. Lehmann, J.M., et al., *Activation of the nuclear receptor LXR by oxysterols defines a new hormone response pathway.* J Biol Chem, 1997. **272**(6): p. 3137-40.
174. Mellon, S.H. and L.D. Griffin, *Neurosteroids: biochemistry and clinical significance.* Trends Endocrinol Metab, 2002. **13**(1): p. 35-43.
175. Koldamova, R.P., et al., *22R-hydroxycholesterol and 9-cis-retinoic acid induce ATP-binding cassette transporter A1 expression and cholesterol efflux in brain cells and decrease amyloid beta secretion.* J Biol Chem, 2003. **278**(15): p. 13244-56.
176. Yao, Z.X., et al., *22R-Hydroxycholesterol protects neuronal cells from beta-amyloid-induced cytotoxicity by binding to beta-amyloid peptide.* J Neurochem, 2002. **83**(5): p. 1110-9.
177. Heverin, M., et al., *Changes in the levels of cerebral and extracerebral sterols in the brain of patients with Alzheimer's disease.* J Lipid Res, 2004. **45**(1): p. 186-93.
178. Griffiths, W.J. and Y. Wang, *Analysis of oxysterol metabolomes.* Biochim Biophys Acta, 2011. **1811**(11): p. 784-99.
179. Lutjohann, D., et al., *Profile of cholesterol-related sterols in aged amyloid precursor protein transgenic mouse brain.* J Lipid Res, 2002. **43**(7): p. 1078-85.
180. Lutjohann, D., et al., *Cholesterol dynamics in the foetal and neonatal brain as reflected by circulatory levels of 24S-hydroxycholesterol.* Acta Paediatr, 2001. **90**(6): p. 652-7.
181. Cali, J.J. and D.W. Russell, *Characterization of human sterol 27-hydroxylase. A mitochondrial cytochrome P-450 that catalyzes multiple oxidation reaction in bile acid biosynthesis.* J Biol Chem, 1991. **266**(12): p. 7774-8.
182. Lund, E., et al., *24-, 25- and 27-hydroxylation of cholesterol by a purified preparation of 27-hydroxylase from pig liver.* Biochim Biophys Acta, 1993. **1166**(2-3): p. 177-82.

183. Compagnone, N.A., et al., *Expression of the steroidogenic enzyme P450scc in the central and peripheral nervous systems during rodent embryogenesis.* Endocrinology, 1995. **136**(6): p. 2689-96.
184. Jelinek, D.F., et al., *Cloning and regulation of cholesterol 7 alpha-hydroxylase, the rate-limiting enzyme in bile acid biosynthesis.* J Biol Chem, 1990. **265**(14): p. 8190-7.
185. Schroepfer, G.J., Jr., *Oxysterols: modulators of cholesterol metabolism and other processes.* Physiol Rev, 2000. **80**(1): p. 361-554.
186. Murphy, R.C. and K.M. Johnson, *Cholesterol, reactive oxygen species, and the formation of biologically active mediators.* J Biol Chem, 2008. **283**(23): p. 15521-5.
187. Kautsky, G.J., et al., *Synthesis and metabolism of 22-ketocholesterol-23-C14.* J Biol Chem, 1958. **233**(6): p. 1340-2.
188. Byon, C.Y. and M. Gut, *Steric considerations regarding the biodegradation of cholesterol to pregnenolone.-exclusion of (22S)-22-hydroxycholesterol and 22-ketocholesterol as intermediates.* Biochem Biophys Res Commun, 1980. **94**(2): p. 549-52.
189. Karlaganis, G. and J. Sjovall, *Formation and metabolism of bile alcohols in man.* Hepatology, 1984. **4**(5): p. 966-73.
190. Heverin, M., et al., *Studies on the cholesterol-free mouse: strong activation of LXR-regulated hepatic genes when replacing cholesterol with desmosterol.* Arterioscler Thromb Vasc Biol, 2007. **27**(10): p. 2191-7.
191. Pikuleva, I. and N.B. Javitt, *Novel sterols synthesized via the CYP27A1 metabolic pathway.* Arch Biochem Biophys, 2003. **420**(1): p. 35-9.
192. Marcos, J., et al., *Cholesterol biosynthesis from birth to adulthood in a mouse model for 7-dehydrosterol reductase deficiency (Smith-Lemli-Opitz syndrome).* Steroids, 2007. **72**(11-12): p. 802-8.
193. Rodriguez-Acebes, S., et al., *Desmosterol can replace cholesterol in sustaining cell proliferation and regulating the SREBP pathway in a sterol-Delta24-reductase-deficient cell line.* Biochem J, 2009. **420**(2): p. 305-15.
194. Yang, C., et al., *Sterol intermediates from cholesterol biosynthetic pathway as liver X receptor ligands.* J Biol Chem, 2006. **281**(38): p. 27816-26.
195. Kelley, R.I. and G.E. Herman, *Inborn errors of sterol biosynthesis.* Annu Rev Genomics Hum Genet, 2001. **2**: p. 299-341.
196. Bjorkhem, I., et al., *Oxysterols in the circulation of patients with the Smith-Lemli-Opitz syndrome: abnormal levels of 24S- and 27-hydroxycholesterol.* J Lipid Res, 2001. **42**(3): p. 366-71.
197. Kratz, L.E. and R.I. Kelley, *Prenatal diagnosis of the RSH/Smith-Lemli-Opitz syndrome.* Am J Med Genet, 1999. **82**(5): p. 376-81.
198. Porter, F.D. and G.E. Herman, *Malformation syndromes caused by disorders of cholesterol synthesis.* J Lipid Res, 2011. **52**(1): p. 6-34.
199. Correa-Cerro, L.S., et al., *Development and characterization of a hypomorphic Smith-Lemli-Opitz syndrome mouse model and efficacy of simvastatin therapy.* Hum Mol Genet, 2006. **15**(6): p. 839-51.
200. Wassif, C.A., et al., *Biochemical, phenotypic and neurophysiological characterization of a genetic mouse model of RSH/Smith--Lemli--Opitz syndrome.* Hum Mol Genet, 2001. **10**(6): p. 555-64.
201. Fitzky, B.U., et al., *7-Dehydrocholesterol-dependent proteolysis of HMG-CoA reductase suppresses sterol biosynthesis in a mouse model of Smith-Lemli-Opitz/RSH syndrome.* J Clin Invest, 2001. **108**(6): p. 905-15.

202. Xu, L., Z. Korade, and N.A. Porter, *Oxysterols from free radical chain oxidation of 7-dehydrocholesterol: product and mechanistic studies.* J Am Chem Soc, 2010. **132**(7): p. 2222-32.
203. Griffiths, W.J., et al., *Analytical strategies for characterization of oxysterol lipidomes: liver X receptor ligands in plasma.* Free Radic Biol Med, 2013. **59**: p. 69-84.
204. Paik, Y.K., et al., *Microsomal enzymes of cholesterol biosynthesis from lanosterol. Solubilization and purification of steroid 8-isomerase.* J Biol Chem, 1986. **261**(14): p. 6470-7.
205. Ali, Z., et al., *On the regulatory role of side-chain hydroxylated oxysterols in the brain. Lessons from CYP27A1 transgenic and Cyp27a1−/− mice.* Journal of Lipid Research, 2013. **54**(4): p. 1033-1043.
206. Heyl, B.L., D.J. Tyrrell, and J.D. Lambeth, *Cytochrome P-450scc-substrate interactions. Role of the 3 beta- and side chain hydroxyls in binding to oxidized and reduced forms of the enzyme.* J Biol Chem, 1986. **261**(6): p. 2743-9.
207. Karu, K., et al., *Nano-liquid chromatography-tandem mass spectrometry analysis of oxysterols in brain: monitoring of cholesterol autoxidation.* Chem Phys Lipids, 2011. **164**(6): p. 411-24.
208. Ramirez, D.M., S. Andersson, and D.W. Russell, *Neuronal expression and subcellular localization of cholesterol 24-hydroxylase in the mouse brain.* J Comp Neurol, 2008. **507**(5): p. 1676-93.
209. Forman, B.M., et al., *The orphan nuclear receptor LXRalpha is positively and negatively regulated by distinct products of mevalonate metabolism.* Proc Natl Acad Sci U S A, 1997. **94**(20): p. 10588-93.
210. Janowski, B.A., et al., *An oxysterol signalling pathway mediated by the nuclear receptor LXR alpha.* Nature, 1996. **383**(6602): p. 728-31.
211. Horton, J.D., J.L. Goldstein, and M.S. Brown, *SREBPs: activators of the complete program of cholesterol and fatty acid synthesis in the liver.* J Clin Invest, 2002. **109**(9): p. 1125-31.
212. Tall, A.R., P. Costet, and Y. Luo, *'Orphans' meet cholesterol.* Nat Med, 2000. **6**(10): p. 1104-5.
213. Kotti, T.J., et al., *Brain cholesterol turnover required for geranylgeraniol production and learning in mice.* Proc Natl Acad Sci U S A, 2006. **103**(10): p. 3869-74.
214. Honda, A., et al., *Side chain hydroxylations in bile acid biosynthesis catalyzed by CYP3A are markedly up-regulated in Cyp27-/- mice but not in cerebrotendinous xanthomatosis.* J Biol Chem, 2001. **276**(37): p. 34579-85.
215. Russell, D.W., *The enzymes, regulation, and genetics of bile acid synthesis.* Annu Rev Biochem, 2003. **72**: p. 137-74.
216. Meaney, S., *Is C-26 hydroxylation an evolutionarily conserved steroid inactivation mechanism?* Faseb j, 2005. **19**(10): p. 1220-4.
217. Taylor, F.R., et al., *24,25-Epoxysterol metabolism in cultured mammalian cells and repression of 3-hydroxy-3-methylglutaryl-CoA reductase.* J Biol Chem, 1986. **261**(32): p. 15039-44.
218. Nelson, J.A., Steckbeck, S. R., and Spencer, T. A. , J. Biol. Chem, 1981. **256**: p. 1067–1068.
219. Iuliano, L., et al., *Measurement of oxysterols and alpha-tocopherol in plasma and tissue samples as indices of oxidant stress status.* Anal Biochem, 2003. **312**(2): p. 217-23.

220. Stapleton, G., et al., *A novel cytochrome P450 expressed primarily in brain.* J Biol Chem, 1995. **270**(50): p. 29739-45.
221. Stiles, A.R., et al., *CYP7B1: one cytochrome P450, two human genetic diseases, and multiple physiological functions.* J Biol Chem, 2009. **284**(42): p. 28485-9.
222. Salen, G., S. Shefer, and V. Berginer, *Familial diseases with storage of sterols other than cholesterol: cerebrotendinous xanthomatosis and sitosterolemia with xanthomatosis.* In The Metabolic Basis of Inherited Disease, 1983. **5th**(J. B. Stanbury, J. B. Wyngaarden, D. S. Fredrickson, J. L. Goldstein, and M. S. Brown, editors. McGraw Hill, New York): p. 713-730.
223. Cali, J.J., et al., *Mutations in the bile acid biosynthetic enzyme sterol 27-hydroxylase underlie cerebrotendinous xanthomatosis.* J Biol Chem, 1991. **266**(12): p. 7779-83.
224. Dahlback, H. and K. Wikvall, *25-Hydroxylation of vitamin D3 by a cytochrome P-450 from rabbit liver mitochondria.* Biochem J, 1988. **252**(1): p. 207-13.
225. Russell DW, S.K., *Bile acid biosynthesis.* Biochemistry, 1992. **31(20)**: p. 4737-49.
226. Bjorkhem, K.B., *Inborn errors in bile acid biosynthesis and storage of sterols other than cholesterol.* The metabolic basis of inherited disease, 1995. **Vol 2**: p. 2073–2102.
227. Lee, M.H., et al., *Fine-mapping, mutation analyses, and structural mapping of cerebrotendinous xanthomatosis in U.S. pedigrees.* J Lipid Res, 2001. **42**(2): p. 159-69.
228. Verrips, A., et al., *Clinical and molecular genetic characteristics of patients with cerebrotendinous xanthomatosis.* Brain, 2000. **123 (Pt 5)**: p. 908-19.
229. Nagai, Y., et al., *Japanese triplets with cerebrotendinous xanthomatosis are homozygous for a mutant gene coding for the sterol 27-hydroxylase (Arg441Trp).* Neurology, 1996. **46**(2): p. 571-4.
230. Menkes, J.H., J.R. Schimschock, and P.D. Swanson, *Cerebrotendinous xanthomatosis. The storage of cholestanol within the nervous system.* Arch Neurol, 1968. **19**(1): p. 47-53.
231. de Sain-van der Velden, M.G., et al., *Elevated cholesterol precursors other than cholestanol can also be a hallmark for CTX.* J Inherit Metab Dis, 2008. **31 Suppl 2**: p. S387-93.
232. Hoshita, T., et al., *Occurrence of bile alcohol glucuronides in bile of patients with cerebrotendinous xanthomatosis.* J Lipid Res, 1980. **21**(8): p. 1015-21.
233. Batta, A.K., et al., *Effect of chenodeoxycholic acid on biliary and urinary bile acids and bile alcohols in cerebrotendinous xanthomatosis; monitoring by high performance liquid chromatography.* J Lipid Res, 1985. **26**(6): p. 690-8.
234. The Jackson Labolatory, B.-C.a.t.E.J.S.i.
235. Repa, J.J., et al., *Disruption of the sterol 27-hydroxylase gene in mice results in hepatomegaly and hypertriglyceridemia. Reversal by cholic acid feeding.* J Biol Chem, 2000. **275**(50): p. 39685-92.
236. Bavner, A., et al., *On the mechanism of accumulation of cholestanol in the brain of mice with a disruption of sterol 27-hydroxylase.* J Lipid Res, 2010. **51**(9): p. 2722-30.
237. Rosen, H., et al., *Markedly reduced bile acid synthesis but maintained levels of cholesterol and vitamin D metabolites in mice with disrupted sterol 27-hydroxylase gene.* J Biol Chem, 1998. **273**(24): p. 14805-12.

238. Norlin, M., et al., *24-hydroxycholesterol is a substrate for hepatic cholesterol 7alpha-hydroxylase (CYP7A).* J Lipid Res, 2000. **41**(10): p. 1629-39.
239. Rose, K.A., et al., *Cyp7b, a novel brain cytochrome P450, catalyzes the synthesis of neurosteroids 7alpha-hydroxy dehydroepiandrosterone and 7alpha-hydroxy pregnenolone.* Proc Natl Acad Sci U S A, 1997. **94**(10): p. 4925-30.
240. Song, W., et al., *Purification and characterization of hamster liver microsomal 7alpha-hydroxycholesterol dehydrogenase. Similarity to type I 11beta-hydroxysteroid dehydrogenase.* J Biol Chem, 1998. **273**(26): p. 16223-8.
241. Mitic, T., et al., *11beta-Hydroxysteroid dehydrogenase type 1 contributes to the regulation of 7-oxysterol levels in the arterial wall through the inter-conversion of 7-ketocholesterol and 7beta-hydroxycholesterol.* Biochimie, 2013. **95**(3): p. 548-55.
242. Xu, L., et al., *Metabolism of oxysterols derived from nonenzymatic oxidation of 7-dehydrocholesterol in cells.* J Lipid Res, 2013. **54**(4): p. 1135-43.
243. Wikvall, K., *Purification and properties of a 3 beta-hydroxy-delta 5-C27-steroid oxidoreductase from rabbit liver microsomes.* J Biol Chem, 1981. **256**(7): p. 3376-80.
244. Schwarz, M., et al., *The bile acid synthetic gene 3beta-hydroxy-Delta(5)-C(27)-steroid oxidoreductase is mutated in progressive intrahepatic cholestasis.* J Clin Invest, 2000. **106**(9): p. 1175-84.
245. Norlin, M., et al., *On the substrate specificity of human CYP27A1: implications for bile acid and cholestanol formation.* J Lipid Res, 2003. **44**(8): p. 1515-22.
246. DeBarber, A.E., et al., *ESI-MS/MS quantification of 7alpha-hydroxy-4-cholesten-3-one facilitates rapid, convenient diagnostic testing for cerebrotendinous xanthomatosis.* Clin Chim Acta, 2010. **411**(1-2): p. 43-8.
247. DeBarber, A.E., et al., *Profiling sterols in cerebrotendinous xanthomatosis: utility of Girard derivatization and high resolution exact mass LC-ESI-MS(n) analysis.* J Chromatogr B Analyt Technol Biomed Life Sci, 2011. **879**(17-18): p. 1384-92.
248. Diczfalusy, U., et al., *Novel pathways for elimination of cholesterol by extrahepatic formation of side-chain oxidized oxysterols.* Scand J Clin Lab Invest Suppl, 1996. **226**: p. 9-17.
249. Matsuda, A., et al., *24(S)-hydroxycholesterol is actively eliminated from neuronal cells by ABCA1.* J Neurochem, 2013. **126**(1): p. 93-101.
250. Heverin, M., et al., *Crossing the barrier: net flux of 27-hydroxycholesterol into the human brain.* J Lipid Res, 2005. **46**(5): p. 1047-52.
251. Li-Hawkins, J., et al., *Disruption of the oxysterol 7alpha-hydroxylase gene in mice.* J Biol Chem, 2000. **275**(22): p. 16536-42.
252. Wu, Z., et al., *Structure and functions of human oxysterol 7alpha-hydroxylase cDNAs and gene CYP7B1.* J Lipid Res, 1999. **40**(12): p. 2195-203.
253. Li, A. and J.C. Bigelow, *The 7-hydroxylation of dehydroepiandrosterone in rat brain.* Steroids, 2010. **75**(6): p. 404-10.
254. Chalbot, S. and R. Morfin, *Dehydroepiandrosterone metabolites and their interactions in humans.* Drug Metabol Drug Interact, 2006. **22**(1): p. 1-23.
255. Biancheri, R., et al., *White matter lesions in spastic paraplegia with mutations in SPG5/CYP7B1.* Neuromuscul Disord, 2009. **19**(1): p. 62-5.

256. Bjorkhem, I. and S. Meaney, *Brain cholesterol: long secret life behind a barrier.* Arterioscler Thromb Vasc Biol, 2004. **24**(5): p. 806-15.
257. Li, X., et al., *Biosynthesis of the regulatory oxysterol, 5-cholesten-3beta,25-diol 3-sulfate, in hepatocytes.* J Lipid Res, 2007. **48**(12): p. 2587-96.
258. Norlin, M., et al., *Oxysterol 7 alpha-hydroxylase activity by cholesterol 7 alpha-hydroxylase (CYP7A).* J Biol Chem, 2000. **275**(44): p. 34046-53.
259. Schule, R., et al., *Marked accumulation of 27-hydroxycholesterol in SPG5 patients with hereditary spastic paresis.* J Lipid Res, 2010. **51**(4): p. 819-23.
260. Van Lier, J.E. and L.L. Smith, *Sterol metabolism. I. 26-Hydroxycholesterol in the human aorta.* Biochemistry, 1967. **6**(10): p. 3269-78.
261. Fieser L. F., H.W.-Y., Bhattacharyya B. K.. *Cholesterol and companions. X. The diol fraction.* . J. Org. Chem. , 1957. **22**: p. 1380–1384.
262. Breslow, J.L., et al., *Cholesterol, 7-ketocholesterol and 25-hydroxycholesterol uptake studies and effect on 3-hydroxy-3-methylglutaryl-coenzyme A reductase activity in human fibroblasts.* Biochim Biophys Acta, 1975. **398**(1): p. 10-7.
263. Kandutsch, A.A. and H.W. Chen, *Regulation of sterol synthesis in cultured cells by oxygenated derivatives of cholesterol.* J Cell Physiol, 1975. **85**(2 Pt 2 Suppl 1): p. 415-24.
264. Lagace, T.A., et al., *Altered regulation of cholesterol and cholesteryl ester synthesis in Chinese-hamster ovary cells overexpressing the oxysterol-binding protein is dependent on the pleckstrin homology domain.* Biochem J, 1997. **326 (Pt 1)**: p. 205-13.
265. Lehto, M. and V.M. Olkkonen, *The OSBP-related proteins: a novel protein family involved in vesicle transport, cellular lipid metabolism, and cell signalling.* Biochim Biophys Acta, 2003. **1631**(1): p. 1-11.
266. Park, K. and A.L. Scott, *Cholesterol 25-hydroxylase production by dendritic cells and macrophages is regulated by type I interferons.* J Leukoc Biol, 2010. **88**(6): p. 1081-7.
267. Gatto, D. and R. Brink, *B cell localization: regulation by EBI2 and its oxysterol ligand.* Trends Immunol, 2013. **34**(7): p. 336-41.
268. Haspot, F., et al., *Human cytomegalovirus entry into dendritic cells occurs via a macropinocytosis-like pathway in a pH-independent and cholesterol-dependent manner.* PLoS One, 2012. **7**(4): p. e34795.

Appendix A
List of Publications

Oxysterols in brain of the cholesterol 24-hydroxylase knockout mouse, Meljon A, Wang Y, Jeffrey G. McDonal JG, Russell DW and Griffiths WJ, Biochem. Biophys. Res. Commun. (accepted)

Synthesis and biological activity of (24E)- and (24Z)-26-hydroxydesmosterol.,Saini R, Kataeva O, Schmidt AW, Wang Y, Meljon A, Griffiths WJ, Knölker HJ, Bioorg. Med. Chem. 2013, 15;21(18):5794-8

Analysis by liquid chromatography-mass spectrometry of sterols and oxysterols in brain of the newborn Dhcr7Δ3-5/T93M mouse: A model of Smith-Lemli-Opitz syndrome., Meljon A, Watson GL, Wang Y, Shackleton CH, Griffiths WJ., Biochem Pharmacol. 2013; 86:43-55

The transcription factor STAT-1 couples macrophage synthesis of 25-hydroxycholesterol to the interferon antiviral response., Blanc M, Hsieh WY, Robertson KA, Kropp KA, Forster T, Shui G, Lacaze P, Watterson S, Griffiths SJ, Spann NJ, Meljon A, Talbot S, Krishnan K, Covey DF, Wenk MR, Craigon M, Ruzsics Z, Haas J, Angulo A, Griffiths WJ, Glass CK, Wang Y, Ghazal P.,Immunity. 2013;38(1):106-18

Chemical Genomics and Proteomics, Chapter 2: Development and Application of Novel Analytical Method in Lipidomics, Wang Y, Meljon A, Ogundare M and Griffiths WJ. 2012; 49-80

Analysis of bioactive oxysterols in newborn mouse brain by LC/MS., Meljon A, Theofilopoulos S, Shackleton CH, Watson GL, Javitt NB, Knölker HJ, Saini R, Arenas E, Wang Y, Griffiths WJ. J Lipid Res. 2012; 53(11):2469-83

Mass Spectrometry Handbook, Mike S. Lee; Section III: Mass Spectrometry for Steroid Analysis. Griffiths WJ, Ogundare M, Meljon A and Wang Y. 2012; 271-338